University of Strathclyde Science

Royal Charter since 1964
Useful Learning since 1796

Strathclyde Institute of Pharmacy and Biomedical Sciences

Investigating the inflammatory pathways and proteomic networks in a rodent model of hypertension:

Exploring HMGB1 expression in the cardiac niche

Zainab Y H A H A Bosakhar

A thesis submitted in fulfilment of the requirements for the degree of Doctor of Philosophy

October 2025

Declarations

‘This thesis is the result of the author’s original research. It has been composed by the author and has not been previously submitted for examination which has led to the award of a degree.’

Signed: 

Date: 10/3/2025

COVID Impact statement

This COVID-19 impact statement highlights the specific challenges and justifications relating to Covid-19 restrictions.

The COVID-19 pandemic has posed significant challenges to research projects, particularly those requiring *in vivo* animal models. For my project on angiotensin II-induced chronic hypertension, lab work was postponed for four months due to COVID restrictions. The completion of practical and theoretical courses requirements is essential for obtaining a necessary Home Office license which is a time and course dependent, this takes a month to be completed and after passing the exams, the license process to be approved that typically takes two months. In addition, project license also needed to start the animal work which also needed to be grant from the Home Office. Theses licenses are necessary qualification for planning and executing my animal experiments, which themselves require a two-week planning period and a month-long execution phase including surgery and end point tissue processing.

After the completion of animal work, data analysis for this work takes time to be completed and procced with *in vitro* laboratory investigations and data analysis. The COVID-19 pandemic has also hindered my access to essential resources and lab supplies. The procurement of antibodies and staining kits, for instance, has been significantly delayed due to supply chain disruptions and increased demand.

Beyond the logistical challenges, the pandemic has also had a profound impact on my emotional well-being and overall health. The stress and uncertainty associated with COVID-19 have taken a toll on my mental health as being abroad alone during the pandemic has exacerbated the emotional strain. The vaccination process, while essential for public health, has had adverse effects on my immune system, and I had suffered with illness and a prolonged recovery period.

Student Signature: Zainab Y H A H A Bosakhar

Supervisor Signature: Margaret Cunningham

Date: 10/10/2025

List of Abbreviations

1K-1C	1 kidneys- 1 clip
2K-1C	2 kidneys-1 clip
2K-2C	2 kidneys- 2 clip
ACE	Angiotensin converting enzyme
AD	Aspartate residue
ADP	Adenosine 5′-diphosphate
Ang II	Angiotensin II
ANP	Atrial natriuretic peptide
AP-A	Aminopeptidase A
ARNI	Angiotensin receptor-neprilysin inhibitors
AT1	Ang II type 1 receptor
AT2	Ang II type 2 receptor
BNP	And brain natriuretic peptide
BP	Blood pressure
BSA	Bovine serum albumin
CCBs	Calcium channel blockers
Cfln1	Cofilin 1
CFU	Colony-forming unit
CFU-MK	Colony-forming unit-megakaryocyte
CMP	Common myeloid progenitor
CSF-1	Colony-stimulating factor-1
CVDs	Cardiovascular diseases
DALYs	Disability-adjusted life-years
DAMPs	Damage-associated molecular patterns
DDA	Dependent acquisition
DEPs	Differential expressed proteins
DNA	Deoxyribonucleic acid

DOCA	Deoxycorticosterone acetate
ECM	Extracellular matrix
ER	Endoplasmic reticulum
FBS	Foetal bovine serum
FDA	Food and Drug Administration
FLI1	Fli-1 proto-oncogene
FN	Fibronectin
GAGs	Glycosaminoglycans
GC–MS	Gas chromatography–mass spectrometry
GO	Gene ontology
GPCRs	G protein-coupled receptors
HF	Heart failure
HFpEF	Heart Failure with Preserved Ejection Fraction
HMGB1	High mobility group box 1 protein
HMW	High molecular weight
HSC	Haematopoietic stem cells
IFNs	Interferons
IL-6	Interleukin-6
KEGG	Kyoto Encyclopedia of Genes and Genomes
LC–MS	Liquid chromatography–mass spectrometry
LFQ	Label free quantification
LFQ	Label free quantitation
L-NAME	N-nitro-L-arginine methyl ester
LVH	Left ventricular hypertrophy
MAPK	Mitogen-activated protein kinase
MAPs	Microtubule-associated proteins
MEG-01	Megakaryoblastic leukaemia cell line
MEP	Megakaryocyte-erythrocyte progenitor
MF	Myocardial fibrosis

MIF	Myocardial interstitial fibrosis
miRNAs	Micrornas
MKs	Megakaryocytes
MLCK	Myosin light chain kinase
MLCP	Myosin light chain phosphatase
MMPs	Matrix metalloproteinases
MRAs	Mineralocorticoid receptor antagonists
mRNA	Messenger RNA
MyD88	Myeloid differentiation protein 88
NETs	Neutrophil extracellular traps
NF-E2	Nuclear factor, erythroid 2
NLRP3	Nucleotide-binding domain, leucine-rich repeat-containing protein 3
NOS	Nitric oxide synthase
PAMPs	Pathogen-associated molecular patterns
PCA	Principal component analysis
PD	Proteome discoverer
PKC	Protein kinase C
PLPs	Platelet like particles
pre-HF	pre-heart failure
PRR	Prorenin renin receptor
PRRs	Pattern recognition receptors
PTMs	Post-translational modifications
RAAS	Renin-angiotensin-aldosterone system
RAGE	Advanced glycation end products
RAS	Renal arterial stenosis
RAS	Renin-angiotensin system
ROS	Reactive oxygen species
RUNX1	Runx family transcription factor 1

STING	Interferon genes
TAT	Thrombin-antithrombin III complex
TIMPs	Natural inhibitors
TLRs	Toll-like receptors
TNF	Tumour necrosis factor
TNF-α	Tumour Necrosis Factor-alpha
VSMCs	Vascular smooth muscle cells

Acknowledgment

I would like to express my deepest gratitude to my primary supervisor Dr Margaret Cunningham, whose guidance and support were instrumental in the completion of my thesis and lab work. I am truly thankful your contributions have shaped most of this work. I am also grateful to my second supervisor, Dr Susan Currie, for your invaluable assistance with the *in vivo* and animal experiments. Your expertise in this area greatly enhanced the quality of my research. I would like to thank Dr Nicholas Rattray and technical support provided by Gillian Farrell for the proteomic experiments carried out at the Strathclyde Centre for Molecular Bioscience.

A special thanks to technician Graeme Mackenzie for your technical support and assistance throughout this project. To my lab partner Ryan, your humour and unconditional help made the lab a more enjoyable and productive place. Thank you for always being there.

I would also like to extend my heartfelt appreciation to my family in Kuwait, especially my sisters, for their unwavering support and encouragement. This mainly give me strength to continue this abroad journey.

To my friends Justin, Abdullah-Alsultan, and Rand, your friendship has been a constant source of strength. Lastly, a big thank you to my gym partner Colin, who keeps me motivated and pushes me to achieve my best. Your support has been invaluable throughout this journey.

Professional Society Membership

British Pharmacological Society ECR Member – Dec 2020-present.

Training: PG Cert Classes, Courses, and Conferences

PG Certificate in Researcher Professional Development Dec 2024.

World Congress of Basic and Clinical Pharmacology 2023 (WCP2023), Glasgow, UK. Poster presentation July 2-7th 2023.

British Pharmacological Society, Pharmacology 2022 Annual Conference Liverpool, UK. Poster presentation Sep 12th-13th 2022.

PIL Personal licence I72786373 granted - Transverse aortic banding or injection/infusion of a pharmacological agent and echocardiography (Protocol number 1). May 16th 2022.

Scottish Accreditation Board for PIL course. PIL certificate & License. Theory: Mouse & Rat. Skills: Mouse & Rat - October 19th - November 2nd 2021.

Generic biomedical and pharmaceutical research skills compulsory course (20 credits). Class complete. April 27th 2021.

4th ERNEST meeting on cell signalling. Online Conference. Attendee. April 12-14th 2021.

Python for beginners' course, Biochemical Society. March 22nd, 2021.

Optical technologies for the imaging and manipulation of excitable cells. University of Glasgow. Attendee. March 9th, 2021.

Scottish Cardiovascular Forum 14th Annual Meeting. Online Conference. Attendee. February 5th, 2021.

Thesis writing masterclass - Watson Research & Training Ltd. December 14th 2020.

Research Outputs

Olatunji, Z., BOSAKHAR, Z. Y. H. A. H. A., MacKenzie, G., Cunningham, M. R., MacQuaide, N., & Currie, S. (2024). Altered regulation of Ca2+ handling proteins in an in vivo rat model of Angiotensin II-induced hypertension. *Medical Science Forum*, *27*((1) 3), Article 2.27. https://doi.org/10.3390/msf2024027003

Bosakhar, Z., MacKenzie, G., Gu, H., Currie, S., & Cunningham, M. (2023). HMGB1 release in the cardiac niche: interplay between HMGB1 and thrombin. *British Journal of Pharmacology*, *180*(S1), 140. Article P0589. https://doi.org/10.1111/bph.16105

Olatunji, Z. O., MacMillan, S., Cameron-Ruiz, M., Bosakhar, Z. Y., MacKenzie, G., Grant, M. H., Tate, R., MacQuaide, N., & Currie, S. (2023). Effects of acute and chronic cobalt treatment on adult rat cardiomyocyte calcium handling. *Heart* , *109*(Supplement 2), Article A6. https://doi.org/10.1136/heartjnl-SCF-2023.18

MacMillan, S., Olatunji, Z. O., Bosakhar, Z. Y., MacKenzie, G., Grant, M. H., Tate, R., Macquaide, N., & Currie, S. (2022). Cobalt-mediated contractile dysfunction in adult hearts and consequent effects on cardiomyocyte calcium transients. *Acta Physiologica*, *236*(S725), 922. Article e13877. https://doi.org/10.1111/apha.13877

MacMillan, S., Olatunji, Z. O., Bosakhar, Z. Y., MacKenzie, G., Grant, M. H., Tate, R., Macquaide, N., & Currie, S. (2022). Concentration- and time-dependent effects of cobalt in rat and human ventricular cardiac fibroblasts. *Acta Physiologica*, *236*(S725), 614. https://doi.org/10.1111/apha.13876

Table of Contents

Declarations II

COVID Impact statement III

List of Abbreviations V

Acknowledgment IX

Professional Society Membership X

Training: PG Cert Classes, Courses, and Conferences X

Research Outputs XI

Table of Contents XII

List of Figures XXI

List of tables XXV

Abstract 1

Graphical abstract 3

..... 3

Chapter 1: 4

General Introduction 4

1.1 Cardiovascular disease (CVD) burden 5

1.1.1 Cardiac cells and alteration in CVD 5

1.1.2 Chronic hypertension 9

1.1.2.1 Pathophysiology and mechanisms of chronic hypertension 9

1.1.2.2 Cardiac remodelling in hypertension 10

1.1.2.3 Histological Characteristics of Cardiac Fibrosis 11

1.1.2.4 Key Characteristics and Homeostasis of Cardiac ECM 13

1.2 Animal models in cardiovascular disease 15

1.2.1 Models of hypertension (essential and secondary) 16
1.2.2 Ang II-induced chronic hypertension 18
1.2.3 Physiological role of the Renin Angiotensin System (RAS) 21
1.2.4 Current anti-hypertensive treatment strategies 24
1.3 Targeting inflammatory proteins as an anti-hypertensive strategy 26
1.3.1. Inflammation, hypertension and CVD injury 26
1.3.2. The role of immune cell signalling in hypertension 27
1.3.3 DAMP mediated TLR4 activation in hypertension 31
1.3.3.1 TLR4 signalling 32
1.4 HMGB1 as a potential biomarker in hypertension 35
1.4.1 Biological and Molecular Characteristics of HMGB1 35
1.4.2 HMGB1 Intracellular and Extracellular Signalling 38
1.4.2.1 Platelets, Extracellular Vesicles (EVs) and HMGB1 in Cardiovascular Disease 40
1.4.3 HMGB1 as inflammation biomarker in CVD 42
1.5. Hypothesis, Aims and Objectives 44
Chapter 2: 46
Materials and Methods 46
2.1 Materials and reagents 47
2.1.1 *in vivo* work materials, reagents and equipment's 47
2.1.2 Buffers and prepared solutions used *in vitro* experiments 48
2.1.2 Key resources used in *in vitro* experiments 49
2.2 Methods 51
2.2.1 Animal ethics 51

2.2.2 Animals 51
2.2.3 Preparation of saline and Angiotensin II mini-pump 53
2.2.4 Animal monitoring pre- and post-surgery 54
2.2.5 Blood pressure measurements 55
2.2.6 Echocardiography studies 55
2.2.7 Heart Dissection and cell culture 58
2.2.8 Bicinchoninic Acid Assay (BCA) Protein Measurement 60
2.2.9 Western blot analysis (Cardiac Tissue) 60
2.2.10 Indirect immunofluorescence on heart tissue sections 60
2.2.11 Picrosirius Red Staining 62
2.2.12 Masson's Trichrome staining 64
2.2.13 Isolation of extracellular vesicles (EVs) 66
2.2.13.1 Rat serum derived EVs 66
2.2.13.2 MEG-01 derived EVs 66
2.2.13.3 Dynamic Light Scattering (DLS) EV Zeta-Sizing 68
2.2.14 Cell culture 69
2.2.14.1 MEG-01 Cell Culture and Sample Preparation: 69
2.2.14.2 Cryopreservation 70
2.2.14.3 Thawing Cells from Cryopreservation 70
2.2.14.4 Cell lysis 70
2.2.15 Trichloroacetic Acid (TCA) + Sodium Deoxycholate (DOC) Precipitation 71
2.2.16 SDS-PAGE and Western Blotting 71
2.2.16.1 Cell Sample Preparation 71

2.2.16.2 Sodium Dodecyl Sulphate-Polyacrylamide Gel Electrophoresis (SDS-PAGE) 72
2.2.16.3 Electrophoretic Transfer of Protein to Membrane and Immunological Detection 72
2.2.16.4 Membrane Stripping and Reprobing. 73
2.2.17 Scanning and Densitometry 73
2.2.18 ImageJ analysis 73
2.2.19 Bright-field Microscopy 74
2.2.20 Fluorescence microscopy 74
2.2.21 LC-MS Proteomics-based heart tissue analysis workflow 76
2.2.21.1 Tissue processing and Sample Preparation for Proteomic Profiling 76
2.2.21.2 Protein Extraction, Trypsin Digestion and Peptide Clean-up 77
2.2. 21.3 Micro-flow LC-MS-based proteomic 78
2.2.21.4 Protein Identification and Quantification. 79
2.2.21.5 Bioinformatics Analyses of Proteomics Data 80
2.2.21.6 GO and KEGG Pathway Analyses 80
2.2.21.7 Protein–Protein Interactions (PPI) and Hub Protein Identification 80
2.2.22 Statistical analysis 81
Chapter 3: 82
In-Vivo Model of Ang II-Induced Chronic Hypertension in Male Rats 82
3.1 Introduction 83
3.1.1 Ang II-induced chronic hypertension model 84
3.2 Chapter Aims and Objectives 86
3.3 Results 88

3.3.1 Evidence for chronic hypertension and hypertrophy following Ang II induction. 88
3.3.1.1 Body Weight Monitoring in Ang II-Induced Hypertension Model..... 88
3.3.1.2 Blood Pressure Monitoring in Ang II-Induced Hypertension Model 89
3.3.1.3 Heart and organs morphology, and heart/body weight ratio 91
3.3.1.4 Transthoracic Echocardiography and Left Ventricular Geometric Patterns 93
3.3.2 Assessment of collagen content and fibrosis progress. 95
3.3.2.1 Collagen deposition in perivascular and interstitial regions 96
3.3.3 HMGB1 association in cardiac remodelling in Ang II induced chronic hypertension 100
3.3.3.1 HMGB1 and high-molecular-weight isoforms detected in cardiac tissue of Ang II-induced hypertensive rats 100
3.3.3.2 HMGB1 localisation and redistribution in Ang II–induced cardiac remodelling 102
3.3.3.3 Collagen with HMGB1 deposition in Ang II infused rats. 106
3.3.4 Analysis of EVs released from the control Rat serum 108
3.3.5 Using the Megakaryoblastic leukaemia cell line (MEG-01) as an alternative model to investigate EV expression of HMGB1 112
3.3.5.1 MEG-01 Derived Extracellular Vesicles (EVs) 116
3.3.5.2 Active release of HMGB1 in MEG-01 cells 120
3.4. Discussion 122
3.4.1 Chronic hypertension and hypertrophy following Ang II induction 122
3.4.2 HMGB1 expression and localisation in Ang II hearts 124
3.5 Chapter conclusion 126

Chapter 4: 128

LC-MS-Based Proteomic Analysis of Left Ventricle Tissues from Ang II-induced Chronic Hypertension in Male Rats 128

4.1 Introduction 129

4.1.1 Overview of Proteomics and high throughput technologies 129

4.1.2 Top-down and bottom-up MS-based proteomic methods 131

4.1.3 Using proteomics to map inflammatory pathways that contribute to cardiovascular dysfunction 133

4.1.4 Pathway Analysis and Protein-Protein Interactions in Hypertension 135

4.2 Chapter Aims and Objectives 136

4.3 Results 138

4.3.1 Proteomics-based LV tissue profiling of Ang II-induced chronic hypertension in male rats 138

4.3.2 Shotgun Proteomics and Protein-Based Bioinformatics 139

4.3.3 Principal Component Analysis (PCA) of Protein Profiles in Ang II, Saline, and Control Groups. 143

4.3.4 Upregulated and Downregulated Proteins in LV Tissue Across Study Groups 146

4.3.5 Common cardiac function markers in hypertension progression 150

4.3.6 HMGB1 Presence, Associated Proteomic Profiles in LV Tissue and protein Interactions 151

4.3.7 Systematic GO and KEGG Pathway Enrichment Analysis of DEPs in the Ang II-Induced Chronic Hypertension Model: Insights into Cardiac Remodelling 155

4.3.7.1 GO annotation and KEGG enrichment analysis of DEPs 155

4.3.8. Mapping Protein Interactions in Cardiac Remodelling via STRING-db 160
4.3.9 Proteins Pathways analysis of the identified DEPs linked to inflammatory response 164
4.3.10 Future Directions in Molecular Characterisation: Unravelling Key Proteins and Pathways in Cardiac Remodelling 167
4.4 Discussion 170
4.4.1 Proteomic Insights into Early Cardiac Remodelling 174
4.4.1.1 Validating the Ang II-Induced Pre-Heart Failure Model in the Absence of Overt Dysfunction 174
4.4.2 Presence of HMGB1 in Proteomic Profiling: A Context-Dependent Regulator in Cardiac Remodelling 176
4.4.3 Distinct and Shared Proteomic Signatures of Cardiac Remodelling and Hypertrophy in Chronic Hypertension 178
4.4.2.1 Mitochondrial Dysfunction and Cardiac Remodelling 180
4.4.2.2 Heat Shock Proteins and Fibrosis 181
4.4.2.3 Cytoskeletal Remodelling and Tubulin Alterations 181
4.4.2.4 Connection between Cardiac Muscle Contractility and Remodelling Markers 184
4.4.2.5 Cytoskeleton Organisation Mechanotransduction and ECM-Integrin Signalling 186
4.2.2.6 Actin Cytoskeleton Remodelling and the Role of Cofilin-1 and Integrin Signalling in Hypertensive Hearts 187
4.4.3 LV DEPs Interactions Related to Cardiac Remodelling that Link to Cardiac Inflammation 188
4.5 Chapter Conclusions 192

Chapter 5: 193

General Discussion 193

5.1 Overview of key findings 194

5.2 Ang II-induced chronic hypertension hypertrophy model in the absence of heart failure 195

5.2.1 Is HMGB1 implicated in the Ang II-induced chronic hypertension hypertrophy model in the absence of heart failure 197

5.2.2 Is increased HMW-HMGB1 expression linked to surgical stress during the mini-pump implantation in the experimental rodent model? 198

5.2.3 Altered HMGB1 localisation in Ang II but not Control or Sal groups – Experimental artifact or a pathological marker of the Ang II disease model? 200

5.2.4 Extracellular release of HMGB1via extracellular vesicles (EV) - A potential consequence of cardiac myocyte HMGB1 redistribution 201

5.2.5 Translating HMGB1 EV release to a human megakaryocytic cell line that secretes platelet-like particles 203

5.2.6 Implications of HMGB1 EV release to cardiovascular dysfunction .. 204

5.3 Did shotgun proteomic analysis of LV tissue offer any new insights into mechanisms of Ang II-induced Hypertension? 205

5.3.1. HMGB1-associated pathways feature in LV proteomics analysis .. 207

5.3.2. Critical evaluation of existing LV proteomic analysis compared to Ang II-induced hypertension experiments 211

5.3.3. Testable hypothesis – the role of Cofilin-associated protein networks as a potential new avenue for experimental follow-up 214

5.4 Limitations of research Conclusion 218

5.5 Future Work 219

References... 222

List of Figures

Chapter 1 Figures

Figure 1.1: Anatomy of the interior of the heart the wall composition and cells. . 6

Figure 1.2: Extracellular matrix (ECM) compartments. 14

Figure 1.3: Schematic illustration classified models of hypertension. 16

Figure 1.4: Angiotensin (Ang) peptides and receptors in RAS signalling. 20

Figure 1.5: Classical renin-angiotensin-aldosterone system (RAAS)..... 23

Figure 1.6: Main components of immune cell involvement and filtration after cardiac injury. 28

Figure 1.7: General innate immune system mechanism. 29

Figure 1.8: Schematic overview of PPRs cellular localisation and signalling upon binding of their preferred ligand. 30

Figure 1.9: Overview of TLR4 signalling in hypertension. 33

Figure 1.10: The structure of HMGB1. 37

Figure 1.11: Mechanisms of signalling by HMGB1. 39

Figure 1.12: HMGB1 localisation and functional roles in cardiovascular homeostasis and inflammation. 42

Chapter 2 Figures

Figure 2.1: Schematics details of three experimental groups. 52

Figure 2.2: Probe position for the parasternal short axis view. 56

Figure 2.3 : M-mode echocardiography from a parasternal short-axis view showing the left ventricular cavity over the cardiac cycle during systole and diastole. 57

Figure 2.4: Schematic description of heart dissection. 59

Figure 2.5: Picrosirius Red Staining for Collagen Detection in Cardiac Tissue Sections. Hearts from three experimental groups (Control, Saline, and Ang II) were sectioned using a cryostat to obtain 10 µm thick transverse sections. Sections were then stained with Picrosirius stain to visualize collagen content. On the second day, images were acquired using an EVOS imaging system.

Image analysis was performed using ImageJ, with consistent image settings applied across all groups. Four areas from each heart section were randomly selected for final quantification of collagen deposition. 63
Figure 2.6: Schematic illustration of Massons trichrome staining workflow. 65
Figure 2.7: Schematic representation of the extracellular vesicle (EV) isolation process from MEG-01 cell culture and rat serum using differential ultracentrifugation. 67
Figure 2.8: Schematic diagram shows the proteomic workflow of left ventricle (LV) tissue form Ang II induced chronic hypertension model. 76
Chapter 3 Figures
Figure 3.1: Body weight progression over 28 days in Ang II-treated, saline-treated, and control groups. Data represent average body weight in gram (g) over 4 weeks. No significant differences were observed between groups, indicating that Ang II infusion did not result in adverse weight loss. 89
Figure 3.2: Blood pressure protocol assessment of all experimental groups. . 90
Figure 3.3: Heart and organs morphology and characteristics. 92
Figure 3.4: Echocardiographic assessment of LV geometry and function in control, saline, and Ang II-infused rats. 94
Figure 3.5: Representative images of Picrosirius red-stained cardiac sections from Ang II, saline, and control groups. 95
Figure 3.6: Collagen deposition in perivascular and interstitial regions of cardiac tissue. 98
Figure 3.7: Illustration of cardiomyocyte hypertrophy in Ang II, compared to saline and control groups. 99
Figure 3.8: HMGB1 expression in different cardiac regions of control, saline, and Ang II groups. 101
Figure 3.9: HMGB1 localisation and expression in cardiac tissue sections from Control, Saline, and Ang II groups. 104

Figure 3.10: Re-localisation of HMGB1 in Ang II heart tissue compared to Control and Saline perfused groups..... 105
Figure 3.11: Histological analysis of collagen deposition and histochemical analysis of HMGB1 localisation. 107
Figure 3.12: DLS analysis for EVs sizes from Rats control group serum represent in intensity and numbers (%). 109
Figure 3.13: Schematic depicting stages of Megakaryocyte (megakaryopoiesis) formation and platelet release (thrombopoiesis)..... 111
Figure 3.14: Live-cell brightfield imaging of MEG-01 cells. 113
Figure 3.15: Characterisation of MEG-01 cell morphology over time. 114
Figure 3.16: Immunofluorescence staining of the MEG-01 cell membrane..... 115
Figure 3.17: Dynamic Light Scattering (DLS) measurements of extracellular vesicles (EVs) isolated from MEG-01 cells. 117
Figure 3.18: HMGB1 expression in MEG-01 cells and HMGB1 localisation in 'pro-platelet's. 119
Figure 3.19: Thrombin-HMGB1 release from MEG-01 cells. 121
Figure 3:20: Distinct intercellular communication mechanisms in the cardiac remodelling process. 127
Chapter 4 Figures
Figure 4.1: Schematic representation of MS-based proteomic strategies top-down and bottom-up. 132
Figure 4.2: Quantitative profiling of left ventricular (LV) tissues from Ang II, saline, and control groups..... 142
Figure 4.3: Principal Component Analysis (PCA) of Protein Expression in Ang II, Saline, and Control Groups. 145
Figure 4.4: Volcano plot of label-free quantitative data for LV tissue, showing upregulated and downregulated DEPs for Ang II vs Saline. 147
Figure 4.5: Volcano plot of label-free quantitative data for LV tissue, showing upregulated and downregulated DEPs for Ang II vs Control. 148

Figure 4.6: Volcano plot of label-free quantitative data for LV tissue, showing upregulated and downregulated DEPs for Saline vs Control. 149
Figure 4.7: STRING Protein-Protein Interaction (PPI) Network of HMGB1 and Differentially Expressed Proteins. 154
Figure 4.8: GO-Functional analysis and KEGG-pathway analysis of the DEPs of G1 (Ang II) vs G2 (Saline). 157
Figure 4.9: GO-Functional analysis and KEGG-pathway analysis of the DEPs of G1 (Ang II) vs G3 (Control). A) The top 10 enriched GO terms for the BP, CC and MF categories. B) The bubble plot lists all the significantly enriched pathways of the DEPs. The bubble size and colour represent the number of DEPs enriched in the pathway and the enrichment significance, respectively. DEPs: differentially expressed proteins; GO: Gene Ontology; BP: biological process; CC: cellular component; MF: molecular function. 158
Figure 4.10: GO-Functional analysis and KEGG-pathway analysis of the DEPs of G2 (Saline) vs G3 (Control). 159
Figure 4.11: STRING Protein-Protein Interaction (PPI) Network of Differentially Expressed Proteins. 161
Figure 4.12: Summary of key findings based on LC-MS-based proteomics analysis of cardiac tissues. 169
Figure 4.13: The Cytoskeleton Network and Its Components. 172

List of tables

Chapter 2 Tables

Table 2.1: Materials and equipment used in *in vivo* experiments 47

Table 2.2: Buffers, prepared media and solutions 48

Table 2.3: Cell lines, reagents, equipment and chemicals 49

Table 2.4: Software and Proteomic Analysis Tools 50

Table 2.5: Demographics of animal model groups. 58

Table 2.6: Echocardiographic measurements in each group after 28 days 58

Table 2.7: List of immunofluorescence stains. 75

Table 2.8: HPLC mobile phase gradient approach. 78

Chapter 4 Tables

Table 4 1: The top 5 Upregulated and Downregulated DEPs Listed in Ang II vs Saline 147

Table 4.2: The top 5 Upregulated and Downregulated DEPs Listed in Ang II vs Control 148

Table 4.3: The top 5 Upregulated and Downregulated DEPs Identified in Saline vs Control 149

Table 4.4: Common Cardiac Biomarkers Identified in The Proteomic Profile Across Experimental Groups. 150

Table 4.5: HMGB1 Expression Levels in LV Proteomic Analysis Across Experimental Groups 151

Table 4.6: Cardiac-Specific Significantly Upregulated Proteins in Ang II-Induced Remodelling: Differential Expression Analysis in Ang II vs saline and Ang II vs control. 162

Table 4.7: Cardiac-Specific Significantly Downregulated Proteins in Ang II-Induced Remodelling: Differential Expression Analysis in Ang II vs saline and Ang II vs control. 163

Table 4.8: Enriched Pathways Associated with Inflammatory Response in Cardiac Remodelling Identified Using PANTHER Analysis of DEPs 165

Abstract

Background: Hypertension is a key risk factor for cardiac remodelling and cardiovascular disease (CVD). Remodelling involves cardiomyocytes, endothelium, vascular smooth muscle, interstitial cells, and the extracellular matrix (ECM), primarily composed of fibrillar collagen. A hallmark of myocardial remodelling is altered collagen turnover, leading to fibrosis. Excess ECM deposition can be triggered by chronic inflammation and damage-associated molecular patterns (DAMPs). High Mobility Group Box 1 (HMGB1), a DAMP elevated in cardiovascular patients, has been linked to inflammatory heart conditions and cardiac hypertrophy, but its role in hypertension and end-organ damage remains unclear.

Project Aim: To assess the contribution of HMGB1 to cardiac/vascular inflammation and remodelling in an *in vivo* male adult rat model of chronic hypertension.

Hypothesis: We hypothesised that HMGB1, particularly its high-molecular-weight isoform (HMW-HMGB1), contributes to inflammation and fibrosis during angiotensin II-induced hypertension, thereby driving cardiac remodelling.

Method: To study HMGB1 contribution in vascular dysfunction, a chronic hypertension model was used. Male Sprague-Dawley rats underwent osmotic mini-pump implantation surgery, ensuring continuous infusion of Ang II for 28 days. Heart tissues were harvested to examine HMGB1 expression for inflammatory pathways. In addition to heart cross-section staining for HMGB1 localisation and collagen distribution, extracellular vesicles (EVs) were examined to explore potential HMGB1 release mechanisms. Due to low serum EV yield from Ang II rats, the human megakaryoblastic cell line (MEG-01) was employed as an in vitro surrogate model for platelet-like particle formation. Dynamic Light Scattering confirmed EV size within the expected exosomal range, and Western

blotting detected HMGB1 within MEG-01 EV cargo, supporting a non-classical vesicular secretion pathway. Furthermore, shotgun liquid chromatography–mass spectrometry (LC-MS)-based proteomic profiling was performed to identify differentially expressed proteins in left ventricular tissue across Ang II, saline, and control groups, providing complementary molecular insights into cardiac remodelling.

Key findings: Chronic hypertension was confirmed with increased cardiac function and changes in echocardiography measurements. Cardiac fibrosis was evident in the Ang II groups, with significant collagen fibre deposition observed using Masson's Trichrome staining. Immunofluorescence analysis revealed enhanced HMGB1 expression and cytoplasmic re-localisation, particularly in perivascular fibrotic regions, supporting its role in inflammatory signalling. Proteomic analysis identified key molecular players, including Acta1, Cfl1, Tubb2a, Itga7, and HMGB1, that may drive cytoskeletal reorganisation and inflammatory signalling in hypertensive cardiac remodelling. These findings provide novel insights into the proteomic landscape of early-stage heart failure (pre-HF), highlighting potential molecular targets for future research and therapeutic intervention.

Graphical abstract

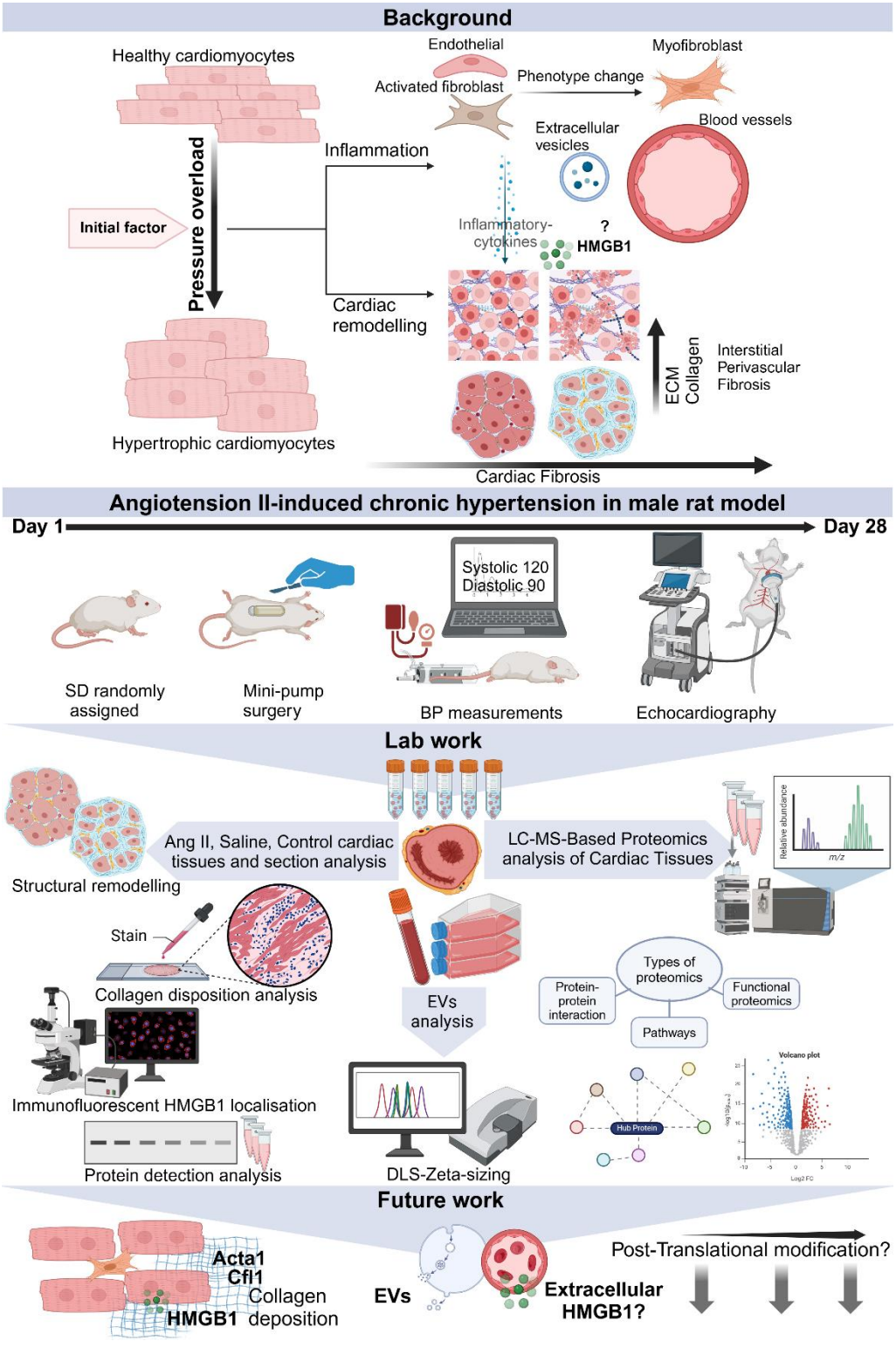

Chapter 1:
General Introduction

1.1 Cardiovascular disease (CVD) burden

The Global Burden of Diseases Study 2022 is a multinational collaboration aimed at estimating the global, regional, and national disease burden. This ongoing effort provides consistent and comparable health estimates from 1990 to 2022 [1]. It applies all available population-level data sources on incidence, prevalence, case fatality, mortality, and health risks to assess population health measures for 204 countries and territories [1]. Cardiovascular disease (CVD) and hypertension continues to be the leading cause of mortality and disability worldwide, surpassing the impact of other factors including occupational, environmental, and lifestyle [2].

1.1.1 Cardiac cells and alteration in CVD

The human heart is a muscular organ composed of various cell types, including cardiomyocytes (CMs), endothelial cells, fibroblasts, and smooth muscle cells (SMCs) [3], illustrated in Figure 1.1. The contractile cells include CMs, which form the contractile myocardium, while SMCs form the contractile coronary vessels [4].

Cardiomyocytes play a vital role in facilitating cardiac contraction and the subsequent circulation of blood throughout the body. This essential function relies on the synchronized depolarization of electrically connected cardiomyocytes in both the atria and ventricles, a process regulated by the cardiac conduction system [5,6]. Sarcomeres are the fundamental contractile unit of CMs. This unit is composed of overlapping, mesh-like thick and thin filaments made up of myosin, actin, tropomyosin, titin, and the troponin complex, which are the key proteins of the contractile apparatus [7,8]. These filaments are organised in a repeating pattern along the length of the myofibril in sarcomeres units. The alignment of these units across myofibrils gives CMs their distinctive striated appearance. Myofibril contraction depends on the binding of Ca^{2+} to the troponin complex, which triggers a conformational change that allows myosin heads to flex and slide along the actin filaments. This process shortens the unit length and generates contractile force [9].

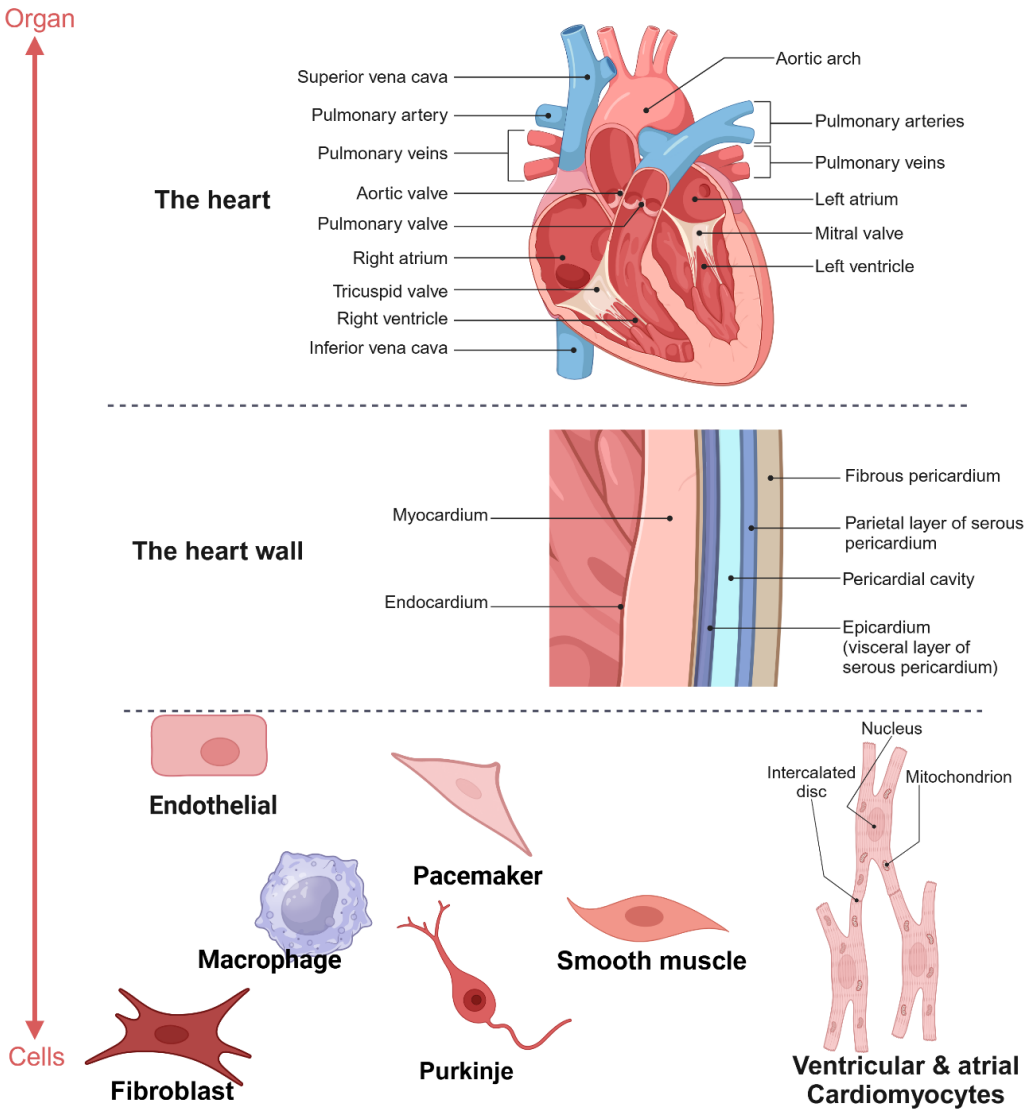

Figure 1.1: Anatomy of the interior of the heart the wall composition and cells.
This figure illustrates the organisation of the heart, from the whole organ to individual cell types. At the organ level, the heart main structures are shown, including the chambers (atria and ventricles), valves (aortic, pulmonary, tricuspid, and mitral), and major blood vessels (aorta, pulmonary arteries and veins, vena cava). These structures work together to pump blood through the body. The heart wall is shown in a cross-section, highlighting its three layers: Epicardium (outer layer) protective covering. Myocardium (middle layer) contains muscle cells responsible for contraction. Endocardium (inner layer) lines the heart chambers and valves. At the cellular level, different heart cell types are illustrated: Cardiomyocytes (heart muscle cells) responsible for contraction. Endothelial cells form the inner lining of blood vessels. Fibroblasts produce structural proteins and support heart tissue. Macrophages immune cells involved in repair and defence. Pacemaker cells generate electrical impulses to regulate heartbeat. Purkinje fibres conduct electrical signals for coordinated contractions. Smooth muscle cells found in blood vessels, controlling their diameter. Created by Biorender. Adapted from [3].

The primary function of the heart is to maintain perfusion of peripheral organs, ensuring their needs are met under both normal and stress conditions. To achieve this in case of increased preload or afterload, the heart and individual cardiomyocytes often undergo enlargement, a condition known as hypertrophy.

Cardiac hypertrophy due to hemodynamic overload presents in two forms [10]. Pressure overload results from conditions like hypertension and aortic stenosis, leading to the addition of sarcomeres in parallel at the cellular level, increasing myocyte cross-sectional area, and resulting in significant thickening of the ventricular wall. Clinically, this is referred to as concentric hypertrophy. Volume overload results from conditions such as mitral regurgitation and aortic regurgitation resulting in eccentric hypertrophy. This is characterised by ventricular dilation, driven by an increase in myocyte length and the addition of sarcomeres.

The cardiac conduction system is crucial for initiating and coordinating the heart's electrophysiology. It consists of the sinoatrial node, atrioventricular node, and the Purkinje system. The sinoatrial node, located in the inflow tract of the right atrium, serves as the primary pacemaker, initiating the cardiac action potential [11].

A study defining the different cell population in mouse heart by cellular markers identified that fibroblasts comprise a relatively minor population whilst endothelial cells constitute most of non-cardiomyocytes [12]. This suggests that endothelial cells might play a greater role in physiological function and response to heart injury. Although cell markers have been historically used to define a specific cell type in the heart, recent advances have been made to develop the first map of cardiac cell diversity by single-nuclei RNA-Seq data and has been specifically annotated for the human heart [3]. Transcriptomic data on six distinct cardiac regions was performed following processing with 10X Genomics and a generative deep variational autoencoder. Mapping revealed 45,870 cells, 78,023 CD45+ enriched cells, and 363,213 nuclei, representing 11 major cell types. These cells included two cardiomyocytes (CMs); atrial cardiomyocytes, ventricular

cardiomyocytes, fibroblasts (FBs), endothelial cells (ECs), mural cells including pericytes and smooth muscle cells (SMCs), adipocytes, mesothelial cells, neuronal cells also known as pacemaker cells and immune cells including myeloid and lymphoid [3].

The endothelial cells are the primary components of blood vessels and located at the interface between the blood vessels and tissues, they sense the environment and signal modulations of vascular function to maintain homoeostasis and host defences against microbial invaders and injury[13]. Endothelial cells are responsible for the rapid release of vaso/bioactive molecules like prostacyclin and nitric oxide through constitutive forms of nitric oxide synthase (NOSIII) and cyclo-oxygenase (COX-1) [14]. In vitro shear stresses were observed to exert a significant impact on the regulation of gene expression in endothelial cells [15]. Specific DNA sequences, including shear-stress response elements, were identified in the regulatory regions of genes involved in disease processes, such as the vascular cell adhesion molecule (VCAM-1) [16]. These elements control gene expression in response to fluid flow, affecting the production of proteins crucial for various biological functions.

Endothelial cells regulate vascular tone through both vasoconstriction and vasodilation and contribute to vascular remodelling, haemostasis and thrombosis, cellular adhesion, smooth muscle cell proliferation, and modulation of vascular inflammation [17]. Damaged cells will disrupt the normal exchange of substances between blood and tissues. In pathological conditions, essential cofactors such as tetrahydrobiopterin (BH4), which is crucial for the enzymatic production of nitric oxide (NO) by endothelial nitric oxide synthase (eNOS), can become depleted. When BH4 levels are insufficient, eNOS becomes uncoupled, leading to the generation of superoxide (O_2^-) instead of NO. This contributes to oxidative stress and reactive oxygen species (ROS) production [18]. These events lead to EC dysfunction. The endothelium plays a vital role in the pathophysiology of

cardiovascular diseases associated with atherosclerosis, including hypertension, heart failure [19].

1.1.2 Chronic hypertension

1.1.2.1 Pathophysiology and mechanisms of chronic hypertension

Hypertension is a global public health issue and a leading risk for death and disability[20]. Even with various accessible treatments, global rates of blood pressure (BP) control stand at only 18-23%, dropping to 10% in certain areas of Asia and Africa [21,22]. Non-adherence to treatment contributes to poor blood pressure control. Additionally, the underlying causes of hypertension remain unclear in most cases. There have been advancements in hypertension drug therapy, including angiotensin receptor antagonists, angiotensin-converting enzyme inhibitors, and calcium channel blockers [23]. However, innovation of new therapeutics is still limited [24]. In addition, these treatments focus on correcting blood pressure levels as a primary symptom but not addressing the underlying disease mechanisms [25].

BP is influenced by several cardiovascular parameters, including blood volume and cardiac output which is the volume of blood the heart pumps per minute. It is also affected by arterial tone, which is influenced by intravascular volume and neurohumoral systems. Maintaining physiological BP levels requires a complex interaction of various elements within an integrated neurohumoral system. This system includes the renin-angiotensin-aldosterone system (RAAS), natriuretic peptides, the endothelium, the sympathetic nervous system, and the immune system. Angiotensin II (Ang II) is at the centre of the pathogenetic role of the RAAS in hypertension [26]. Ang II is linked to endothelial dysfunction and exhibits pro-fibrotic and pro-inflammatory effects, primarily through increased oxidative stress, leading to renal, cardiac, and vascular injury. These mechanisms play a crucial role in targeted organ damage associated with hypertension. Therefore,

hypertension is a complex pathophysiology that is coupled with a systemic inflammatory reaction, marked by the activation of complement, myeloid cells, inflammasome activation, and vascular cells disturbances. These factors contribute to renal and vascular dysfunction, exacerbating blood pressure elevation and terminating in end organs damage [27].

Left ventricular hypertrophy (LVH) is a compensatory consequence of chronic systemic hypertension, aortic stenosis and hypertrophic cardiomyopathy. In addition, it is an independent risk factor for complications like hypertension [28], arrhythmias [29], myocardial infarction [30], and stroke [31]. Therefore, models of cardiac hypertrophy are useful for studying underlying adverse cardiovascular events that may be reduced or reversed by targeting specific cellular pathways.

Cardiac hypertrophy is accompanied by changes in gene expression, which induce changes in metabolism, contractility, and cardio myocyte survival [10]. Specific biomarkers include indicators of wall stress and necrosis, such as atrial natriuretic peptide (ANP) and brain natriuretic peptide (BNP). Pro-thrombotic markers include the thrombin-antithrombin III complex (TAT), while markers of wall stress and myonecrosis include troponin T and troponin C. Additionally, inflammatory markers such as interleukin-6 (IL-6) and tumor necrosis factor-alpha (TNF-α) are also relevant. [32]. Pathological cardiac hypertrophy is often closely associated with myocardial fibrosis (MF) and with chronic inflammation, which is accompanied by infiltration of immune cells into the heart and the presence of increased inflammatory cytokines. Therefore, unravelling inflammatory signals that may accompany cardiac remodelling has significant clinical implications.

1.1.2.2 Cardiac remodelling in hypertension

Uncontrolled or chronic hypertension can result in myocardial hypertrophy leading to changes in the myocardial structure and coronary vasculature, resulting in cardiovascular disease [33]. It is considered as a transitional phase in the

progression toward heart failure. Cardiac remodelling refers to structural and functional changes in the heart, including alterations in size, shape, geometry, wall thickness, cavity diameter, and the composition of the left ventricle. These changes occur in response to cardiac load or injury [34]. There are two forms of cardiac hypertrophy resulting from hemodynamic overload [35]. Pressure overload, caused by conditions like hypertension and aortic stenosis, leads to the parallel addition of sarcomeres, increased myocyte cross-sectional area, and significant thickening of the ventricular walls. Clinically, this is known as concentric hypertrophy [36]. Volume overload, seen in conditions such as mitral and aortic regurgitation, results in eccentric hypertrophy, characterised by ventricular dilation. This occurs due to an increase in myocyte length and the addition of sarcomeres in series [36].

In the early stage of hypertrophy triggered by pressure overload stress, cardiac efficiency is preserved and initially induced as adaptive or compensatory phase. During this phase, myocytes thicken to manage the increased pressure on the ventricular wall and maintain cardiac output. However, prolonged hypertension-induced hypertrophy can lead to a shift from adaptive to maladaptive remodelling, characterised by reduced ejection fraction as contractile dysfunction and left ventricular dilation [10].

Pathological hypertrophy is often associated with interstitial and perivascular fibrosis, along with cardiomyocyte death, marked by elevated levels of type I collagen and the activation of myofibroblasts.

1.1.2.3 Histological Characteristics of Cardiac Fibrosis

Myocardial fibrosis (MF) is defined as the excessive accumulation of extracellular matrix (ECM) proteins in the myocardium and represents a hallmark of chronic cardiac diseases, including hypertension and cardiomyopathy [37,38]. This process disrupts myocardial structure and underpins adverse cardiac remodelling [39]. MF

contributes to the progression of heart failure and is recognised as having prognostic implications in both ischemic and non-ischemic conditions [40].

In hypertensive heart disease and hypertrophic cardiomyopathy, myocardial interstitial fibrosis (MIF) is the predominant form, characterised by diffuse collagen deposition that reduces ventricular compliance and impairs diastolic filling. Collagen types I and III are the main fibrillar proteins: type I provides tensile strength but increases stiffness, while type III contributes elasticity; imbalance between the two alters myocardial mechanical properties and accelerates dysfunction [37 39 40].

Key regulators of ECM turnover include matrix metalloproteinases (MMPs) and their endogenous tissue inhibitors (TIMPs). Under physiological conditions, the MMP/TIMP axis maintains a balance between collagen degradation and deposition [41 42,43]. Under hypertensive stress, dysregulation of this axis results in impaired collagen degradation, pathological ECM accumulation, and progressive fibrosis [44]. MMP-2 and MMP-9 are particularly important, as they exhibit dual roles in both tissue remodelling and inflammation. For example, increased MMP-9 activity contributes to early hypertension by degrading collagen and weakening arterial walls [44], while TIMPs promote fibrosis by inhibiting MMP-driven matrix turnover [42,43].

Beyond matrix regulation, MMP/TIMP imbalance links fibrosis to inflammation. Increased MMP activity during hypertension promotes vascular remodelling, smooth muscle cell proliferation, and monocyte infiltration [45] . Conversely, TIMPs can suppress immunomodulatory MMP functions, further complicating this relationship. This highlights that myocardial fibrosis is not merely structural but also a dynamic inflammatory process, where ECM turnover, immune activation, and fibroblast signalling interact to drive remodelling [46] . Importantly, damage-associated molecular patterns (DAMPs) such as HMGB1 have been shown to

activate fibroblasts and enhance ECM remodelling, providing an additional inflammatory link to fibrosis progression [47] .

1.1.2.4 Key Characteristics and Homeostasis of Cardiac ECM

The cardiac ECM provides both structural stability and dynamic signalling capacity, ensuring that cardiomyocytes remain mechanically integrated while responding to physiological stress [48,49]. Collagens I and III dominate the fibrillar network: type I supplies tensile strength and stiffness, whereas type III contributes elasticity, together maintaining ventricular compliance [50–52]. Smaller amounts of collagens IV and V, fibronectin, laminin, and proteoglycans link this fibrillar scaffold to basement membranes, securing cohesion between myocytes and fibroblasts [53].

Beyond structure, the ECM serves as a signalling reservoir. It binds and regulates cytokines, growth factors, chemokines, matrix metalloproteinases (MMPs), their tissue inhibitors (TIMPs), and noncoding RNAs such as microRNAs [54,55]. Through these interactions, the ECM fine-tunes cellular growth, differentiation, and repair processes.

Functionally, the ECM is organised into two regions. The basement membrane/pericellular matrix surrounds individual cells, supporting polarity, differentiation, and migration through integrin-mediated outside-in signalling [56–58]. The interstitial matrix, dominated by collagens I and III, provides tensile and elastic support across the myocardium, distributing mechanical load and enabling synchronous contraction [59,60]. These distinct regions illustrate how ECM remodelling directly links to both mechanical load and inflammatory signalling in hypertension (see Figure 1.2).

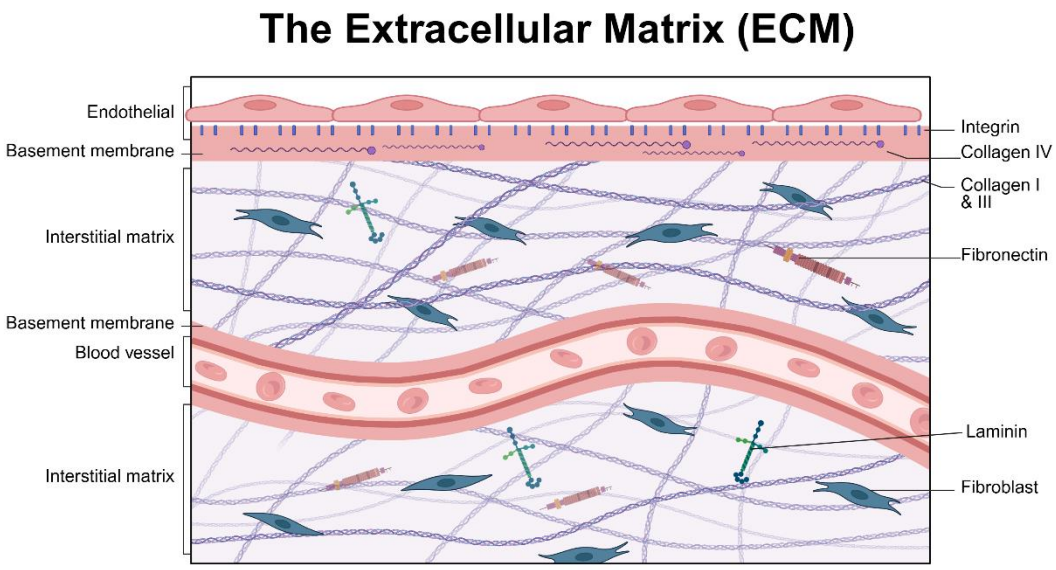

Figure 1.2: Extracellular matrix (ECM) compartments.
Summarises these two ECM compartments and their principal molecular components. This organisation emphasises how mechanical properties and biochemical signals are inseparable in cardiac tissue homeostasis. Created by Biorender.

During remodelling, the balance between matrix metalloproteinases (MMPs) and their inhibitors (TIMPs) governs collagen turnover. MMP activity facilitates collagen degradation and repair, but when dysregulated, it leads to pathological accumulation of extracellular matrix proteins [61,62]. Such imbalance is a hallmark of hypertensive cardiac remodelling, where excessive collagen cross-linking reduces compliance and contributes to diastolic dysfunction.

Previous studies across cardiovascular disease models have demonstrated that ECM dysregulation is not purely structural but is also closely linked with inflammatory signalling and fibroblast activation [63]. In this context, hypertension provides a valuable model for identifying specific protein alterations that couple inflammatory stress with fibrosis progression, offering mechanistic insight into early disease stages relevant to this thesis.

1.2 Animal models in cardiovascular disease

Several small animal models including mice and rats have been generated to mimic various pathological mechanisms contributing to hypertension[65] [64] and heart failure (HF) [65]. Despite certain limitations, animal models have significantly advanced our understanding of the pathogenesis of various CVD aetiologies, providing crucial insights into underlying mechanisms and aiding the development of effective therapies. In particular, animal models of hypertension serve as invaluable tools for studying disease progression and hypertension-induced cardiac remodelling, as patient data on the cellular and molecular remodelling of the heart remain limited [66] .

The rat model offers significant advantages due to the availability of various genetic strains showing spontaneous hypertensive traits either naturally or induced by environmental factors [64,66]. Moreover, rats are easy to care for and breed, cost-effective to maintain, and their size accommodates most analytical studies, including long-term investigations, dynamic cardiovascular monitoring, and blood and tissue sampling. These rat models, mirroring many phenotypic features seen in human hypertension, have been extensively utilised to explore the genetic and mechanistic underpinnings of hypertension [64].

1.2.1 Models of hypertension (essential and secondary)

Animal models of hypertension have proven valuable for studying the pathophysiology of hypertension and for developing new treatments [64]. The rodent is a crucial model organism for studying diseases like hypertension. Numerous inbred rat models have been developed and thoroughly characterised for this condition. Secondary and primary-essential hypertensions models can be classified according to aetiology, which is illustrated in Figure 1.3 [67].

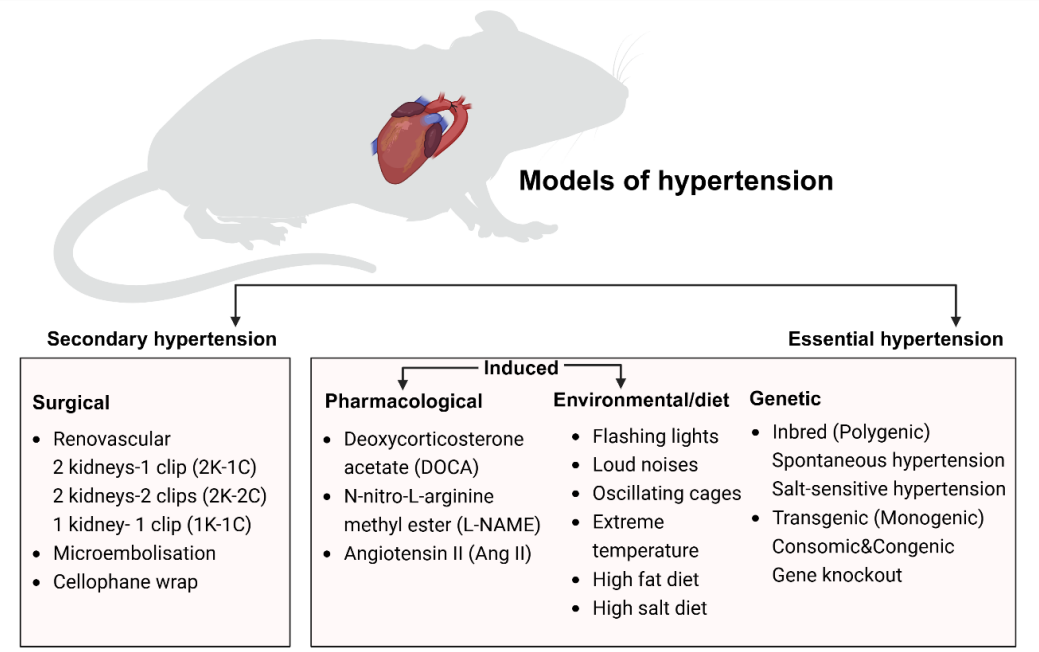

Figure 1.3: Schematic illustration classified models of hypertension.
This figure categorises different animal models of hypertension into secondary hypertension and essential hypertension, based on their underlying mechanisms. Secondary hypertension models are induced through surgical interventions, including renovascular hypertension (2K-1C, 2K-2C, 1K-1C), microembolization, and cellophane wrap methods, which mimic conditions such as renal artery stenosis and fibrosis-related hypertension. Essential hypertension models are classified into three major groups: pharmacological induction, using agents like deoxycorticosterone acetate (DOCA), N-nitro-L-arginine methyl ester (L-NAME), and angiotensin II (Ang II) to induce hypertension by altering vascular tone and renal function. Environmental and dietary factors, including flashing lights, loud noises, oscillating cages, extreme temperatures, high-fat diets, and high-salt diets, which contribute to hypertension by influencing stress and metabolic pathways. Genetic models, including inbred (polygenic) strains, spontaneous hypertensive rats, salt-sensitive hypertension models, and transgenic (monogenic), consomic, and congenic models, as well as gene knockout models, which help study hereditary factors in hypertension. Created by Biorender.

In surgical models, major causes of secondary hypertension are renal diseases including renal arterial stenosis (RAS). RAS has been modelled by the 2 kidneys-1 clip hypertension model (2K-1C) and has previously been used to examine kidney damage induced by hypertension [68]. The 1 kidney-1 clip hypertension model (1K-1C) was used to assess the role of the vascular angiotensin II-generating system by using specific blockers [69]. Another method is 2 kidney-2 clip hypertension model (2K-2C). Other systems have been developed to examine the pathophysiology of renal parenchymal hypertension, perinephric fibrosis and renal ischemia such as animal model of coronary microembolisation [70] and cellophane wrap of the kidney [71].

Essential hypertension models including pharmacological methods using a nitric oxide synthase (NOS) selective inhibitor such as N-nitro-L-arginine methyl ester (L-NAME), used in rat to induce hypertension [72]. Another method involves activating the RAAS using the Ang II and the deoxycorticosterone acetate (DOCA)-induced model which copies the effects of mineralocorticoid and glucocorticoid-induced hypertension and are used with sodium chloride in unilateral nephrectomised rats to induce hypertension. Induction of environmental stresses, including separate or simultaneous introduction of flashing lights, loud noises and oscillating cages and high temperature, have also been performed to induce hypertension. Noise and air pollution are recognised environmental risk factors that induce hypertension and dysregulation of the heat shock proteins [73].

Genetic models of hypertension include polygenic models, such as spontaneously hypertensive models, which are used to study hypertrophy and fibrosis [74] , Dahl salt-sensitive rats and other rat strains are also used as models of hypertension and renal injury to investigate disease phenotypes [75]. Other salt sensitive such as salt-Induced models of hypertension was used to examine cortical expression of COX-2, which is associated with significant end organ injury specifically the kidneys and increased intrarenal RAS activation and urinary excretion [76].

Other monogenic models, such as transgenic models including consomic and congenic strains, combined with gene knockout techniques, have been employed to investigate the mechanistic basis of essential hypertension [77]. A congenic and consomic strains is created by selectively transferring a portion of the genome from one rat strain to another through backcrossing a donor strain to a recipient strain, with careful selection. For consomic strains (chromosome substitution), an entire chromosome is transferred, while in congenic strains, only a specific chromosomal segment (the differential segment) is transferred.

Among the various models of hypertension, the Ang II-induced model, categorised under pharmacological induction, is widely used to study chronic hypertension and its impact on cardiovascular remodelling. This model effectively mimics key pathological features of human hypertension, leading to sustained elevations in blood pressure, vascular dysfunction, inflammation, and extracellular matrix remodelling. Which provides valuable insights into the molecular and cellular mechanisms driving hypertension-induced cardiac remodelling, including the interplay between inflammatory pathways, fibrosis, and structural changes in the heart.

1.2.2 Ang II-induced chronic hypertension

The broader physiological role of the renin–angiotensin–aldosterone system (RAAS) is discussed in Section 1.2.3; here, the focus narrows to the experimental Ang II–induced chronic hypertension model, which reproduces sustained RAAS activation and its cardiovascular consequences.

Chronic infusion of Angiotensin II (Ang II) in rodents reliably reproduces the pathophysiological features of human hypertension, including sustained blood pressure elevation, vascular dysfunction, inflammation, and cardiac remodelling [78]. This approach reflects neurohumoral activation of the renin–angiotensin–aldosterone system (RAAS), resulting in elevated circulating Ang II and aldosterone, which drive systemic haemodynamic and tissue-level effects [79].

Ang II exerts its effects primarily via binding to two receptors: the Ang II type 1 receptor (AT1R) and type 2 receptor (AT2R) [80]. AT1R signalling promotes vasoconstriction, sodium and water retention, sympathetic nervous system activation, oxidative stress, and aldosterone secretion. Collectively, these actions raise blood pressure and promote maladaptive changes such as hypertrophy, fibrosis, and vascular remodelling [80,81]. By contrast, AT2R signalling counterbalances AT1R effects, inducing vasodilation, natriuresis, and anti-fibrotic, anti-inflammatory responses [80].

In addition to hemodynamic regulation, Ang II directly activates intracellular pathways such as NADPH oxidase, resulting in reactive oxygen species (ROS) generation and mitochondrial dysfunction, further linking hypertension to oxidative stress [82]. Locally, Ang II and prorenin acting on the prorenin receptor (PRR) activate ERK1/2 and p38 MAPK cascades, which can promote fibrosis and cellular hypertrophy in cardiomyocytes, endothelial cells, mesangial cells, and vascular smooth muscle cells (VSMCs) independently of systemic RAAS activation [83].

Beyond Ang II itself, RAAS produces a family of bioactive peptides. Ang II is converted by aminopeptidase A (AP-A) into Ang III, which continues AT1R-mediated actions, and further into Ang IV by aminopeptidase N (AP-N), which binds AT4R. Parallel counter-regulatory pathways involve angiotensin-converting enzyme 2 (ACE2), which cleaves Ang II into Ang-(1–7) or Ang I into Ang-(1–9). These peptides act on the Mas receptor (MasR) or the Mas-related GPCR (MrgDR), producing vasodilatory, antifibrotic, and cardioprotective effects [84] 83. Reduction in ACE2 activity lowers Ang-(1–7) generation and exacerbates vascular injury, highlighting the importance of the ACE2/Ang-(1–7)/MasR axis in counteracting the classic ACE/Ang II/AT1R pathway.

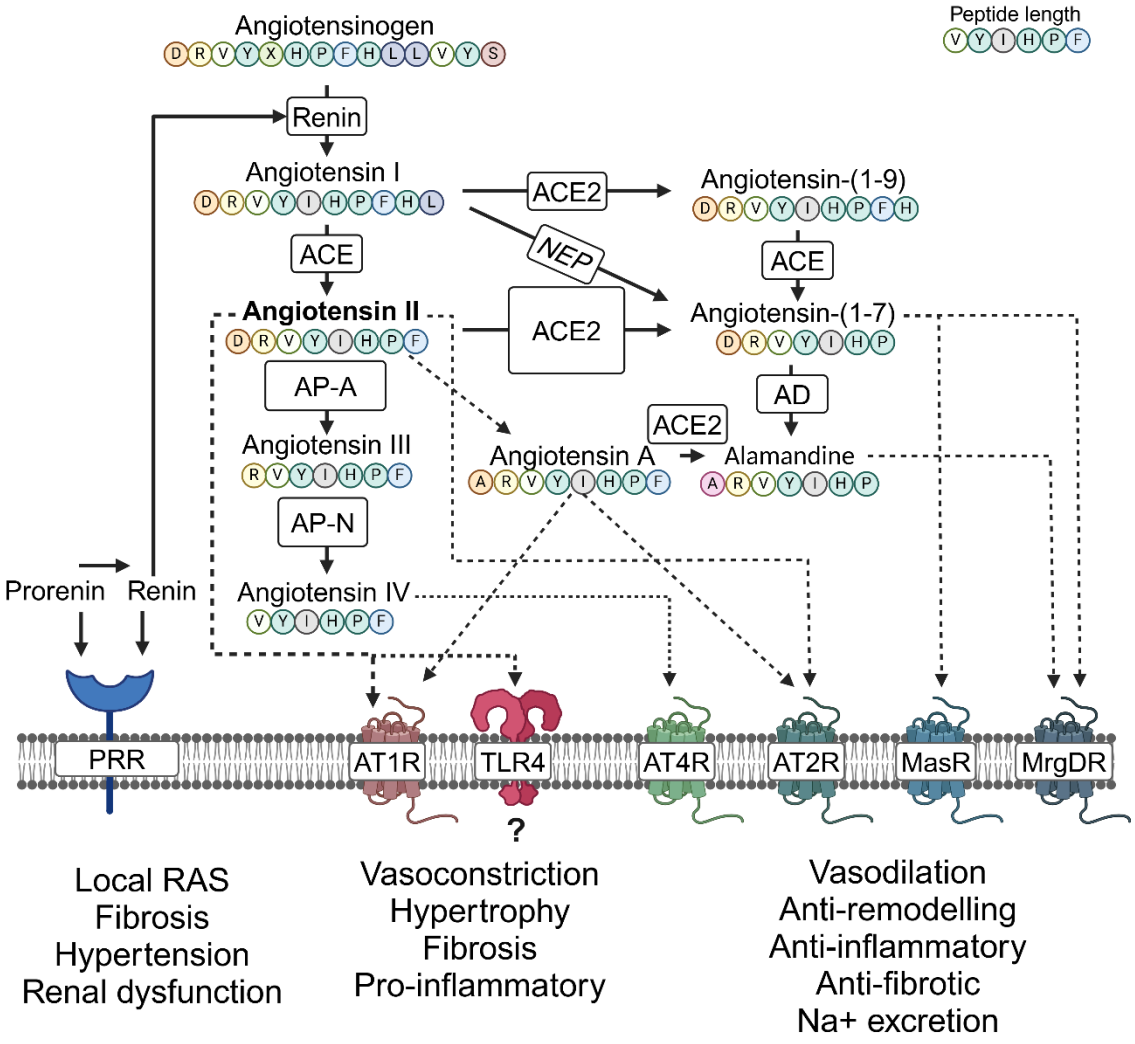

Figure 1.4: Angiotensin (Ang) peptides and receptors in RAS signalling.
Prorenin and renin bind the prorenin receptor (PRR), activating ERK1/2 and p38 MAPK pathways. Renin also cleaves angiotensinogen to Ang I, which is converted by angiotensin-converting enzyme (ACE) to Ang II. Ang II acts on AT1R to promote vasoconstriction, fibrosis, and inflammation, and on AT2R to mediate vasodilation and antifibrotic effects. Ang II can also be converted to Ang-(1–7) by ACE2, acting on MasR/MrgDR to provide cardioprotection, or to Ang III/IV by AP-A and AP-N, acting through AT1R/AT4R. Abbreviations: AT1R, Ang II type 1 receptor; AT2R, Ang II type 2 receptor; ACE, angiotensin-converting enzyme; ACE2, angiotensin-converting enzyme 2; AP-A, aminopeptidase A; AP-N, aminopeptidase N; MasR, Mas receptor; MrgDR, Mas-related G protein-coupled receptor D; PRR, prorenin receptor; ROS, reactive oxygen species. Figure created with BioRender.

Preclinical studies underscore this protective arm: treatment with recombinant human ACE2 reduced blood pressure, oxidative stress, and cardiac remodelling in spontaneously hypertensive rats and Ang II–infused rodents [85]. Conversely, ACE2 deficiency accelerates fibrosis and inflammatory mediator expression in Ang II models [86]. More recently, alamandine, derived either from Ang-(1–7) or Ang A, has been shown to exert cardioprotective effects by activating the AMPK–NO pathway via MrgDR, attenuating Ang II–induced hypertrophy [87,88]. Together, these findings establish Ang II–induced hypertension as a model that integrates hemodynamic, renal, oxidative, and inflammatory mechanisms, reflecting the dual balance of classical and non-classical RAAS axes [89].

1.2.3 Physiological role of the Renin Angiotensin System (RAS)

While Section 1.2.2 described how Ang II infusion in rodent models chronic hypertension, this section outlines the physiological and pathophysiological functions of the RAAS in the wider systemic context, which is crucial for interpreting findings from the animal model.

The renin–angiotensin–aldosterone system (RAAS) is a central hormonal pathway that regulates cardiovascular, renal, and metabolic homeostasis [90 91 92]. It controls blood pressure by modulating vascular tone, sodium–water balance, and systemic vascular resistance. Renin, secreted by juxtaglomerular cells in response to reduced renal perfusion, sympathetic nervous system (SNS) activation, or decreased sodium delivery, cleaves hepatic angiotensinogen into angiotensin I. Angiotensin-converting enzyme (ACE), mainly from pulmonary endothelium, converts angiotensin I into angiotensin II (Ang II), the key effector peptide [90 91] .

The physiological and pathological effects of Ang II are primarily mediated via two receptor subtypes: the Ang II type 1 receptor (AT1R) and type 2 receptor (AT2R), both members of the G protein–coupled receptor (GPCR) family [80 93]. AT1R activation drives vasoconstriction, aldosterone secretion, renal sodium–water

retention, oxidative stress, and sympathetic outflow, collectively leading to blood pressure elevation and adverse cardiovascular remodelling [80,81] [82] [94] [95]. In addition, AT1R signalling promotes vascular smooth muscle cell (VSMC) hypertrophy, fibrosis, and pro-inflammatory cytokine release, which are central to hypertension-induced organ damage [96] [97] .

By contrast, AT2R activation generally opposes AT1R effects. It promotes vasodilation, natriuresis, anti-fibrotic, and anti-inflammatory pathways through G protein–independent signalling mechanisms and crosstalk with the ACE2/Ang-(1–7)/Mas axis [84] [85] [98] [99]. AT2R signalling therefore serves as a protective arm of RAAS, balancing AT1R-mediated injury and remodelling.

Beyond haemodynamic control, RAAS integrates neurohumoral and metabolic regulation. Unlike the baroreceptor reflex, which provides rapid short-term pressure control, RAAS governs both acute and chronic adaptations to stress. Classically described as a three-component system (renin, Ang II, aldosterone) [91], RAAS is now recognised as a multifaceted network that includes angiotensinogen, multiple ACE isoforms, Ang II metabolites (e.g., Ang III, Ang IV), and receptor subtypes (AT1R, AT2R, MasR) [92] [100] (98,99). Persistent activation of this system drives long-term tissue injury and remodelling in hypertension. The classical RAAS pathway is illustrated in Figure 1.5.

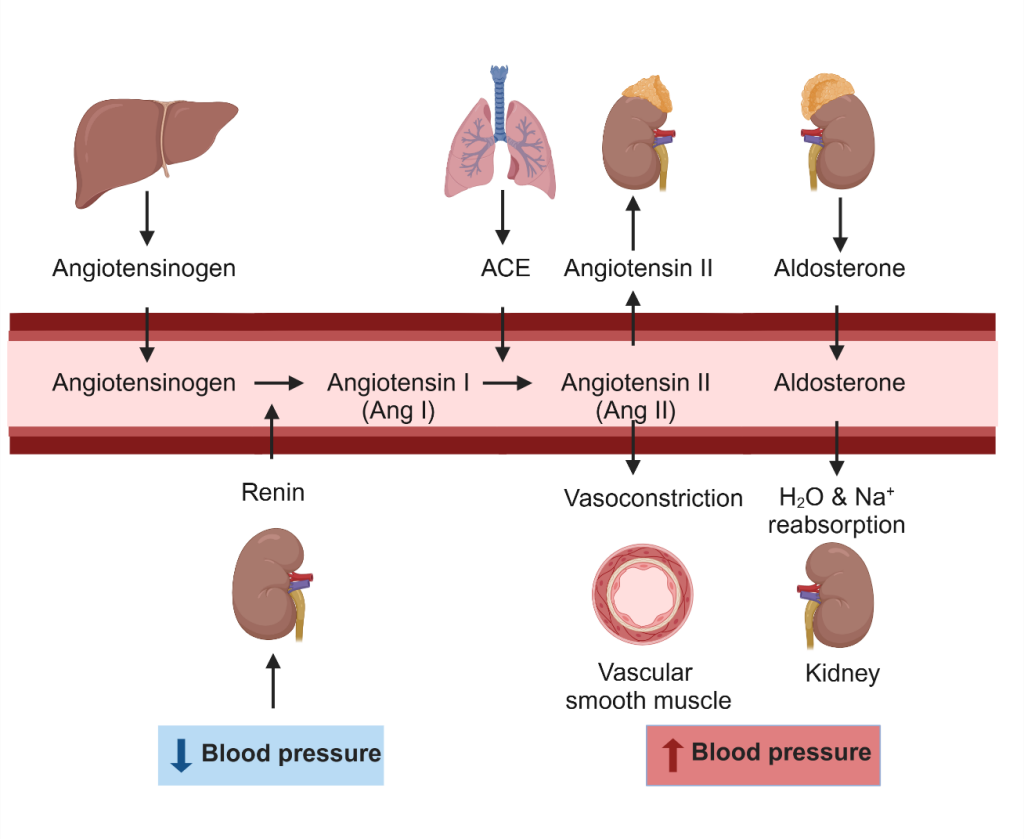

Figure 1.5: Classical renin-angiotensin-aldosterone system (RAAS)
When blood pressure falls, juxtaglomerular cells release renin, which cleaves liver-derived angiotensinogen into angiotensin I. Ang I is converted by ACE into Ang II, which acts on AT1R to induce vasoconstriction, sodium–water retention, and aldosterone release, while the ACE2/Ang-(1–7)/Mas axis provides opposing protective actions. Abbreviations: ACE, angiotensin-converting enzyme; ACE2, angiotensin-converting enzyme 2; AT1R, Ang II type 1 receptor; AT2R, Ang II type 2 receptor; MasR, Mas receptor. Created by Biorender. Adapted from [101].

Angiotensinogen, an α-globulin produced mainly by the liver and circulating in plasma, is the substrate for RAAS. Reduced renal perfusion, increased sympathetic outflow, or decreased distal tubular NaCl delivery stimulates juxtaglomerular renin release, which cleaves angiotensinogen to angiotensin I (decapeptide 1–10). Endothelial ACE predominantly pulmonary converts angiotensin I to angiotensin II (Ang II), which mediates systemic effects via AT1R/AT2R [101] . In the kidney, AT1R-driven Ang II actions promote aldosterone secretion (zona glomerulosa) and enhance tubular sodium and water

reabsorption, expanding intravascular volume [102] . Physiologically, RAAS maintains water–electrolyte balance, vascular resistance, and arterial pressure; pathologically, sustained activation drives oxidative stress, endothelial dysfunction, inflammation, and fibrotic remodelling, contributing to hypertension, kidney disease, and heart failure [103] .

1.2.4 Current anti-hypertensive treatment strategies

Antihypertensive therapy includes several pharmacological classes that target distinct pathways regulating blood pressure and organ protection. Among these, inhibitors of the renin–angiotensin–aldosterone system (RAAS) remain first-line treatments, particularly for patients with target organ damage such as heart failure or renal impairment. Clinical trials have demonstrated that angiotensin-converting enzyme inhibitors (ACEi), angiotensin II receptor blockers (ARBs), angiotensin receptor–neprilysin inhibitors (ARNIs), and mineralocorticoid receptor antagonists (MRAs) are effective in lowering blood pressure and delaying target organ damage [104] .

Beta-blockers, which antagonise β-adrenergic receptors, are also widely prescribed to control blood pressure and heart rate by suppressing sympathetic nervous system activity. However, compared to diuretics, ACEi, ARBs, and calcium channel blockers (CCBs), beta-blockers show less efficacy in reducing stroke incidence and all-cause mortality, and are often used as adjunct rather than first-line therapy [105] .

CCBs, which inhibit calcium influx into vascular smooth muscle, induce vasodilation and reduce vascular stiffness, and have been shown in large trials to reduce cardiovascular events in elderly or isolated systolic hypertension patients [106,107]. Diuretics, particularly loop diuretics like torasemide, demonstrate anti-fibrotic effects: in chronic heart failure patients treated with torasemide, collagen volume fraction (CVF) and procollagen type I levels were significantly reduced,

compared to baseline or to furosemide treatment where no such change was observed [108].

Despite their clinical benefits, current antihypertensives have limitations. ACE inhibition can be bypassed by non-ACE enzymatic pathways generating Ang II, while ARBs increase plasma renin activity, raising Ang II levels that continue to compete for AT1R binding [109–110] . Moreover, many standard therapies effectively reduce blood pressure but do not consistently reverse myocardial fibrosis or eliminate residual cardiovascular risk.

These gaps have prompted the development of novel therapeutic strategies. Investigational approaches include activators of the ACE2/Ang-(1–7)/Mas axis, neprilysin inhibition, soluble guanylyl cyclase stimulation, dual-acting bispecific peptides, non-steroidal MRAs, antioxidants, and aminopeptidase A (AP-A) inhibitors [111] . Beyond hemodynamic control, increasing attention is directed toward therapies targeting inflammation and immune signalling, including modulation of cytokine release and immune cell activation, which could attenuate vascular remodelling and end-organ damage in chronic hypertension.

1.3 Targeting inflammatory proteins as an anti-hypertensive strategy

1.3.1. Inflammation, hypertension and CVD injury

The idea of focusing on vascular or cardiac inflammation to prevent CVD makes sense both in theory and in practice, as shown by recent studies [112] . However, one major challenge with the idea of residual inflammatory risk is with the uncertainty around the reliable quantification and it depend on the CVD condition in question. The most widely accepted strategies to detect vascular or cardiac inflammation currently include the measurement of circulating levels of inflammatory biomarkers or biomolecules [113]. These tests are often used in combination with imaging techniques, such as echocardiography and cardiac magnetic resonance imaging, to better diagnose and monitor cardiovascular conditions [114] .

Biomarkers can provide valuable insights into the disease and inflammatory process, enabling early diagnosis and effective treatment. Commonly used biomarkers include for cardiac fibrosis include TGF-β, connective tissue growth factor and platelet-derived growth factor-D [115]. For vascular inflammation markers include high-sensitivity C-reactive protein (hs-CRP), interleukin-6 (IL-6), and troponin [116]. Biomarkers for hypertrophy and inflammation associated with hypertrophic cardiomyopathy (HCM) for example, in the acute inflammatory phase response, include cytokines such as interleukin (IL)-1 and IL-6. These drive production of reactant proteins, including C-reactive protein which are independently associated with the risk of major adverse cardiovascular events [117]. Inflammatory biomarkers that have been most studied in HCM patients are IL-6 and TNF-α [32]. TNF-α and IL-6 might be involved in the HCM pathogenesis, but there is no clear activation mechanism. Increased mechanical stress might trigger the release of IL-6 and TNF-α [118] . IL-6 might induce the expression of MMPs and TNF-α in hypertensive patients [45] could lead to fibrosis. Current trends in

identifying the biomarkers that may consistently support prognosis in the early stages of diseases such as hypertension are limited. Identifying novel biomarkers of hypertension might provide clinicians and researchers with a deeper understanding of its underlying mechanisms, leading to increased motivation for addressing the difficult task of lowering hypertension and its associated cardiovascular diseases.

Genome-wide association studies have identified numerous genetic variants linked to blood pressure regulation or hypertension, but their individual impact on blood pressure is relatively small [119]. Researching a complex disease with multiple causes, defined subjectively by a blood pressure threshold, is challenging. Hypertension is often asymptomatic, leading to limited awareness of the condition until significant organ damage develops, such as due to stroke, myocardial infarction, or heart failure. Thus, the relationship between inflammation and CVD is complex, bidirectional, and only partly identified. Various proposed mechanisms include, but are not limited to, immune-mediated damage through autoantibody deposition, cytokine signalling, TLR activation, inflammasome activation, and inflammation, all of which contribute to end-organ damage [120] .

1.3.2. The role of immune cell signalling in hypertension

Immune cells play a dual role in cardiac tissue, contributing to both damage and repair, including scar formation and left ventricle remodelling [121–123]. Damaged or dead cardiomyocytes exposes damage-associated molecular patterns (DAMPs) that are recognised by pattern recognition receptors (PRRs) located on the surface or within the cytoplasm of resident macrophages and non-classical patrolling monocytes [124]. This recognition triggers the production of inflammatory cytokines and chemokines. In response to chemokines and cytokines, immune system cells migrate to the site of injury and initiate inflammation response [122,125].

A summary of main immune cell involvement and filtration after cardiac injury is illustrated in Figure 1.6.

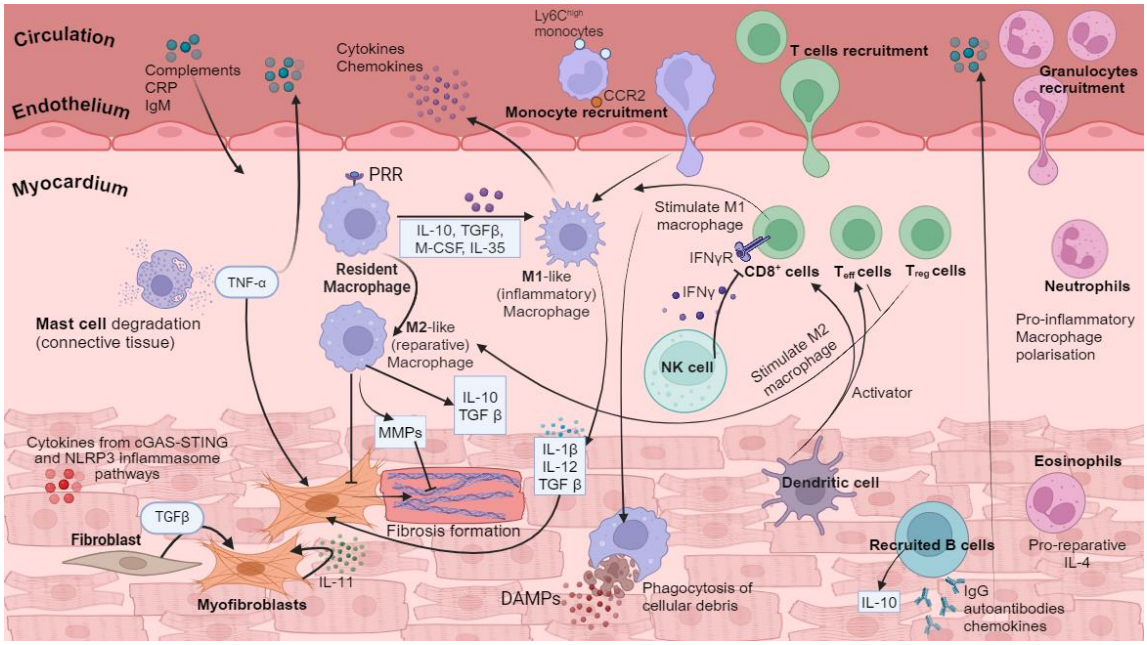

Figure 1.6: Main components of immune cell involvement and filtration after cardiac injury. Stressed cardiomyocytes initiate inflammatory secretory programs through the cytosolic DNA sensing cGAS-STING and NLRP3 pathways. Damaged and dead cells release DAMPs which act as potent signalling molecules. CRP, IgM, and other circulating factors filter the injured heart. Tissue-resident macrophages proliferate also CCR2+ monocytes are recruited from circulation. Macrophages polarise between two phenotypes M1-like inflammatory and M2-like reparative. Dendritic cells are potent activators of recruited all T cell types, are main immune infiltrates. CD8+ cytotoxic and several Teff cells signal with M1 macrophages and many other pro-fibrotic inflammatory and pro-reparative pathways. While some Teff and Treg cells infiltrate the heart and stimulate M2-like macrophages reparative phenotype, ECM remodelling, and overall cardiac repair. B cells produce many cytokines, chemokines, and autoantibodies. NK cells are recruited and have reparative role. Granulocytes such as neutrophils are recruited, and they stimulate M1-like macrophages and secrete proinflammatory cytokines. Eosinophils infiltrate the heart and help stimulate tissue recovery. One of the major downstream targets of this inflammatory scene are cardiac fibroblasts. Tissue-resident fibroblasts proliferate and resident in activated form into myofibroblasts and produce damaging fibrosis. Abbreviation: IL indicates interleukin; MMP, matrix metalloproteinase; TGFβ, transforming growth factor β; and TNFα, tumour necrosis factor-α; damage-associated patterns (DAMPs); CRP (C-reactive protein); CCR2+ (C-C chemokine receptor type 2); effector T cells (Teff cells); regulatory T cells (Treg cells); ECM (extracellular matrix); Natural killer (NK); M-CSF, Colony-Stimulating Factor-1. Created by Biorender. Adapted from [126] .

The inflammatory response triggered by tissue damage involves the coordination of numerous cellular and molecular events. Pathogen recognition is a crucial step in initiating an appropriate immune response. The activation and polarisation of immune cells begin with the recognition of conserved molecular patterns associated with pathogens and tissue damage, mediated by PRRs [127] .A general mechanism of innate immune system recognition is illustrated in Figure 1.7.

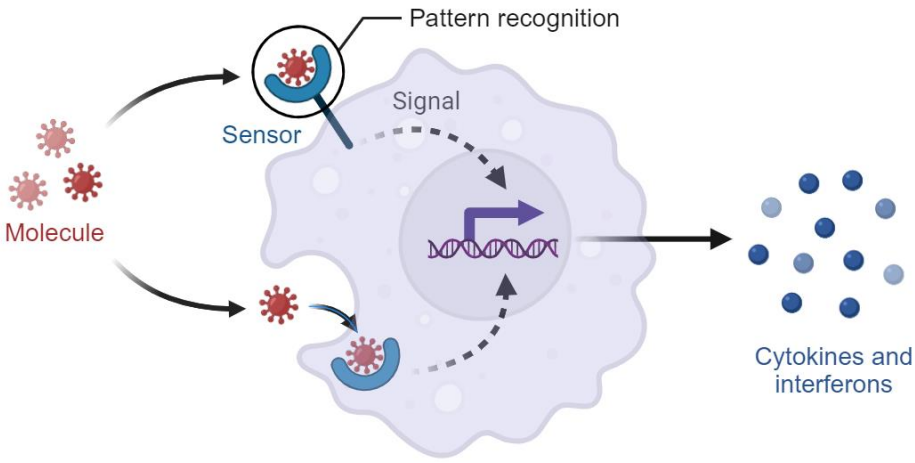

Figure 1.7: General innate immune system mechanism.
Innate immunity trigger sensors that detect unusual molecules or activities, known as pattern recognition. Once molecule patterns are detected by pattern recognition receptors (PRRs), they trigger immediate alarm through secretion of cytokines and interferons. Figure created by Biorender.

Cells in different organs and tissues express a diverse range of PRRs. PRRs are sensors that detect two classes of molecules including the exogenous danger signals, often referred to as pathogen-associated molecular patterns (PAMPs), which are highly conserved motifs in microbial pathogens like viruses, bacteria, fungi, and parasites. Endogenous danger signals, referred to as DAMPs, are proteins, cytokines, chemokines, and other molecules [127]. Since DAMPs initiate inflammatory responses that occur independently of pathogen infection, they are known to contribute to sterile inflammation under conditions of cellular stress or injury [128] .

PPRs have been classified into two major groups based on their cellular location. the transmembrane protein families are the toll-like receptors (TLRs) and C-type lectin receptors. The second class is the cytoplasmic protein families including the retinoic acid-inducible gene-like receptors (RLRs), absent in melanoma 2-like receptors, cytosolic DNA receptors, and nucleotide-binding oligomerization domain (NOD)-like receptors (NLRs) [129,130]. An overview of PPRs cellular localisation and signalling upon binding of their preferred ligand is illustrated in Figure 1.8.

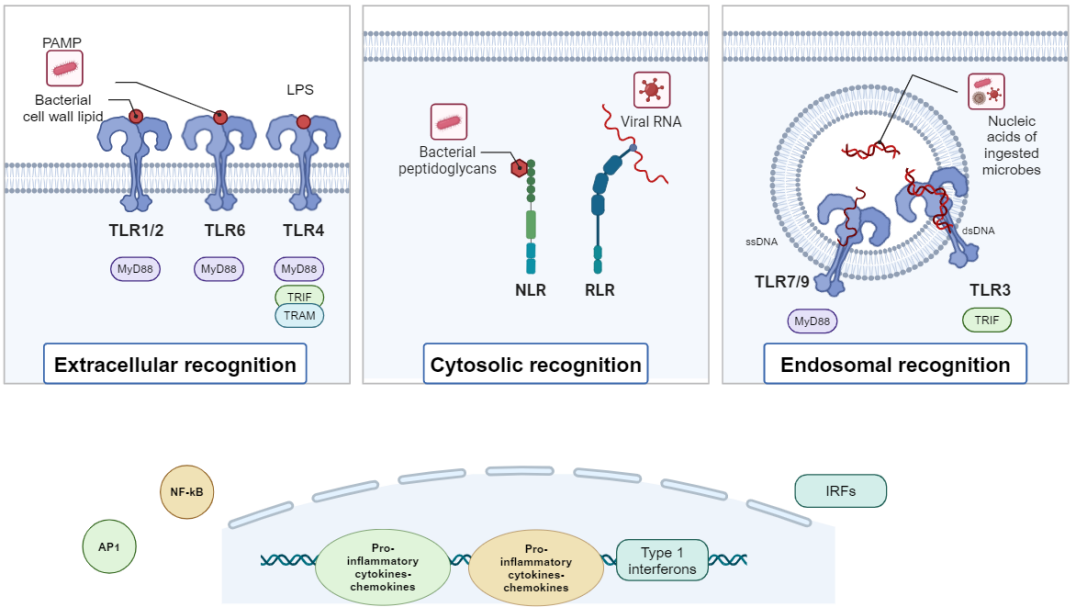

Figure 1.8: Schematic overview of PPRs cellular localisation and signalling upon binding of their preferred ligand.
TLRs are involved in alarming the immune system against extracellular or endosomal PAMPs like bacterial lipopolysaccharides and nucleic acids. NLRs are involved in regulation of inflammatory and apoptotic responses; RLRs are associated with intracellular recognition of RNA virus replication. Ligand binding leads to TLR dimerization of the cytosolic TIR domains where a signalling complex can be formed. The four adapter proteins MyD88, MAL, TRIF, and TRAM are the first to assemble. The signalling cascades that ensue result in the activation of the transcriptional activators AP1, NF-κB, IRF3, and IRF7. AP1 and NF-κB induce the expression of proinflammatory genes whereas IRFs induce the expression of type I interferon genes. MyD88-dependent signalling often results in the expression of the former genes, TRIF dependent signalling often results in the expression of the latter genes. TLR4 signalling induced by TRIF, as indicated by the dotted line, is initiated in the endosome. Created by Biorender. Adopted from [131,132]

1.3.3 DAMP mediated TLR4 activation in hypertension

Homeostatic disturbances lead to tissue injury through cellular stress or direct damage, DAMPs are released from the affected area and act as ligands for PRRs. DAMPs include cell-derived nucleic acids, fatty acids, heat shock proteins (HSPs), HMGB1, and ECM components such as proteoglycans, hyaluronic acid, and fibronectin [133]. The activation of TLRs by DAMPs serves a protective function by signalling cellular damage and promoting its resolution and repair. However, excessive or prolonged DAMP-mediated stimulation of these innate immune receptors can induce a chronic inflammatory state, which contributes to the persistence of hypertension [134]. DAMP-induced activation of TLRs triggers intracellular adaptor protein-dependent signalling cascades, leading to the upregulation of pro-inflammatory gene expression [135].

TLR4 is unique among TLRs as it recruits four adaptor molecules and signals through two distinct pathways to induce the production of pro-inflammatory cytokines and chemokines [136]. Cells commonly associated with cardiovascular diseases, such as macrophages, renal epithelial cells, cardiomyocytes, VSMCs, endothelial cells, glial cells, and neurons, express TLR4 [137]. TLR4 activation, primarily driven by DAMPs, contributes to cardiovascular dysfunction and remodelling which suggest that DAMP-induced TLR4 stimulation may be the critical link between inflammation and hypertension.

Hypertension-related DAMPs are proposed to modulate TLR4. For example, in VSMCs from SHR, Ang II increased TLR4 mRNA levels and this effect was reduced by losartan [138]. This indicates the involvement of AT1 receptor in such induction. In addition, TLR4 inhibition attenuated the Ang II-induced increases in NADPH oxidase activity, superoxide anion production, as well as VSMC migration and proliferation, thus indicates a role for TLR4 in the increased oxidative stress induced by Ang II.

1.3.3.1 TLR4 signalling

TLR4 consists of an extracellular domain with leucine-rich repeats and an intracellular toll-IL-1 receptor (TIR) domain responsible for signal transduction. Upon activation, TLR4 signalling proceeds through two pathways including the MyD88-dependent pathway and the MyD88-independent, TRIF-dependent pathway [135]. Both signalling cascades induce the production and release of pro-inflammatory cytokines, chemokines and pro-inflammatory factors. In addition, TLR4 endocytosis is required for the TRIF-dependent pro-inflammatory signalling and for the following degradation of the receptor and termination of the signalling [139]. An overview of TLR4 signalling in hypertension is illustrated in Figure 1.9.

The most common pathway for initiating immune responses is MyD88-dependent. In this process upon activation, TLR4 recruits the TIR domain-containing adaptor protein, MyD88 adaptor-like protein (TIRAP/MAL). This links MyD88 to the TIR domain, thereby initiating the MyD88-dependent signalling pathway [140]. MyD88 subsequently recruits and activates IL-1 receptor-associated kinase 4 (IRAK4), forming a signalling complex known as the myddosome[141]. Myddosome is a cluster consists of five components, MyD88, IRAK2, IRAK1, TRAF6, and TGF-β-activated kinase 1 (TAK1) [142]. IRAK4 (interacting protein 4 of the interleukin-1 receptor-associated kinases) facilitates the recruitment, phosphorylation, and degradation of IRAK1 and IRAK2, after which these IRAKs dissociate from MyD88 to bind TNF receptor-associated factor 6 (TRAF6) [143]. TRAF6 plays a critical role in signal transduction downstream of IRAK4 and IRAK1/2 [144]. Combining with TAK1 binding proteins TAB2 and TAB3, TAK1 activates the IκB kinase (IKK) complex and MAPK pathways [133]. Within the IKK pathway, two catalytic subunits, IKKα and IKKβ, along with a regulatory subunit (IKKγ/NEMO), degrade IκB proteins via phosphorylation and ubiquitination [145]. TLR4-mediated activation of the IKK pathway leads to the early nuclear translocation and activation of NF-κB [146].

TLR4's impact on downstream MAPKs is likely a key factor in cytokine and chemokine production. The MAPK family is highly conserved and divided into three subfamilies including ERKs, JNKs, and p38/stress-activated protein kinases (SAPKs) [147].

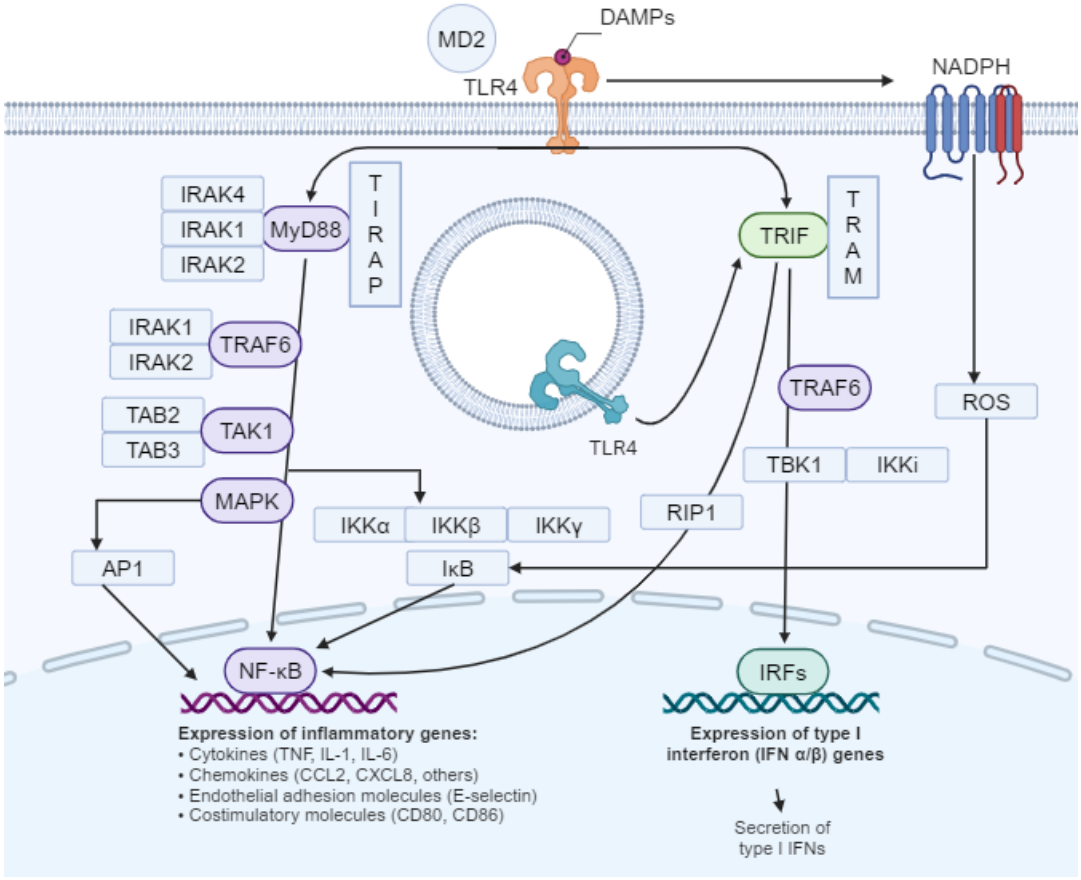

Figure 1.9: Overview of TLR4 signalling in hypertension.
TLR4 activation by DAMPs, may involve a primary interaction with myeloid differentiation factor 2 co-receptor (MD2). Upon activation, TLR4 initiates the early MyD88-dependent and late TRIF-dependent phase cascades. The MyD88-dependent pathway TIRAP associates with the receptor TIR domain, facilitating MyD88 association where MyD88 recruits and activates IRAKs, leading to stimulation of TRAF6 and TAK1. The downstream MAPK and IKK pathways eventually result in the nuclear translocation of activator protein 1 (AP-1) and NF-κB transcription factors and production of pro-inflammatory mediators. In the delayed TRIF-dependent signalling, recruitment of TRAM to the TIR domain allows TRIF binding and upregulates IRF3 expression through TRAF3. TRAM recruitment also activates NF-κB through RIPK1 (RIP1). Created by Biorender. Adapted from [148] .

The alternative TRIF-dependent pathway involves proteins, including TRIF, TRAF3, and receptor-interacting serine/threonine protein kinase 1 (RIP1) which comprise the pathway signalling complex [149,150]. TLR4 links to TRIF via TRAM and interacts with TRAF3 to activate IKK pathways. This lead to translocation of NF-κB, via adapter kinase receptor-interacting protein (RIPK) 1 and IFN regulatory factor (IRF) 3 stimulation. Activation of TANK-binding kinase 1 (TBK1) by TRIF leads to the activation of IRF3, which then translocate to the nucleus, potentially regulating IFN-β synthesis [151]. Additionally, the TRIF-dependent pathway can trigger inflammation through TRAF6 activation of the NF-κB pathway [152].

TLR4 is also implicated in the canonical activation of the NLRP3 inflammasome. The NLRP3 inflammasome is a multimeric complex composed of NLRP3, ASC, NEK7, and pro-caspase-1, which facilitates autoproteolysis and the activation of caspase-1. Activated caspase-1 cleaves pro-IL-1β and pro-IL-18 into their secreted forms. Additionally, caspase-1 catalyses the cleavage of gasdermin D, which binds to the inner surface of the plasma membrane, forming pores that can lead to either pyroptotic cell death or the release of IL-1β from living cells [153]. Activation of TLR4 in human and murine macrophages serves as a priming signal (Signal 1) which induces the expression of NLRP3 and pro-IL-1β. This also promotes post-translational modifications of NLRP3. The assembly of a fully active inflammasome requires a second stimulus (Signal 2), which is typically provided by various PAMPs and DAMPs [154]. Although the precise mechanism by which these structurally diverse molecules initiate inflammasome formation is unclear, they seem to induce cellular stress, such as K+ efflux, mitochondrial dysfunction, or lysosomal damage, which is subsequently detected by NLRP3 [155]. As NLRP3 expression is regulated by NF-κB, both MyD88 and TRIF-dependent TLR4 signalling pathways may be involved. Consistent with this, caspase-1 cleavage and activation were observed in LPS-stimulated macrophages from

MyD88 or TRIF-knockout mice, while the double knockout did not support inflammasome activation [156,157].

Activation of the non-canonical inflammasome occurs independently of TLR4 and is triggered by the presence of cytosolic LPS. LPS directly binds to and activates caspase-11 (or caspase-4 and -5 in humans), which in turn activates the primed NLRP3 inflammasome, leading to the release of IL-1 and the induction of pyroptosis. The LPS internalisation in the cytosol is not clear, however, recent studies indicate that it can be internalised via the receptor for advanced glycation end-products (RAGE) following its binding to HMGB1 [158]. DAMPs such as extracellular HMGB1 triggers TLR4 and RAGE and as an inflammatory mediator contributes to CVD and it has attracted great attention [159], yet its specific CVD inflammatory pathophysiology remains limited.

1.4 HMGB1 as a potential biomarker in hypertension

1.4.1 Biological and Molecular Characteristics of HMGB1

Non-histone nuclear protein groups with high electrophoretic mobility were discovered in 1973 and labelled as high mobility group (HMG) proteins [160]. This protein family bind to DNA in a non-sequence-specific manner and includes HMGN, HMGA, HMGB based on the specific functional domains via which they recognise individual DNA structures on chromatin [161]. The HMGA protein family has an AT-hook, which is a DNA-binding motif with a preference for A/T rich areas. Those in the HMGN family have a nucleosome binding domain (NBD), whereas the HMGB family have A-box and B-box functional motifs. The HMGB family includes HMGB1, HMGB2, HMGB3, and HMGB4 [162] and are ubiquitous and abundant in most cells and can bind to DNA without sequence specificity [163,164].

HMGB1 is the most abundant non-histone nucleoprotein in the HMGB gene family. It is encoded by the human HMGB1 gene, also known as Amphoterin or

HMG1. It is a highly conserved, cytokine-like, nuclear protein that is expressed in nearly all mammalian cell types [165]. It is secreted by immunocompetent cells, including monocytes [166], neutrophils [167], macrophages [168] and microglial cells [169]. Other non- immune cells that express and secrete HMGB1 including platelets [170–172], endothelial [173] epithelial cells [174,175], fibroblasts [176], neurons [177] hepatocytes [178] and cardiomyocytes [179].

HMGB1 is highly conserved cross-species, with a sequence homology of more than 98% between mice and humans [180]. The HGMB1 protein is comprised of 215 amino acid residues (25–30 kDa) and forms two homologous box domains (A and B), which are DNA-binding motifs (shown in Figure 1.10). Structurally, HMGB1 contains three alpha-helices separated by loops and an acidic C-terminal tail. The C-tail is negatively charged, contains a string of glutamic and aspartic acid. It acts as a DNA binding and bending regulator by interacting with its DNA-binding domains or histones H1/H3 [181–183]. Box A domain binds DNA [184], while box B domain binds and facilitates DNA bending [185]. HMGB1 has two nuclear localisation signals (NLSs). NLS1 (amino acids 28-44) is located in A box, and NLS2 (amino acids 179-185) in the B box. As the name suggests, these motifs are responsible for HMGB1 nuclear localisation under the homeostatic, steady-state conditions [186]. Nuclear localisation is also regulated by the nuclear importin karyopherin (KAP)-α1 [185].

Studies have since identified regions of HMGB1 responsible for engagement with different substrates, including RAGE receptor binding (amino acids 150–183) and TLR4 receptor binding (89–108) [187,188]. Other structural features within the Box A domain include a heparin-binding domain (residues 6-12) and a thrombin-mediated proteolytic cleavage site (residues 10-11) [189,190]. Residues responsible for binding the p53 transactivation domain and thus increasing gene transcription have also been identified [191]. Previous studies conducted in a venous thrombosis model proposed that the disulphide form of HMGB1 released from platelets and neutrophils could promote neutrophil recruitment and neutrophil extracellular

traps (NETs) formation. This process contributes to thrombosis through activation of redundant pattern recognition receptors [192]. Thus, the disulphide form of HMGB1 might promote thrombosis derived from inflammation.

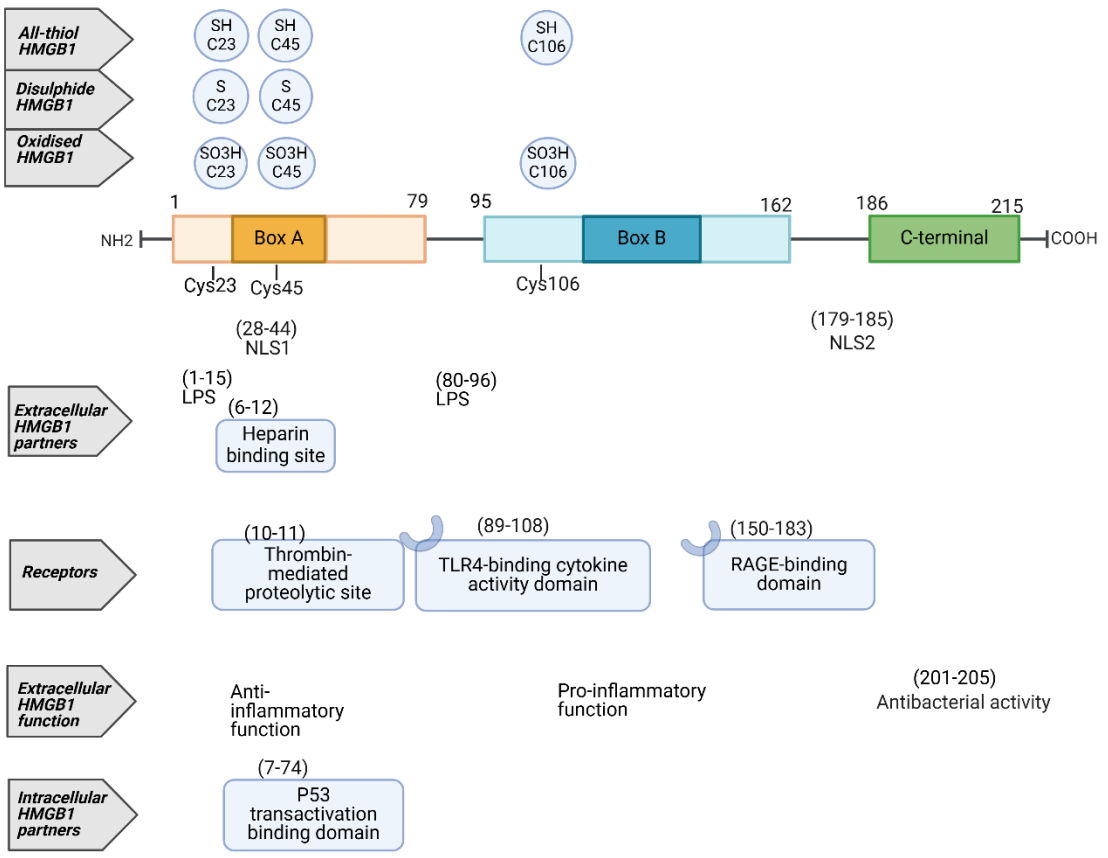

Figure 1.10: The structure of HMGB1.
This protein is composed of 215 amino acid residues and divided into three functional domains: box A, box B, and acidic C-terminal tail. Three redox-sensitive cysteine residues at the 23rd, 45th, and 106th positions regulate HMGB1 functions in response to oxidative stress. All-thiol HMGB1 exhibited all reduced cysteine residues at C23, C45, and C106, oxidised HMGB1 was termed as all three oxidized cysteines at C23, C45, and C106 and disulphide HMGB1 was formed by a disulphide bond between C23 and C45, which result in HMGB1 acting as a chemokine, a nonimmune factor, and an inflammatory factor, respectively. The ligand-binding sites and activate signalling mechanisms: heparin-binding site (6-12 aa), TLR4 binding site (89-108 aa), and RAGE binding site (150-183 aa), thrombin site (10-11aa). Abbreviations: NLS, nuclear localisation sequences; LPS, lipopolysaccharide; TLR4, toll-like receptor 4; RAGE, advanced glycation end products. Adapted from [193].

1.4.2 HMGB1 Intracellular and Extracellular Signalling

HMGB1 normally resides in the nucleus due to nuclear localisation signals (NLSs), where it stabilises nucleosomes and regulates gene transcription [194]. Under cellular stress, HMGB1 undergoes post-translational modifications such as hyperacetylation, leading to its translocation into the cytosol and subsequent release [195] . HMGB1 can be secreted actively by immune cells or passively released from necrotic or damaged cells [196] . This occurs through non-classical ER/Golgi-independent pathways, reflecting its unconventional mode of secretion [197] .

Once released, HMGB1 acts as a prototypical damage-associated molecular pattern (DAMP), bridging innate immunity and sterile inflammation [198] [199] [196] (194–196). Extracellular HMGB1 interacts with pattern-recognition receptors, including TLR2, TLR4, and RAGE [200,201] [202]. These interactions activate downstream signalling cascades (MyD88, IRFs, NF-κB, MAPKs, PI3K), promoting cytokine release, immune cell recruitment, and tissue inflammation. Figure 1.11 illustrates HMGB1 release and its major signalling pathways.

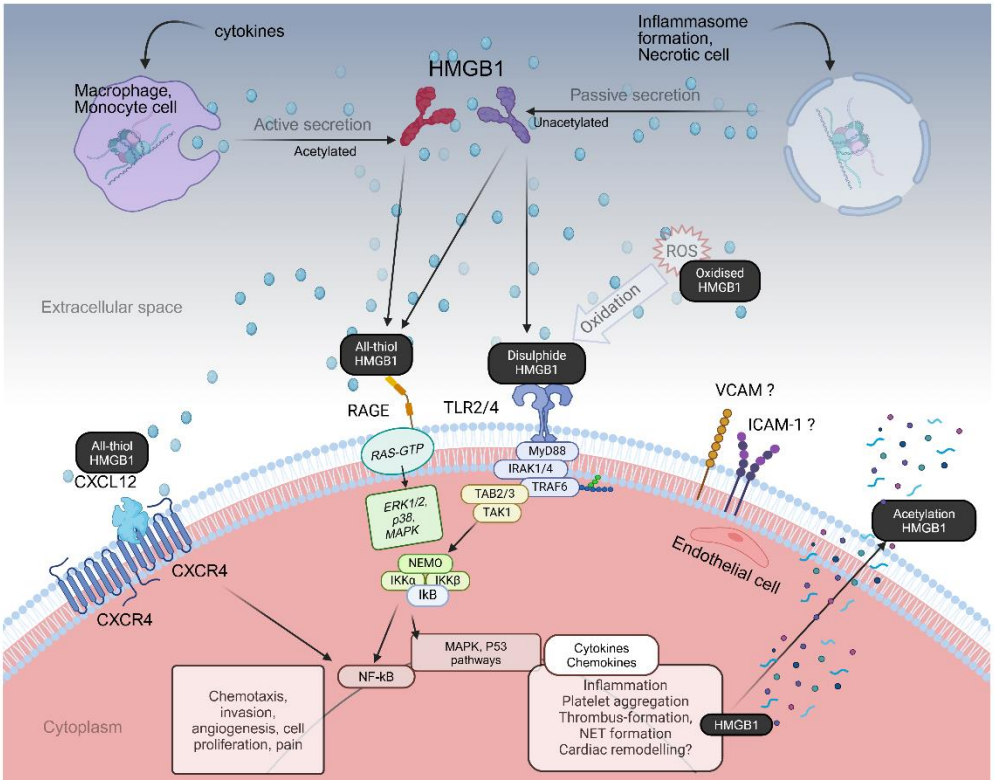

Figure 1.11: Mechanisms of signalling by HMGB1.

HMGB1 can be actively secreted or passively released, subsequently activating multiple receptors. Through TLR2/4 and RAGE, HMGB1 induces cytokine production, cell migration, proliferation, and differentiation. Distinct redox states confer different activities, including disulphide HMGB1 signalling through TLR4 and all-thiol HMGB1 interacting with CXCL12. Abbreviations: LPS, lipopolysaccharide; RAGE, receptor for advanced glycation end products; TNF, tumour necrosis factor; IL-1β, interleukin-1 beta; VCAM, vascular cell adhesion molecule-1; ICAM, intercellular adhesion molecule-1. Created with BioRender.

RAGE, a multiligand receptor of the immunoglobulin superfamily, is expressed in endothelial cells, neurons, monocytes, other tissues [203,204] and platelets [205]. HMGB1 binding to RAGE amplifies pro-inflammatory signalling and has been implicated in diabetes nephropathy [206], cancer [207], neurodegeneration [208,209] , and cardiovascular disease including atherosclerosis [210] . Beyond RAGE, HMGB1 also activates TLR2 and TLR4, reinforcing its role as a central mediator of sterile inflammation and vascular injury [211] .

1.4.2.1 Platelets, Extracellular Vesicles (EVs) and HMGB1 in Cardiovascular Disease

Platelets and extracellular vesicles (EVs) play complementary roles in sterile inflammation and cardiovascular disease, extending beyond their classical haemostatic functions. Upon activation, platelets rapidly release EVs including microparticles and exosomes that transport bioactive molecules such as cytokines, lipids, and damage-associated molecular patterns (DAMPs) [212] [213] [214]. Among these, HMGB1 has emerged as a key mediator of vascular inflammation and remodelling. EVs provide a non-classical secretion pathway for HMGB1, enabling its stable circulation and efficient delivery to target cells, thereby linking cellular stress to fibrosis progression.

Extracellular vesicles (EVs), including exosomes (50–150 nm) and microvesicles (0.1–1 μm), are recognised mediators of intercellular communication, transferring proteins, nucleic acids, and lipids between cardiovascular cells [212] [213] . EVs can exert both protective and pathological effects. For instance, fibroblast-derived EVs can promote cardioprotection and recovery after ischemic damage [215] , whereas EVs isolated from myocardial infarction patients or hypoxic cardiomyocytes were enriched in miR-30a and impaired autophagic responses in recipient cells [216] . Such dual roles highlight that EV cargo, including HMGB1, may strongly influence cardiovascular outcomes. This provided the rationale for examining HMGB1 trafficking in platelet-like particles derived from MEG-01 cells in this project.

HMGB1 is a key cargo of platelet-derived EVs. Once externalised, it engages receptors such as TLR4 and RAGE on endothelial and immune cells, thereby amplifying leukocyte recruitment, vascular inflammation, and thrombosis [156,157] [166] [172]. Elevated HMGB1-enriched EVs have been reported in hypertension, atherosclerosis, and myocardial infarction, linking platelet activity to vascular pathology [168] [173] [170].

EV-mediated HMGB1 release ensures stability in circulation and facilitates propagation of inflammatory signalling, thereby connecting vascular stress to myocardial remodelling [215] [216]. In hypertension, platelet activation contributes to vascular stiffening, endothelial dysfunction, and myocardial fibrosis [171] [176] . This provides a mechanistic basis for selecting MEG-01 cells as a surrogate model for platelet-derived EVs in this project, enabling controlled investigation of HMGB1 trafficking and release *in vitro*.

Together, these insights position platelet- and EV-derived HMGB1 as important mediators of cardiovascular inflammation and remodelling

1.4.3 HMGB1 as inflammation biomarker in CVD

HMGB1 acts as a nuclear regulator under homeostatic conditions and as a danger-associated molecular pattern (DAMP) during stress and injury (see Figure 1.12).

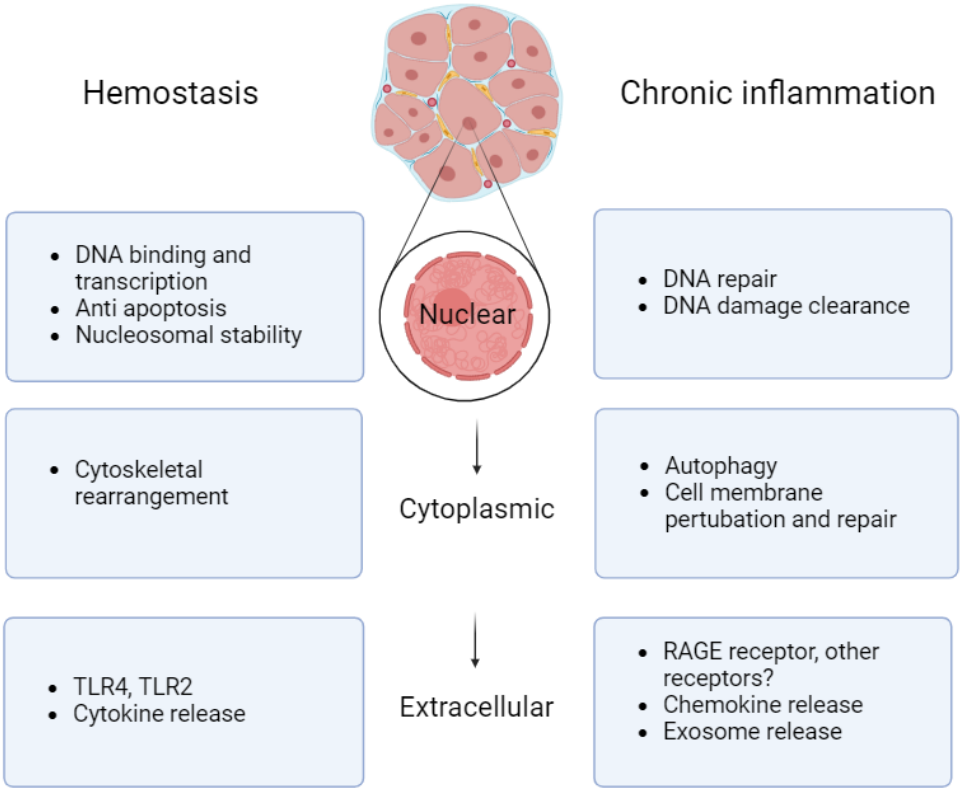

Figure 1.12: HMGB1 localisation and functional roles in cardiovascular homeostasis and inflammation.
Schematic illustration showing how HMGB1 functions vary by subcellular compartment. In the nucleus, HMGB1 supports DNA binding, transcription, anti-apoptotic signalling, nucleosomal stability, DNA repair, and damage clearance. In the cytoplasm, HMGB1 contributes to cytoskeletal rearrangement, autophagy, and cell membrane repair. Once released into the extracellular space, HMGB1 engages receptors such as TLR2, TLR4, and RAGE, triggering cytokine and chemokine release and promoting exosome-mediated intercellular signalling. These context-dependent roles highlight its dual functions in maintaining homeostasis and driving chronic inflammation. Created in Biorender. Adapted from [217].

HMGB1 has emerged as a context-dependent biomarker in cardiovascular disease (CVD), where its expression, localisation, and post-translational modifications determine its functional impact. Elevated extracellular HMGB1 levels have been reported in cardiac remodelling, myocardial infarction, heart failure, pulmonary hypertension, atherosclerosis, and hypertrophy, where it contributes to inflammation and fibrosis [159] [218] [219] .

In pressure-overload and hypertensive models, reduced nuclear HMGB1 with cytoplasmic translocation has been linked to maladaptive inflammation and progression to heart failure, whereas preservation of nuclear HMGB1 mitigates hypertrophy and dysfunction [220] . This highlights its potential use not only as a marker of disease severity but also as an indicator of remodelling dynamics.

Importantly, HMGB1 functions are highly context dependent. While disulphide-HMGB1 promotes cytokine release through TLR4 signalling, all-thiol HMGB1 supports chemotaxis via CXCL12, and oxidised HMGB1 is functionally inert [159] [221] . These isoform-specific actions may explain its paradoxical effects in CVD, acting as both a driver of sterile inflammation and a facilitator of tissue repair.

Recent studies link HMGB1 to the DNA damage response (DDR) in Ang II–induced hypertrophy, suggesting its utility as a biomarker of stress signalling and progression to heart failure [222] . Additionally, high-molecular-weight (HMW) forms generated by post-translational modifications such as acetylation and phosphorylation may serve as novel biomarker candidates, though their roles in hypertension-induced remodelling remain underexplored [223] .

1.5. Hypothesis, Aims and Objectives

Important questions in HMGB1 biology and its role in cardiovascular dysfunction remain to be fully addressed. Valuable findings from the Cunningham laboratory have identified a new soluble high molecular weight (HMW) form of HMGB1, HMW-HMGB1 (*Domoto, Butler, Plevin Kawabata & Cunningham, unpublished)*.

We hypothesise that this HMW-HMGB1 contributes to the inflammation associated with the progression of cardiovascular dysfunction during hypertension. This project aims to assess changes in HMGB1 expression and determine if HMW-HMGB1 is detected during pathological conditions using an *in vivo* model of Ang II induced chronic hypertension.

In the event that no significant effects are observed in HMGB1/HMW-HMGB1 expression or localisation, we will employ an alternative strategy to further understand the disease mechanisms. Specifically, we will leverage LC-MS-based proteomics to gain insights into broader pathological changes in protein expression within this model of hypertension. This approach will allow us to identify potential compensatory pathways, novel biomarkers, or alternative inflammatory mediators that may contribute to cardiovascular dysfunction.

These findings will provide valuable direction for future investigations into therapeutic targets for hypertension.

The objectives of the project were to:

- Establish and optimise a male rat model of *in vivo* Ang II induced chronic hypertension and monitor parameters such as blood pressure, organ weights and echocardiography (Chapter 3).
- Observe interstitial and perivascular fibrosis by analysing collagen marker using specific staining (Chapter 3).

- Analyse HMGB1 / HMW-HMGB1 expression, localisation and inflammatory role in Ang II induced chronic hypertension male rat model Translate key findings to relevant human cell models (Chapter 3)
- Carry out untargeted LC-MS based proteomics to profile compare the proteome of the control, saline and Ang II induced chronic hypertension rat model (Chapter 4).

Chapter 2:
Materials and Methods

2.1 Materials and reagents

2.1.1 *in vivo* work materials, reagents and equipment's

Table 2.1: Materials and equipment used in *in vivo* experiments

Solutions/chemicals/ peptides/treatments	**Source**	**Composition / Drug dosages**
Krebs buffer		mM: 120 NaCl, 5.4 KCl, 0.52 NaH_2PO4, 20 Hepes, 11.1 glucose, 3.5 $MgCl_2$, 20 taurine and 10 creatine; pH 7.4
Homogenisation buffer		20mM tris base, 100mM DDT, 100mM protease inhibitor, pH 7.4
Normal saline 0.9%	Baxter Holging	
Angiotensin-II Human	Sigma Aldrich	400 ng/kg/min, Ang II stock 25mg/ml
Heparin Sodium	Wockhardt	5000 I.U/ml - 0.1 m/ml/kg
Carprofen (Rimadyl)	Zoetis	50mg/ml- 5ml/kg
Overdose anaesthesia	Vetoquinol	Dolethal (pentobarbital sodium 200mg/ml) - (1mg/ml/kg)
Isoflurane (Isofane)	Covetrus	100% w/w inhalation vapour, liquid
Equipment	**Source**	**Description**
Micro-osmotic pump system with flow moderator in place, 2ML4 model	ALZET©	Includes filling tube, flow moderator and pump body. 2ml reservoir volume. M1004 model https://www.alzet.com/products/alzet_pumps/
Surgical instruments		Scissors, forceps
Suture	ETHICON®	Coated-Vicryl™3-0

Echocardiography machine-Philips	Philips-SONOS 5500	Includes ultrasound gel, heat mat, probe size 15mm
Nuvo lite oxygen concentrator	NIDEK Nuvo Lite Range	Isofluorane 2% with continuous flow oxygen up to 5 litres per minute, connected with anaesthesia device

2.1.2 Buffers and prepared solutions used *in vitro* experiments

Table 2.2: Buffers, prepared media and solutions

Buffer 1 (western blot)	1.5 M Tris-HCL (pH 8.8) + 500mM Sodium dodecyl sulphate (SDS) in dH_2O_2
Buffer 2 (western blot)	500mM Tris base-HCL (pH 6.8) + 14mM SDS in dH_2O_2
Stripping buffer 1L	31 mM Tris-HCl (pH 6.7) + 35mM SDS in dH_2O_2
Running buffer 1L	25mM Tris base + 192mM Glycine, 3.5mM SDS in dH_2O_2
Transfer buffer 1L	25mM Tris base + 192mM Glycine, in 20% (v/v) menthol in dH_2O_2
TBS-Tween (TBS-T) 1L	20mM Tris base (pH 7.5) + 150 mM sodium chloride (NaCl), 0.1% (v/v) Tween-20 in dH_2O_2
Blocking buffer	2% BSA diluted in TBS-T
ECL1(western blot)	10% 1M Tris base (pH 8.5) + 1% 250mM Luminol + 0.5% 250mM Coumaric acid+ 89% (v/v) dH_2O_2
ECL2(western blot)	10% 1M Tris base (pH 8.5) + 0.1% (v/v) Hydrogen peroxide+ 89% dH_2O_2
Roswell Park Memorial Institute 1640 (RPMI-1640)	RPMI 1640 + 2mM Glutamine + 10% Foetal Bovine Serum (FBS) + 1% Pen/Strep.

2.1.2 Key resources used in *in vitro* experiments

Table 2.3: Cell lines, reagents, equipment and chemicals

Reagents	**Source**
Cell lines	
MEG-01	*Merck KGaA, Darmstadt, Germany, Sigma-Aldrich®*
Culture media	
Roswell Park Memorial Institute 1640 (RPMI-1640)	*CORNING (USA)*
Foetal Bovine Serum (FBS)	*BIOSERA*
2 mM glutamine	*GIBCO*
Equipment	
Tissue culture hood	*MCH Class II*
Bright-field microscopy	*Nikon*
Leica Confocal SP8 microscope	*Leica Microsystems (Milton Keynes, UK)*
All tissue culture flasks, 10cm dishes, (6, 12 and 24) well plates, graduated pipettes and falcon tubes	*Corning B.V (Buckinghamshire, UK)*
Heraeus Fresco 21 micro centrifuge	*Thermo Fisher Scientific UK Ltd (Leicestershire, UK)*
Chemicals and peptides	
Sodium dodecyl sulphate (SDS) NuPAGE LDS sample buffer (4x)	*Thermo Fisher Scientific UK Ltd (Leicestershire, UK)*
-Glycine -methanol -sodium chloride -Tween-20	*Sigma-Aldrich Co Ltd (Poole, Dorset, UK)*

-p-coumeric acid -Luminol -Trizma Base -Dithiothreitol (DTT) -2-Mercaptoethanol -N,N,N',N'-tetramethylene diamine (TEMED)	
Bovine Serum Albumin (BSA) Phosphate buffered saline (PBS) tablets Poly-L-lysine solution, 0.1 % (w/v) in H2O cOmplete™ Protease Inhibitor Cocktail Triton x100 Dimethyl sulfoxide (DMSO) and ethanol.	*Sigma-Aldrich Co Ltd (Poole, Dorset, UK)*

Table 2.4: Software and Proteomic Analysis Tools

Software/applications	**Source**
ImageJ 1.53J	*National Institutes of Health*
Graph Prism 8	*GraphPad Software*
Bio render	https://app.biorender.com/
PANTHER v.14.0 database	http://www.pantherdb.org/
STRING v12.0	https://string-db.org

2.2 Methods

2.2.1 Animal ethics

All procedures were performed under sterile conditions and in accordance with the Guide for the Care and Use of Laboratory Animals (US National Institutes of Health, NIH Publication No. 85-23, revised 1996) and Directive 2010/63/EU of the European Parliament. This project was carried out under UK Home Office Project Licence PP0204578 (licence holder: Dr Susan Currie) and Personal Licence I72786373 (Zainab Bosakhar), approved for modules E1, L, A practical, A skills, PIL B, and K theory for rats and mice.

Group sizes were determined in line with previously published studies using pressure overload models to induce cardiac hypertrophy and left ventricular failure [224]. Typically, n=6–8 animals per group has been shown to detect ~20–25% differences in hypertrophic outcomes with adequate statistical power (α=0.05, power ~0.8). A formal power analysis was not performed; however, the chosen group sizes are consistent with established experimental standards in the field.

Animal welfare monitoring pre- and post-procedure was carried out and compared with institutional standards for animal husbandry, under the oversight of the Animals in Science Regulation Unit (ASRU).

2.2.2 Animals

The study was performed using weight-matched male Sprague Dawley rats (250–313 g; University of Strathclyde, The Biological Procedures Unit, BPU). The animals were housed two per cage on a 12-hour light/dark cycle, with access to standard chow and purified water ad libitum. All procedures were conducted in accordance with The Animals in Science Regulation Unit (ASRU) and approved under UK Home Office Project Licence PP0204578.

Rats were randomly assigned to three groups: control (n = 6), sham (saline mini-pump; n = 8), and Angiotensin II (Ang II) mini-pump infusion (n = 12). Ang II was delivered at a dose of 400 ng/kg/min for 28 days via subcutaneous osmotic mini-pumps (Alzet Model 2004, DURECT Corporation, USA), which were implanted as described in Section 2.2.3. Sham animals received identical pumps containing sterile saline. Baseline systolic blood pressure was measured in all animals (day 1), followed by weekly recordings at week 1 and week 4 (end-point). Echocardiography was performed to assess LV internal diameters (LVDD, LVDS) and fractional shortening (%FS). At termination, animals were euthanised with an overdose of Dolethal (pentobarbital sodium 200mg/ml) - (1mg/ml/kg)) containing Heparin (5000 I.U/ml - 0.1 m/ml/kg), and hearts were rapidly excised for histological and molecular analyses.

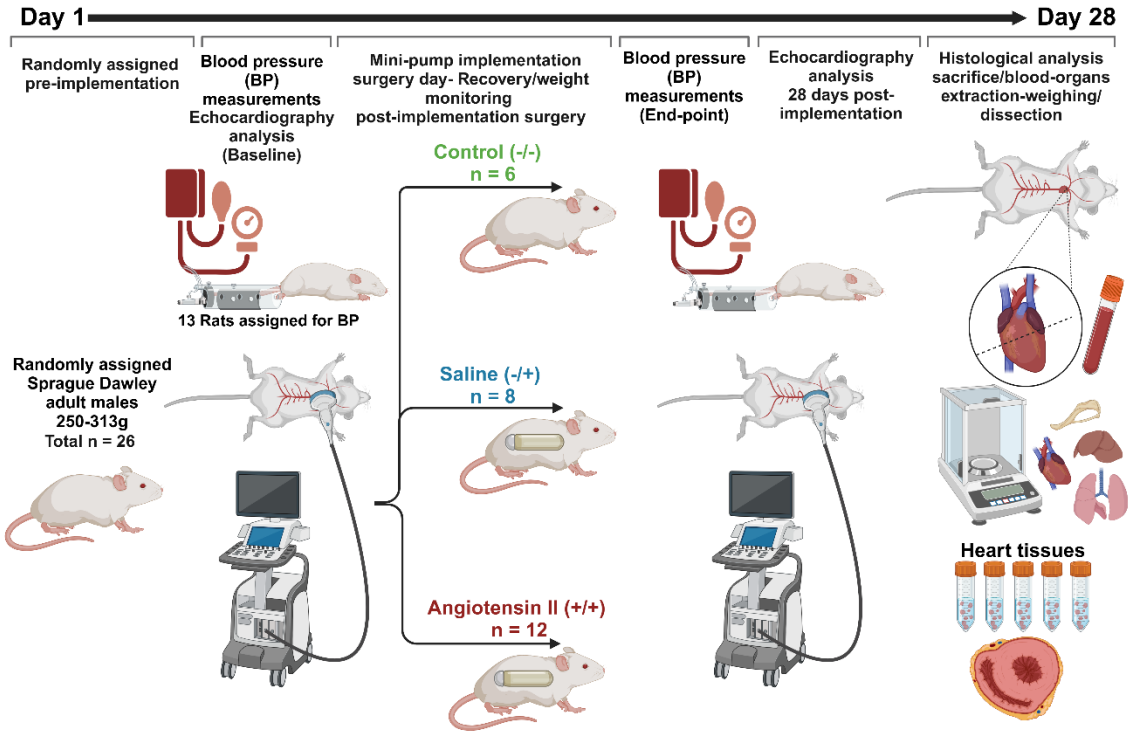

Figure 2.1: Schematics details of three experimental groups.
The experimental workflow for the cardiac function tracking of sham-operated (Saline) group (n=8), control group (n=6) and Angiotensin II-induced chronic hypertension model (n=12) using blood pressure (n=13) and echocardiography analysis as baseline and post-implementation endpoint. Scarification, organ collection and histological analysis obtained after 28 days. Created by Biorender software.

2.2.3 Preparation of saline and Angiotensin II mini-pump

All procedures were performed with standard aseptic technique. Surgical instruments were autoclaved, along with surgical gowns the day before. Angiotensin II stock of 25mg/ml was prepared according to the drug solubility and stored at -20^{o}C. The appropriate amount and concentration using flow rate and required doses were calculated for each Rat according to their weight. Pump information is in µl per hour and prepared stock Ang-II is 25mg/ml, 300µg was prepared in sterile Saline vehicle by using the Alzet website to calculate the required dose of 0.567mg/kg/day and the working concentration, final volume for each Rats depending on their weights. (see https://www.alzet.com/formulating-the-solution/).

Mini pumps were prepared the day before implementation, the pumps were weighed together with its flow moderator before and after filling. The pumps were filled with the required doses and topped up with saline as a vehicle, clear from air bubbles. The mini pumps were stored in bijoux/universal tube filled with 0.9% saline and primed at room temperature overnight before the surgery day. Priming allows the pump to equilibrate, ensuring immediate and consistent drug delivery upon implantation.

2.2.3.1 Mini Pump Surgical Implementation

All procedures were performed under standard aseptic conditions using 70% ethanol, Hibiscrub, and Sterillium®. Rats were randomly assigned to sham-operated controls (saline, n = 8) or Ang II-treated groups (n = 12). The Ang II group received continuous subcutaneous infusion of Ang II (Sigma-Aldrich, UK) via osmotic mini-pumps (Alzet®, model 2004; DURECT Corporation, USA), implanted to induce chronic hypertension. Pumps were filled to deliver Ang II at a rate of 400 ng/kg/min (pump delivery rate 0.25 µL/hr) for 28 days. Sham-operated

animals underwent the same surgical procedure with pumps filled with sterile saline.

Anaesthesia was induced with 3% isoflurane in 95% O_2 and 5% CO_2 in an induction chamber and maintained at 1.5–2% isoflurane via nose cone. Depth of anaesthesia was monitored by respiratory rate and toe-pinch reflex. Analgesia (Carprofen, 5 mg/kg, subcutaneous; Zoetis, UK) was administered prior to surgery, and a second dose given orally in softened food 24 hours post-surgery to minimise pain.

The surgical site (mid-scapular region, right dorsum) was shaved and disinfected with Hibiscrub. A small subcutaneous incision was made, and tissue gently separated with haemostat forceps to create a pouch for pump placement. The pump was inserted with the flow moderator oriented posteriorly and positioned below the incision to prevent interference and allow optimal healing. The incision was closed using absorbable sutures (Ethicon® Vicryl 3-0, Johnson & Johnson, USA), typically requiring 5–8 interrupted sutures.

2.2.4 Animal monitoring pre- and post-surgery

Animals' welfare was carefully monitored. Body weight was recorded on the day of surgery, checked immediately after surgery and monitored regularly during the entire treatment period. Weights were checked daily for the first week to make sure no body weight loss of 20% or more, then three times weekly for the rest of the treatment period. Animals were monitored for evidence of post-operative pain or infection, signs of weight loss, lack of mobility, abnormal posture, failure to groom, and excessive licking or biting of the incision area. Baby food was introduced prior and post-surgery as a treat, and a buddy was introduced in the cage with the experimental rat on the second day.

2.2.5 Blood pressure measurements

Systolic/diastolic Blood Pressure Measurements

Systolic and diastolic blood pressure (SBP/DBP) were measured using a non-invasive tail-cuff plethysmography system (BP-2000 Series II™, Visitech Systems, Apex, NC, USA).

Rats were first placed in a preheated chamber (32–34 °C) for 15–20 minutes to improve tail blood flow and acclimatise them to handling. After warming, each rat was gently transferred into an individual rat jacket restrainer, with the tail positioned through the rear opening for cuff placement.

An occlusion cuff and a volume–pressure recording cuff were positioned near the tail base. Automated inflation–deflation cycles (~90 seconds) were performed, and data were acquired via the BP-2000 system software. To minimise variability, all measurements were carried out by the same operator in a quiet environment at the same time of day.

Animals underwent a one-day acclimatisation session in which six inflation cycles were performed but not recorded. During actual measurement sessions, 6–8 cycles were taken per rat, and six stable cycles were averaged to generate mean SBP/DBP values. Baseline values (Day 0) were determined across two consecutive measurement days. Follow-up BP recordings were obtained between Days 7–10 and Day 28 for control, sham-operated, and Ang II-infused groups.

2.2.6 Echocardiography studies

A non-invasive protocol for transthoracic echocardiography assessment of cardiac anatomy and function for adult rats was followed [224,225]. Inhalation anaesthesia using isoflurane was commenced in an induction chamber starting at 3% and was maintained at 1.5 - 2% in 95% oxygen using a nose cone. After confirming a depth of anaesthesia by lack of response to the toe-pinch reflex, the left side of the sternum with the index mark turned to the right shoulder was shaved. A two-dimensional parasternal short-axis view of the left ventricle was

obtained by transthoracic echocardiography using a 15mHz linear array probe and ultrasound transmission gel. The probe was positioned as shown (Figure 2.2). All data are means of three consecutive cardiac cycles recorded for each animal. 2D guided M-mode recordings were obtained from the parasternal short-axis view of the left ventricle at the level of the papillary muscles. The angle of the M-mode flash was focused on the middle of the LV. Parasternal short axis M-mode tracings were recorded and used to determine LVIDd and LVIDs which are the Left ventricular internal diameter end diastole and end systole, and fractional shortening (FS). FS is calculated by measuring the percentage change in the LV diameter during systole by measuring the end-systole and -diastole by using the formula %FS=(LVEDD−LVESD)/LVEDD x 100. All the measurements were captured over three cardiac cycles, and the average is estimated.

Figure 2.2: Probe position for the parasternal short axis view.
Rotate the probe 90 degrees clockwise so that the indicator is now pointing towards the animal left shoulder.

Animal characteristics and the morphology of the heart were investigated following echocardiography are detailed in Figure 2.3.

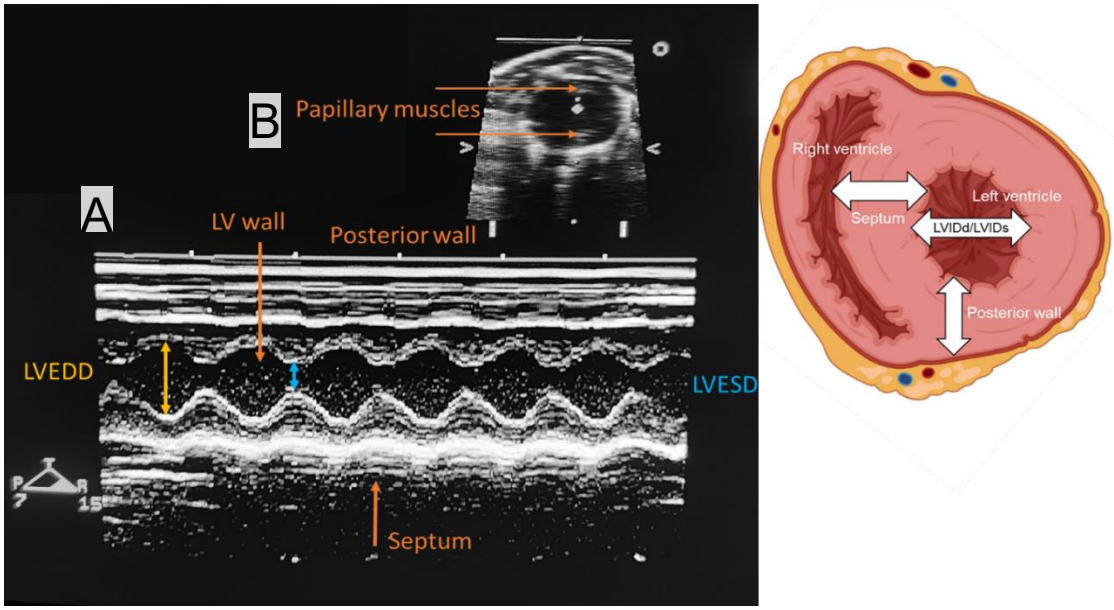

Figure 2.3 : M-mode echocardiography from a parasternal short-axis view showing the left ventricular cavity over the cardiac cycle during systole and diastole.
(A) Measurements of the widest diameter of the LV during diastole (LVEDD) displayed in yellow and the narrowest diameter during systole (LVESD) in blue to calculate %FS. Left ventricular, posterior wall and septum are indicated in orange. (B) image of the left ventricular short axis view. The cursor should be placed as indicated preferably at the level of the papillary muscles. Abbreviations: LV left ventricle; LVEDD, left ventricle end-diastolic dimension; LVESD, left ventricle end-systolic dimension.

The three Rat models under investigation were comparable with respect to body weight, heart weight and size. Echocardiography measurements were detailed in Table 2.5. Left ventricular fractional shortening (FS%) was calculated using the formula FS(%) =(LVIDD−LVISD)/LIDD X 100 shown in Table 2.6.

Table 2.5: Demographics of animal model groups.

Experimental group	Control (n=6)	Saline (n=5-6)	Ang II (n=12)
Average mean			
Heart weight (g)	1.24	1.31	1.48
Liver weight (g)	14.77	14.62	13.08
Lungs weight (g)	1.52	1.55	1.57

Table 2.6: Echocardiographic measurements in each group after 28 days

Experimental group	Control (n=6)	Saline (n=8)	Ang II (n=12)
Average mean			
LVIDD (cm)	0.737	0.716	0.663
LVISD (cm)	0.361	0.347	0.292
FS (%)	50.85%	51%	57%

2.2.7 Heart Dissection and cell culture

Immediately after echocardiography, an overdose of Dolethal (Pentobarbital sodium 1mg/ml/kg), mixed with Heparin (0.02ml/100g) was given intraperitoneally. Anaesthetic depth was assessed with reaction to nociceptive stimulus by checking toe-pinch reflex. After the reactions were lost, the anterior chest hair was shaved and by using scissors quickly cut the diaphragm and the sides of the rib cage to expose the content of the chest cavity, along the sternum to harvest the lungs, liver, and heart and cardiac tissue cleansed using Krebs to remove any remaining blood for weighing.

Hearts were cut along the short axis into two parts for biochemical and histological examination. Trunk blood up to 5ml was taken for DLS analysis of extracellular vesicles sizes. The cardiac tissues (LV; left ventricle, RV; right ventricle, LA; left atrium, RA; right atrium, S; septum) were collected and placed in homogenisation buffer for preparation of whole cardiac homogenates then homogenates were aliquoted and stored in -80 freezer (see Figure 2.4).

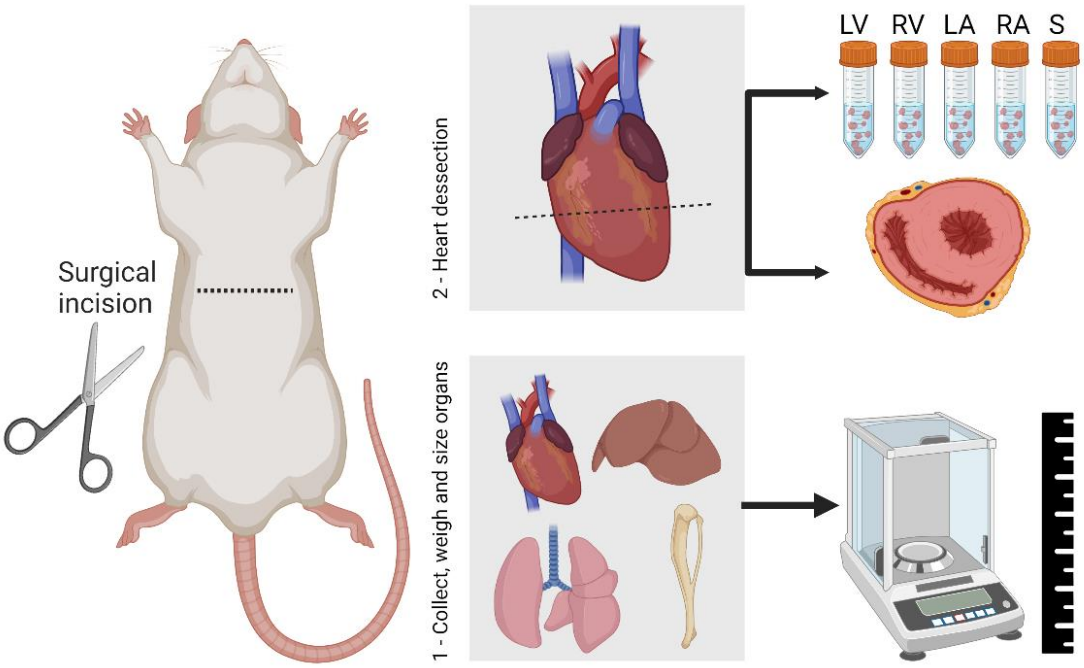

Figure 2.4: Schematic description of heart dissection.
Overdose of Dolethal performed with confirmation of death. Chest surgical incision was made to collect the heart, lung, liver, and tibia. First weighing and measuring size of organs then dissecting the heart to collect cardiac tissues and half crossed part. Created by Biorender.

2.2.8 Bicinchoninic Acid Assay (BCA) Protein Measurement

The concentration of total cellular proteins, prepared in standard RIPA buffer, and EV proteins were determined using a bicinchoninic acid assay (Pierce™ BCA Protein Assay Kit, Thermo Scientific). A BCA protein assay kit was used to measure total protein concentrations of whole homogenates for optimisation using bovine serum albumin as standard. Where appropriate, tissues were prepared with 4x lysis buffer, boiled at 95 C°/5 minutes and stored at -20 degrees ready for experiment.

2.2.9 Western blot analysis (Cardiac Tissue)

Equal amounts of protein from each sample ($10\mu\gamma$g) were separated by 15% SDS-PAGE gel, and transferred to a polyvinylidene fluoride membrane (PVDF, Bio-Rad Laboratories) under electrophoretic conditions (300 mA, 2 h). Membranes were blocked in Tris-buffered saline with Tween solution (TBST, 50 mM Tris-HCl, PH 7.5, 150 mM NaCl, and 0.5% Tween-20) containing 2% BSA for 1 h at room temperature. The blots were then incubated with primary antibody HMGB1, (at 1:5000 dilution) overnight at room temperature. The following day, blots were rinsed in TBST 3 times, 5 min each, and incubated for 1 h with anti-rabbit secondary antibodies (at 1:7500 dilution). After being rinsed in TBST for 3 times for 5 min, target proteins were visualised as black bands by using enhanced chemiluminescence and analysed by ImageJ.

2.2.10 Indirect immunofluorescence on heart tissue sections

Cardiac tissue embedded in OCT was sectioned on the Leica CM1950 apparatus with a chamber set temperature of -15 ◦C and a cutting holder temperature of -20 ◦C. Sections were acquired, starting from the apex with a thickness of 12 microns. The sectioned tissue was placed on a microscopic slide and dried by storing them in -80 freezer prior to immunofluorescent staining.

The OCT residue was removed from the tissue by two washes of 5 minutes with PBS in Coplin jars. The tissues were fixed with 3.6% (v/v) paraformaldehyde in PBS for 10 minutes. Tissues then were washed with PBS two times for 5 minutes' interval to remove the paraformaldehyde. For permeabilisation, tissues were washed with 0.25% (v/v) Triton-X-100 in PBS for 10 minutes. Tissues were washed with PBS two times for 5 minutes' interval and blocked in 1% (w/v) BSA in PBS for one hour and incubated with the primary antibody HMGB1 (1:100) in a humidified atmosphere overnight. Samples were washed with PBS three times for 5 minutes' interval to remove residual primary antibody and tissues were blocked with 1% (w/v) BSA in PBS for 30 min. the tissues were incubated with the required light sensitive secondary antibody Alex flour 488 anti-Rabbit (1:100) for 2 hours in dark room. The tissues were washed with PBS, 3 times for 5-minute intervals. Rhodamine phalloidin staining (1:40) and 4',6- diamidino-2-phenylindole (DAPI. 500nM in PBS, (1:2000)) nuclear counterstain were applied to the tissues for 20 minute and incubated in the dark room. The stains were removed with three washes of PBS for 5minute interval. Mowiol mounting media was added on top of the tissues and covered by a 0.13-0.17mm thick cover glass and left in a dark room overnight to be dried and ready for confocal microscopy analysis.

2.2.11 Picrosirius Red Staining

Picrosirius Red staining was performed to assess collagen deposition in cardiac tissue sections (see Figure 2.5). Where the red colour staining represents collagen fibres as a marker.

The frozen tissue samples were sectioned in 10um, rehydrated through graded ethanol series of 100%,80% and 40% and fixed in 3.6% formaldehyde. Sections were then incubated with Picro-Sirius Red Stain Kit (Cardiac Muscle) (cat# ab245887, abcam ©) which specifically binds to collagen fibres.

Single section from each animal in group was viewed and photographed with an EVOS LF Auto digital camera (Thermo Fischer Scientific, UK) under x4 magnification selecting random areas and x10 for whole heart. Quantification of collagen content was performed; fibrosis was calculated by quantifying the % red of areas using the colour threshold tool through converting the image to black and white based on the selected threshold settings by ImageJ software.

The results for each animal were then averaged for subsequent statistical analysis and presented as total collagen area %.

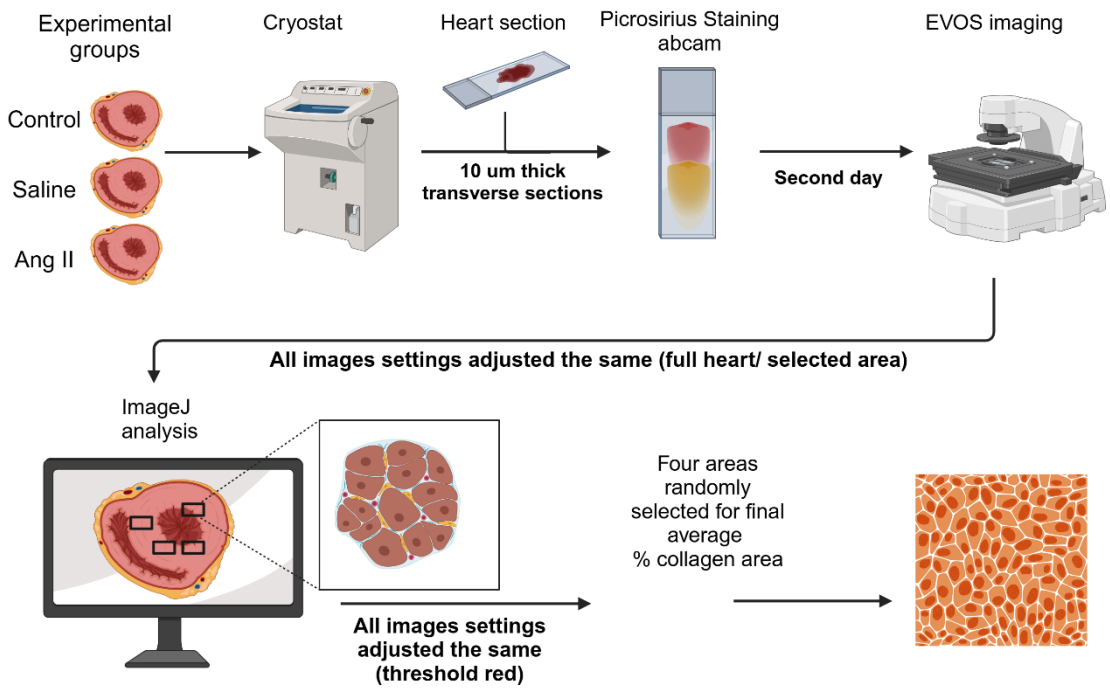

Figure 2.5: Picrosirius Red Staining for Collagen Detection in Cardiac Tissue Sections. Hearts from three experimental groups (Control, Saline, and Ang II) were sectioned using a cryostat to obtain 10 µm thick transverse sections. Sections were then stained with Picrosirius stain to visualize collagen content. On the second day, images were acquired using an EVOS imaging system. Image analysis was performed using ImageJ, with consistent image settings applied across all groups. Four areas from each heart section were randomly selected for final quantification of collagen deposition.

2.2.12 Masson's Trichrome staining

Masson's trichrome staining was used to determine cardiac fibrosis (see figure 2.6), where the blue colour staining represents collagen fibres as a marker. Masson's Trichrome kit (cat# ab150686, abcam ©, United Kingdom, SIGMA-ALDRICH ©) was used to stain 10 µm paraffin transverse heart sections that is fixed at 3.6% formaldehyde before staining. Perivascular (PV) and interstitial (INT) fibrosis was calculated by quantifying the % blue of areas using the colour threshold tool through converting the image to black and white based on the selected threshold settings (blue 140-180/190) by ImageJ software (https://imagej.net/).

A single section from each animal in group was viewed and photographed with an EVOS LF Auto digital camera (Thermo Fischer Scientific, UK) under ×10 for whole heart and ×4 for perivascular and interstitial collagen area magnifications. Visual representation and quantification of the fibrosis area was carried out by two individuals who were blinded to the treatments. First observer imaged the whole heart a minimum of six area separate images from different, nonoverlapping regions of the left ventricle midmyocardium and the perivascular cortex areas. Second observer carried out the quantification selecting random area. The results for each animal were then averaged for subsequent statistical analysis and presented as total collagen area %.

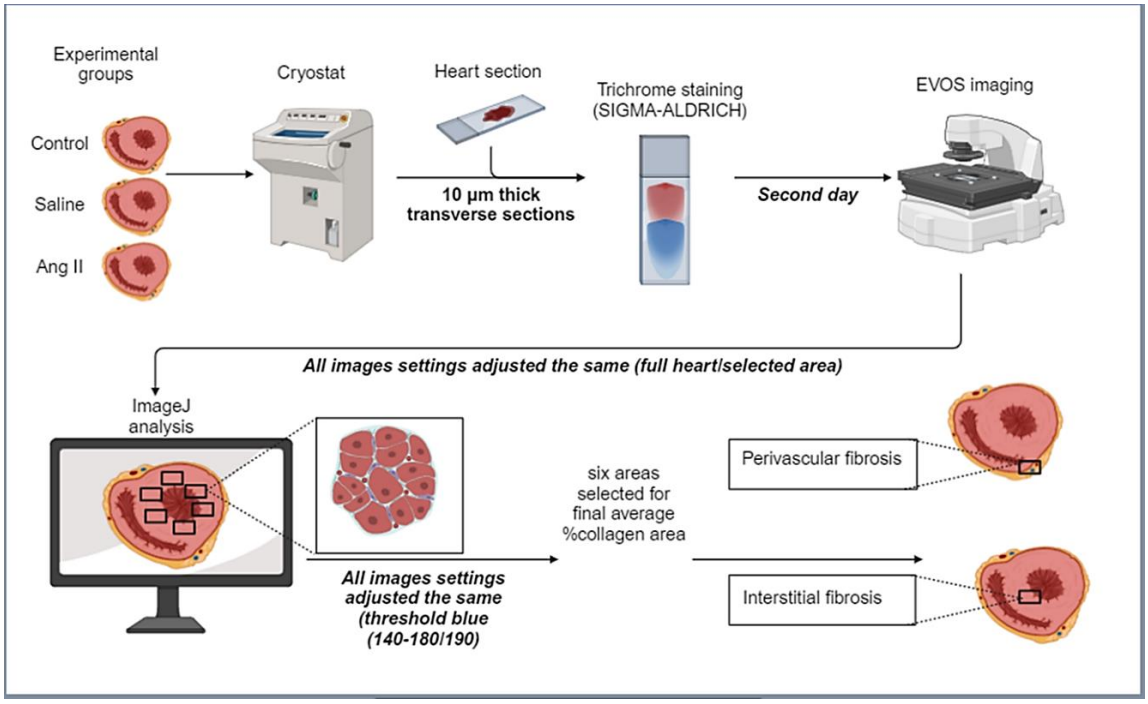

Figure 2.6: Schematic illustration of Massons trichrome staining workflow.
Hearts from three experimental groups (Control, Saline, and Ang II) were sectioned using a cryostat to obtain 10 µm thick transverse sections. Sections were then stained with Masson's trichrome to visualize collagen content. On the second day, images were acquired using an EVOS imaging system. Image analysis was performed using ImageJ, with consistent image settings applied across all groups. Six areas from each heart section were selected for final quantification of collagen deposition. Fibrosis was quantified separately in perivascular and interstitial regions.

2.2.13 Isolation of extracellular vesicles (EVs)

2.2.13.1 Rat serum derived EVs

For EVs isolation from blood, approximately 6 mL of blood was obtained per rat. Ultracentrifugation methods were used, and serum was prepared and centrifuged at 2000 × g for 30 minutes to discard cells and at 12 000 × g for 45 minutes to discard microvesicles. The resulting supernatant was centrifuged at 110 000 × g for 70 minutes to collect the EV-enriched fraction. EVs were washed once in PBS and centrifuged as before to resuspend the final pellet in PBS and store it at −80°C.

2.2.13.2 MEG-01 derived EVs

For EVs isolation from MEG-01 cells, the media was thawed on ice and multiple centrifugation cycles were performed. The media was first centrifuged at 3500xg for 10 minutes and the supernatant was carefully removed, pellet discarded and further centrifuged at 10,000xg for 20 minutes. The supernatant was carefully removed, pellet discarded and centrifuged at 100,000xg for 60 minutes. The supernatant was removed, and the tubes were inverted onto tissue paper for 10 minutes. The EV pellet obtained was suspended in sterile filtered PBS and re-centrifuged at 100,000xg for 60 minutes. The EV fraction obtained was then suspended in a final volume of 0.6ml PBS. These were aliquot into 0.1ml fractions and frozen at -80 for experimental use.

Figure 2.7 illustrates the stepwise protocol used for EV isolation from MEG-01 cell culture supernatant and rat blood serum, involving sequential centrifugation steps to remove debris and isolate small EVs. For both sources, differential centrifugation was performed, starting with low-speed spins to remove cell debris, followed by higher-speed ultracentrifugation to pellet small EVs. The isolated EVs were then resuspended in Phosphate-Buffered Saline (PBS) for Dynamic Light Scattering (DLS) zeta-sizing analysis, ensuring consistency in size distribution measurements between the two sample types.

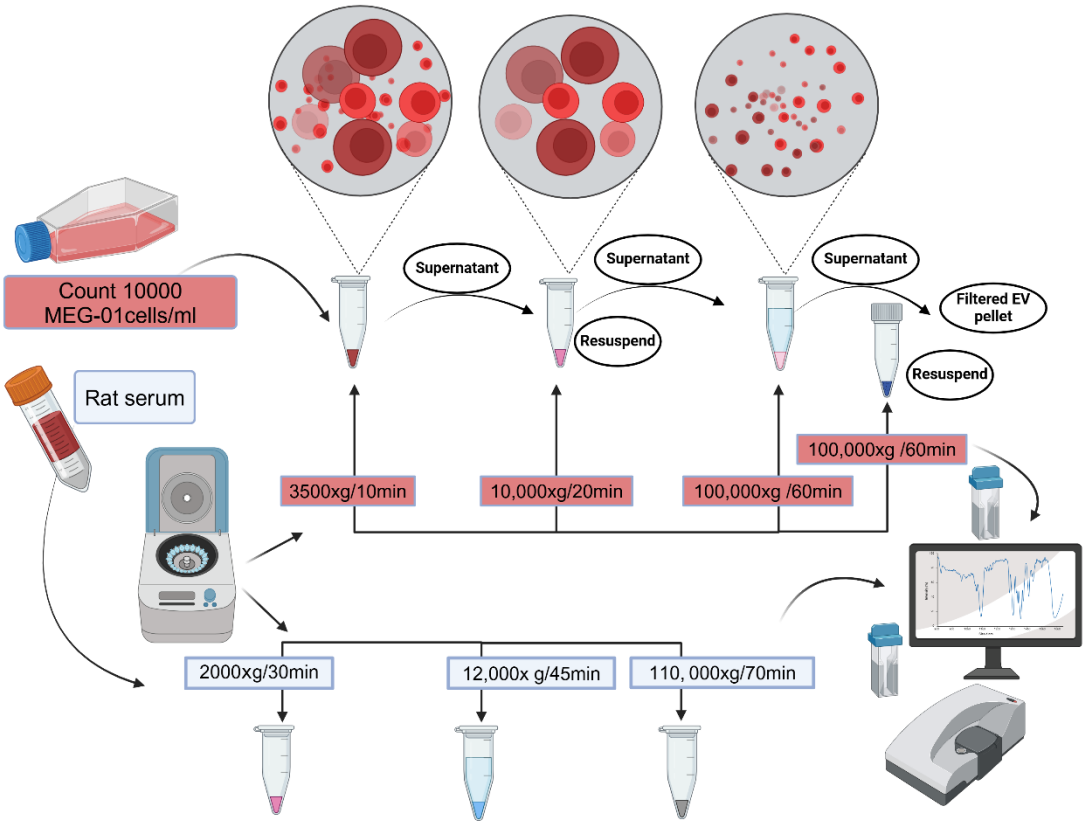

Figure 2.7: Schematic representation of the extracellular vesicle (EV) isolation process from MEG-01 cell culture and rat serum using differential ultracentrifugation.
MEG-01 cells were counted at 10,000 cells/mL and subjected to sequential centrifugation steps (3,500 × g for 10 min, 10,000 × g for 20 min, and 100,000 × g for 60 min) to remove debris and isolate EVs. Similarly, rat serum underwent differential centrifugation (2,000 × g for 30 min, 12,000 × g for 45 min, and 110,000 × g for 70 min) to obtain purified EV fractions. The final EV pellet was resuspended and analysed using dynamic light scattering (DLS) for zeta-sizing and particle characterisation. Image created by Biorender.

2.2.13.3 Dynamic Light Scattering (DLS) EV Zeta-Sizing

The final EV pellet was resuspended in PBS and stored (as mentioned in above section). Defrosted samples were diluted with 0.9ml PBS for final volume of 1.0ml, as minimum volume for analysis required is ≥0.4ml which transferred into cuvette tubes for zeta potential and size distribution analysis using DLS. This protocol ensures a purified EV sample for accurate characterisation of EVs and size distribution. For zeta potential and size distribution measurements, five technical replicates were performed for each biological replicate to ensure data reproducibility and minimise variability. Each replicate was measured under identical conditions, maintaining consistent temperature, choosing media composition, and sample handling procedures to reduce experimental bias.

DLS measurements were conducted using a laser-based scattering system, where fluctuations in scattered light intensity were analysed to determine the hydrodynamic diameter and surface charge (zeta potential) of EVs. The results were averaged across replicates to provide a robust and reproducible characterisation of the EV population. DLS analysis was performed using both intensity-weighted and number-weighted distributions to assess EV size heterogeneity and stability. The intensity-based distribution highlighted larger EVs due to their stronger scattering signal, while the number-based analysis provided a more accurate representation of the actual EV population it corrects for the bias toward large particles. A main peak in the 30–150 nm range indicated successful enrichment of exosomes/small EVs, whereas secondary peaks (>200 nm) suggested minor aggregation or contamination.

2.2.14 Cell culture

All cell culture was conducted in Class II laminar flow hood under aseptic conditions.

2.2.14.1 MEG-01 Cell Culture and Sample Preparation:

MEG-01 cells (human megakaryoblastic leukemia cell line) were selected as an in vitro surrogate model because they differentiate into platelet-like particles and secrete extracellular vesicles (EVs), providing a controlled and renewable source of platelet-derived vesicles. This rationale was particularly important in this project, as limited blood availability from Ang II rats restricted serum EV analyses. The MEG-01 model therefore allowed investigation of HMGB1 trafficking and release via EVs under reproducible laboratory conditions, complementing the *in vivo* data.

MEG-01 cells were purchased from Merck (see Table 2.3), maintained and cultured in growth media at 37 ºC / 5% CO_2 in a HeraCell incubator, and used between passage 5–20. The cell line population was adjusted and seeded into 25-cm² flasks at a concentration of 2–4 × 10^5 cells/mL in Roswell Park Memorial Institute (RPMI) medium supplemented with 2 mM L-Glutamine and 10% Foetal Bovine Serum (FBS).

Cells were checked daily and maintained by feeding them every 2–3 days, as the doubling time is ~36–48 hours, until they reached 80–90% confluency. Maintenance was achieved by direct dilution with fresh serum-containing media (1–2 mL added per flask). For passaging, cells were reseeded at 1:3 (v/v). A sterile scraper was used to gently detach adherent cells, which were collected into sterile 15 mL tubes and centrifuged at 1000 rpm for 5 minutes at room temperature. Cells were then resuspended, counted using a haemocytometer, and used for experiments when required.

2.2.14.2 Cryopreservation

Cells at early passages and 80–90% confluence were preserved for storage. Following routine passaging, cell pellets were resuspended in a solution of 90% FCS and 10% dimethyl sulfoxide (DMSO). Aliquots of 1 mL were transferred into cryogenic vials and immediately stored at –80 °C for short-term storage. For long-term storage, vials were transferred into liquid nitrogen.

2.2.14.3 Thawing Cells from Cryopreservation

Cryopreserved cells were rapidly thawed and transferred into sterile 15 mL Falcon tubes, followed by dropwise addition of fresh RPMI medium. Cells were centrifuged at 1000 rpm for 5 minutes to pellet, and the supernatant was aspirated to remove DMSO. The cell pellet was resuspended in fresh medium and transferred to T75 flasks for recovery and propagation. Cells were subsequently maintained as described in Section 2.2.14.1.

2.2.14.4 Cell lysis

Cells were counted, seeded at the required density, and allowed to recover for 48 hours in 6-well plates before experimentation. The medium was removed, and cells were harvested by centrifugation, washed once in PBS, and exposed to lysis buffer (50 mM Tris-HCl pH 7.4, 1% Triton X-100, plus Roche Mini Protease Inhibitor cocktail freshly added). Lysates were homogenised using a syringe and transferred to 1.5 mL microfuge tubes. Samples were rotated for 1 hour at 4 °C, then centrifuged at 10,000 rpm at 4 °C for 10 minutes. Protein content was quantified using the Pierce BCA assay according to manufacturer’s instructions. For whole-cell lysates, 2X NuPage LDS sample buffer and 50 mM DTT were added in a 1:1 ratio to normalised lysates, heated at 95 °C for 5 minutes, and stored at –20 °C until analysis (within 6 months).

2.2.15 Trichloroacetic Acid (TCA) + Sodium Deoxycholate (DOC) Precipitation

MEG-01 cells at 80-90% confluency was manually counted, prepared at 3×10^5 and treated with 1U/ml thrombin for time course stimulation (5,15,30,60,120 minutes) and zero time was used as control. Cells were centrifuged at 1500xg/5min to collect supernatant in Eppendorf tubes. Sodium deoxycholate monohydrate of 125ul/ml (0.00125g/ml) was prepared and 10ul added into each tube for 15 minutes on ice. Trichloroacetic acid of 60ul was carefully added in each tube to give a final concentration of 6% and centrifuged at 4◦C, 12000xg speed for 30 minutes. Supernatant was carefully removed by aspiration and pellets were washed with 1ml cold Acetone and centrifuged at 4◦C, 12000xg speed for 5 minutes. Acetone was removed and protein residues were prepared with 2x SDS, homogenised, boiled at 95◦C and stored in -20◦C for experiment.

2.2.16 SDS-PAGE and Western Blotting

2.2.16.1 Cell Sample Preparation

MEG-01 cells were transferred into 1 mL Eppendorf tubes at a density of 2–4 × 10^5 cells/mL or seeded into 6-well plates and cultured in RPMI medium with serum-free conditions until 70–80% confluence. Cell counts for all MEG-01 suspension experiments were determined using a haemocytometer. A density of 3 × 10^5 cells was collected in 1 mL Eppendorf tubes and centrifuged at 1500 rpm for 5 minutes. The supernatant was removed, and pellets were incubated in serum-free media for 2 hours. Cells were then stimulated with thrombin (1 U/mL) for 5, 15, 30, 60, or 120 minutes, as indicated, and processed as described in Section 2.2.14.4 for further experimentation.

2.2.16.2 Sodium Dodecyl Sulphate-Polyacrylamide Gel Electrophoresis (SDS-PAGE)

SDS-PAGE was performed using Bio-Rad Mini-Protean Tetra systems with 10–15% resolving gels for HMGB1 protein separation. Gels were prepared with 15% (v/v) acrylamide solution, 3 mL Buffer 1, 3 mL dH_2O, 10% (w/v) ammonium persulphate (APS), and 0.02% (v/v) TEMED. Gels were poured into pre-assembled gel chambers with 1.5 mm thickness. A 4% stacking gel was layered on top, prepared with 0.75% (v/v) acrylamide solution, 0.19% Buffer 2, 10% (w/v) APS, and 0.02% (v/v) TEMED. Well-forming combs (10- or 15-well, 1.5 mm) were gently inserted, and gels were left to polymerise.

2.2.16.3 Electrophoretic Transfer of Protein to Membrane and Immunological Detection

Normalised MEG-01 and cardiac tissue protein samples were separated by SDS-PAGE (15% gels for HMGB1) alongside molecular weight markers. Electrophoresis was performed at 130 V until the dye front reached the bottom of the gel. Proteins were electro-transferred onto nitrocellulose membranes (300 mA, 105 minutes) in transfer buffer. Membranes were incubated on an orbital shaker for 120 minutes in blocking solution (2% BSA in TBS-T) to prevent non-specific binding.

Primary antibodies against HMGB1 were diluted 1:5000 (v/v) in 0.2% BSA/TBS-T and incubated overnight at room temperature on a shaker. After three 5-minute washes in TBS-T, membranes were incubated with HRP-conjugated secondary antibodies (1:7500 v/v in 0.2% TBS-T) for 90 minutes at room temperature. Specific protein bands were visualised using enhanced chemiluminescence (ECL) substrate, and signals were detected on autoradiography film. Band intensities were quantified using ImageJ software.

2.2.16.4 Membrane Stripping and Reprobing.

For normalisation and reprobing, membranes were stripped using 15 mL stripping buffer (100 mM β-mercaptoethanol, 2% SDS, 62.5 mM Tris-HCl, pH 6.7) at 60 °C for 15 minutes with shaking. Stripping buffer was removed, and membranes were rinsed three times in TBS-T (5 minutes each) to eliminate residual buffer. Membranes were reprobed for housekeeping proteins (tubulin and GAPDH) following the same immunodetection protocol described in Section 2.2.16.3.

2.2.17 Scanning and Densitometry

Autoradiography films were scanned at a minimum resolution of 300 dpi using an HP Deskjet 2540 scanner. Adjustments to global brightness, contrast, and density were applied in ImageJ before analysis.

2.2.18 ImageJ analysis

ImageJ software was used for densitometric analysis of scanned autoradiography films. The area of interest was selected using a rectangular region of interest (ROI). Under the “Analyse → Gels” tool, the first lane was selected, and the same process was repeated for subsequent lanes. The area under the curve (AUC) was determined by drawing a straight baseline across each lane using the line selection tool, and peak areas were measured by plotting lane profiles. The wand tool was then used to automatically detect object edges and quantify the traced AUC. Raw data were exported into Excel spreadsheets for statistical analysis.

For Masson’s trichrome staining, the area of interest was cropped, and all images were converted to binary format using a defined colour threshold for blue (140–180/190). Collagen-positive areas were quantified as a percentage of total myocardial area.

2.2.19 Bright-field Microscopy

Cell imaging was performed to evaluate morphology. MEG-01 cells were grown to 80% confluence in complete medium prior to imaging. Time-lapse live-cell imaging was performed at ×10 magnification at 37 °C in an environmental chamber using a Nikon inverted epifluorescence microscope. Images were captured with MetaMorph software in bright-field mode.

2.2.20 Fluorescence microscopy

MEG-01 cells suspension was cultivated to 80% confluence. The cells were labelled with 5μM DiI for 10minutes at 37°C in a humidified environment with 5% CO_2. Cells were washed twice with PBS followed by fixation with 4% formaldehyde for 15 minutes in the incubator followed by 3 washes in PBS. Cells were permeabilised in 0.1% triton in PBS for 10 minutes followed by 2% BSA/PBS block for 1 hr, with centrifugation at 1.500 rpm for 5 minutes between steps. HMGB1 antibodies were used (1:200 dilution) and incubated in 2% BSA/PBS overnight at room temperature with gentle rotation to promote cell suspension mixing and enhance antibody binding. The cells were washed a further 3 times with 1X PBS, centrifugation at 300rpm for 5 minutes between each wash and blocked in 2% BSA/PBS for a further15 minutes. Cells were pelleted by centrifugation as before and tubes were then covered to protect from light and incubated 1:200 (v/v) with Alexa Fluor 488 secondary antibodies for 2 hours at room temperature. Cells were washed with 1XPBS and centrifugation, as previously described, and counterstained for 5 minutes with the nuclear marker 4',6- diamidino-2-phenylindole (DAPI, 500nM in PBS). Cells were washed a final time in PBS to remove residual DAPI stain and mounted on to slides and coverslips using Mowiol.

Table 2.7: List of immunofluorescence stains.

Name	Concentration	Source
DAPI (4′,6-diamidino-2-phenylindole)	500 nM	*Sigma©*
DiI Stain (1,1'-Dioctadecyl-3,3,3',3'-Tetramethylindocarbocyanine Perchlorate ('DiI'; DiIC18(3)))	5µM	*ThermoFisher© Invitrogen™*
Alexa Fluor 488 Polyclonal Antibody	1:200 dilution (v/v)	*ThermoFisher© Invitrogen™*
Rhodamine Phalloidin	1:40 -1:100 (v/v)	*ThermoFisher© Invitrogen™*

2.2.21 LC-MS Proteomics-based heart tissue analysis workflow

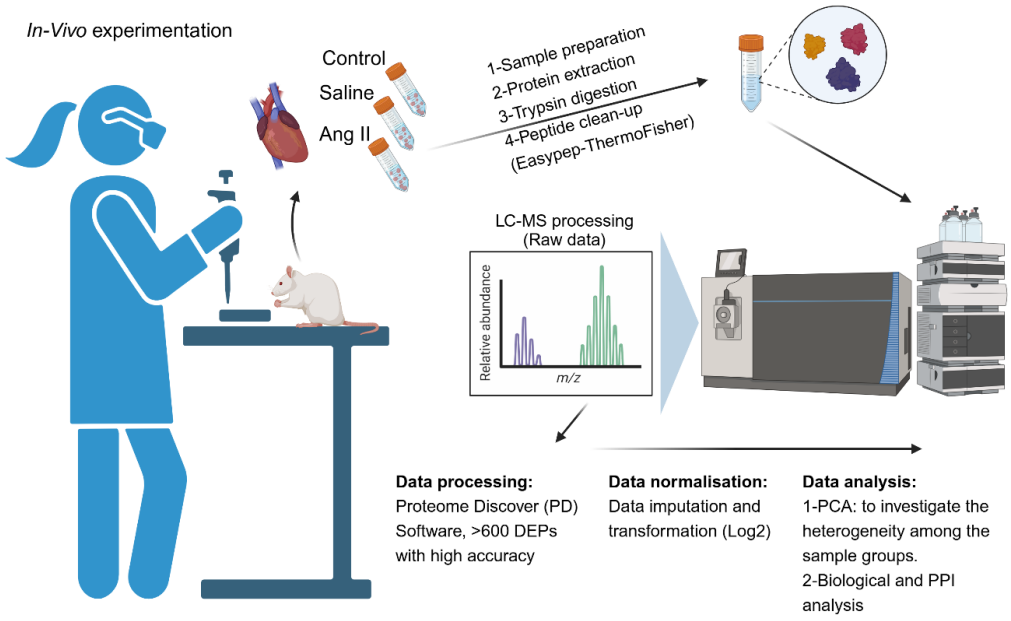

Figure 2.8: Schematic diagram shows the proteomic workflow of left ventricle (LV) tissue form Ang II induced chronic hypertension model.
Samples analysed by LC-MS of LV samples for Ang II, saline and control. Samples were characterised using a novel microflow label-free shotgun proteomics approach. The raw LC–MS data were processed using proteome discover, followed by further data filtering of normalisation and imputation and data transformation (log2), generating a total of >600 proteins in each experiment. DEPs under the threshold values (log2 Fold change 1 and $p \leq 0.05$) were captured, their biological analysis of functional (GO), and pathway (KEGG) and PPI were reported. Abbreviation: LC-MS: liquid chromatography-mass spectrometry; PD: Proteome Discoverer; DEPs: differentially expressed proteins; PCA: principal component analysis; PPI: Protein-protein interaction.

2.2.21.1 Tissue processing and Sample Preparation for Proteomic Profiling

Sprague Dawley male rats were treated with Ang II or saline for 28 days. At the end of the study, Ang II rats presented significantly higher systolic blood pressure and HW/BW ratios compared to Control and Saline groups, confirming the presence of chronic hypertension and cardiac hypertrophy. Heart tissue was processed, and samples were prepared from each group for LC–MS-based proteomic analysis following the ThermoFisher® protocol.

2.2.21.2 Protein Extraction, Trypsin Digestion and Peptide Clean-up

Protein samples were prepared for mass spectrometry (MS) analysis using the EasyPep™ Mini MS Sample Prep Kit (Thermo Scientific, Cat No. A40006). LV Tissue samples (5mg) were homogenised in 100 µL of Lysis Solution with 1 µL of Universal Nuclease and centrifuged at 16,000 × g for 10 minutes. Protein concentration was determined using the Pierce™ BCA Protein Assay Kit (Product. No. 10495315; Thermo Fisher, Rockford, IL, USA), and 50 µg of protein was subjected to reduction with 50 µL of Reduction Solution, followed by alkylation with 50 µL of Alkylation Solution, and incubation at 95°C for 10 minutes using a heat block. Protein digestion was performed by adding 50 µL of reconstituted Trypsin/Lys-C Protease Mix and incubating at 37°C for 2 hours in an Eppendorf ThermoMixer C (Thermo Fisher, San Jose, CA, USA) with agitation (600rpm). Digestion was terminated using 50µL of Digestion Stop Solution. Peptides were purified using Peptide Clean-up Columns by sequential washing with Wash Solution A and Wash Solution B, followed by elution in Elution Solution.

Peptide concentrations were quantified using the Pierce Quantitative Fluorometric Peptide Assay, using the Flexstation III microplate-based detection method. This assay relies on an amine-reactive fluorescent reagent to label the N-terminal primary amines of peptides. All assay components were equilibrated to room temperature before use and steps followed the manufacturer's guidelines. Briefly, the Peptide Digest Assay Standards (0–1000 µg/mL) were prepared by serial dilution in ultrapure water to generate a standard curve. For each measurement, 10 µL of peptide standard or sample was pipetted into a black 96-well microplate, followed by the addition of 70 µL of Fluorometric Peptide Assay Buffer and 20 µL of Fluorometric Peptide Assay Reagent. The plate was incubated at room temperature for 5 minutes before fluorescence measurement at Ex 390 nm/Em 475 nm using a Flextstation III fluorescence plate reader. A standard curve was generated by plotting fluorescence intensity against peptide concentration, and

the peptide concentrations of unknown samples were determined accordingly. All samples were analysed in triplicate to ensure accuracy linear, and measurements were within the range of 5–1000 µg/mL, enabling reliable and high-throughput peptide quantification for proteomic studies.

The final peptides were normalised and then collected and evaporated to dryness using a Thermo Scientific Savant SpeedVac (Thermo Fisher, San Jose, CA, USA). Dried peptides were reconstituted in 100 µL of 0.1% formic acid in water and transferred to LC–MS glass vials (Cat. No. 6PSV9-03FIVAPT; Thermo Fisher) for analysis.

2.2. 21.3 Micro-flow LC-MS-based proteomic

2.2.21.3.1 Data Acquisition

Peptide separation was performed using a Thermo Vanquish UHPLC system. Twenty microlitres of peptide solution were injected onto a Thermo Acclaim C18 PepMap 100 column (150 mm × 1 mm, 3 µm) and separated over a 100-minute method at 40 °C (autosampler at 5 °C, flow rate 50 µL/min). Solvent A was 99.9% water with 0.1% formic acid, and Solvent B was 99.9% acetonitrile with 0.1% formic acid. The gradient is shown in Table 2.8. All post columns viper fittings had a 75µm internal diameter (black colour code).

Table 2.8: HPLC mobile phase gradient approach.

No.	Time	Flow (ml/min)	%B
1	0.000	Run	
2	0.000	0.050	3.0
3	65.000	0.050	20.0
4	70.000	0.050	40.0
5	74.000	0.050	95.0
6	79.000	0.050	95.0

7	84.000	0.050	3.0
8	100.000	0.050	3.0
9			
10	100.000	Stop Run	

The bottom-up proteomics was performed on a high-resolution Exploris 240 Orbitrap mass spectrometer (Thermo Fisher Scientific) using positive ionisation (HESI+). Spray voltage was 3400 V; ion transfer tube temperature 320 °C; vaporiser temperature 75 °C. Sheath and aux gas flows were 25 and 5 Arb, respectively. MS1 survey scans were acquired at 120,000 resolution, RF lens 70%, scan range 275–1500 m/z, with a Top 20 DDA method. MS/MS scans were acquired at 15,000 resolutions with a 1.2 m/z isolation window and normalised HCD energy of 30%. Cycle time was 3 s. High-purity nitrogen was used for nebulisation and collision.

2.2.21.4 Protein Identification and Quantification.

Proteome Discoverer (PD) v3.0 software (Thermo Fisher, San Jose, CA, USA) was used, at which the MS raw data were searched against the UniProtKB Rattus norvegicus (Rat) Reference Proteome database (v22.07.13; 79,740 entries), including common contaminants (247 entries), using the SEQUEST and Percolator algorithms involved in modified label-free quantification (LFQ) standard processing and consensus workflows. The precursor mass tolerance was set to 10 ppm and 0.02 Da for-fragment mass tolerance. Full tryptic digestion was selected, with up to two missed cleavages were accepted. The minimum and maximum peptide lengths were set at 6 and 144 amino acids. Cysteine carbamidomethylation was set as a static modification, and oxidation of methionine (Met), Met loss and N-terminal acetylation were set as dynamic modifications. Three modifications were allowed per peptide as a maximum number. A concentrated target-decoy approach was applied for the false

discovery rate (FDR) calculation, which was set to 1% for highly confident peptide hits.

To assess protein abundance, the Feature Mapper node was selected. Chromatographic alignment of the raw files was conducted, allowing for a 10-minute retention time shift. A signal to noise threshold of 5 was established for feature linking and mapping. For quantifying precursor peptide abundance, precursor chromatographic intensities were utilized, with total peptide amount chosen as the normalisation mode to mitigate experimental bias. Quantification of identified proteins was based on unique and razor peptides.

2.2.21.5 Bioinformatics Analyses of Proteomics Data

Data processing was conducted in R v4.3.0. Dimensionality reduction was performed using PCA (mixOmics package). Differentially expressed proteins (DEPs) were identified using cut-offs of $\log_2$ fold change ≥ 1 and $p \leq 0.05$.

2.2.21.6 GO and KEGG Pathway Analyses

GO and KEGG enrichment analyses of DEPs were performed using the enrichDAVID function in the clusterProfiler package [226]. Terms with $p < 0.05$ (hypergeometric test) and minimum count of 5 were considered significant.

2.2.21.7 Protein–Protein Interactions (PPI) and Hub Protein Identification

DEPs were analysed in STRING (Rattus norvegicus, confidence ≥ 0.4). Pathway enrichment was performed using PANTHER v14.0. Over- or under-representation of pathways was assessed by Fisher's Exact Test [227] . Raw *p*-values were reported. Hub proteins were identified by betweenness centrality within the PPI network.

2.2.22 Statistical analysis

All data are presented as mean ± standard deviation (SD). Western blot densitometry was quantified using ImageJ (NIH, USA), with protein signals normalised to tubulin loading controls and processed in Excel. Graphs and statistical tests were performed in GraphPad Prism 8 (GraphPad Software, USA). For animal experiments (blood pressure, echocardiography, heart/weight ratio, collagen area fraction %, HMGB1 immunofluorescence quantification), statistical analysis was conducted using one-way ANOVA followed by Tukey's post hoc multiple comparisons test, after confirming normality and variance assumptions. Statistical significance was set at $p < 0.05$.

For proteomic analyses, three independent biological replicates were used per group. Data were processed in R v4.3.0. One-way ANOVA with FDR correction (0.5%) was applied for multiple group comparisons. For selected pairwise comparisons, Student's t-tests were used with FDR-adjusted thresholds to control false discovery.

Chapter 3:
In-Vivo Model of Ang II-Induced Chronic Hypertension in Male Rats

3.1 Introduction

In vivo models continue to play essential roles in our understanding of biology, physiology, and pathophysiology and target validation for various reasons. To provide insights about whole body interactions and disease progression in a physio-pathological context [228]. Chronic hypertension is a common complex condition that is the key risk factor for developing CVD. Evolved experimental animal models of hypertension enables a clearer understanding of underlying features of blood pressure regulation, hypertensive trait inheritance, and cellular responses to injury as well as end organ damage [64,65].

The use of animal studies in translational medical research has faced growing scrutiny due to issues like risk of bias, low reproducibility, inadequate experimental design and execution, analytical and logical flaws, and incomplete reporting [229–231]. Following recommendations on ways to mitigate these issues should be considered for animal models studies. The Animals in Science Regulation Unit (ASRU) Home Office authorities the use of animals in scientific research while outlining specific restrictions on which animals can be used and for what purposes [232]. The government is dedicated to the principles of replacement, reduction, and refinement commonly known as the 3Rs (Replacement, Reduction and Refinement) in the use of animals for research purposes.

Designing models for studies on cardiac pathophysiology presents significant challenges due to the complexity of cardiovascular disease, which arises from multiple causes and comorbidities, leading to a multi-organ condition, particularly in aging populations. Available models for studying cardiovascular disease include human subjects, laboratory animals, and stem cell-derived systems. These models allow for the investigation of various aspects such as cellular pathophysiology mechanisms, cardiac development, organ-organ interactions, and a wide range of measurable parameters [228]. Several models facilitate a reduction in the number of studies involving laboratory animals, as they enable

initial steps in identifying pathophysiology mechanisms. However, organ-organ interactions can only be fully examined in living models, such as humans or animals. Studying chronic hypertension as a primary contributor of organ damage could provide more insight about cardiovascular diseases progression and inflammatory related impacts.

3.1.1 Ang II-induced chronic hypertension model

Ang II, the primary peptide hormone of the renin-angiotensin system, plays a pivotal role in the development of hypertension [80]. Inhibitors targeting this system are an effective and first line choice as hypertension treatment. However, meta-analyses indicate that overall adherence to angiotensin converting enzyme inhibitors and angiotensin receptor blockers is only 50–60% [233]. Untreated, chronic systolic blood pressure of ≥140 mm Hg or diastolic blood pressure of ≥90 mm Hg, is associated with raised relative and absolute possibilities for cardiovascular disease outcomes. Vascular remodelling, marked by medial thickening, fibrosis, and the accumulation of inflammatory cells, is the mechanism through which hypertension exacerbates organ damage and increases the risk of cardiovascular disease [234].

Inflammation is a key contributor to the development and progression of hypertensive cardiac remodelling [235] . Ang II is a crucial element of the RAS, which promotes the early infiltration of pro-inflammatory cells, particularly monocytes and macrophages, during hypertensive cardiac remodelling [236]. Monocytes and macrophages secrete pro-fibrotic cytokines that induce the differentiation of resident cardiac fibroblasts into myofibroblasts, resulting in the excessive production of ECM [237]. A previous study demonstrated that HMGB1 released from injured lungs regulates mitochondrial metabolism of macrophages seeded within the abdominal aorta [238]. This indicates the crosslink between cardiac and immune cells that enhance the release of pro-inflammatory molecules. In addition, decreased expression of nuclear HMGB1 is observed in human failing hearts

compared to normal hearts which was associated with cardiomyocyte hypertrophy and fibrosis as assessed by a significant negative correlation of collagen amount and nuclear HMGB1 levels [222]. This was confirmed by using Ang II induced hypertrophy for 2 weeks on mice model with HMGB1 Tg nuclear as showed a reduction in hypertrophic changes. In addition, HMGB1 Tg nuclear with ATM DNA damage inhibitor mice showed less fibrosis in the left ventricular sections after Ang II induction compared with that of wild type mice. Interestingly, there was no significant difference in blood pressure after Ang II infusion between wild type and HMGB1 Tg mice. This suggests that HMGB1 might have independent role in cardiac remodelling.

3.2 Chapter Aims and Objectives

This chapter aims to establish and characterise an Ang II-induced model of chronic hypertension in male rats, investigate cardiac remodelling with a specific focus on HMGB1 expression and localisation, and complement in vivo findings with MEG-01 experiments to explore platelet/EV-mediated HMGB1 release.

Objectives of this Chapter

1. Establish and validate an Ang II-induced chronic hypertension model in male rats
    - Confirm induction of chronic hypertension through continuous Ang II infusion.
    - Monitor physiological parameters, including blood pressure, organ morphology, and cardiac function by echocardiography.
2. Investigate structural changes associated with hypertensive cardiac remodelling
    - Characterise perivascular and interstitial fibrosis by histological staining and collagen quantification.
    - Assess cardiomyocyte hypertrophy in response to Ang II infusion.
3. Determine the expression and localisation of HMGB1 in the hypertensive heart
    - Quantify HMGB1 protein levels in distinct cardiac chambers (LV, RV, LA, RA) by Western blotting.
    - Assess HMGB1 localisation in cardiac sections, focusing on perivascular and interstitial regions, under control, saline, and Ang II-infused groups.
4. Characterise HMGB1 release and EV/PLP contribution using MEG-01 cells
    - Characterise MEG-01-derived EVs under basal conditions (size distribution, morphology).
    - Detect HMGB1 in MEG-01-derived platelet-like particles (PLPs).

- Assess HMGB1 release dynamics in MEG-01 cells and supernatant following thrombin stimulation.

3.3 Results

3.3.1 Evidence for chronic hypertension and hypertrophy following Ang II induction.

Hypertension is the most common aetiology underlying various cardiovascular diseases and is recognised as a modifiable risk factor for global morbidity and mortality. Uncontrolled regulation of the RAAS in primary hypertension has made the Ang II rodent model a reliable one to study hypertension and related diseases [239]. A dose of 400 $ng \cdot kg^{-1} \cdot min^{-1}$ or lower, which is considered a slow-pressor, over prolonged infusion results in a gradual increase in BP and associated end-organ damage which mimics essential hypertension in humans [240,241].

3.3.1.1 Body Weight Monitoring in Ang II-Induced Hypertension Model

Throughout the 28-day experimental period, all rats were closely monitored in accordance with animal welfare guidelines, with particular attention to body weight to ensure overall health and to detect any adverse effects associated with Ang II infusion. Body weights were recorded weekly, starting from day 0, across all groups: Ang II-treated, saline-treated, and control. The project license restricted that no animal should experience more than a 20% reduction in body weight, as per Home Office regulations. The data in Figure 3.1 indicated no significant weight loss in the Ang II group compared to controls over the 4-week period, suggesting that chronic Ang II infusion did not adversely affect the general health of the animals.

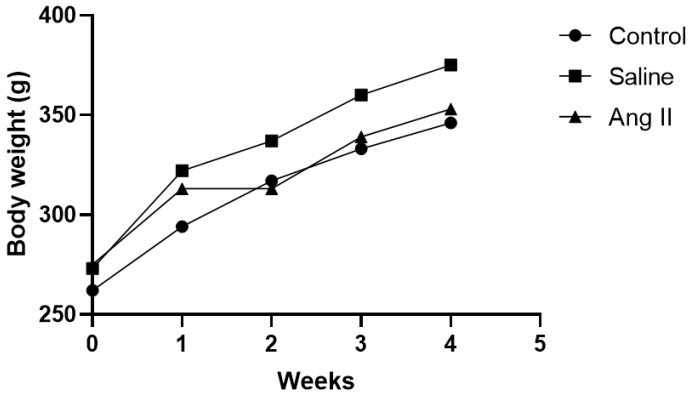

Figure 3.1: Body weight progression over 28 days in Ang II-treated, saline-treated, and control groups. Data represent average body weight in gram (g) over 4 weeks. No significant differences were observed between groups, indicating that Ang II infusion did not result in adverse weight loss.

3.3.1.2 Blood Pressure Monitoring in Ang II-Induced Hypertension Model

BP assessment began 2 days before minipump implantation to habituate the Rats to the procedure and continued at three different intervals (days 0, 7-9, and 28) for measurements. Rats were placed on a heating platform for 15-20 min before blood pressure assessment and restrained with a specific animal jacket that they felt comfortable in to remain calm. A minimum of 4 measurements (systolic and diastolic) were taken until the blood pressure stabilised and, then a minimum of six measurements were taken per Rat and averaged for analysis. BP was monitored by the same person at the same time of the day.

Systolic BP (mmHg) was significantly elevated in the Ang II group compared with control and saline groups at Days 7–9 and Day 28 (one-way ANOVA, $p < 0.0001$; Figure 3.2B)

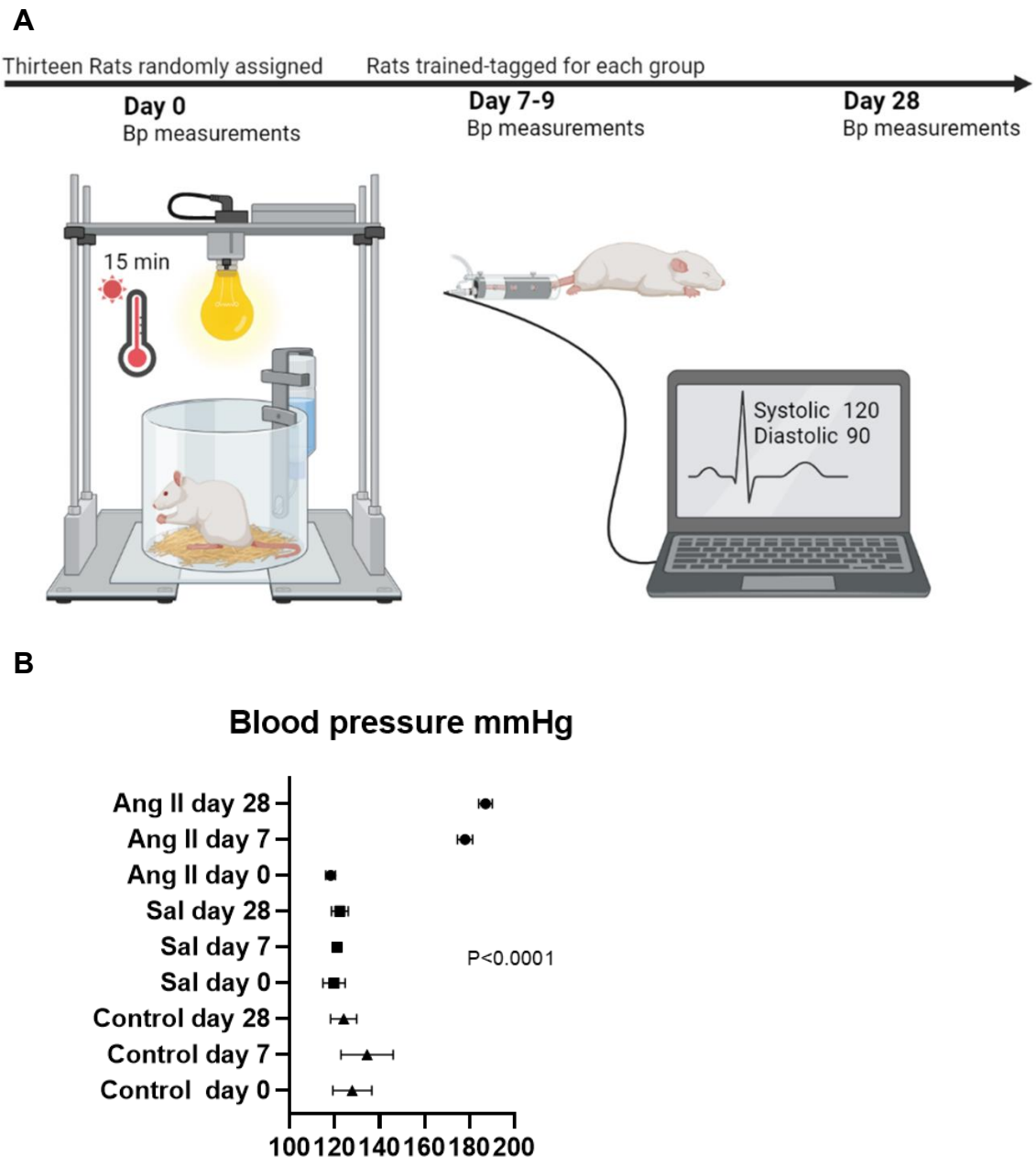

Figure 3.2: **Blood pressure protocol** assessment of all experimental groups.
(A) Workflow of BP measurements: baseline (Day 0), mid-study (Days 7–9), and endpoint (Day 28). Rats were pre-warmed under a heat lamp for 15–20 minutes before placement into restraining jackets for tail-cuff measurements. (B) Systolic blood pressure (mmHg) in all groups (Control n=6; Saline n=8; Ang II n=12). One-way ANOVA showed significant increases in Ang II rats at Days 7–9 and 28 compared to controls ($p < 0.0001$)

3.3.1.3 Heart and organs morphology, and heart/body weight ratio

In this study, cardiac hypertrophy was assessed by measuring absolute heart weight and the heart weight-to-body weight (HW/BW) ratio after 28 days of Ang II infusion, compared with Control and Saline groups. Baseline body weights were similar among all groups (245 ± 50 g).

Heart weight differed significantly among groups (one-way ANOVA, p = 0.0001). Mean values were Control 1.237 ± 0.050 g (n = 6), Saline 1.310 ± 0.147 g (n = 6), and Ang II 1.482 ± 0.090 g (n = 12). Tukey's post hoc test confirmed that Ang II hearts were significantly heavier than both Control (***p = 0.0002) and Saline (**p = 0.0066), whereas Control and Saline did not differ (p = 0.4286).

The heart weight to body weight (HW/BW) ratio was also significantly increased in Ang II rats (0.004270 ± 0.0003445) compared to Control (0.003265 ± 0.0002610) and Saline (0.003406 ± 0.0001351) (one-way ANOVA, p < 0.0001). Tukey's post hoc test confirmed significant increases in Ang II versus both Control (***p < 0.0001) and Saline (***p < 0.0001), while Control vs. Saline was not significant (p = 0.6775).

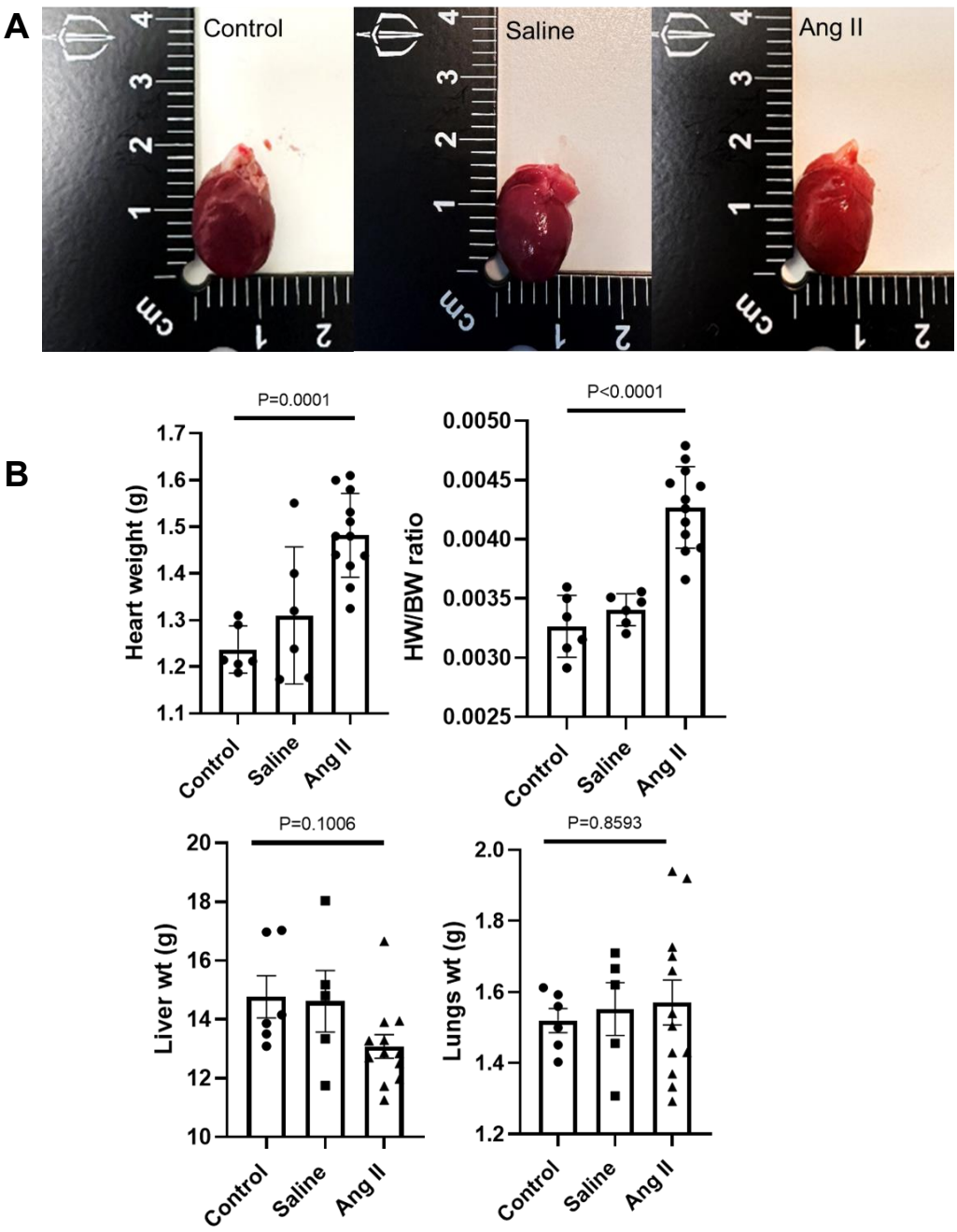

Figure 3.3: Heart and organs morphology and characteristics.
(A) Heart weights of Ang II (n = 12), Control (n = 6), and Saline (n = 6) groups. (B) Heart weight-to-body weight ratio (HW/BW) across groups. Data are presented as mean ± SD. Statistical analysis was performed by one-way ANOVA followed by Tukey's multiple comparison test. Only ANOVA p-values are shown in the figure for clarity; detailed post hoc results are reported in the text. Liver and lungs weights were compared between groups. Abbreviation: Angiotensin II; Ang II.

3.3.1.4 Transthoracic Echocardiography and Left Ventricular Geometric Patterns

Cardiac morphology and function were assessed by transthoracic echocardiography. Representative M-mode echocardiograms were obtained from Control, Saline, and Ang II-infused rats after 28 days (Figure 3.4A).

Fractional shortening (FS%) was significantly different among groups (one-way ANOVA, $p = 0.0105$). Mean values were Control 50.85 ± 4.15% ($n = 6$), Saline 50.68 ± 3.16% ($n = 8$), and Ang II 56.83 ± 5.53% ($n = 12$). Tukey's post hoc test showed that FS% was significantly increased in Ang II compared to both Control (*$p = 0.0421$) and Saline (*$p = 0.0205$), while Control vs. Saline was not significant ($p = 0.9973$).

The left ventricular diastolic internal diameter (LVIDd) also showed significant group differences (ANOVA, $p = 0.0216$). Control: 0.7365 ± 0.0406 cm, Saline: 0.7159 ± 0.0569 cm, Ang II: 0.6629 ± 0.0565 cm. Tukey's test confirmed a significant reduction in Ang II compared with Control (*$p = 0.0298$), while Control vs. Saline ($p = 0.7585$) and Saline vs. Ang II ($p = 0.0988$) were not significant.

Similarly, the systolic internal diameter (LVIDs) was significantly altered (ANOVA, $p = 0.0021$). Control: 0.3610 ± 0.0285 cm, Saline: 0.3466 ± 0.0397 cm, Ang II: 0.2864 ± 0.0487 cm. Tukey's test indicated Ang II values were significantly reduced compared with both Control (**$p = 0.0050$) and Saline (*$p = 0.0130$), while Control vs. Saline was not significant ($p = 0.8059$).

These echocardiographic data demonstrate increased FS% together with reduced LVIDd and LVIDs in Ang II rats compared with controls (Figure 3.4B).

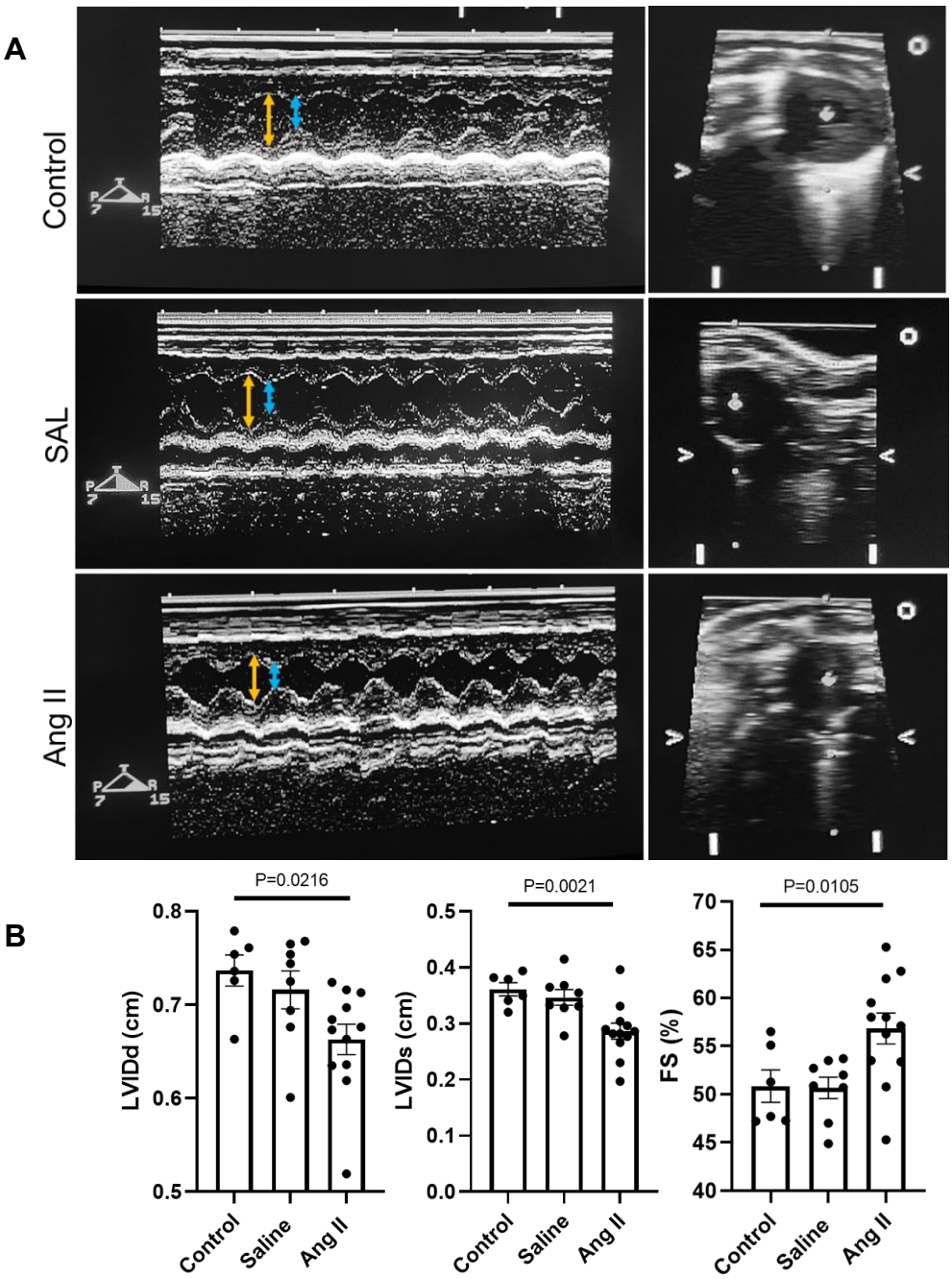

Figure 3.4: Echocardiographic assessment of LV geometry and function in control, saline, and Ang II-infused rats.
(A) Representative short-axis echocardiography with M-mode tracings showing LV diastolic internal dimension (LVIDd, blue arrow) and LV systolic internal dimension (LVIDs, yellow arrow). (B) Quantification of LVIDd, LVIDs, and fractional shortening (FS%). Data are expressed as mean ± SD. One-way ANOVA was used to compare groups (LVIDd: p = 0.0216; LVIDs: p = 0.0021; FS%: p = 0.0105). Tukey's post hoc comparisons are reported in the text. Group sizes: Control (n = 6), Saline (n = 8), Ang II (n = 12).

3.3.2 Assessment of collagen content and fibrosis progress.

Initially, Picrosirius red staining was attempted to assess collagen deposition in cardiac tissue sections across all experimental groups. However, the staining quality was inconsistent, making it challenging to obtain reliable and reproducible results. Given the study timeline and the limited availability of heart tissue samples, an alternative approach was pursued to avoid unnecessary sample depletion. Masson's trichrome staining was subsequently performed, and it yielded consistent and reproducible results on the first attempt. Therefore, this method was chosen for collagen quantification, allowing for a complete and standardized analysis across all samples. Although Picrosirius red staining was not used for the final analysis, a preliminary attempt (n=2 per group) was documented, and collagen percentage quantification from this attempt is presented for reference (Figure 3.5).

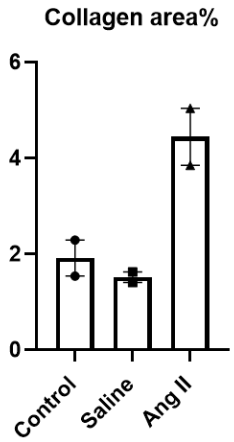

Figure 3.5: Representative images of Picrosirius red-stained cardiac sections from Ang II, saline, and control groups.
All sections are stained with picrosirius red and viewed at the same magnification (×40) using standard light microscopy (EVOS). The accompanying bar graph quantifies collagen percentage across groups (*n*=2 biological replicate per group), demonstrating the preliminary assessment. Figures represent areas randomly selected from the full heart section (not shown).

3.3.2.1 Collagen deposition in perivascular and interstitial regions

Collagen content was assessed in perivascular and interstitial regions of the left ventricle after 28 days of Ang II infusion. Representative trichrome-stained images are shown in Figure 3.6.

Perivascular collagen area was significantly increased in Ang II rats (7.87 ± 1.93%) compared with Control (3.76 ± 0.56%) and Saline (4.34 ± 0.96%) groups (one-way ANOVA, $p = 0.0026$). Tukey's test confirmed significant differences between Ang II vs. Control (**$p = 0.0066$) and Ang II vs. Saline (**$p = 0.0094$), whereas Control vs. Saline was not significant ($p = 0.8732$).

Interstitial collagen was also significantly elevated in Ang II rats (7.30 ± 1.39%) compared with Control (4.26 ± 0.70%) and Saline (4.53 ± 1.14%) (ANOVA, $p = 0.0078$). Tukey's test showed Ang II differed from Control (*$p = 0.0160$) and Saline (*$p = 0.0169$), while Control vs. Saline remained non-significant ($p = 0.9506$).

Together, these results confirm that collagen accumulation was significantly greater in Ang II rats compared with both Control and Saline groups, while no trend was observed between Control and Saline (Figure 3.6).

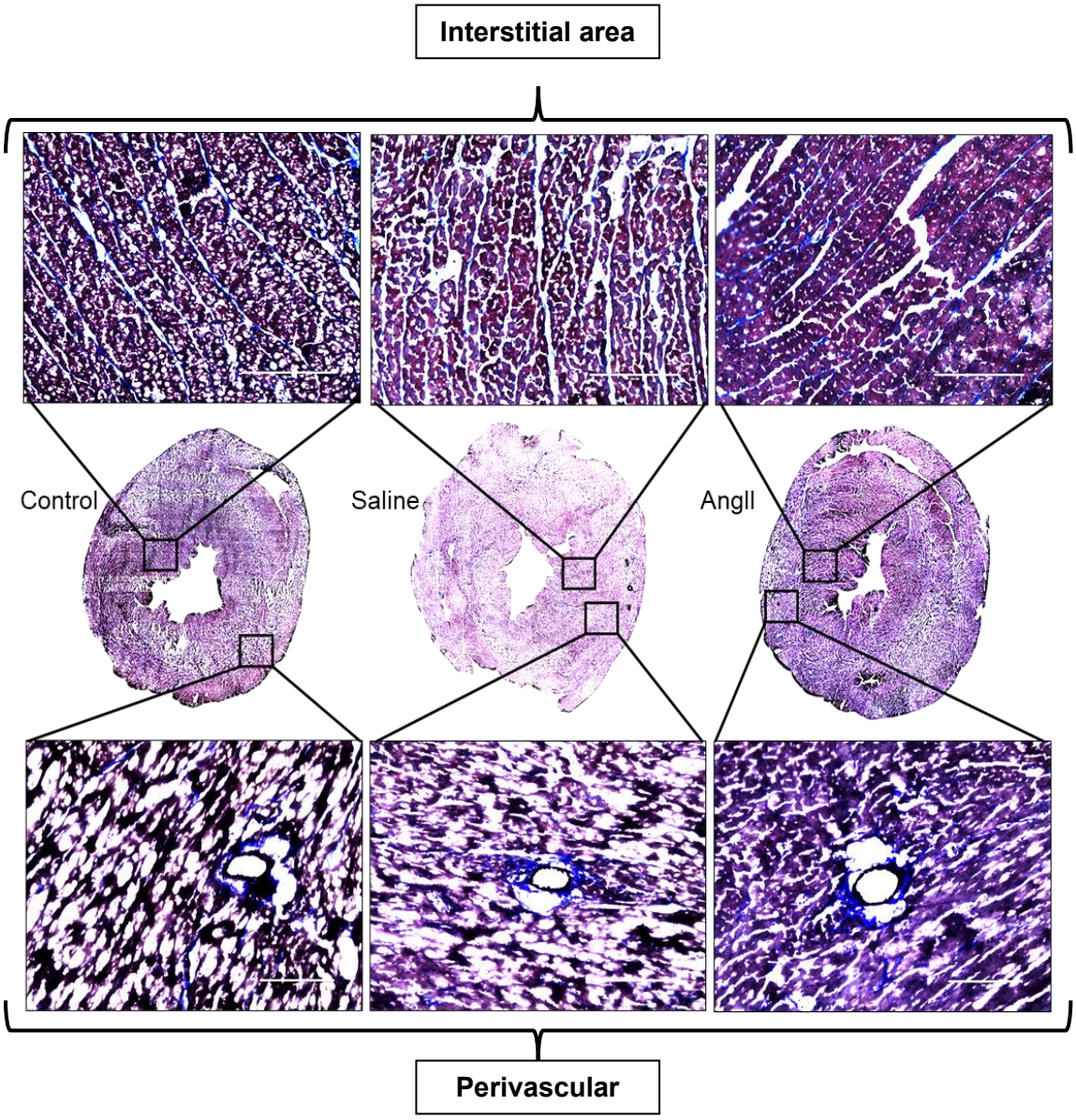
Interstitial area
Control
Saline
AngII
Perivascular

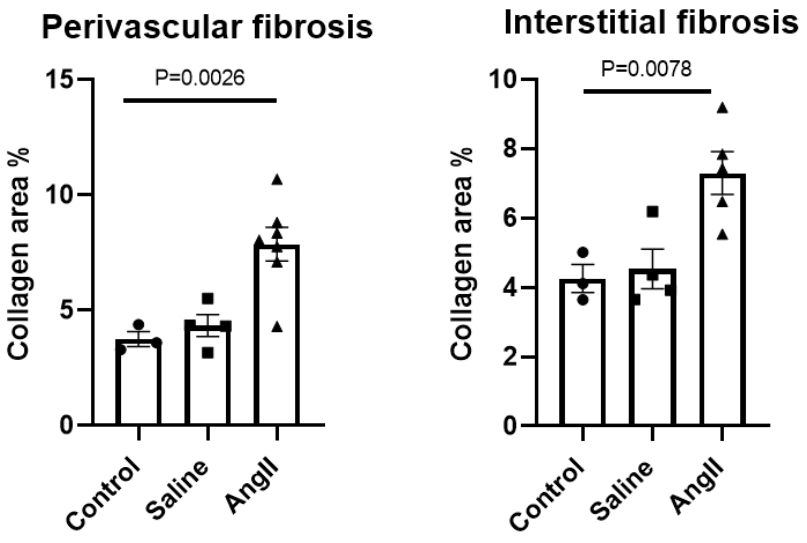

Figure 3.6: Collagen deposition in perivascular and interstitial regions of cardiac tissue.
Masson's trichrome staining shows collagen in blue. Representative sections are displayed at 10× (whole section) and 20× (higher magnification) from Control, Saline, and Ang II groups. Quantification confirmed significantly higher collagen area (%) in Ang II rats compared with both Control and Saline groups (perivascular: ANOVA p = 0.0026; interstitial: ANOVA p = 0.0078, Tukey post hoc in text). Scale bar = 200 μm.

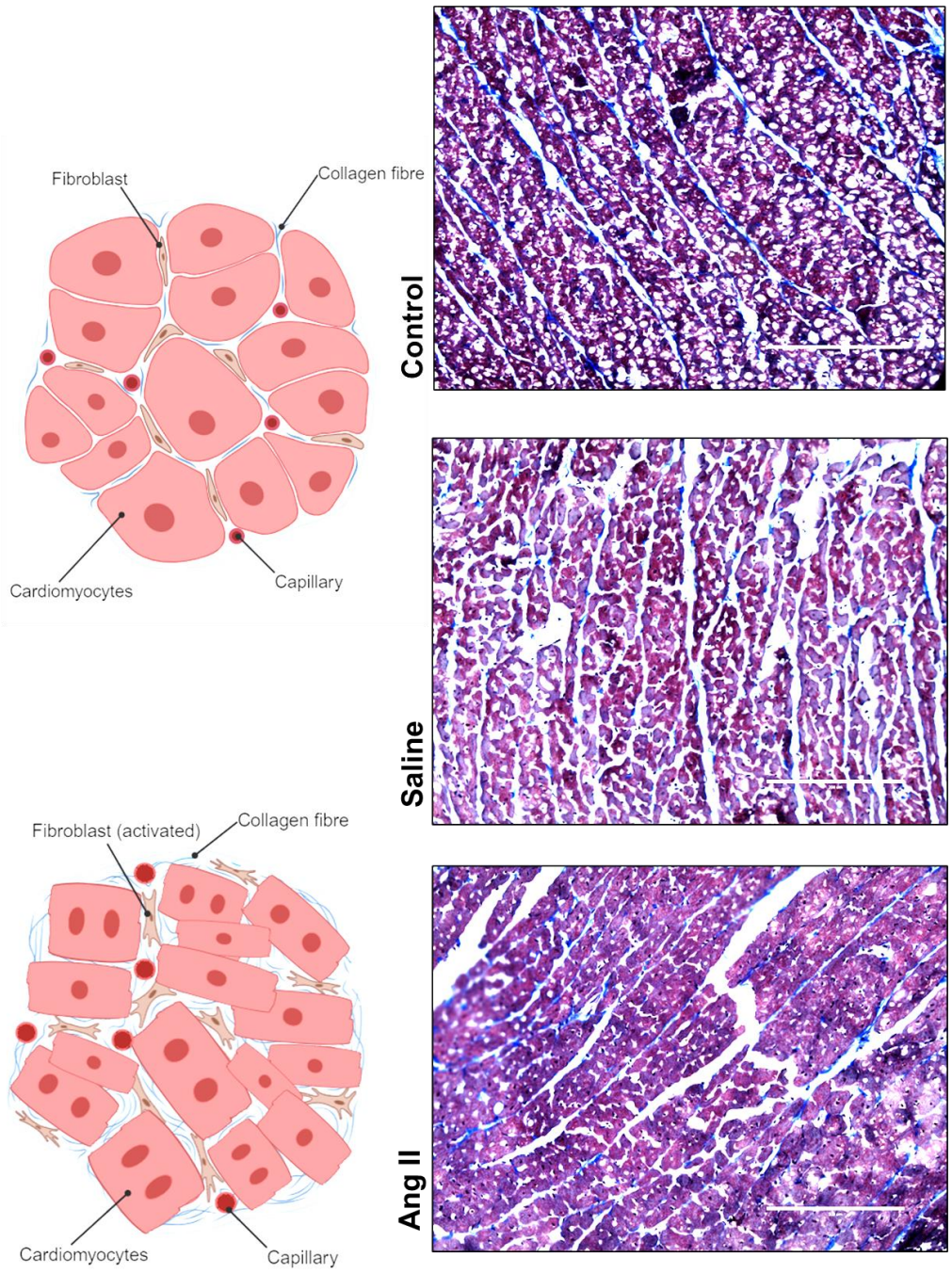

Figure 3.7: Illustration of cardiomyocyte hypertrophy in Ang II, compared to saline and control groups.
Representative images show cardiomyocyte cross-sectional area differences among groups, highlighting hypertrophic changes in the Ang II-treated group compared to saline and control groups. Cardiomyocyte enlargement is evident in the Ang II group, indicative of pathological remodelling associated with chronic hypertension. Scale bar 200um. Created by Biorender.

3.3.3 HMGB1 association in cardiac remodelling in Ang II induced chronic hypertension

3.3.3.1 HMGB1 and high-molecular-weight isoforms detected in cardiac tissue of Ang II-induced hypertensive rats

Western blot analysis was used to assess HMGB1 expression across different cardiac chambers (left ventricle, right ventricle, left atrium, right atrium) in control, saline, and Ang II–infused rats (Figure 3.8). HMGB1 was consistently detected at ~29 kDa, and an additional high–molecular weight (HMW-HMGB1) band was observed. Quantitative analysis showed no statistically significant differences in HMGB1 or HMW-HMGB1 expression between groups (all ANOVA p-values > 0.1). A trend toward higher HMW-HMGB1 in the right atrium of Ang II rats ($p = 0.1363$) was noted but did not reach significance.

These findings indicate that HMGB1 is expressed in both monomeric and higher–molecular weight forms in cardiac tissues, but without significant group-dependent changes.

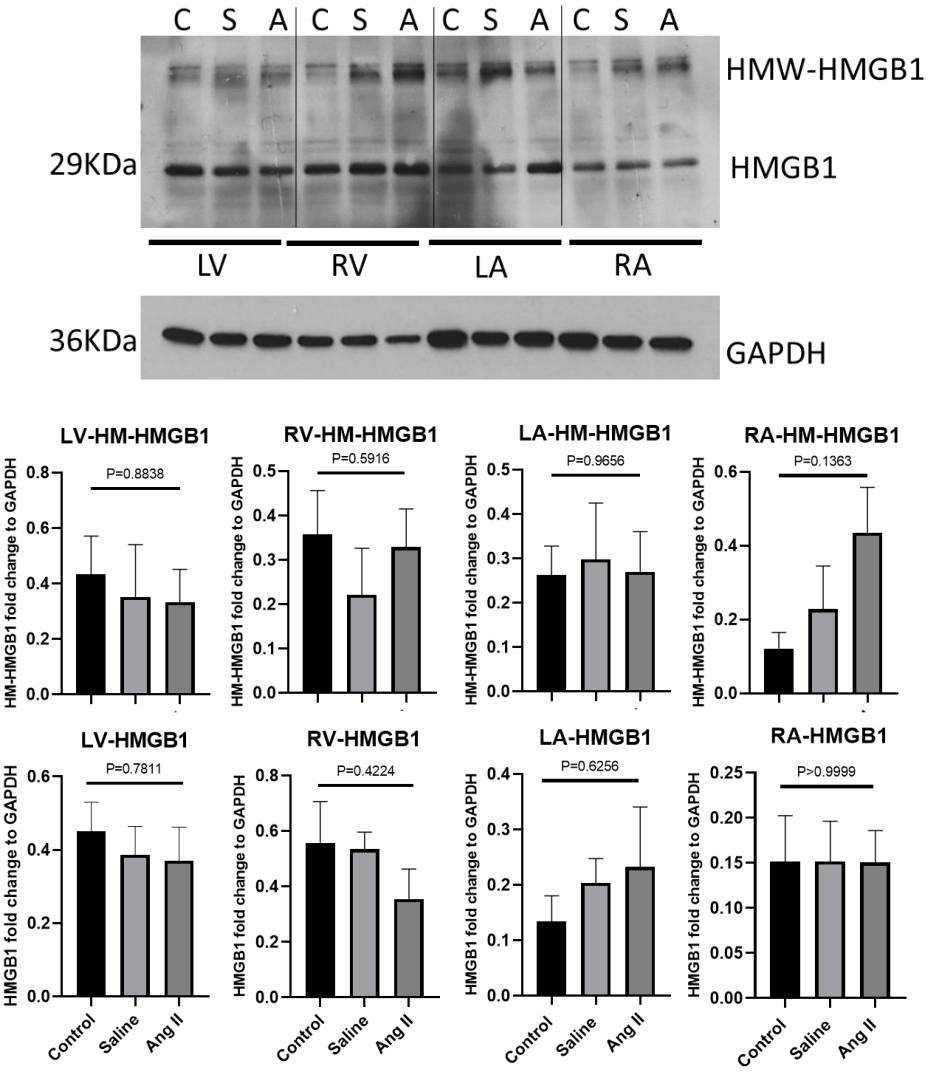

Figure 3.8: HMGB1 expression in different cardiac regions of control, saline, and Ang II groups. Western blots show monomeric HMGB1 (~29 kDa) and high-molecular weight HMGB1 (HMW-HMGB1). Data represent n = 4 biological replicates per group. Quantification graphs show fold change normalised to GAPDH. Statistical analysis by one-way ANOVA (all comparisons non-significant). Abbreviations: C, Control; S, Saline; A, Angiotensin II.

3.3.3.2 HMGB1 localisation and redistribution in Ang II–induced cardiac remodelling

Immunofluorescence staining with confocal imaging was performed on transverse heart sections from control, saline-treated, and Ang II-infused rats (Figure 3.9). HMGB1 (green) was visualised alongside Rhodamine–phalloidin F-actin (red) and DAPI-stained nuclei (blue).

Panel A shows representative localisation of HMGB1 across the three groups. In control and saline hearts, HMGB1 was mainly observed in the nuclear region, whereas Ang II-treated hearts displayed a broader distribution with areas of increased cytoplasmic signal. This qualitative shift indicates altered HMGB1 localisation under hypertensive stress.

Panel B presents quantitative analysis of HMGB1 expression, measured as corrected total cell fluorescence (CTCF). Mean fluorescence intensity was significantly different among groups (one-way ANOVA, $p = 0.0163$). Values were Control 199,366 ± 22,936 a.u. ($n = 3$), Saline 176,739 ± 65,956 a.u. ($n = 4$), and Ang II 323,568 ± 82,583 a.u. ($n = 6$). Tukey's post hoc test confirmed significantly higher HMGB1 expression in Ang II compared with Saline (*$p = 0.0208$), whereas differences between Ang II and Control ($p = 0.0705$) and between Control and Saline ($p = 0.9054$) did not reach statistical significance.

Signal intensity profiling further supported these findings by highlighting stronger HMGB1 signal in selected regions of Ang II hearts compared with controls (Figure 3.10). While this analysis suggests redistribution of HMGB1, the imaging approach does not allow firm conclusions regarding nuclear versus cytoplasmic compartmentalisation.

A

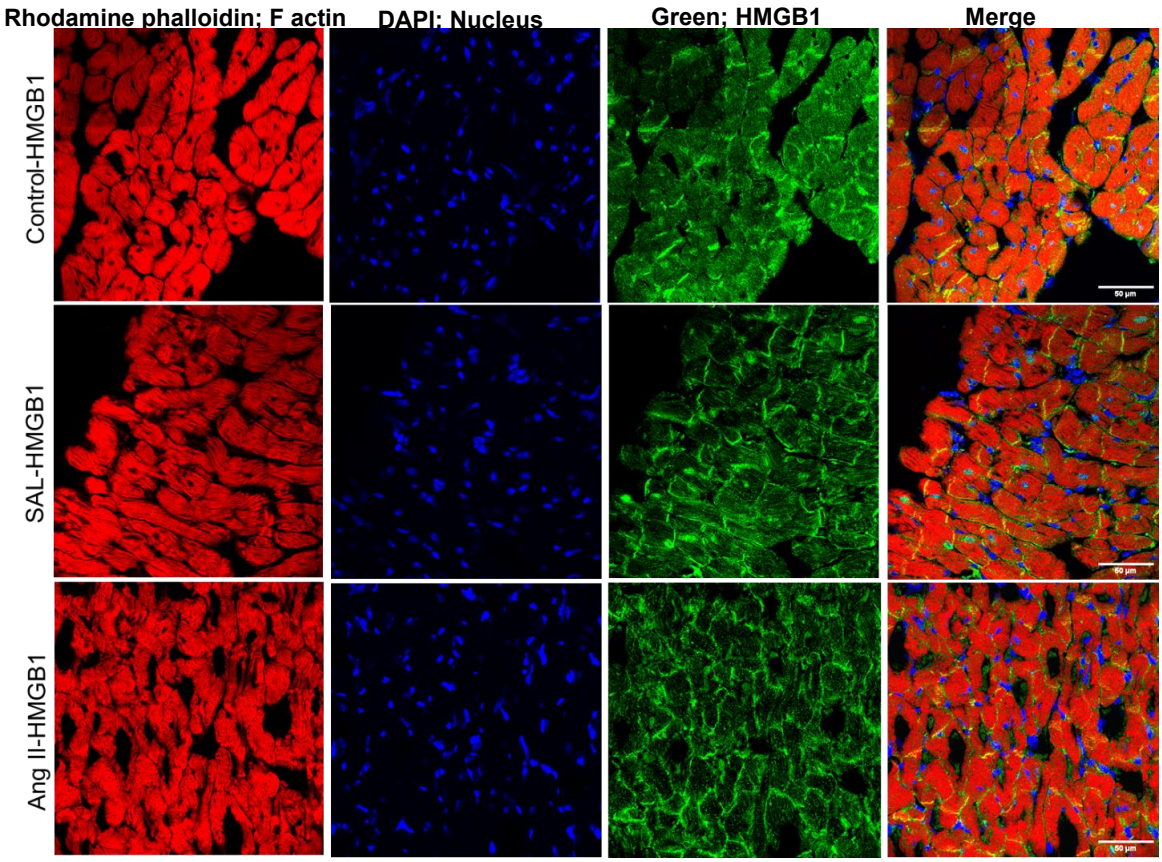
Rhodamine phalloidin; F actin
DAPI; Nucleus
Green; HMGB1
Merge
Control-HMGB1
SAL-HMGB1
Ang II-HMGB1

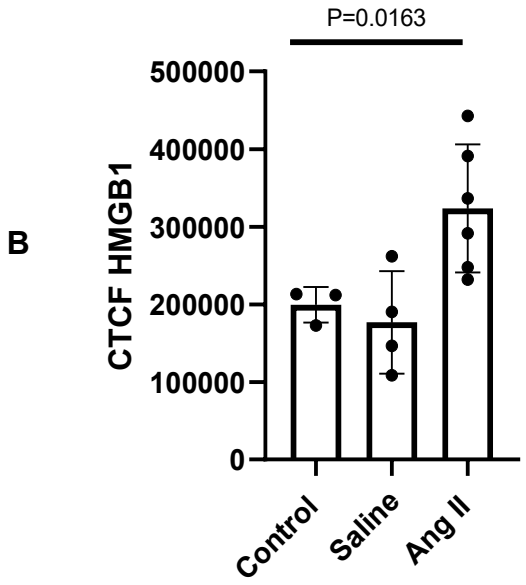

Figure 3.9: HMGB1 localisation and expression in cardiac tissue sections from Control, Saline, and Ang II groups.
(A) Indirect immunofluorescence and confocal imaging of transverse heart sections showing HMGB1 (green), F-actin labelled with Rhodamine–phalloidin (red), and nuclei stained with DAPI (blue). Representative images are shown for Control (n = 3), Saline (n = 4), and Ang II (n = 6) groups. Scale bar 50 μm. (B) Quantification of HMGB1 expression as corrected total cell fluorescence (CTCF, arbitrary units). One-way ANOVA showed a significant difference among groups (p = 0.0163). Data are presented as mean ± SD.

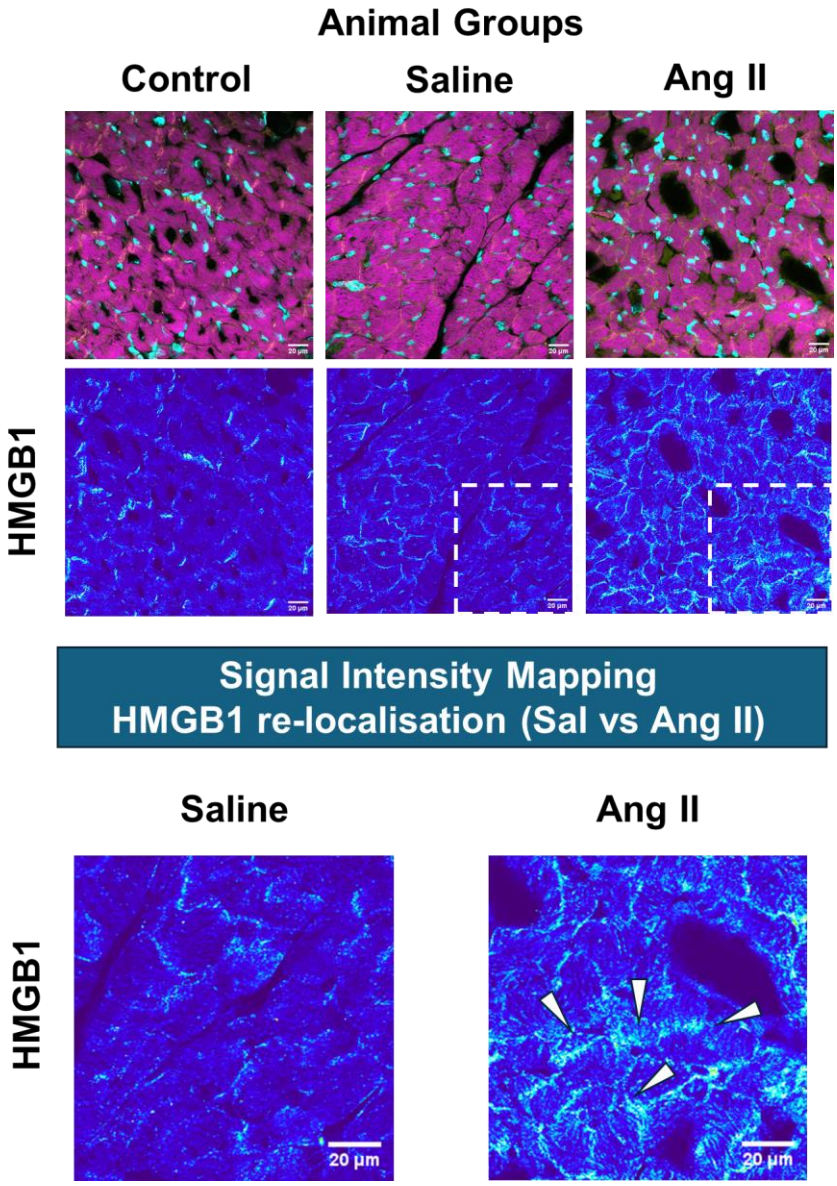

Figure 3.10: Re-localisation of HMGB1 in Ang II heart tissue compared to Control and Saline perfused groups.
Indirect immunofluorescence and confocal imaging were carried out in Control, Saline, and Ang II treated Rat. Signal intensity profiling of the HMGB1 signal across the cardiac tissue samples was carried out to visualise changes in HMGB1 localisation. Changes in HMGB1 localisation intensity profiles is shown (Lower panels, white arrows). Rhodamine phalloidin F-actin and DAPI are shown for reference (magenta/cyan, top panel). All data shown represent analysis taken from rats in control (*n*=3), Sham-Operated-Saline (*n*=4) and Ang II treated (*n*=6) groups. Scale bar 20um. Qualitative data.

3.3.3.3 Collagen with HMGB1 deposition in Ang II infused rats.

Hypertension has a chronic inflammatory status characterised as the transmigration, accumulation, and activation of inflammatory cells and pro-inflammatory cytokines [242]. Hypertension triggers numerous organ-specific alterations, one of them is left ventricular hypertrophy [243], which display an abnormal increase in left ventricular mass. This is a marker for and contributes to coronary dysfunction which lead to stroke, heart failure, peripheral arterial disease, and cardiovascular mortality in patients with hypertension. Cardiac fibrosis is a pathological process involving the remodelling of the ECM, resulting in abnormal matrix composition and quality, which ultimately impairs cardiac muscle function not only in schematic scar but also in conditions with absence of ischemia, including hypertensive heart disease and hypertrophy [244]. In a simplified view of fibrosis progression, there is a significant shift in both the relative amount and distribution of interstitial and basement membrane collagens. This process is accompanied by changes in vascularisation, immune cell infiltration, and is influenced by the specific underlying aetiologies and progression [245]. For example, collagens that are typically found around blood vessels or cells may spread into areas where they shouldn't be, contributing to stiffening and dysfunction of the heart muscle.

Therefore, HMGB1 as DAMPs molecule released under cellular stress or recurring tissue injury, it was assessed in heart section of Ang II using indirect immunofluorescence staining. Trichrome staining used to compare with collagen distribution and deposition in Ang II infused rats (see Figure 3.11).

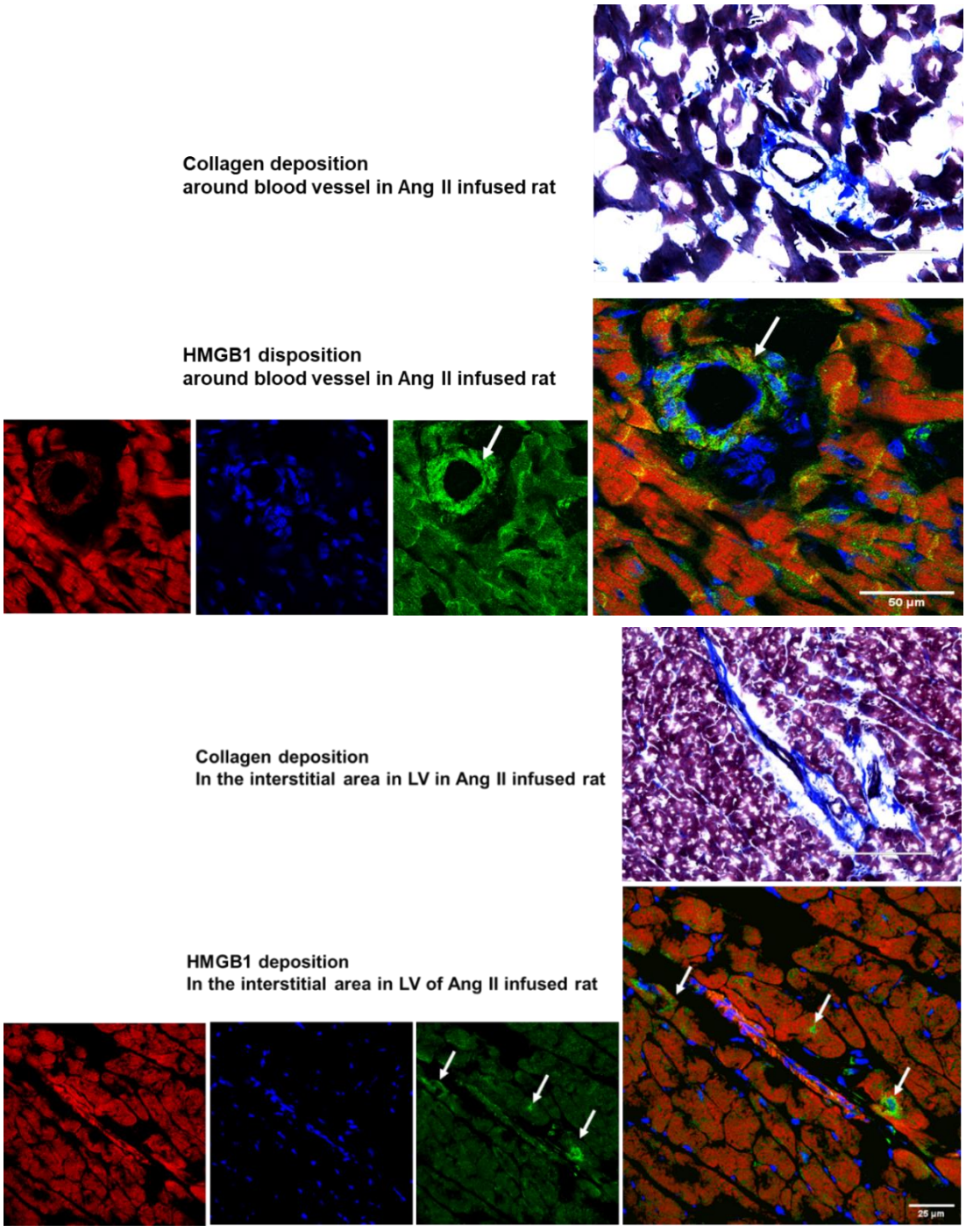

Figure 3.11: Histological analysis of collagen deposition and histochemical analysis of HMGB1 localisation.
Top panel: Masson's trichrome staining to assess the collagen deposition which indicated tissue fibrosis in blue of both perivascular and interstitial area (Scale bar: 200µm). Bottom panel: representative images of HMGB1 localisation in Ang II infused rat (scale bar 25-50um) (Qualitative data).

Given that we observed a re-localisation of HMGB1 in cardiac tissue, where in addition to an overall increase in total expression, its cytosolic distribution shifted towards the cell membrane. This finding suggested that HMGB1 may be actively mobilized for extracellular release. Given HMGB1's known role in inflammatory signalling and its ability to be secreted via non-classical pathways, we hypothesised that extracellular vesicles (EVs) could serve as a key mechanism for its release. We examined EVs isolated from control rat serum.

3.3.4 Analysis of EVs released from the control Rat serum

In this project, EVs of healthy, control rats were examined to determine their sizes. For polydispersity assessment, the Z-Ave (average particle size) was paired with the Polydispersity Index (PdI) to evaluate the sample heterogeneity. The PdI is a measure of the heterogeneity of particle sizes in a sample, ranging from 0 (monodisperse, uniform size) to 1 (highly polydisperse, broad size distribution).

Dynamic Light Scattering (DLS) confirmed that the EVs particles from rat serum were polydisperse (0.546 ± 0.046), ranging from 10-1000 nm in diameter, results presented at intensity and number-based distributions (%) mean diameter 408.3 nm and 27.1 nm respectively. Results suggests a broad size distribution, possibly due to the presence of different EV subtypes. Unfortunately challenges in isolating whole blood from the Ang II rodent model meant that we were unable to compare EV’s between control and Ang II groups.

Whilst EV isolation from control rat serum and DLS characterisation was successful (Figure 3.12), challenges were faced when attempting to isolate whole blood from Ang II rats. We were therefore unable to characterise HMGB1 expression in rat EV lysates. Low EV protein expression and poor sample yield was a critical barrier for onwards HMGB1 experimentation to investigate secretory pathways of HMGB1 in this mode.

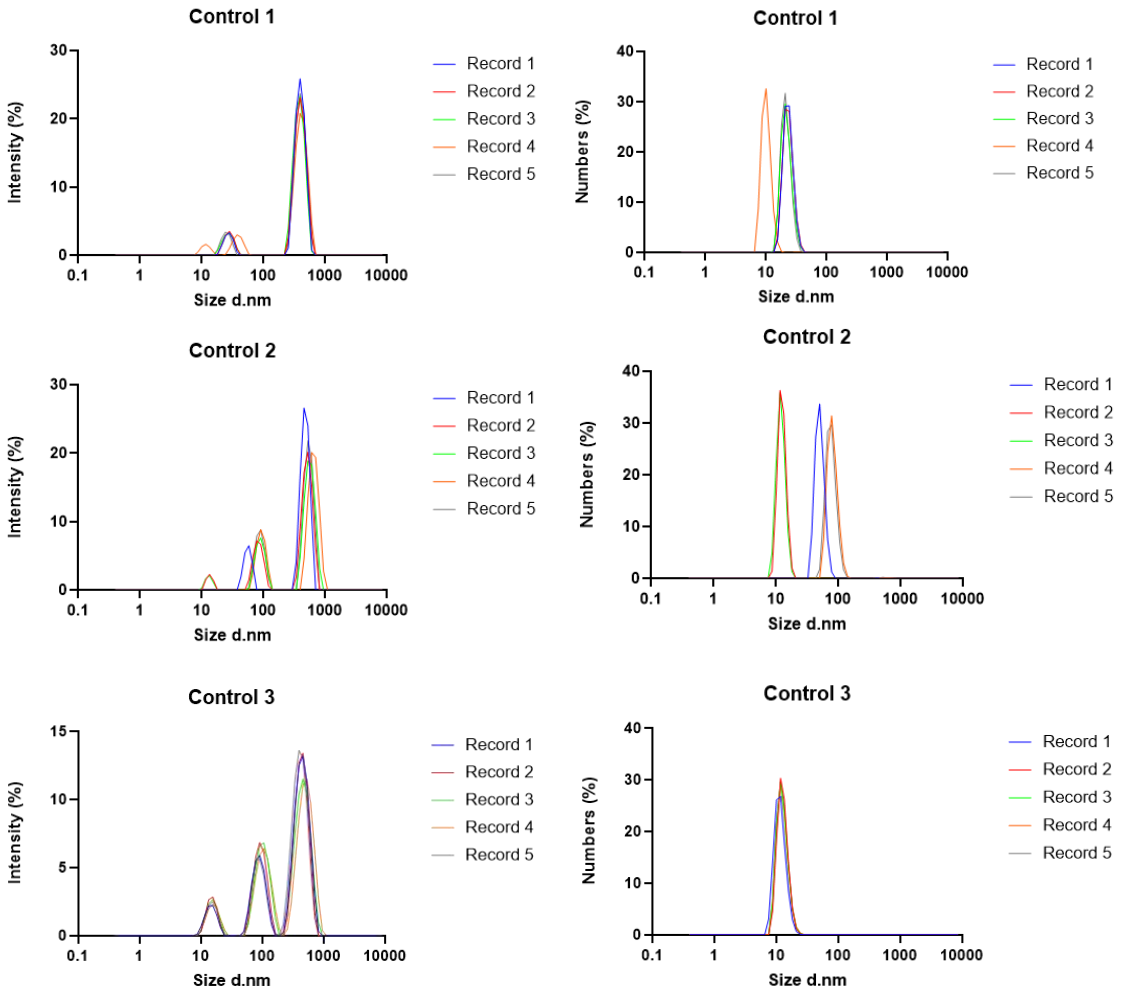

Figure 3.12: DLS analysis for EVs sizes from Rats control group serum represent in intensity and numbers (%).
DLS analysis was performed to assess the size distribution of EVs isolated from the serum of control rats, represented in both intensity and particle number (%). The intensity-based size distribution revealed prominent peaks within the 10–1000 nm range, indicating the presence of larger EV populations contributing more to the scattering signal. In contrast, the number-based distribution showed peaks primarily within the 10–100 nm range. Experiments represent *n*=3 independent biological replicates and 5 technical records for accuracy.

Table 3.1 represent a summary of DLS zeta-sizing analysis, including Z-average (Z-ave) represent intensity distribution, polydispersity index (PdI), number distribution, and the mean of all recorded measurements. The Z-average represents the intensity-weighted mean hydrodynamic diameter of particles, while the PdI indicates the uniformity of the size distribution. The intensity distribution in the graph above reflects the proportion of scattered light from different particle sizes, whereas the number distribution accounts for the relative proportion of particles based on count rather than scattering intensity. Mean values were calculated from multiple measurements to ensure result accuracy and reliability.

Table 3.1: Dynamic Light Scattering (DLS) Analysis of Particle Size (Z-Ave), Polydispersity Index (PdI), and numbers of (EVs) Isolated Rat Blood of control Samples.

Control1	Records	Type	Z-Ave d.nm	PdI	Number d.nm
	1	Size	405.2	0.641	23.65
	2	Size	399.1	0.554	23.66
	3	Size	397	0.485	22.16
	4	Size	391.6	0.564	10.3
	5	Size	390.2	0.529	21.7
	Mean		396.6	0.555	20.29
	Std Dev		6.048	0.057	5.655
Control2	**Records**	**Type**	**Z-Ave d.nm**	**PdI**	**Number d.nm**
	1	Size	564.7	0.669	51.77
	2	Size	529.2	0.56	12.62
	3	Size	524.6	0.552	12.14
	4	Size	570.9	0.591	85.97
	5	Size	578.4	0.605	80.98
	Mean		553.6	0.595	48.7
	Std Dev		24.87	0.047	35.63
Control3	**Records**	**Type**	**Z-Ave d.nm**	**PdI**	**Number d.nm**
	1	Size	264.6	0.528	11.68
	2	Size	311.2	0.455	12.76
	3	Size	261.3	0.464	12.58
	4	Size	262.6	0.529	12.63
	5	Size	274	0.474	12.71
	Mean		274.7	0.49	12.47
	Std Dev		20.98	0.036	0.4482

Although EVs could be successfully isolated and characterised from control rat serum, attempts with Ang II serum samples were unsuccessful due to low yield and poor protein recovery. Nevertheless, the control data confirmed the feasibility of EV isolation and DLS characterisation in this model. Importantly, these findings complement the in vivo HMGB1 localisation results, where increased cytosolic redistribution in Ang II heart tissue suggested extracellular release. EVs therefore represent a plausible mechanism for HMGB1 export, providing the rationale for the subsequent use of MEG-01 cells as a surrogate system to investigate HMGB1 trafficking and release (Figure 3.13).

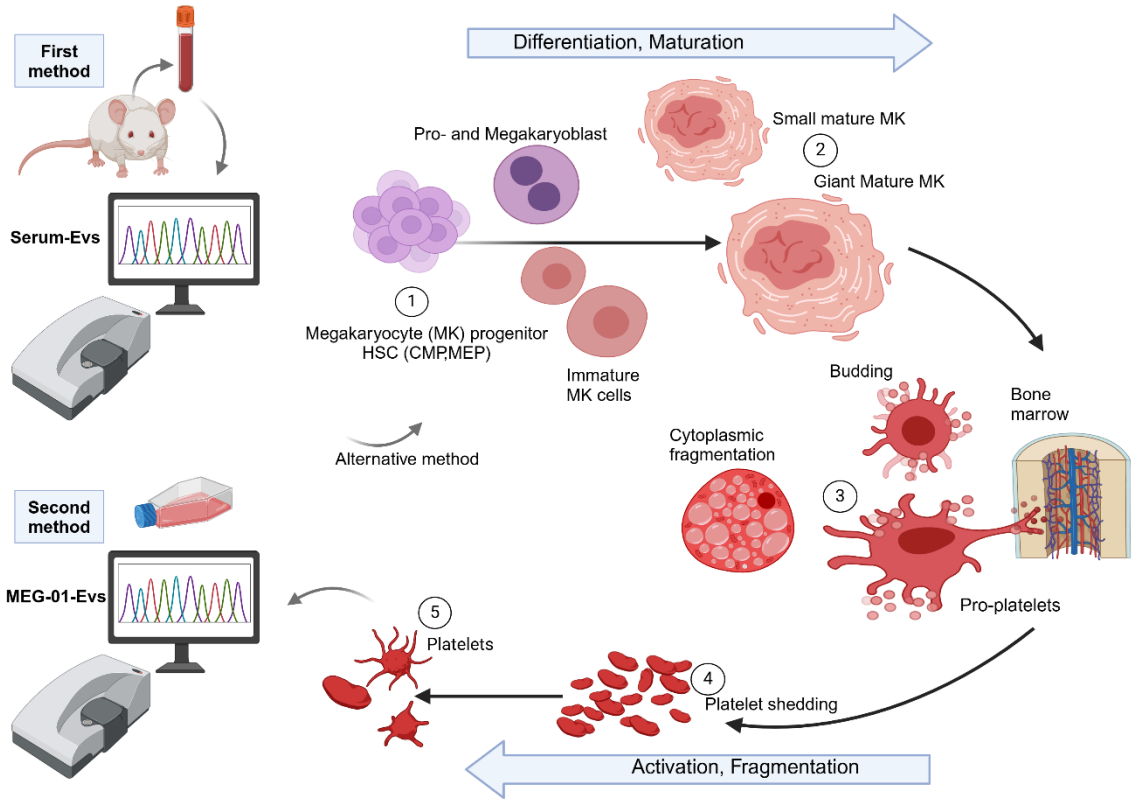

Figure 3.13: Schematic depicting stages of Megakaryocyte (megakaryopoiesis) formation and platelet release (thrombopoiesis).
HSC gives rise to the CMP, MEP and after multiple rounds of endomitosis, (2) the pro and megakaryoblast go through maturation process resulted in small or giant MK cells. (3) Mature cells transferred into cytoplasmic fragmentation or produce budding and pro-platelets through bone marrow sinusoids (4) following platelet shedding and (5) platelet releasing from the cell into circulation. Abbreviations: MK; megakaryocyte. HSC; haematopoietic stem cells. MEP; megakaryocyte-erythroid progenitor. CMP; common myeloid progenitor. Created by Biorender and adapted from [246].

3.3.5 Using the Megakaryoblastic leukaemia cell line (MEG-01) as an alternative model to investigate EV expression of HMGB1

While *in vivo* models provide critical insights into disease mechanisms, their complexity makes it challenging to isolate specific cellular contributions to disease pathology. The transition to the MEG-01 cell line allows for a more controlled investigation of HMGB1 expression, release, and EV-mediated transport without systemic influences. By using MEG-01-derived platelet-like particles (PLPs), we were able to specifically analyse HMGB1 secretory processes. The rationale for these experiments was to complement *in vivo* findings and strengthen our understanding of HMGB1's role in hypertensive cardiac remodelling.

MEG-01 cells were captured using bright-field microscopy of 500µl cells at x20 magnification to assess cell differentiation as platelets are shed from mature megakaryocytes by a series of events of platelet production. Figure 3.14 shows (A) the MEG-01 cells grow as a mixture of adherent and suspension cells at 80% confluency in full media. The blue arrows indicate mature cells with one or two lobulated nucleuses. Under the usual culture conditions, less than half of the cells adhered to the flask with an extension of pseudopods (green arrows). The yellow arrow is a good example of a nucleated giant cell with a few cytoplasmic vacuoles, cytoplasmic protrusions, and small platelet-like particles on the surface (pro-platelets). The red arrow shows the release of numerous platelet-like particles. (B) showed zoomed images of (i) large mature MEG-01 with two nucleus (ii) pseudopods formation (iii) proplatelets formation and (iv) platelets release. This MEG-01 cell differentiation events are simplified in schematic figure as shown in panel (C).

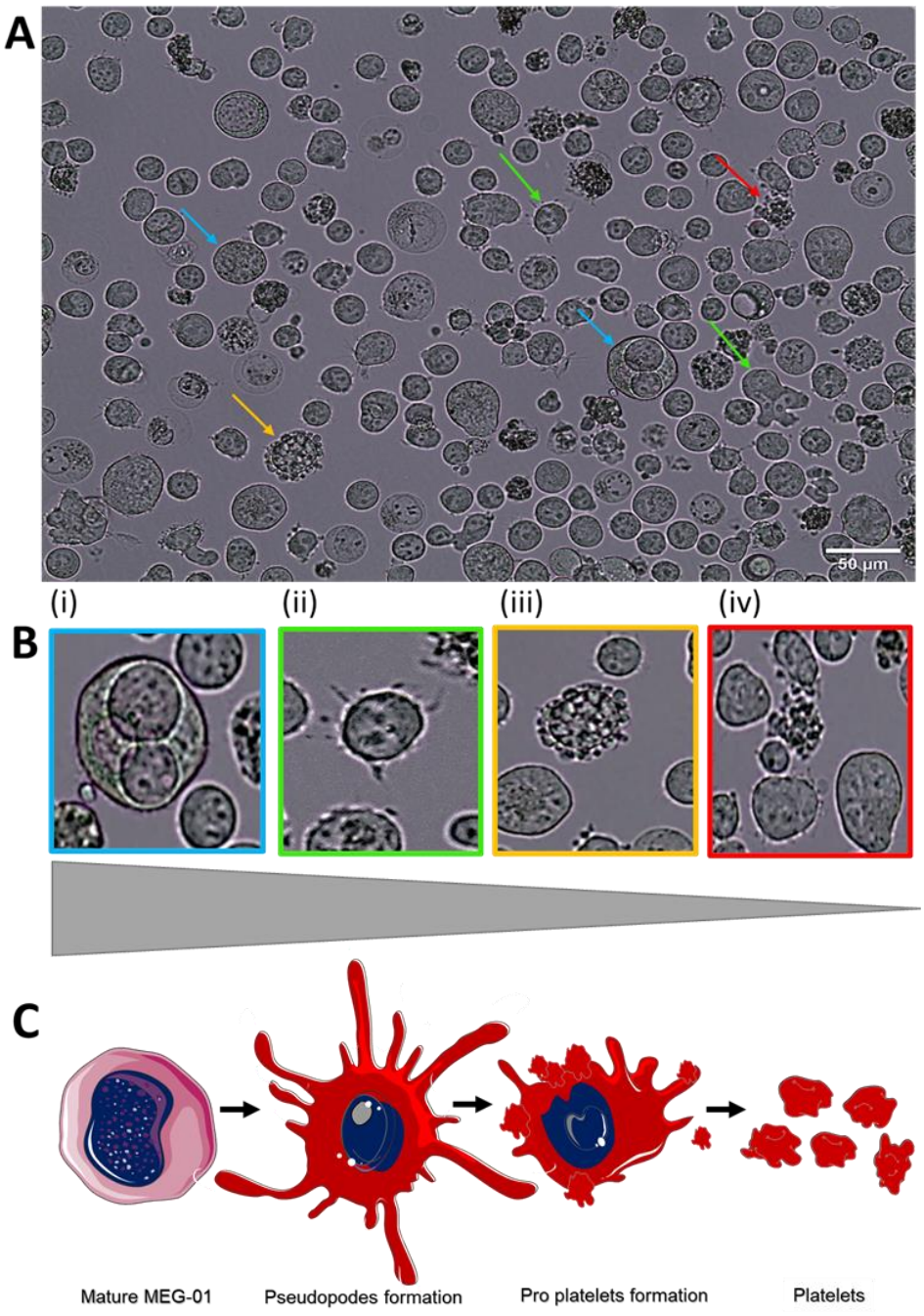

Figure 3.14: Live-cell brightfield imaging of MEG-01 cells.
(A) Cells differentiate into diverse shapes, and sizes indicated by different arrow colours. Blue arrows show different cell sizes and one with two nuclei. Green arrows show the extended shape of cells. The yellow arrow shows the cell budding of platelet-like particles on the cell surface. The red arrow shows exposed cells with platelets-like particles. (B) zoomed of diverse cell differentiation, maturation, and platelets formation. Cells were visualised by using a brightfield microscope at x20 magnification. Images are representative of 5 independent experiments. Scale bar 50um.

Figure 3.15 shows different characterisation of MEG-01 morphology taken in time-lapse video captured every 10min for 60 min duration at 10x magnification by using bright field microscope. Cells were visualised without stimulation only grown in full media. (A) Most cells are typically spheroid in appearance however the ability of the cells to become adherent over time was captured (yellow arrow). By 60 minutes (B, white dashed frame) MEG-01 cell shape changed from round into cell with an extension of pseudopods, with an adherent phenotype.

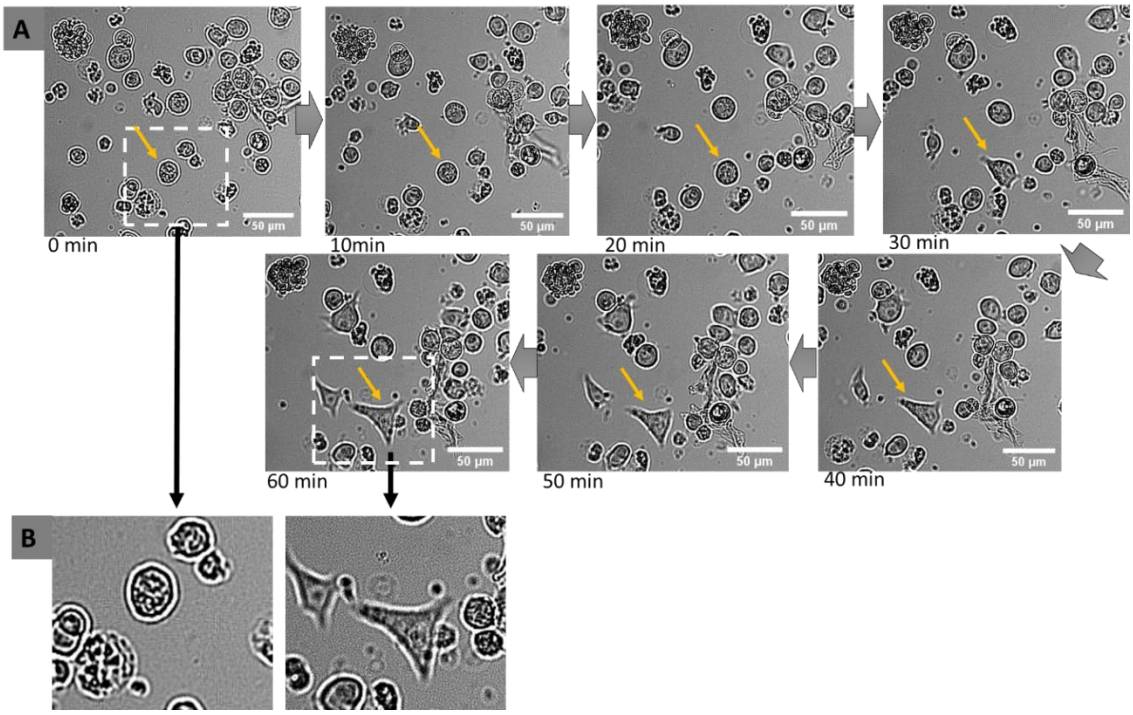

Figure 3.15: Characterisation of MEG-01 cell morphology over time.
(A) images captured every 10 minutes over 60 minutes duration. (B) zoomed images of the start time zero minute and the end time 60 minutes. By using a brightfield microscope at x10 magnification, representative of 5 independent experiments. Scale bar size 50µm and 10µm zoomed.

Immunofluorescence microscopy was used to detect the morphological changes in the MEG-01 cells membrane. Figure 3.16 shows (A) DAPI staining labelled the nucleus with blue colour, and DiI membrane localisation is indicated in magenta. (B) The unique demarcation membrane system of the MEG-01 cell shows the extension of pseudopods (zoomed shown in C). Cells were visualised at 43x (oil) magnification using confocal microscopy. These budding events are typically observed during pro-platelet formation and release and represent the dynamic processes these cells undergo.

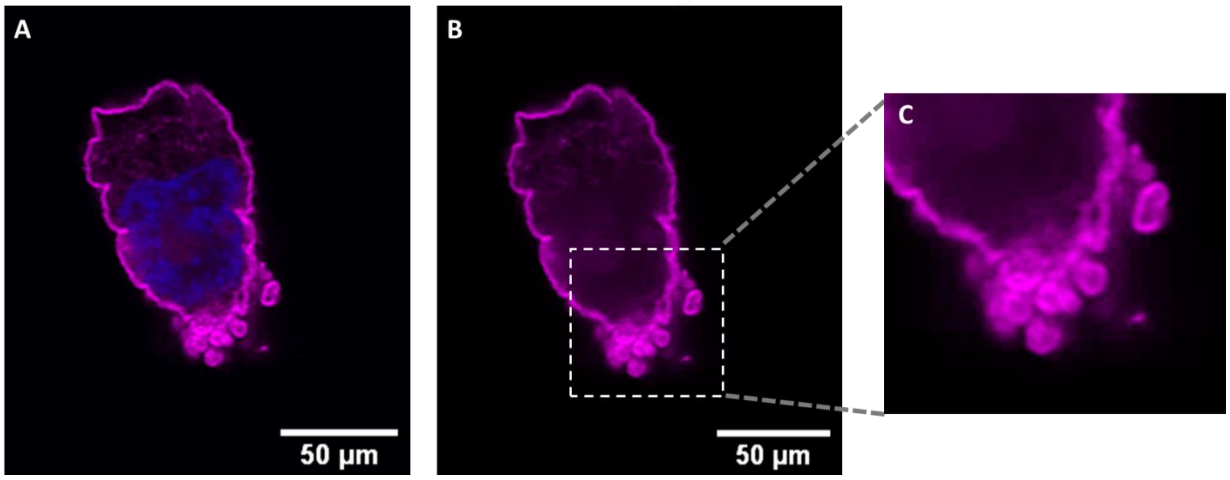

Figure 3.16: Immunofluorescence staining of the MEG-01 cell membrane.
Live cell staining of the MEG-01 cell membrane (magenta), DAPI labelled the nucleus (blue). (B) The cell membrane with extension of pseudopods. (C) in zoomed capture. Cells were visualised at 43x (oil) magnification using confocal microscopy, with images representative of 5 independent qualitative experiments. Scale bar 50µm.

3.3.5.1 MEG-01 Derived Extracellular Vesicles (EVs)

MEG-01 cell line terminally differentiates to release platelets from long cytoplasmic processes termed proplatelets that release platelets like particles. Three different populations of MEG-01 cultures are found including nucleated floating, nucleated attached, and platelet-like particles. As PLP are very small particles, DLS analysis was used for particles size detection.

EVs isolation was carried out by multiple ultracentrifugation and the supernatant was collected for further analysis. There are typically two different types of analysis performed on the isolated vesicles, which is physical and chemical/biochemical/compositional analysis. Here we used the physical analysis DLS, which provides insight to particle size and concentration. EVs are small (0.03–5 μm in diameter) and are divided into subtypes including micro-vesicles (MVs), exosomes, and apoptotic bodies [213]. The standard size distributions of EVs were obtained using the nanoparticle tracking analysis of dynamic light scattering. Analysis showed each sample represented in intensity % and numbers % (Figure 3.17) confirmed that the EVs particles from MEG-01 supernatant were polydisperse (0.808± 0.085 mean/SD), results presented at intensity and number-based distributions % mean diameter 377 nm and 223 nm respectively.

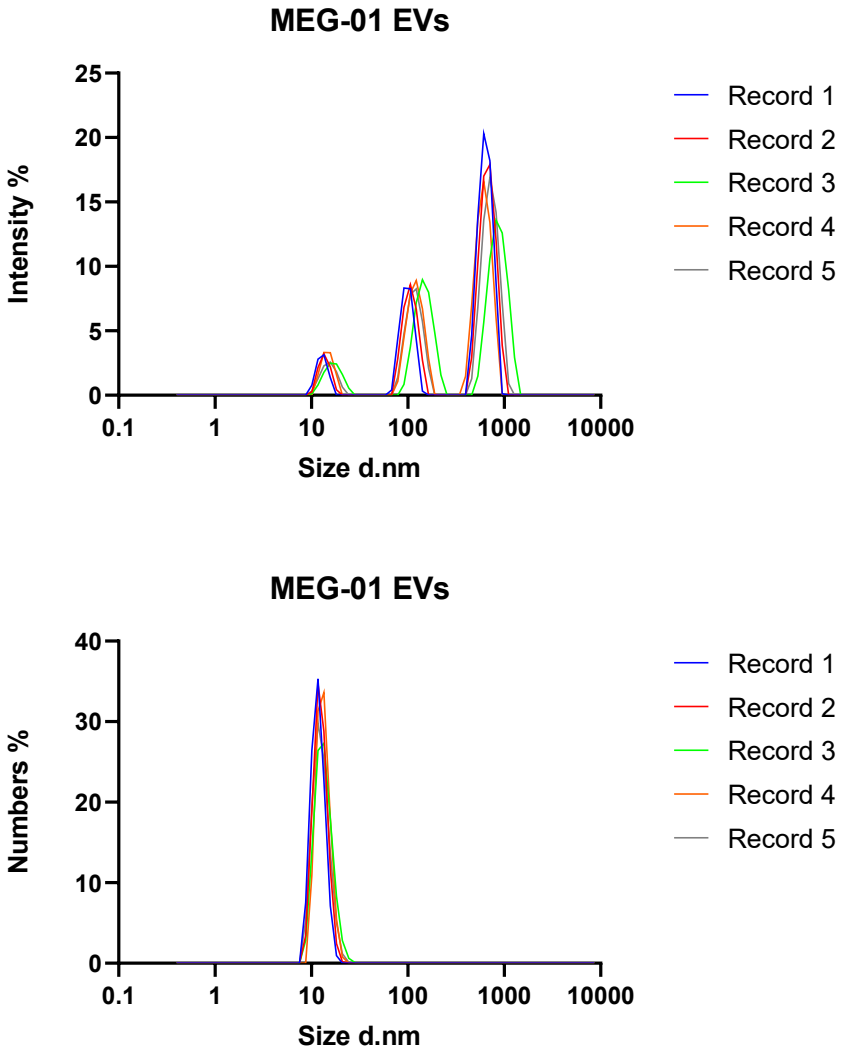

Figure 3.17: Dynamic Light Scattering (DLS) measurements of extracellular vesicles (EVs) isolated from MEG-01 cells.
DLS measurements were performed to determine the size distribution of EVs derived from MEG-01 cells. The figure shows EV populations represented by both intensity and number (%) distributions. Consistent peaks were observed in the 10–1000 nm range for intensity measurements and in the 10–90 nm range for number-based distribution, indicating a predominant presence of smaller EVs despite the greater scattering contribution from larger particles. Data are presented from *n* = 3 independent technical replicates and 5 records for technical accuracy.

Table 3.2 presents a summary of DLS zeta-sizing analysis for MEG-01 cells, including Z-average (Z-ave), which represents the intensity distribution, polydispersity index (PdI), number distribution, and the mean of all recorded measurements. The Z-average reflects the intensity-weighted mean hydrodynamic diameter of the particles, while the PdI indicates the uniformity of the size distribution. The intensity distribution in the graph above illustrates the proportion of scattered light from particles of varying sizes, whereas the number distribution represents the relative proportion of particles based on count rather than scattering intensity. Mean values were calculated from multiple measurements to ensure accuracy and reliability of the results.

Table 3.2: Dynamic Light Scattering (DLS) Analysis of Particle Size (Z-Ave), Polydispersity Index (PdI), numbers of EVs Isolated from MEG-01 Cells

MEG-01 1	Record	Type	Z-Ave d.nm	PdI	Number d.nm
	1	Size	781.3	0.691	302
	2	Size	836.5	0.739	4.425
	3	Size	676.5	0.541	371.3
	4	Size	764.6	0.647	5.438
	5	Size	771	0.608	376.2
	Mean		766	0.645	211.9
	Std Dev		57.54	0.076	191.2
MEG-01 2	**Record**	**Type**	**Z-Ave d.nm**	**PdI**	**Number d.nm**
	1	Size	713.1	0.641	293.2
	2	Size	796.7	0.597	9.161
	3	Size	755.9	0.568	360.6
	4	Size	693.1	0.426	436.7
	5	Size	732.5	0.416	486.7
	Mean		738.3	0.53	317.3
	Std Dev		40.1	0.103	187.3
MEG-01 3	**Record**	**Type**	**Z-Ave d.nm**	**PdI**	**Number d.nm**
	1	Size	942.9	0.57	0.6739
	2	Size	825.7	0.613	0.6863
	3	Size	975.2	0.75	307.9
	4	Size	830.7	0.643	0.7864
	5	Size	1031	0.726	391.4
	Mean		921.1	0.66	140.3
	Std Dev		90.49	0.076	193.4

Immunofluorescence microscopy was used to detect the HMGB1 expression and localisation in the MEG-01 cells. Figure 3.18 shows (A) DAPI staining labelled the nucleus with blue colour, DiI membrane localisation is indicated in magenta and the HMGB1 stained with green. (B) The unique demarcation membrane system of the MEG-01 cell shows the extension of pseudopods and (C) the evidence of HMGB1 expressed in the cargo indicated in green. Cells were visualised at 43x (oil) magnification using confocal microscopy. These budding events are typically observed during pro-platelet formation and release and represent the dynamic processes these cells undergo.

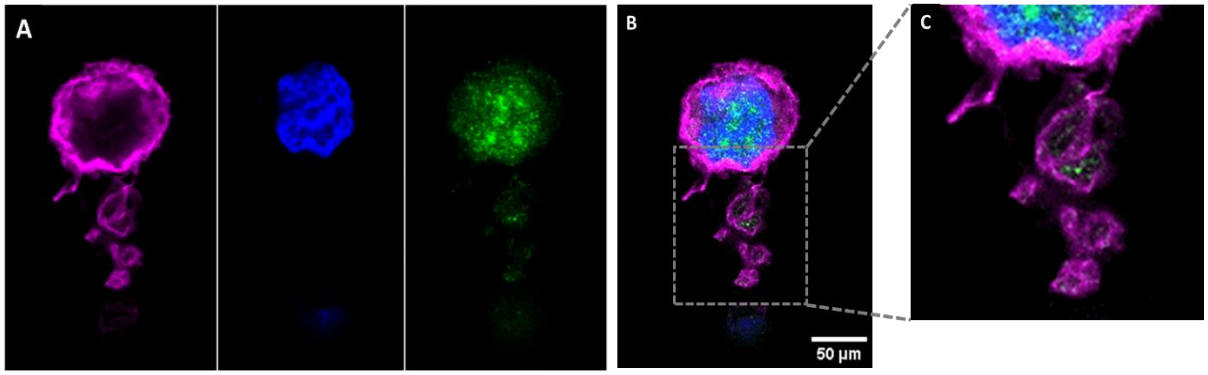

Figure 3.18: **HMGB1 expression in MEG-01 cells and HMGB1 localisation in 'pro-platelet's.** Live cell staining of (A) the MEG-01 cell membrane (magenta), and DAPI labelled the nucleus (blue) and HMGB1 in green. (B) Dashed frame showed cell membrane extension of pseudopods and the present of HMGB1 in the cargo. (C) zoomed capture. Cells were visualised at 43x (oil) magnification using confocal microscopy. Scale bar 50µm. (qualitative data).

3.3.5.2 Active release of HMGB1 in MEG-01 cells

Thrombin, a key serine protease in the coagulation cascade, is known to activate platelets and megakaryocytes, EV release. Given its role in cellular activation and vesiculation, we investigated whether thrombin stimulation of MEG-01 cells could influence HMGB1 release in these cells. Changes in HMGB1 expression in MEG-01 cell (0.03 $x10^6$cells) upon thrombin (1U/ml) treatment (0-120 minutes) was assessed by Western blotting and by measuring the intensities of the immunoreactive bands at 29kDa, as shown Figure 3.19. Thrombin activating peptide increased HMGB1 expression in MEG-01 cells 15-minute post-treatment (1.222±0.035 fold compared to Tubulin p=0.0035, n=5). Extracellular HMGB1 also was detected in the cell supernatant with variant expression. Unstimulated cells (0 minutes) were used as control. Tubulin was used for protein expression quantification. An increase in HMGB1 release was observed after 5 minutes of thrombin treatment.

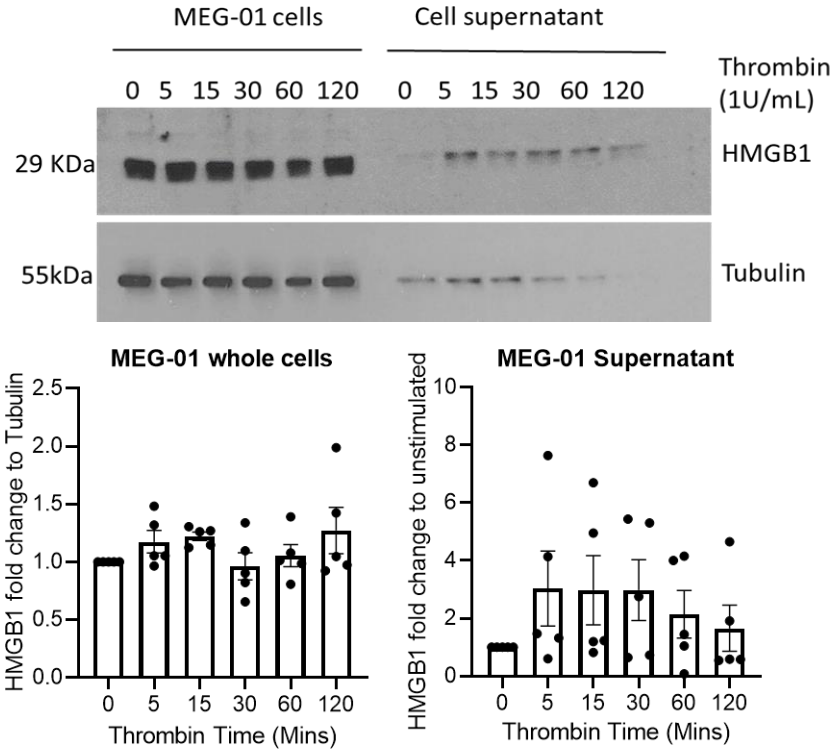

Figure 3.19: Thrombin-HMGB1 release from MEG-01 cells.
Quantitative immunoblotting of time course (0-120 mins) thrombin (1U/ml) treatment. HMGB1 fold change to tubulin for MEG-01 cells, HMGB1 fold change to unstimulated cells for MEG-01 supernatant. All experiments represent *n*=5 independent technical replicates.

3.4. Discussion

3.4.1 Chronic hypertension and hypertrophy following Ang II induction

In this project, an Ang II-induced chronic hypertension model was successfully established in male rats, representing pre-HF hypertrophy. Elevated blood pressure (Figure 3.2) and increased HW/BW ratio (Figure 3.3) confirmed hypertrophy, while echocardiographic parameters (LVIDd, LVIDs, FS%) showed preserved systolic function (Figure 3.4). This indicates structural, but not functional, remodelling consistent with early hypertensive heart disease [247]. Similar adaptive responses, where LVH maintains cardiac output under pressure overload, have been reported in both experimental and clinical settings [248]. Clinical and animal studies have shown that cardiac remodelling in response to pressure overload is more favourable in females than in males, with females exhibiting less fibrosis, left ventricular dilation, and dysfunction [249–252]. Because of these sex differences in cardiac remodelling, most researchers focus on using male mice to investigate the mechanisms underlying pressure overload–induced cardiac hypertrophy and HF.

In this project, both perivascular and interstitial fibrosis were significantly increased in Ang II-infused rats compared with control and saline groups, supporting their role as key pathological features of hypertensive cardiac remodelling (Figure 3.6). Cardiac remodelling progression cause fibrosis which characterised by the excessive deposition of ECM proteins, primarily collagen fibres, in the interstitium and perivascular areas, is a critical pathological response to chronic inflammation [253]. In fibrotic tissue, the most consistent results are found for the two markers, collagens I and III, the main forms of collagen in the cardiac ECM [254]. A human study examined different cardiovascular non-ischemic heart failure and found that interstitial collagen volume fraction was similar among the groups [255]. In addition, perivascular fibrosis ratio was higher in the hypertrophic

cardiomyopathy and hypertensive heart disease groups. Perivascular fibrosis is associated with the impairment of coronary blood flow. This suggests that hypertension which leads to hypertrophy have different function of perivascular and interstitial fibrosis types. As targeting perivascular fibrosis to improve coronary microcirculation impairment that could be caused by pro-inflammatory accumulation and secretion into the circulation.

In this project, the pro-inflammatory HMGB1 localisation was examined by indirect immunofluorescence dyes and was significantly higher in Ang II infused rats compared to saline and control groups (see Figure 3.9). In addition, HMGB1 was depositional with collagen of perivascular area (figure 3.11). The abnormal accumulation of extracellular matrix within the heart, cardiac fibrosis, is linked to almost all forms of heart disease, including hypertensive condition. Hypertension induces perivascular and interstitial fibrosis in the heart, resulting in arterial stiffness, diastolic dysfunction, and myocardial hypertrophy [37].

Cardiac fibroblasts produce MMPs that degrade the ECM and collagen deposition facilitating injured region progression [256]. This study presented that myofibroblast specific heat shock protein (Hsp)47 deletion in mice showed reduced cardiac hypertrophy after TAC compared with control which assessed by echocardiography, cardiomyocyte area measured in histological heart sections and induction of hypertrophic marker genes. These results suggest that inhibition of collagen production with ECM accumulation from cardiac myofibroblasts reduces the cardiac hypertrophic response with pressure overload stimulation by inhibiting cellular stress molecules. Cardiac remodelling triggers innates immune signalling, while the secretion of pro-inflammatory molecules can promote cell infiltration/differentiation into the damaged area associated with collagen deposition. In a study, cardiac fibroblasts and myofibroblasts were proliferation, migration, and expression MMP and TIMP after HMGB1 stimulus [257]. TIMPs, the tissue inhibitors of MMPs are important regulators of ECM turnover, tissue remodelling, and cellular behaviour. Plasma multi-biomarker panel consisting of

increased MMP7, MMP9, TIMP1 predicted the presence of left ventricle hypertrophy [258].

3.4.2 HMGB1 expression and localisation in Ang II hearts

Extracellular release of HMGB1 into the circulation has been recognised as a key contributor to cardiovascular disease progression, primarily through nuclear-to-cytoplasmic translocation and subsequent secretion as a danger signal (DAMP) [159]. Inflammation is a central feature of pressure overload–induced cardiac hypertrophy and remodelling, although the exact mechanisms linking HMGB1 to this process are still under investigation.

In this project, both the canonical 29 kDa HMGB1 and higher molecular weight forms (HMW-HMGB1) were detected in cardiac tissue extracts (Figure 3.8). Interestingly, HMW-HMGB1 was observed in saline and Ang II groups but absent in non-operated controls, raising the possibility that surgical stress itself may trigger certain post-translational modifications. This is consistent with previous reports that sham or surgical procedures can alter systemic inflammatory signalling and proteomic signatures, even in the absence of the primary insult [259,260].

Indirect immunofluorescence analysis further demonstrated that HMGB1 expression and localisation were altered in Ang II-treated animals, with evidence of increased cytoplasmic redistribution (Figures 3.9–3.10). Such nuclear-to-cytoplasmic translocation is a hallmark of HMGB1 activation and often precedes extracellular release. Supporting our findings, in vivo silencing of HMGB1 has been shown to improve left ventricular function and reduce collagen deposition in diabetic rats [261], while in vitro studies have demonstrated that HMGB1 promotes collagen synthesis and fibroblast activation [262]. Together, these findings reinforce the role of HMGB1 as a pro-inflammatory mediator of fibrosis and hypertrophy.

To investigate whether HMGB1 release occurred via extracellular vesicles (EVs), pilot experiments were performed using serum-derived EVs from control rats. Dynamic light scattering confirmed successful EV isolation, but poor yield from Ang II serum prevented further comparative analysis. Nonetheless, these control findings provide proof-of-principle that circulating vesicles can be isolated in this model, and they align with the observed HMGB1 redistribution in cardiac tissue, which is suggestive of extracellular release.

To overcome the limitations of serum analysis, an *in vitro* surrogate system was established using MEG-01 cells, which are widely used to study megakaryocyte and platelet biology [246] . HMGB1 was detected in MEG-01-derived EV cargo under basal conditions and was further enhanced following thrombin stimulation in western blot (Figures 3.18-3.19). These results indicate that platelets and megakaryocytes may represent an important source of HMGB1 release during hypertension, consistent with studies showing platelet-derived EVs carry pro-inflammatory molecules and contribute to cardiovascular pathology [263]. Importantly, this *in vitro* evidence complements our *in vivo* observations by demonstrating a possible mechanism for HMGB1 export via EVs.

Collectively, these findings show that HMGB1 expression is altered in Ang II-induced cardiac remodelling, with cytoplasmic re-localisation supporting its active release. While direct serum confirmation was limited by technical constraints, MEG-01 studies provided supportive evidence that HMGB1 can be packaged into EVs and secreted, strengthening the link between tissue-level redistribution and systemic release mechanisms.

3.5 Chapter conclusion

In this chapter, we successfully established and validated an Ang II-induced chronic hypertension model in male rats, demonstrating hallmark features of hypertension including elevated blood pressure, cardiac hypertrophy, and increased fibrosis. We also identified a significant increase in HMGB1 expression within the cardiac niche, with evidence of its re-localisation to the cell membrane, suggesting a potential role in extracellular signalling during hypertensive remodelling.

Challenges with low yield and poor protein quality from rat serum limited the ability to confirm circulating HMGB1. To overcome this, we used an *in vitro* MEG-01 cell model, where pilot studies showed an increase in HMGB1 release following thrombin stimulation, supporting the hypothesis that HMGB1 may be secreted via non-classical pathways such as EVs.

Overall, these results highlight a clear association between Ang II-induced hypertension, fibrosis, and HMGB1 expression. However, the precise mechanistic role of HMGB1 in the hypertensive heart remains to be fully defined. Figure 3.20 provides a visual overview of the main findings reported in this chapter.

To gain broader insight into molecular changes associated with Ang II-induced hypertension, we adopted an untargeted, shotgun proteomics approach in the next chapter. This strategy enabled a global assessment of protein expression alterations across control, saline, and Ang II-treated groups, aiming to identify key pathway-specific changes that may contribute to hypertension-induced cardiac remodelling and inflammation.

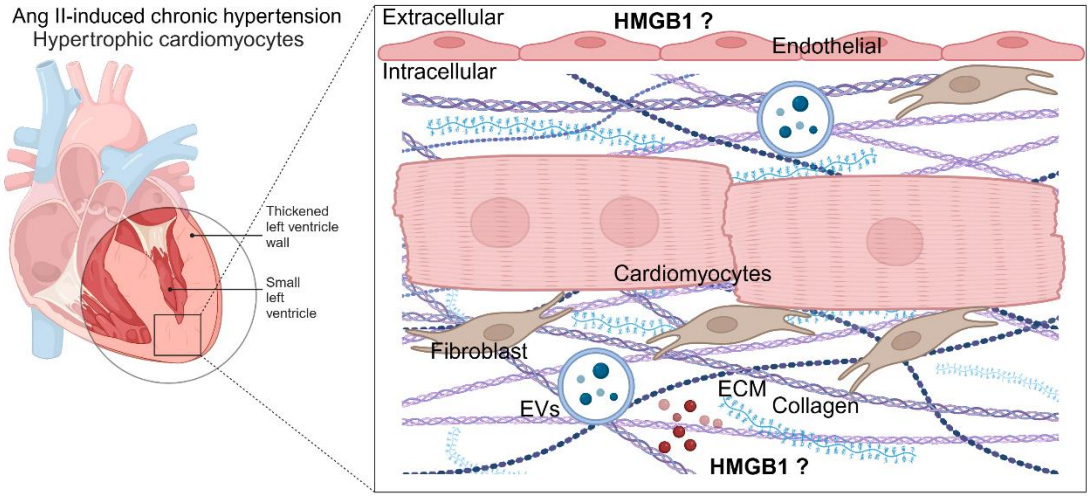

Figure 3:20: Distinct intercellular communication mechanisms in the cardiac remodelling process. At longer distances, the secretion of soluble cytokines, growth factors, or extracellular vesicles can modify the behaviour of target cells. Connecting various cardiac cell populations, the extracellular matrix provides structural support, which degrades due to cardiac hypertrophy, affects multiple bioactive factors, and signal transduction, thus dysregulating intercellular communication. HMGB1 is a multifunctional protein that plays a crucial role in cardiac remodelling, mediating inflammation, fibrosis, and cellular signalling. HMGB1 contributes to this process through the following mechanisms: as a pro-inflammatory protein activating TLR4, triggering downstream pro-inflammatory signalling pathways. This activation promotes the release of cytokines and chemokines, which exacerbate inflammation and contribute to the adaptive mechanism and further to maladaptive remodelling. In addition, HMGB1 influences cardiac fibrosis by stimulating myofibroblast activation and collagen synthesis. It modulates the secretion of matrix metalloproteinases (MMPs) and tissue inhibitors of metalloproteinases (TIMPs), leading to dysregulated extracellular matrix (ECM) turnover. This disrupts the ECM's structural and signalling role, contributing to intercellular communication disturbances and fibrosis progression in the hypertrophic, leading to a failing heart. Finally, HMGB1 is released and involved in regulating extracellular vesicles (EVs), such as exosomes and microvesicles, which serve as carriers of signalling molecules like microRNAs, proteins, and lipids. By modulating EV release and content, HMGB1 affects intercellular communication between cardiomyocytes, fibroblasts, endothelial cells, and immune cells, thereby influencing the overall remodelling process. Image created by Biorender.

Chapter 4:
LC-MS-Based Proteomic Analysis of Left Ventricle Tissues from Ang II-induced Chronic Hypertension in Male Rats

4.1 Introduction

4.1.1 Overview of Proteomics and high throughput technologies

Omics is a branch of biology focused on the comprehensive study and characterisation of the complete set of biological molecules within a cell, tissue, organism, or ecosystem. This approach aims to understand the structure, functions, and interactions of these molecules on a systemic level, in a global-unbiased approach [264] . Omics approaches enable the generation and analysis of extensive datasets, including those of the genome, transcriptome, and metabolome, which represent biological dynamics [265]. One of the first high-throughput technologies, DNA microarrays, was developed for large-scale gene expression analysis by measuring mRNA abundance through hybridisation-based detection [266]. With the advancement of sequencing-based omics, recent high-throughput technologies have significantly improved proteomics, enabling more comprehensive analysis of proteins and their functions through sophisticated methodologies. Mass spectrometry (MS)-based proteomics has become a fundamental approach in the field, allowing for the identification and quantification of proteins in complex biological samples with high sensitivity and accuracy [267]. Proteomics approaches are generally divided into gel based and gel-free methods, such as chromatography are usually classified into three basic types according to the mobile phase used including liquid chromatography (LC) [268], gas chromatography (GC) [269] and a technique that uses nuclear magnetic resonance (NMR) [270] . Each have their uses, with pros and cons depending on the research question being addressed.

Early protein separation techniques, such as two-dimensional polyacrylamide gel electrophoresis (2D-PAGE), enabled the resolution of proteins based on charge in the first dimension and mass in the second, with separation efficiency influenced by gel size [271]. An advancement of this method, two-dimensional differential gel electrophoresis (2D-DIGE), employs CyDye fluorophores to label

proteins, allowing for the simultaneous detection of multiple protein samples by exciting the dye at specific wavelengths [272] .

Modern proteomics has largely integrated these gel-based approaches with online chromatography-mass spectrometry techniques for enhanced protein identification and quantification [273] . Within this framework, two primary strategies are employed: label-based approaches, which involve chemical modification of proteins or peptides using various labelling techniques [274], and label-free methodologies, which rely on direct quantification without chemical labelling [275].

Proteomics, a key branch of omics sciences, involves the large-scale study of proteins—the dynamic molecular effectors that regulate virtually all biological processes. By investigating protein expression, interactions, modifications, and functions, proteomics provides critical insights into cellular mechanisms and disease pathways [276,277]. Unlike the relatively static genome, the proteome is highly dynamic and changes in response to various stimuli and conditions [278]. This dynamic nature makes proteomics a powerful tool for understanding cellular functions and disease mechanisms. A major limitation of genomic or transcriptomic profiling studies is that the data provides only indirect measurements of cellular states which may not accurately reflect the corresponding changes in protein levels. This includes changes in posttranslational modifications (PTMs), such as phosphorylation and protein degradation that could be obtained from proteomics. Differential proteomics, previously known as expression proteomics, involves creating quantitative maps of protein expression from tissues or cells [279]. This technique assesses the differences in protein composition between samples of interest, such as between a normal, or control sample and its diseased counterparts.

Proteomics methods have advanced from traditional techniques such as immunohistochemistry (IHC) staining, Western blot, and enzyme-linked immunosorbent assay (ELISA), to high-throughput approaches such as tissue microarray (TMA), protein pathway array, and mass spectrometry (MS) [280] . These

high-throughput proteomics techniques not only reduce analysis time but also enhance the accuracy and depth of proteome coverage. With advancements in bioinformatics and modern multi-analyte omics technologies, proteomics has gained unprecedented depth and accuracy in analysing protein expression and function. However, both omics-based and traditional biochemical approaches remain complementary, as traditional methods play a crucial role in validating protein-level findings

4.1.2 Top-down and bottom-up MS-based proteomic methods

Protein identification through MS typically employs either top-down proteomics, which involves analysing intact proteins, or bottom-up proteomics, where proteins are digested into smaller peptides via enzymatic or chemical methods before analysis. Various more efficient MS-based proteomic strategies have been developed to address diverse biological analytical challenges (see figure 4.1). A critical aspect of both bottom-up and top-down approaches is the separation of peptides and proteins, which plays a key role in enhancing the accuracy and depth of proteomic analyses.

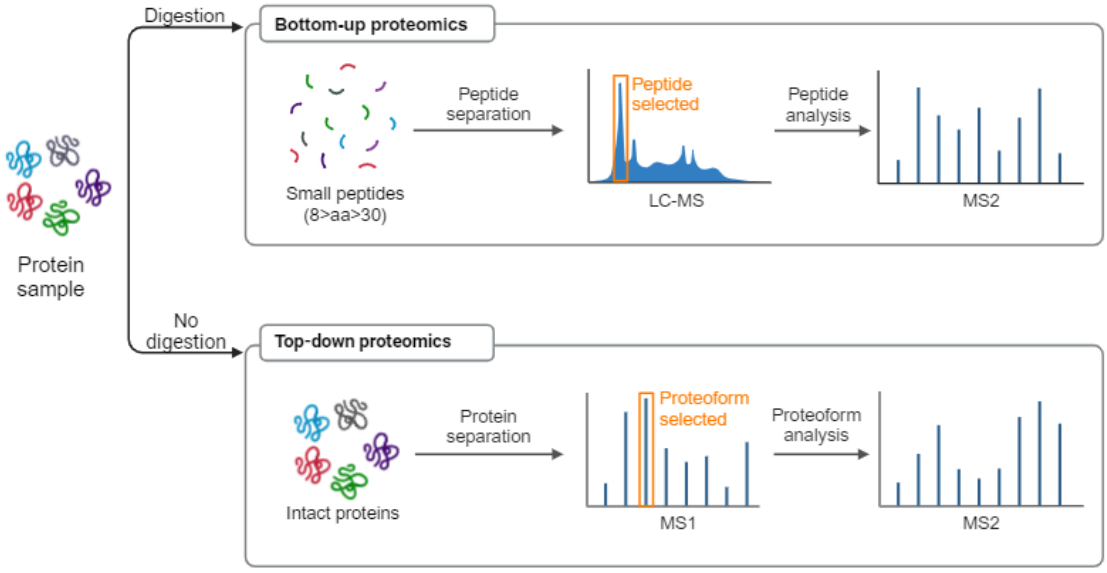

Figure 4.1: Schematic representation of MS-based proteomic strategies top-down and bottom-up. For top-down, the intact proteins are separated and individually characterised. In bottom up, proteins are first digested by proteolytic enzymes and the separated peptides are analysed by MS. Created by Biorender. Adapted from [281] .

In the top-down proteomics method, a full-length protein is directly sent for MS analysis, where it can be fragmented within the mass spectrometer, and the masses of the fragments are recorded [282]. This approach analyses intact proteins, allowing for the study of protein isoforms and post-translational modifications, although it is technically more challenging. Due to analytical challenges, the depth of protein coverage that is achievable by top-down proteomics is considerably less than that of bottom-up proteomics [283]. Bottom-up has advantages over the top-bottom method as peptides can be easily ionised and fractionated.

The bottom-up approaches, also known as shotgun proteomics, use data-dependent acquisition (DDA) workflows which are fundamental in proteomics. In these workflows, peptide identification is typically achieved by matching fragment spectra to a protein sequence database [284]. The most abundant precursor ions are selected for MS analysis. The bottom-up proteomic workflow starts with

sample preparation of the protein sample, which are typically extracted from biological sources such as tissues, cells, or bodily fluids. Bottom-up proteomics methods employ individual proteases or protease mixtures to selectively cleave proteins at multiple amino acid sites, resulting in a mixture of small peptides. The optimal peptide length for bottom-up MS is 6–50 amino acid residues for effective computational analysis. Trypsin digestion is commonly used as it produces peptides with an average length of 14 amino acids [285], therefore producing peptides that are well-suited for MS analysis. This step is crucial as it generates manageable peptide fragments that can be more easily analysed than intact proteins. Digesting proteins into small peptide fragments offers several advantages, including improved separation efficiency, a limited number of charges on each peptide, and increased sample homogeneity - all of which enhance MS detection.

These techniques are impossible without the use of bioinformatics, as in shotgun analysis the spectra that are acquired are just data. There are a multitude of software packages commercially available for example Proteome Discoverer (PD) [286] that enable proteomic workflows to be applied to the analysis of the wide variety of studies.

4.1.3 Using proteomics to map inflammatory pathways that contribute to cardiovascular dysfunction

Numerous pathological mechanisms contribute to the onset and progression of high blood pressure. Inflammation is one such process that has been extensively linked to hypertension. Research has shown elevated levels of inflammatory markers in individuals with hypertension, suggesting a strong association between inflammation, the onset of hypertension, and subsequent organ damage [287].

Key events driving cardiac remodelling include oxidative stress-induced hypertrophy, immune cell infiltration, and myofibroblast activation, leading to

extracellular matrix (ECM) reorganisation and fibrosis. These structural modifications are critical contributors to the progression of heart failure [288]. High-throughput technologies enable the investigation of a large set of proteins in a single sample, thus, to connecting several biomarkers from distinct pathophysiological pathways.

Back in 2005, a study conducted proteomic profiling of left ventricular myocardia in spontaneously hypertensive rats and Wistar-Kyoto rats at different ages using 2D-DE in combination with MALDI-TOF/TOF MS/MS [289]. Whilst proteomic analysis was primitive when compared to the advanced approaches today, the findings revealed significant modifications in proteins involved in cellular energy metabolism and oxidative stress. Further proteomic studies in mice predisposed to hypertrophic cardiomyopathy analysed three groups: non-transgenic mice and cardiac-specific transgenic mice overexpressing either the wild-type or mutant cardiac troponin I gene [290] . Interestingly, biological process classification revealed that most identified proteins were associated with cell structure and muscle contraction. A recent human study analysed serum proteomic data from the Qatar Biobank to identify protein expression differences among individuals with normal blood pressure, prehypertension, and hypertension, aiming to uncover biological pathways linked to hypertension progression [291]. Pathway analysis revealed a cluster of proteins, the majority of which were associated with actin cytoskeleton remodelling.

Previous studies have not examined cardiac tissue to evaluate biological pathways involved in the pre-heart failure (pre-HF) stage of a non-genetic rat model of Ang II-induced chronic hypertension, compared to controls. This study aims to address this gap while minimizing potential confounding factors. In addition, it seeks to profile proteins associated with these effects, including inflammation-related responses, by analysing differentially expressed proteins (DEPs) and performing a protein network analysis.

4.1.4 Pathway Analysis and Protein-Protein Interactions in Hypertension

Protein pathways consist of a series of cellular reactions that drive specific biological effects. The proteins directly involved in these processes, along with regulatory molecules, are compiled into pathway databases. Several well-established resources provide extensive data on protein pathways, including KEGG, Ingenuity, the Pathway Knowledge Base, Reactome, and BioCarta, which offer insights into metabolism, signalling, and molecular interactions [292,293].

Overrepresentation analysis is a statistical approach used to identify gene or protein sets that appear more frequently within a list of differentially expressed genes/proteins (DEGs/DEPs) than expected by chance. This method detects significantly enriched pathways and biological processes, helping to interpret large-scale omics data [294]. In addition, topology-based approaches build upon traditional enrichment analyses by incorporating pathway architecture and network interactions. Unlike methods that focus solely on gene sets without considering relationships between molecules, topology-based strategies map interactions within biological networks, offering deeper insights into functional connectivity [295]. These approaches account not only for gene presence but also for their interactions and regulatory influence, enhancing our understanding of complex biological systems.

To support pathway and network analysis, several specialized databases have been developed. For instance, GenMAPP provides insights into signal transduction pathways [296] , while PANTHER facilitates protein classification based on evolutionary relationships [297] . These public databases offer high connectivity, aiding in protein identification, interaction mapping, and novel discoveries. Additionally, the STRING database integrates data from multiple sources, including literature mining, to analyse protein-protein interactions [298] . STRING enables researchers to visualize interaction networks derived from known and

predicted associations, offering a valuable tool for deciphering functional relationships and regulatory mechanisms in complex biological processes.

4.2 Chapter Aims and Objectives

This chapter aims to investigate the biological functions and pathways underlying Ang II-induced chronic hypertension in the left ventricle of male rats. By integrating a ‘bottom-up’ proteomic, in combination with analyses that utilises network-based approaches, the study seeks to identify key molecular drivers of hypertensive cardiac remodelling and identify pathways for future validation that may reveal critical proteins that contribute to inflammation and extracellular matrix reorganisation in the cardiac niche.

Objectives of this Chapter

1. Use bottom-up proteomics to map the molecular impact of Ang II-induced chronic hypertension
    - Analyse global protein expression changes in the left ventricle tissue of Ang II-infused rats compared to sham-operated and control groups.
    - Identify differentially expressed proteins (DEPs) associated with hypertensive cardiac remodelling.
2. Identify key regulatory proteins and pathways involved in hypertensive remodelling
    - Perform pathway enrichment and protein network analysis to uncover biological processes contributing to structural and functional changes in the heart.
    - Investigate inflammatory and extracellular matrix-related proteins linked to hypertension-induced remodelling.

The left ventricle (LV) is the primary cardiac compartment extensively studied in the context of cardiovascular dysfunction due to its critical role in maintaining systemic circulation and its susceptibility to hypertensive remodelling. Investigating the proteomic landscape of the LV in response to Ang II-induced chronic hypertension provides a well-characterized foundation for understanding molecular mechanisms underlying cardiac remodelling.

This study will not only contribute to existing knowledge but also serve as a stepping stone for future proteomic analyses of other cardiac regions. Notably, preliminary findings have indicated an increase in high-molecular-weight HMGB1 (HMW-HMGB1) in the right atrium, suggesting its potential involvement in disease progression. Therefore, establishing a comprehensive proteomic framework in the LV will facilitate comparative studies and future investigations into right atrial remodelling, broadening our understanding of regional cardiac responses to hypertension.

4.3 Results

4.3.1 Proteomics-based LV tissue profiling of Ang II-induced chronic hypertension in male rats

Left ventricular hypertrophy (LVH) is well recognised as a key focus for hypertension-induced organ damage and its role as a reliable predictor of adverse cardiovascular events has been well-established [28]. As a complex pathological phenomenon, hypertension-driven cardiac remodelling involves alterations in a multitude of proteins, making proteomic analysis a powerful approach to identify, characterise, and quantify global changes in the protein landscape. This strategy has been effectively employed to investigate myocardial protein profiles in spontaneously hypertensive rats a well-established model of essential hypertension compared to normotensive controls [299]. Notably, this research underscores the advantages of LC-MS/MS over traditional 2D-PAGE, as it offers greater sensitivity, higher throughput, and a more comprehensive characterisation of proteomic alterations associated with disease progression.

Previous proteomic studies have provided critical insights into novel pathophysiological processes, potential therapeutic targets, and biomarkers within the context of cardiovascular diseases. For example, bottom-up proteomic analysis of human adult cardiac tissue and isolated cardiomyocytes has yielded valuable data on the specific molecular alterations within cardiac tissue [300]. Additionally, research has examined the implications of plasma clusterin levels in LV remodelling following myocardial infarction (MI), revealing its significant involvement in cardiac hypertrophy [301]. Despite these advances, there remains a notable lack of comprehensive, in-depth analysis of the protein changes associated with Ang II-induced chronic hypertension, particularly when compared to control groups. This gap highlights a critical need for further proteomic investigations to uncover the molecular mechanisms driving hypertension-

induced cardiac remodelling, which may offer opportunities for the identification of novel therapeutic targets and biomarkers for cardiovascular diseases.

4.3.2 Shotgun Proteomics and Protein-Based Bioinformatics

4.3.2.1 Proteome Profiling of LV Tissue from Ang II, sham-operated Saline, and Control

In this study, samples of Ang II-induced chronic hypertension in rats were used and compared to control and sham-operated saline groups to examine protein profile alterations or differences. Protein expression profiles of these 3 groups were analysed in triplicate. Bottom-up label free quantification (LFQ) was used for this analysis, whereby proteins derived from isolated LV-tissue undergo proteolytic digestion with trypsin, and the resulting peptides or fragments are subsequently analysed via MS.

The LFQ proteomic method was employed to profile proteins and investigate the underlying mechanisms of Ang II-induced chronic hypertension, with the goal of identifying key implicated targets. After processing the raw data from tryptic peptides using Proteome Discoverer v3.1 (PD) software, several critical steps were undertaken, including data filtering with a false discovery rate (FDR) of less than 1% for both peptides and proteins, as well as normalisation and imputation via the NormalyzerDE [302] and NAguideR [303] platforms. This rigorous approach resulted in the identification of over 600 proteins across the various comparison groups, providing a comprehensive overview of the protein alterations associated with the hypertensive model.

In the quality assessment process, box plots were used to visually compare the distribution of log2-transformed LFQ intensities across different experimental groups. The pairwise comparisons included (A) Ang II vs saline (G1 vs G2), (B) Ang II vs control (G1 vs G3), and (C) saline vs control (G2 vs G3) groupings. These box plots revealed that the median protein intensities were comparable

across all samples within each group, indicating a consistent distribution of protein expression within the groups. This suggests that there were no significant outliers or skewed data, ensuring the quality and reliability of the data for further analysis. The results of these comparisons are shown in Figure 4.2, which provides a visual representation of the data distributions and confirms the consistency of the protein profiles within each group.

A)

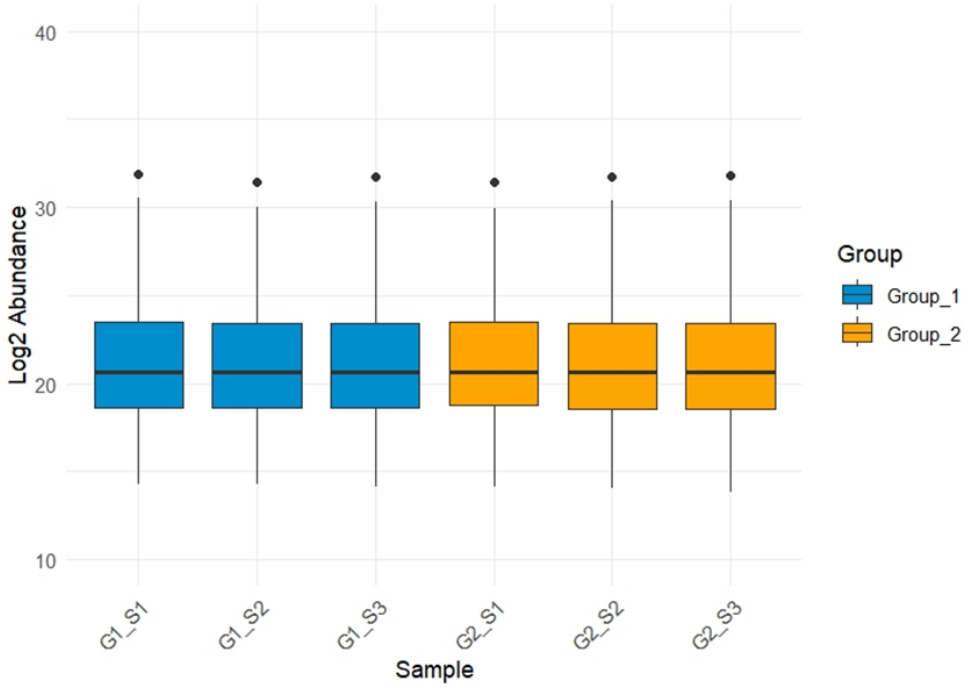
40
30
20
10
Log2 Abundance
G1_S1
G1_S2
G1_S3
G2_S1
G2_S2
G2_S3
Sample
Group
Group_1
Group_2

B)

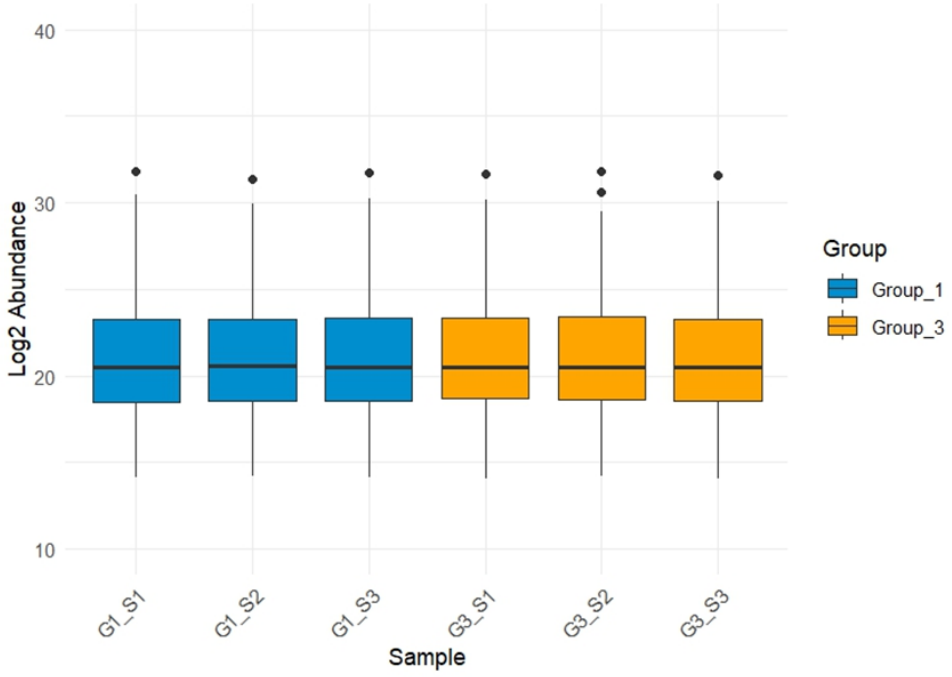
40
30
20
10
Log2 Abundance
G1_S1
G1_S2
G1_S3
G3_S1
G3_S2
G3_S3
Sample
Group
Group_1
Group_3

C)

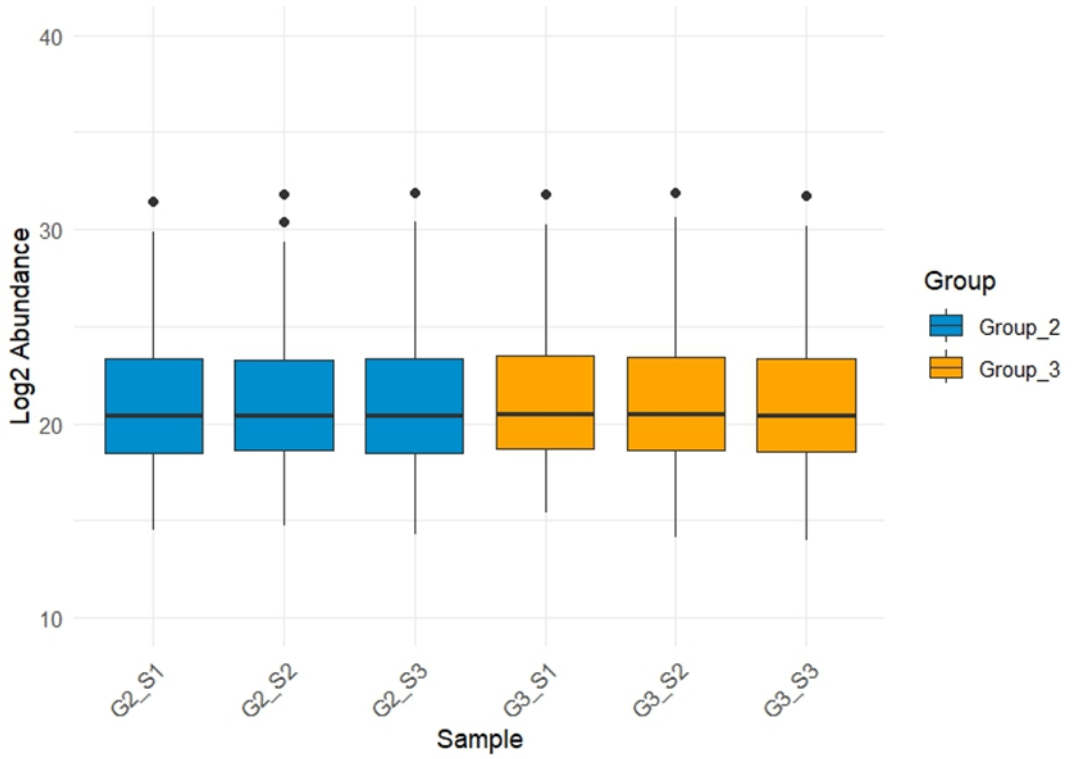

Figure 4.2: Quantitative profiling of left ventricular (LV) tissues from Ang II, saline, and control groups.
The box plot displays the log2-transformed LFQ intensity values for each sample in the three experimental groups. Data represent three technical replicates for each group: (A) Ang II vs saline (G1 vs G2), (B) Ang II vs control (G1 vs G3), and (C) saline vs control (G2 vs G3). The box plots provide a visual comparison of protein expression levels across the groups, with the central line indicating the median and the box representing the interquartile range. Abbreviations: LFQ: Label-Free Quantification; S: Technical Replication.

4.3.3 Principal Component Analysis (PCA) of Protein Profiles in Ang II, Saline, and Control Groups.

To assess the overall heterogeneity of the sample groups and explore the underlying variations in protein expression, Principal Component Analysis (PCA) was applied to the proteomic data. PCA is an unsupervised dimensionality reduction technique that identifies patterns and relationships within complex datasets by transforming them into principal components that account for the greatest variance. This approach is highly effective in visualising how different sample groups relate to one another based on protein expression profiles.

In our experiments, the PCA analysis revealed important distinctions among the experimental groups. Notably, there was significant overlap between the Ang II (G1) and Saline (G2) groups (Figure 4.3A), suggesting that the protein expression profiles in these two groups were quite similar. This observation indicates that the saline treatment did not significantly alter the protein profile in comparison to the Ang II infusion, which could be attributed to the minimal impact of saline on the cardiac tissue. However, a clear separation between the Ang II (G1) and Control (G3) groups was evident (Figure 4.3B), highlighting the distinct molecular changes induced by chronic hypertension following Ang II infusion. These findings underscore the significant differences in protein expression between hypertensive and non-hypertensive conditions, with Ang II treatment driving notable alterations in the cardiac proteome. Interestingly, Saline (G2) and Control (G3) groups observed a difference, which may indicate that the surgical procedure may have an impact on changes to LV protein expression.

Some overlap between Saline and Ang II samples also suggests that variability from the surgical procedure itself could represent a potential confounding factor in the PCA analysis (see Figure 4.3).

A)

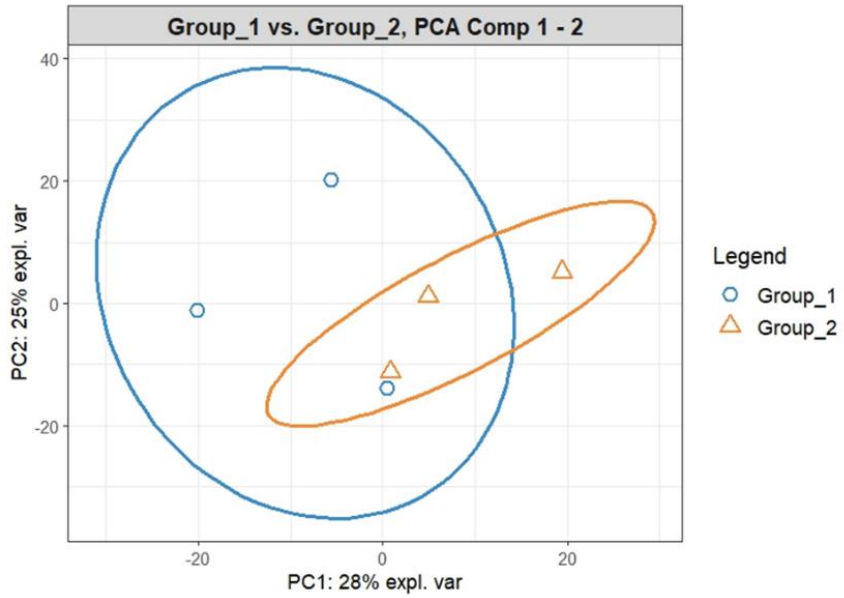
Group_1 vs. Group_2, PCA Comp 1 - 2
PC2: 25% expl. var
PC1: 28% expl. var
40
20
0
-20
-20
0
20
Legend
Group_1
Group_2

B)

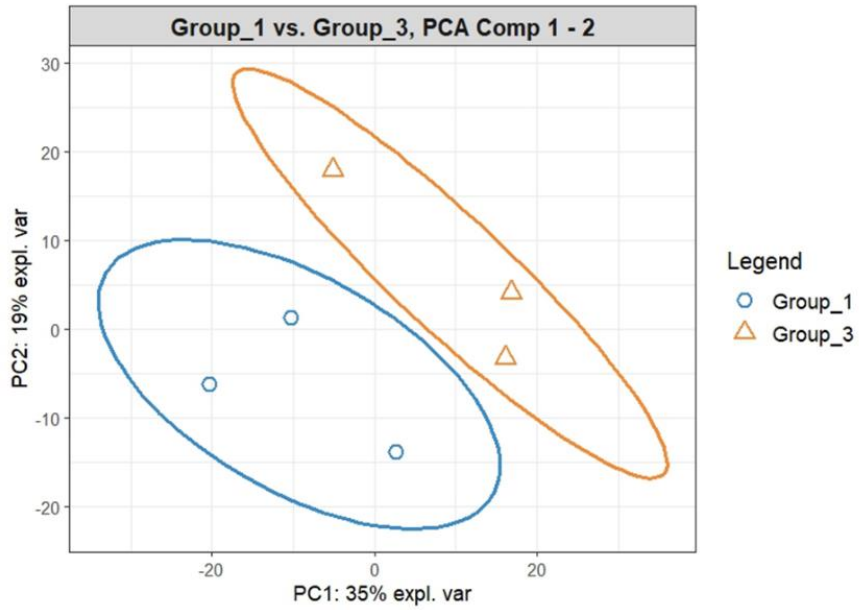
Group_1 vs. Group_3, PCA Comp 1 - 2
PC2: 19% expl. var
PC1: 35% expl. var
30
20
10
0
-10
-20
-20
0
20
Legend
Group_1
Group_3

C)

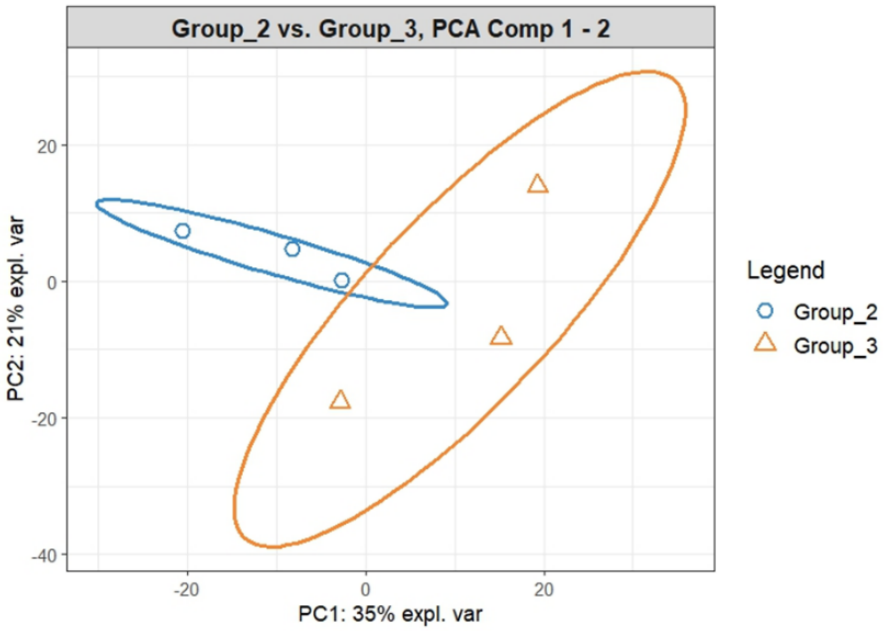

Figure 4.3: Principal Component Analysis (PCA) of Protein Expression in Ang II, Saline, and Control Groups.
PCA score plots illustrate the distribution and separation of the sample groups based on their protein expression profiles. The plots represent pairwise comparisons between the three groups: Ang II vs Saline, Ang II vs Control, and Saline vs Control. Shaded circles in the plots represent the 90% confidence intervals for each group, indicating the region where 90% of the individual sample points fall. Coloured dots and triangles correspond to individual samples within each group, visually depicting their positions relative to one another in the principal component space. Notably, while there is considerable overlap between the Ang II and Saline groups, a distinct separation is observed between the Ang II and Control groups, suggesting a marked difference in protein expression between hypertensive and normotensive conditions.

4.3.4 Upregulated and Downregulated Proteins in LV Tissue Across Study Groups

To identify the differentially expressed proteins (DEPs) responsible for the separation and clustering observed in the PCA results, volcano plots were generated based on the threshold values (log2 fold change ≥ 0.5 and p ≤ 0.05). The analysis revealed a total of 594 DEPs for the Ang II vs saline comparison (Group1 vs Group2, Shown in Figure 4.4), 624 DEPs for Ang II vs control (Group1 vs Group3, Figure 4.5), and 630 DEPs for saline vs control (Group2 vs Group3, Figure 4.6). Among these, 12, 8, and 12 proteins were upregulated (red dots), and 7, 23, and 27 proteins were downregulated (green dots) in the respective groups, as illustrated in the figures with the top 5 upregulated and downregulated DEPs were selected based on statistical significance and fold change criteria are listed in Table for Ang II vs Saline (Group1 vs Group2), Table for Ang II vs Control (Group1 vs Group3) and Table for Saline vs Control (Group2 vs Group3) below.

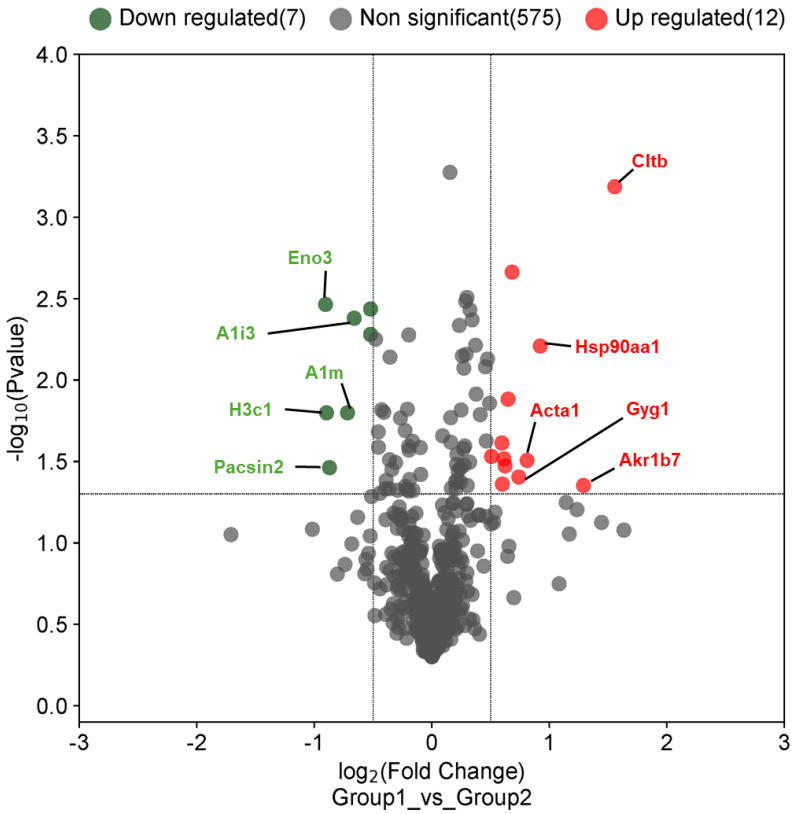

Figure 4.4: Volcano plot of label-free quantitative data for LV tissue, showing upregulated and downregulated DEPs for Ang II vs Saline.
Volcano plots highlight statistically significant upregulated proteins (red dots, $P < 0.05$) and downregulated proteins (green dots, $P < 0.05$) in the comparisons between Ang II vs saline (Group 1 vs Group 2, shown in A). The plots were generated using a log2 fold change threshold of 0.5 and a −log10 *p*-value threshold of < 0.05 with proteins not meeting these criteria shown in grey. Abbreviation: LV = Left Ventricle, DEPs = Differentially Expressed Proteins.

Table 4 1: The top 5 Upregulated and Downregulated DEPs Listed in Ang II vs Saline

Ang II vs Saline (Group1 vs Group2)	
Top 5 downregulated DEPs	**Protein ID (UniProt)**
Beta-enolase	**Eno3**
Histone H3.1	**H3c1**
Protein kinase C and casein kinase substrate in neurons 2 protein	**Pacsin2**
Alpha-1-macroglobulin	**A1m**
Alpha-1-inhibitor 3	**A1i3**
Top 5 upregulated DEPs	**Protein ID (UniProt)**
Clathrin light chain B	**Cltb**
Aldo-keto reductase family 1 member B7	**Akr1b7**
Heat shock protein HSP 90-alpha	**Hsp90aa1**
Actin, alpha skeletal muscle	**Acta1**
Glycogenin-1	**Gyg1**

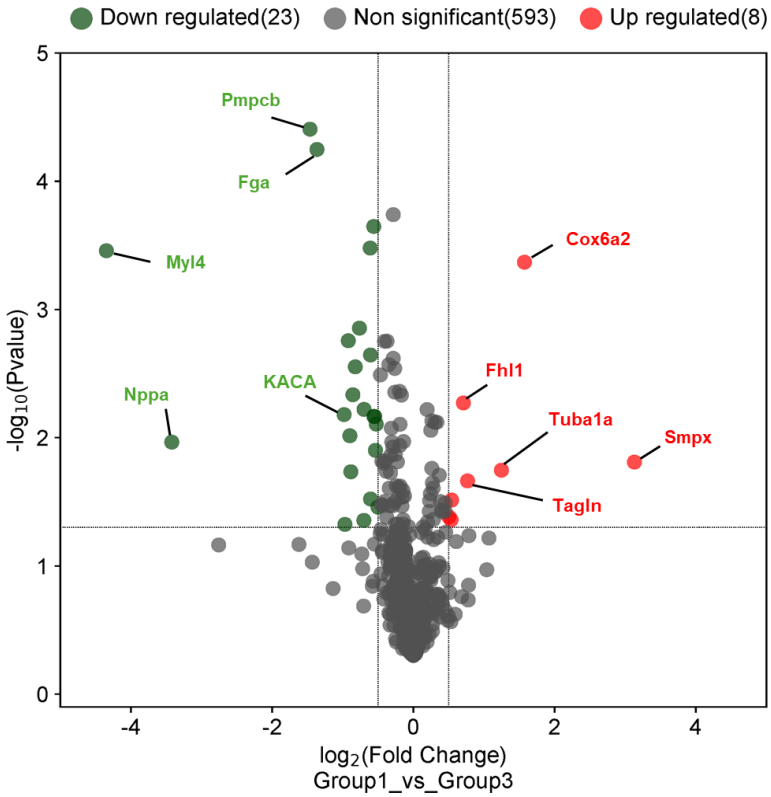

Figure 4.5: Volcano plot of label-free quantitative data for LV tissue, showing upregulated and downregulated DEPs for Ang II vs Control.
Volcano plots highlight statistically significant upregulated proteins (red dots, $P < 0.05$) and downregulated proteins (green dots, $P < 0.05$) in the comparisons between Ang II vs saline (Group1 vs Group3, shown in A). The plots were generated using a log2 fold change threshold of 0.5 and a −log10 *p*-value threshold of < 0.05 with proteins not meeting these criteria shown in grey. Abbreviation: LV = Left Ventricle, DEPs = Differentially Expressed Proteins.

Table 4.2: The top 5 Upregulated and Downregulated DEPs Listed in Ang II vs Control

Ang II vs Control (Group1 vs Group3)	
Top 5 downregulated DEPs	**Protein ID (UniProt)**
Myosin light chain 4	**Myl4**
Natriuretic peptides A	**Nppa**
Mitochondrial-processing peptidase subunit beta	**Pmpcb**
Fibrinogen alpha chain	**Fga**
Ig kappa chain C region, A allele	**KACA**
Top 5 upregulated DEPs	**Protein ID (UniProt)**
Four and a half LIM domains protein 1	**Fhl1**
Transgelin	**Tagln**
Tubulin alpha-1A chain	**Tuba1a**
Cytochrome c oxidase subunit 6A2, mitochondrial	**Cox6a2**
Small muscular protein	**Smpx**

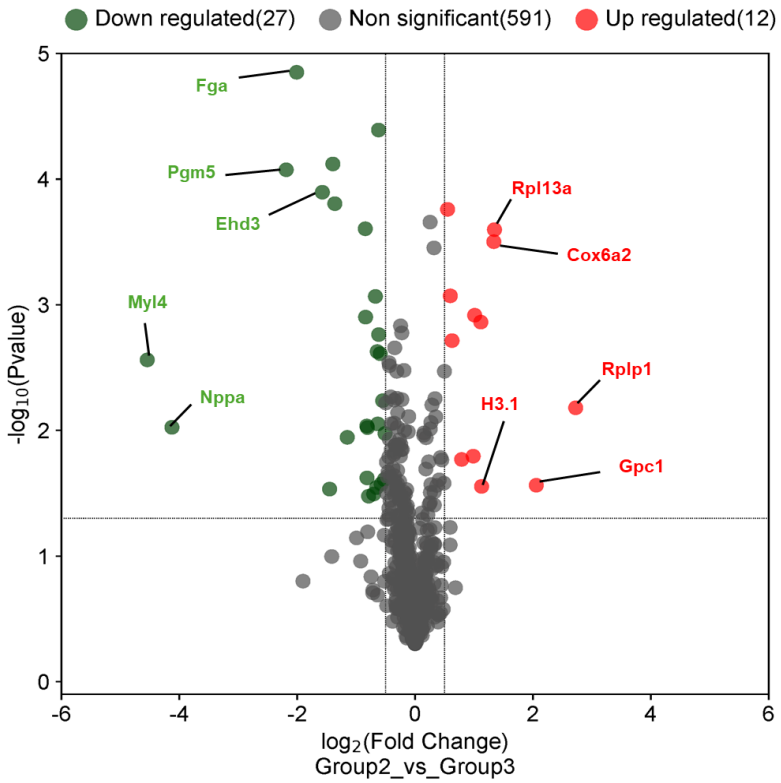

Figure 4.6: Volcano plot of label-free quantitative data for LV tissue, showing upregulated and downregulated DEPs for Saline vs Control.
Volcano plots highlight statistically significant upregulated proteins (red dots, $P < 0.05$) and downregulated proteins (green dots, $P < 0.05$) in the comparisons between Ang II vs saline (Group2 vs Group3). The plots were generated using a log2 fold change threshold of 0.5 and a −log10 *p*-value threshold of < 0.05 with proteins not meeting these criteria shown in grey.
Abbreviation: LV = Left Ventricle, DEPs = Differentially Expressed Proteins.

Table 4.3: The top 5 Upregulated and Downregulated DEPs Identified in Saline vs Control

Saline vs Control (Group2 vs Group3)	
Top 5 downregulated DEPs	**Protein ID (UniProt)**
Myosin light chain 4	**Myl4**
Natriuretic peptides A	**Nppa**
Phosphoglucomutase-like protein 5	**Pgm5**
Fibrinogen alpha chain,	**Fga**
EH domain-containing protein 3	**Ehd3**
Top 5 upregulated DEPs	**Protein ID (UniProt)**
Histone H3.1	**H3.1**
Cytochrome c oxidase subunit 6A2, mitochondrial	**Cox6a2**
Large ribosomal subunit protein uL13,	**Rpl13a**
Glypican-1	**Gpc1**
Large ribosomal subunit protein P1	**Rplp1**

4.3.5 Common cardiac function markers in hypertension progression

An analysis of the proteomic profile, including both significant and non-significant DEPs, was conducted to identify common cardiac biomarkers, further validating the Ang II-induced model of cardiac remodelling in the absence of evident cardiac dysfunction. Among the identified proteins, cardiac troponins Troponin I (Tnni3) and Troponin T (Tnnt2) were detected across all experimental groups, though with varying p-values and without reaching statistical significance. Additionally, natriuretic peptide A (Nppa), a key marker of cardiac stress and hypertrophy, was significantly downregulated in both Ang II vs. control and saline vs. control comparisons, suggesting a potential adaptive or compensatory response rather than pathological dysfunction typically associated with heart failure. This downregulation, alongside the presence but non-significance of troponins, may indicate that while structural remodelling occurs, the hypertrophic signalling pathways leading to decompensated cardiac dysfunction are not significantly activated in this model. Table 4.4 presents the detected levels of Tnni3, Tnnt2, and Nppa, along with their corresponding p-values.

Table 4.4: Common Cardiac Biomarkers Identified in The Proteomic Profile Across Experimental Groups.

Groups	**DEPs (ID uniPort)**	***P*-value**	**logFc**
Ang II (G1) vs Saline (G2)	Troponin T (Tnnt2)	0.287427	0.05627
Ang II (G1) vs control (G3)	Troponin T (Tnnt2)	0.263746	0.06222
Saline (G2) vs control (G3)	Troponin T (Tnnt2)	0.477163	0.00662
Groups	**DEPs (ID uniPort)**	***P*-value**	**logFc**
Ang II (G1) vs Saline (G2)	Troponin I (Tnni3)	0.440784	-0.0139
Ang II (G1) vs control (G3)	Troponin I (Tnni3)	0.322919	0.02441
Saline (G2) vs control (G3)	Troponin I (Tnni3)	0.261014	0.07166
Groups	**DEPs (ID uniPort)**	***P*-value**	**logFc**
Ang II (G1) vs Saline (G2)	Natriuretic peptide A (Nppa)	Not found	Not found
Ang II (G1) vs control (G3)	Natriuretic peptide A (Nppa)	0.010822	-3.42199
Saline (G2) vs control (G3)	Natriuretic peptide A (Nppa)	0.009448	-4.12566

4.3.6 HMGB1 Presence, Associated Proteomic Profiles in LV Tissue and protein Interactions

Given HMGB1 established role as a pro-inflammatory mediator in cardiac remodelling, its presence in the proteomic profiling of LV tissue was specifically examined to determine its potential involvement in Ang II-induced pathological changes. High mobility group protein B1 (Hmgb1) was detected in all groups; however, its expression levels varied across conditions and did not reach statistical significance in the differential expression analysis.

Comparative analysis revealed that HMGB1 expression in the Ang II group relative to the saline and control groups showed no significant difference (Ang II vs. Saline: p = 0.3797, logFC = -0.03745; Ang II vs. Control: p = 0.4891, logFC = -0.01026). Similarly, the comparison between the saline and control groups indicated no significant change (p = 0.4525, logFC = -0.05013). These findings suggest that while HMGB1 is present in the LV proteome across all groups, its expression levels do not exhibit substantial differential regulation under Ang II-induced remodelling conditions (Table 4.5). The logFC values are very close to zero across comparisons suggesting that HMGB1 expression remains relatively stable between the Ang II, saline, and control groups, with no substantial up- or downregulation.

Table 4.5: HMGB1 Expression Levels in LV Proteomic Analysis Across Experimental Groups

Groups	**DEPs (ID uniPort)**	**P-value**	**logFc**
Ang II (G1) vs Saline (G2)	High mobility group protein B1 (Hmgb1)	0.379695	-0.03745
Ang II (G1) vs control (G3)	High mobility group protein B1 (Hmgb1)	0.489127	-0.01026
Saline (G2) vs control (G3)	High mobility group protein B1 (Hmgb1)	0.452549	-0.05013

To further explore HMGB1-associated pathways, a PANTHER (Protein ANalysis THrough Evolutionary Relationships) analysis was conducted, incorporating all significantly identified DEPs plus HMGB1. The PANTHER database is a powerful tool widely used for analysing and interpreting large-scale proteomic datasets. It offers a comprehensive array of biological pathways, providing insights into the molecular interaction networks associated with specific proteins or gene functions. PANTHER is particularly beneficial in proteomic analysis because it not only classifies proteins by their functions but also offers evolutionary insights into their biological roles across different species. This enables a deeper understanding of how proteins interact within the larger cellular context.

One of the key advantages of using the PANTHER database for pathway analysis is its ability to pinpoint biologically significant pathways that are overrepresented among a set of DEPs. For example, in this study, we utilised PANTHER to identify significantly enriched pathways ($P < 0.05$) or not significant including all results of the DEPs that could be associated with the inflammatory response in cardiac remodelling. This approach aims to assess potential clustering patterns and pathway associations that may provide further insights into HMGB1 involvement in cardiac remodelling processes. Results revealed that HMGB1 was categorised under the p53 signalling pathway in all groups, though with different *p*-values (Ang II vs. saline = 0.0839, Ang II vs. control = 0.127, and saline vs. control = 0.161).

To further explore HMGB1 interactions, STRING PPI analysis was performed. Protein interactions play a crucial role in mediating major biological processes, controlling metabolic and signalling pathways, cellular functions, and organismal systems. These interactions form intricate networks that regulate both health and disease mechanisms. To gain deeper insight into these processes, a focused protein-protein interaction (PPI) network analysis was performed by mapping the up- and down-regulated differentially expressed proteins (DEPs) onto the STRING database (http://string.embl.de/). This analysis offers a more

comprehensive topological assessment of protein interactions, incorporating metrics such as node degree and betweenness centrality.

In the PPI network, the edges represent both functional and physical protein associations, with the line thickness indicating the strength of these associations. A minimum interaction scores of >0.4 was applied, which serves as a threshold for determining the confidence level of the interactions. Additionally, the PPI enrichment p-value was used to assess whether the proteins interact more frequently than would be expected by chance, based on a random set of proteins with the same size and degree distribution. This enrichment suggests that the proteins are biologically linked as a cohesive group.

The results revealed condition-specific networks. Notably, in Ang II vs. saline, HMGB1 interacted with Histone H3.1, which was subsequently linked to Acta1 with PPI enrichment ($p = 3.78^{E-04}$). In the Ang II vs. control comparison, HMGB1 exhibited no direct interactions, yet the overall protein network was significant $p = 3.56^{E-13}$). In Saline vs. Control, HMGB1 clustered with Histone H3.1 and microtubule-associated proteins (MAP1A/1B light chain 3A), though this network did not reach significance ($p = 8.17^{E-02}$). The line thickness in the network represents the strength of data support, while the node colours indicate upregulated (red) and downregulated (green) proteins and HMGB1 in (purple). The protein interaction networks for each group are presented in Figure 4.7 below.

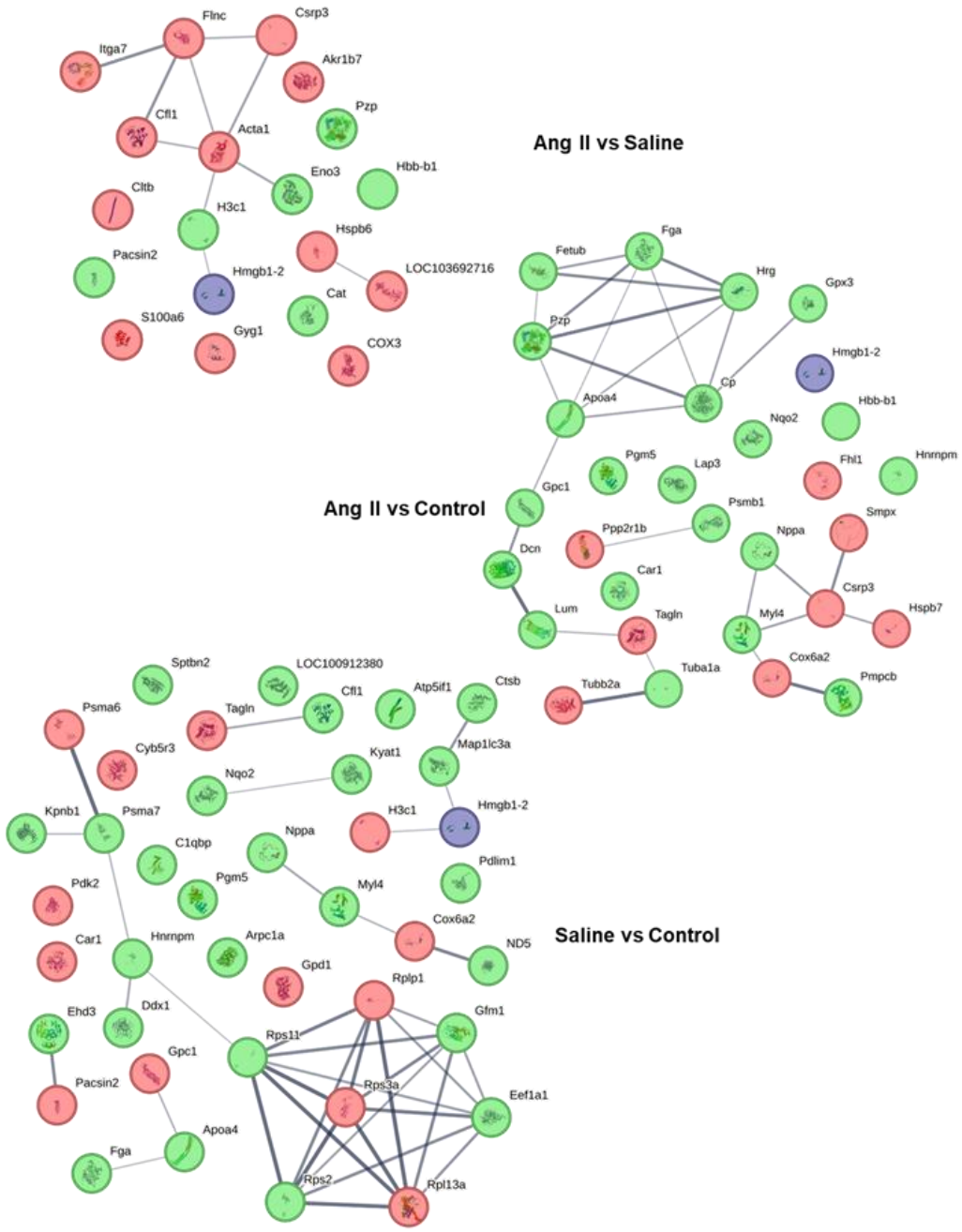

Figure 4.7: STRING Protein-Protein Interaction (PPI) Network of HMGB1 and Differentially Expressed Proteins.
This figure represents the Protein-Protein Interaction (PPI) network analysis of upregulated (red) and downregulated (green) differentially expressed proteins (DEPs) identified in this study, along with HMGB1 (HMGB1-2) (purple). The network visualizes both functional and physical interactions between these proteins, with edges representing predicted associations. Solid lines indicate direct experimental evidence, while line thickness reflects the strength of supporting data, with thicker lines representing stronger, more reliable interactions. This network provides insights into potential protein collaborations and regulatory influences within the context of the treatment groups.

4.3.7 Systematic GO and KEGG Pathway Enrichment Analysis of DEPs in the Ang II-Induced Chronic Hypertension Model: Insights into Cardiac Remodelling.

Pathway enrichment analysis is a powerful approach for interpreting complex omics datasets, offering valuable insights from a biological perspective [294]. To gain a systematic understanding of the biological functions and pathways associated with the DEPs, we first conducted an overrepresentation analysis using Gene Ontology (GO) and Kyoto Encyclopaedia of Genes and Genomes (KEGG) enrichment pathways. This analysis was performed through the enrichDAVID function of the clusterProfiler package, enabling robust data analysis and visualisation of the enriched biological processes and pathway

4.3.7.1 GO annotation and KEGG enrichment analysis of DEPs

To explore the functional characteristics of the differentially expressed proteins (DEPs), Gene Ontology (GO) and Kyoto Encyclopedia of Genes and Genomes (KEGG) enrichment analyses were performed using the clusterProfiler package. GO terms were grouped into biological process (BP), cellular component (CC), and molecular function (MF), with significance defined as $p < 0.05$ and a minimum count of 5 proteins.

Ang II vs Saline (G1 vs G2). Enriched BP terms included hydrogen peroxide catabolic process, oxygen transport, platelet aggregation, and cytoskeleton organisation. Significant CC terms were cytosol, hemoglobin complex, mitochondria, and sarcolemma. MF terms included protein binding, oxygen transporter activity, and protein kinase binding (Figure 4.8A). KEGG enrichment identified neurodegeneration-related pathways (Huntington's disease, prion disease, amyotrophic lateral sclerosis) and diabetic cardiomyopathy as significant, alongside metabolic pathways and neutrophil extracellular trap formation (Figure 4.8B).

Ang II vs Control (G1 vs G3). Enriched BP terms included regulation of heart contraction force, platelet aggregation, and cardiac muscle contraction. CC terms included extracellular space, intercalated disc, and sarcolemma, while MF terms included protein binding, metal ion binding, and structural roles in the cytoskeleton (Figure 4.9A). KEGG analysis showed enrichment in adrenergic signalling in cardiomyocytes, cardiac muscle contraction, hypertrophic and dilated cardiomyopathy, tight junctions, the cGMP–PKG pathway, and neutrophil extracellular trap formation (Figure 4.9B).

Saline vs Control (G2 vs G3). Enriched BP terms included cell mobility and response to immobilisation stress. CC terms included mitochondria, synapse, cytoplasm, and cytosol. MF terms included protein binding and cytochrome c oxidase activity (Figure 4.10A). KEGG analysis indicated enrichment in cardiac muscle contraction, metabolic pathways, dilated cardiomyopathy, actin cytoskeleton regulation, and several neurodegenerative pathways (ALS, prion disease, Huntington's disease), as well as oxidative phosphorylation and diabetic cardiomyopathy (Figure 4.10B).

A)

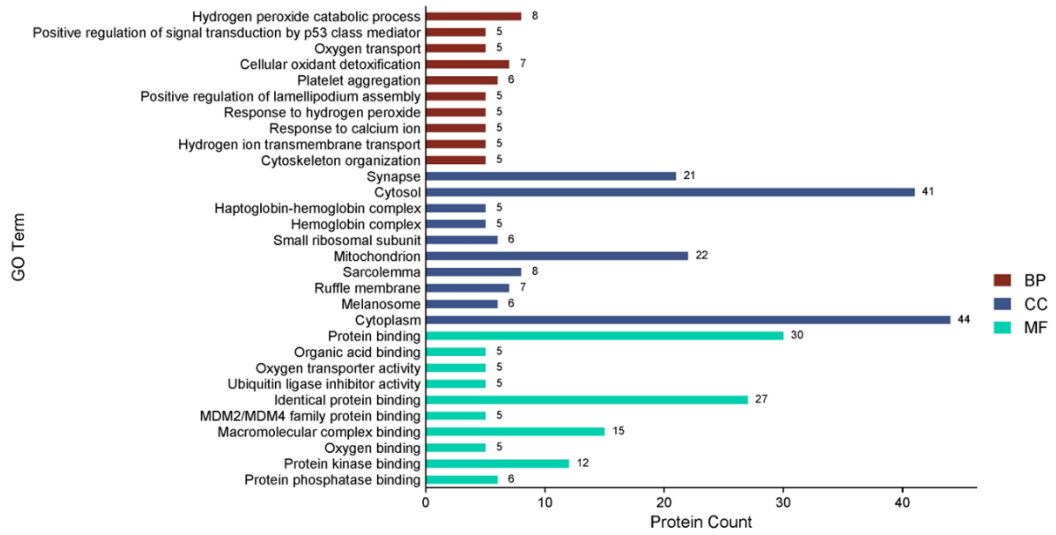

B)

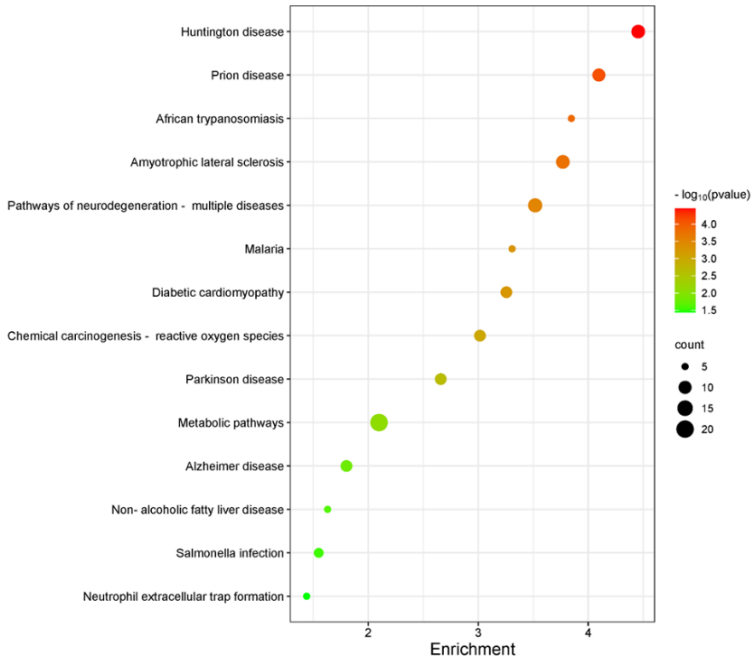

Figure 4.8: **GO-Functional analysis and KEGG-pathway analysis of the DEPs of G1 (Ang II) vs G2 (Saline)**.
A) The top 10 enriched GO terms for the BP, CC and MF categories. B) The bubble plot list all the significantly enriched pathways of the DEPs. The bubble size and colour represent the number of DEPs enriched in the pathway and the enrichment significance, respectively. DEPs: differentially expressed proteins; GO: Gene Ontology; BP: biological process; CC: cellular component; MF: molecular function.

A)

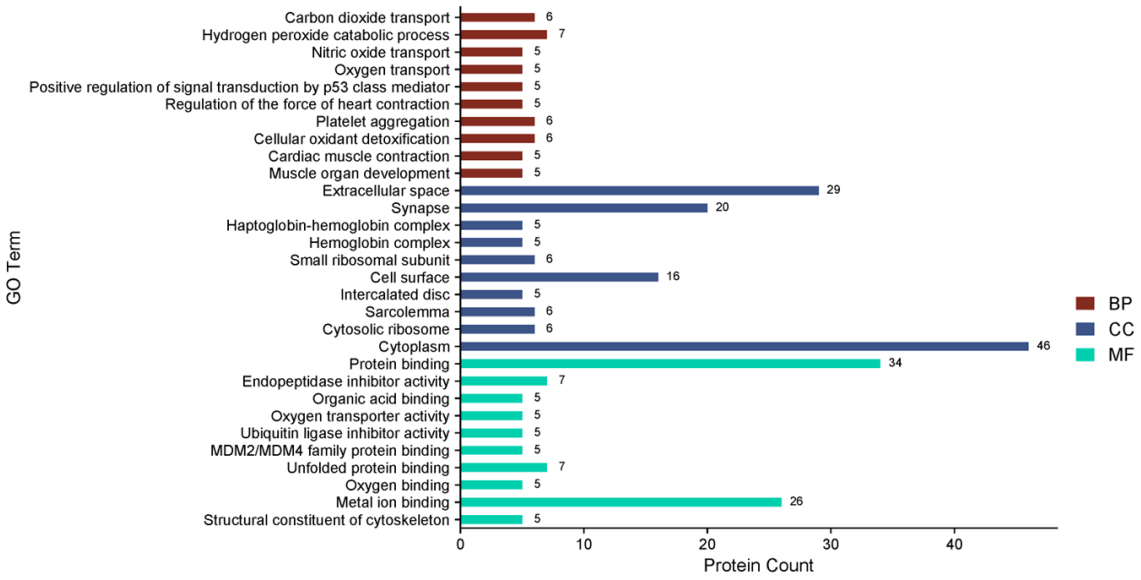

B)

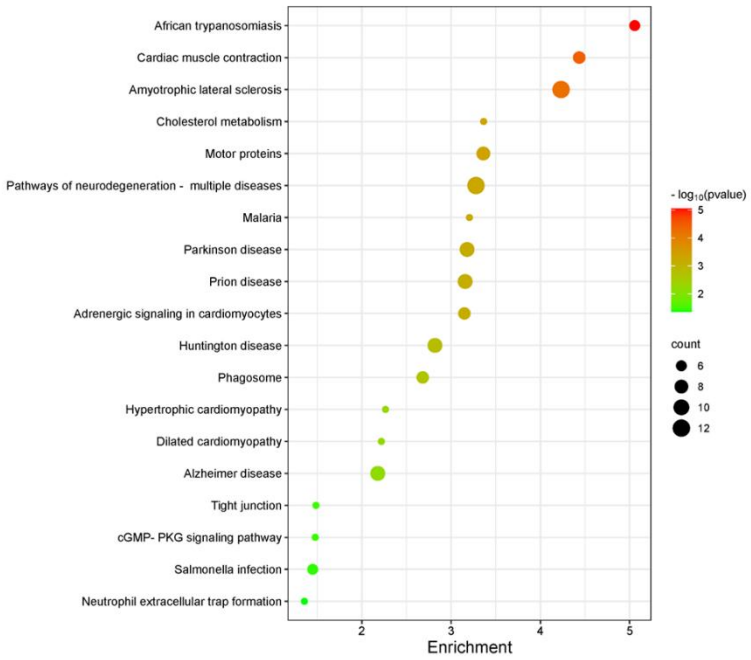

Figure 4.9: GO-Functional analysis **and KEGG-pathway analysis** of the DEPs of G1 (Ang II) vs G3 (Control). A) The top 10 enriched GO terms for the BP, CC and MF categories. B) The bubble plot lists all the significantly enriched pathways of the DEPs. The bubble size and colour represent the number of DEPs enriched in the pathway and the enrichment significance, respectively. DEPs: differentially expressed proteins; GO: Gene Ontology; BP: biological process; CC: cellular component; MF: molecular function.

A)

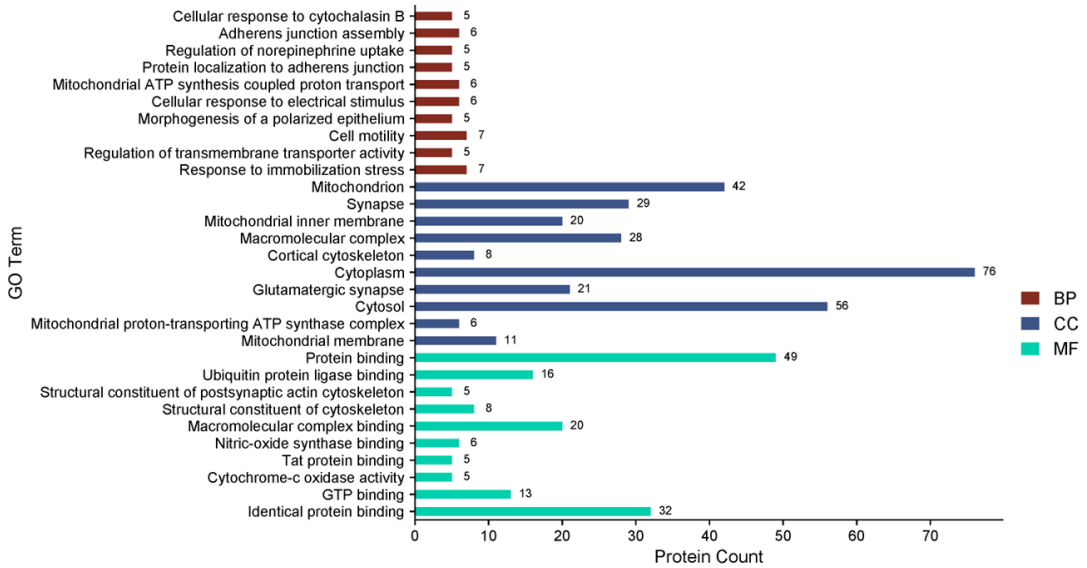

B)

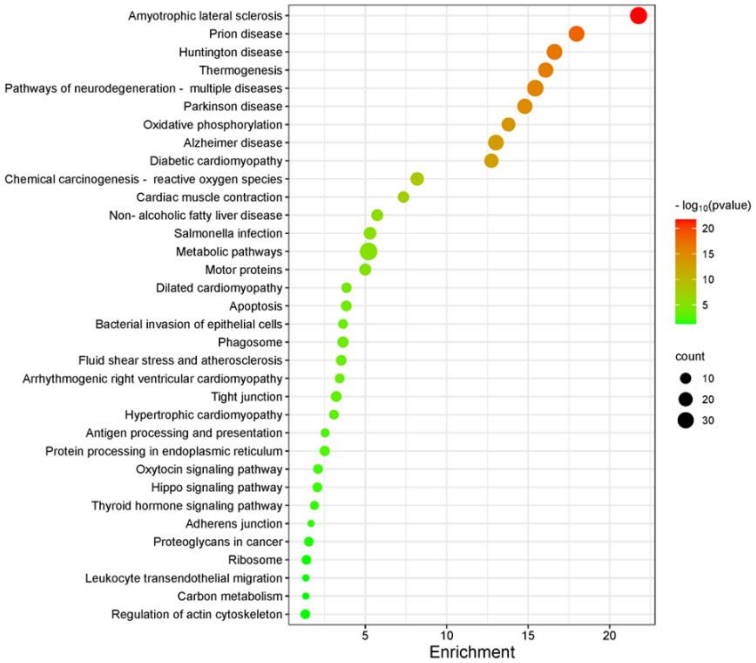

Figure 4.10: GO-Functional analysis and KEGG-pathway analysis of the DEPs of G2 (Saline) vs G3 (Control).
A) The top 10 enriched GO terms for the BP, CC and MF categories. B) The bubble plot list all the significantly enriched pathways of the DEPs. The bubble size and colour represent the number of DEPs enriched in the pathway and the enrichment significance, respectively. DEPs: differentially expressed proteins; GO: Gene Ontology; BP: biological process; CC: cellular component; MF: molecular function.

4.3.8. Mapping Protein Interactions in Cardiac Remodelling via STRING-db

Protein interactions play a crucial role in mediating major biological processes, controlling metabolic and signalling pathways, cellular functions, and organismal systems. These interactions form intricate networks that regulate both health and disease mechanisms.

In total, 11 significantly enriched pathways (P= 6.28^{E-05}) were identified in the Ang II vs saline comparison, and 28 significant pathways (P= 2.74^{E-14}) were found in the Ang II vs control comparison. In contrast, 35 pathways were identified for the saline vs control comparison, but they did not reach statistical significance (P= 0.0993). The line thickness in the network represents the strength of data support, while the node colours indicate upregulated (red) and downregulated (green) proteins. The protein interaction networks for each group are presented in Figure 4.11 below.

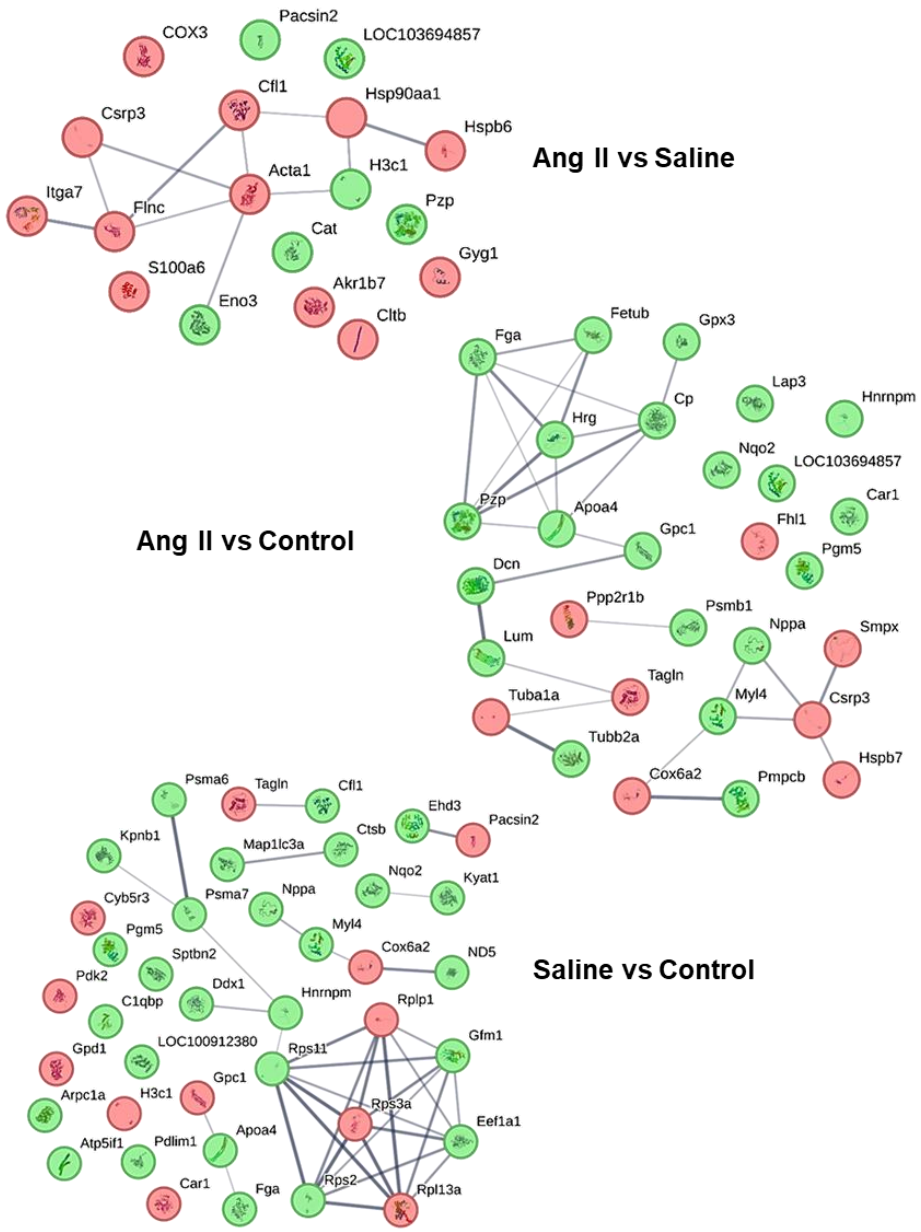

Figure 4.11: STRING Protein-Protein Interaction (PPI) Network of Differentially Expressed Proteins.

This figure displays the protein-protein interaction (PPI) network of the differentially expressed proteins identified in the study, generated using the STRING database. The network visualizes both functional and physical interactions between proteins, with edges representing these associations. Upregulated proteins are shown in red, while downregulated proteins are depicted in green, providing a clear distinction between the two categories. The solid lines connecting proteins indicate direct experimental evidence supporting the interaction, while the thickness of the lines reflects the strength of the data supporting each interaction, with thicker lines representing more reliable interactions. This network allows for a detailed view of how these proteins may collaborate or influence each other within the context of the treatment groups compared.

The tables below represent the top proteins with the most significant difference in abundance which are up-regulated (Table 4.6) and down-regulated (Table 4.7) between groups. These proteins are classified under the selected potential KEGG pathway and functional GO oncology of cardiac related function associated with the hypertension or remodelling.

Table 4.6: Cardiac-Specific Significantly Upregulated Proteins in Ang II-Induced Remodelling: Differential Expression Analysis in Ang II vs saline and Ang II vs control.

Proteins upregulated	KEGG	GO
Cofilin-1, (**Cfl1),** non-muscle		Positive regulation of lamellipodium assembly (I) Cytoskeleton organisation (I) Ruffle membrane (II)
Filamin-C **(Flnc)**		Sarcolemma (II)
Integrin alpha-7 (**Itga7)**		Sarcolemma (II) Macromolecular complex binding (III)
Heat shock protein HSP 90-alpha (**Hsp90aa1)**		Positive regulation of lamellipodium assembly (I) Ruffle membrane (II) Mitochondrion (II)
Cysteine and glycine-rich protein 3 (**Csrp3)**		Cardiac muscle contraction (I) Regulation of the force of heart contraction (I) muscle organ development (I)
Four and a half LIM domains protein 1 (**Fhl1)**		Negative regulation of cell growth (I) muscle organ development (I)
Tubulin alpha-1A chain (**Tuba1a)**		structural constituent of cytoskeleton (III)
Cytochrome c oxidase subunit 6A2, (**Cox6a2)**	Cardiac muscle contraction	
Cytochrome c oxidase subunit 3 **(COX3**)	Diabetic cardiomyopathy	Mitochondrion (II)
Heat shock protein beta-6 (**Hsp20**) Hspb6		Mitochondrion (II)
Cysteine and glycine-rich protein 3 (**Csrp3**)		Cytoplasm (II) Cardiac muscle contraction (I) Regulation of the force of heart contraction (I) muscle organ development (I)

Highlighting the GO oncology and KEGG related to cardiac remodeling. Abbreviations; (I): Biological process; (II): cellular localization; (III): molecular function.

Table 4.7: Cardiac-Specific Significantly Downregulated Proteins in Ang II-Induced Remodelling: Differential Expression Analysis in Ang II vs saline and Ang II vs control.

Proteins downregulated	**KEGG**	**GO**
Protein kinase C and casein kinase substrate in neurons 2 protein (**Pacsin2**)		Cytoskeleton organisation (I) Ruffle membrane (II)
Myosin light chain 4, Myosin light chain 1, atrial isoform (**Myl4)**	Cardiac muscle contraction Adrenergic signalling in cardiomyocytes	cardiac muscle contraction (I) regulation of the force of heart contraction (I)
Natriuretic peptides A (**Nppa)**		negative regulation of cell growth (I)
Fibrinogen alpha chain (**Fga)**	Neutrophil extracellular trap formation	platelet aggregation (I) positive regulation of ERK1 and ERK2 cascade (I) Endoplasmic reticulum (II)
Phosphoglucomutase-like protein 5 **(Pgm5)** No interaction		Intercalated disc (II) Sarcolemma (II)
Tubulin beta-2A chain **(Tubb2a)**		Cytoplasm (II) Structural constituent of cytoskeleton (III)
Histidine-rich glycoprotein (**Hrg)**		negative regulation of cell growth (I)
Histone H3.1 (**H3c1**)	Neutrophil extracellular trap formation	

Highlighting the GO oncology and KEGG related to cardiac remodeling. Abbreviations; (I): Biological process; (II): cellular localization; (III): molecular function.

4.3.9 Proteins Pathways analysis of the identified DEPs linked to inflammatory response

After conducting KEGG and GO analysis, using PANTHER pathway analysis provided additional biological insights. PANTHER Pathways are curated from a different database than KEGG, focusing on functional and evolutionary classifications of proteins, often capturing additional signalling mechanisms that may not be well-annotated in KEGG. KEGG Pathway Analysis maps proteins to well-established biological pathways with a strong emphasis on metabolic, signalling, and disease-related pathways based on curated molecular interactions.

This approach allowed us to focus on specific biological processes and signalling pathways relevant to the condition, providing valuable insights into the molecular mechanisms driving cardiac alterations. Moreover, the PANTHER approach is crucial when attempting to extrapolate biological meaning from proteomic data, especially in comparative studies of disease states. By placing the identified DEPs within the context of known, well-characterized biological pathways, PANTHER enables a more accurate interpretation of how changes in protein expression contribute to disease mechanisms. This is essential for bridging the gap between proteomics data and actionable biological insights. The results of this analysis are presented in Table 4.8, offering a clearer picture of the inflammatory pathways implicated in the study. These results will help to pave the way for future follow-up investigation, which is beyond the scope of the current study.

However, it should be noted that not all pathways identified reached statistical significance (Table 4.8). These non-significant enrichments are reported here for transparency but are considered exploratory, hypothesis-generating findings rather than definitive results.

Table 4.8: Enriched Pathways Associated with Inflammatory Response in Cardiac Remodelling Identified Using PANTHER Analysis of DEPs

Ang II vs Saline			
PANTHER categories	**PANTHER enrichment P-value**	**Protein**	**Protein alteration from DEPs analysis**
DNA replication	0.0246	H3.1	Downregulated
Cytoskeletal regulation by Rho GTPase	0.00209	Acta1, Cfl1	Upregulated
Blood coagulation	0.0399	Pzp	Downregulated
Huntington disease	0.00874	Cltb, Acta1	Upregulated
Nicotinic acetylcholine receptor signalling pathway	0.0738	Acta1	Upregulated
Integrin signalling pathway	0.0106	Itga7, Acta1	Upregulated
Heterotrimeric G-protein signalling pathway-Gq alpha and Go alpha mediated pathway	0.0952	Cltb	Upregulated
Cadherin signalling pathway	0.0974	Acta1	Upregulated
Alzheimer disease-presenilin pathway	0.0974	Acta1	Upregulated
Heterotrimeric G-protein signalling pathway-Gi alpha and Gs alpha mediated pathway	0.123	Cltb	Upregulated
Inflammation mediated by chemokine and cytokine signalling pathway	0.188	Acta1	Upregulated
Wnt signalling pathway	0.204	Acta1	Upregulated
Ang II vs Control			
PANTHER Categories	**PANTHER enrichment P-value**	**Protein**	**Protein alteration from DEPs analysis**
Plasminogen activating cascade	0.0208	Fga	Downregulated
Blood coagulation	0.00188	Fga, Pzp	Downregulated
Cytoskeletal regulation by Rho GTPase	0.102	Tubb2a	Downregulated
Parkinson disease	0.122	Psmb1	Downregulated
FGF signalling pathway	0.154	Ppp2r1b	Upregulated
Huntington disease	0.202	Tubb2a	Downregulated
Gonadotropin-releasing hormone receptor pathway	0.272	Tuba1a	Upregulated
Saline vs Control			
PANTHER Categories	**PANTHER enrichment P-value**	**Protein**	**Protein alteration from DEPs analysis**
TCA cycle	0.0203	Pdk2	Upregulated
Plasminogen activating cascade	0.0269	Fga	Downregulated
DNA replication	0.0499	H3.1	Downregulated
Cytoskeletal regulation by Rho GTPase	0.00863	Arpc1a, Cfl1	Downregulated

Blood coagulation	0.0803	Fga	Downregulated
Parkinson disease	0.0124	Psma6, Psma7	Downregulated
Huntington disease	0.0344	Arpc1a, Capns1	Downregulated
Integrin signalling pathway	0.277	Arpc1a	Downregulated
Inflammation mediated by chemokine and cytokine signalling pathway	0.348	Arpc1a	Downregulated

4.3.10 Future Directions in Molecular Characterisation: Unravelling Key Proteins and Pathways in Cardiac Remodelling

Based on the proteomic analysis conducted as part of this investigation, future molecular characterisation studies would prioritise HMGB1, Acta1, Cofilin 1, Tubba2 and Itga7. Each of these proteins represents a promising set of targets for deeper investigation, given their interconnected roles in cardiac remodelling under chronic hypertension and pre-HF condition. It is important to acknowledge that not all these proteins were significantly altered in the present dataset; their inclusion here reflects their established biological relevance and potential involvement in cardiac remodelling. Therefore, they are presented as candidates for hypothesis-driven validation in future studies, rather than as definitive outcomes of this proteomic screen.

These proteins are not only central to inflammation, actin dynamics, and cell adhesion but also key regulators of hypertrophic and fibrotic pathways in the heart. By examining the molecular mechanisms that link HMGB1 with Acta1 and Cofilin 1 in the context of inflammatory signalling and exploring the functional consequences of Itga7 in fibrosis and cell migration, we can gain critical insights into the cellular events driving pathological changes in the left ventricle.

Targeting these pathways could open new avenues for therapeutic intervention in diseases like hypertension, where cardiac remodelling contributes to disease progression. Therefore, validating these proteins and their associated pathways through advanced molecular techniques, such as gene knockdown or overexpression studies, will help solidify their roles in the disease process and offer potential biomarkers or therapeutic targets for managing cardiac dysfunction.

The most interesting observation from the PANTHER classification of pathways analysis in Table 4.8 is the upregulation of Cofilin 1 in the Ang II vs Saline comparative analysis, whilst cofilin was downregulated in Saline vs Control samples. Cfl1/Cofilin-1 is a widely distributed intracellular actin-modulating protein

that binds and depolymerises filamentous F-actin and inhibits the polymerization of monomeric G-actin in a pH-dependent manner [304,305]. Increased expression and phosphorylation of Cofilin-1 by LIM kinase aids in Rho-induced reorganisation of the actin cytoskeleton [306]. Ongoing Cofilin research in the Cunningham laboratory, make this candidate a logical step forward given the availability of tools already available.

In the context of Ang II-induced cardiac remodelling, the detection of HMGB1 within the p53 pathway, despite its non-significant differential expression, suggests a nuanced role in cardiac pathophysiology. HMGB1, a nuclear protein involved in DNA organisation and transcriptional regulation, has been implicated in both intracellular and extracellular signalling pathways. In cardiac tissues subjected to Ang II stimulation, HMGB1 role appears multifaceted. Ang II has been shown to upregulate HMGB1 expression through activation of AT1 and AT2 receptors, contributing to cardiac remodelling [307]. Moreover, decreased nuclear HMGB1 expression correlates with increased DNA damage responses and adverse cardiac remodelling, suggesting its protective role within the nucleus [222]. The presence of HMGB1 within the p53 pathway in Ang II-treated tissues may reflect its involvement in DNA repair mechanisms. The lack of significant differential expression does not exclude functional relevance, as post-translational modifications, subcellular localisation shifts, or protein-protein interactions may alter HMGB1 activity. Further investigations are warranted to elucidate the precise mechanisms by which HMGB1 interfaces with the p53 pathway in the setting of Ang II-induced cardiac remodelling.

The validation of proteomic data is currently ongoing, with a summary of the key chapter findings illustrated in Figure 4.12.

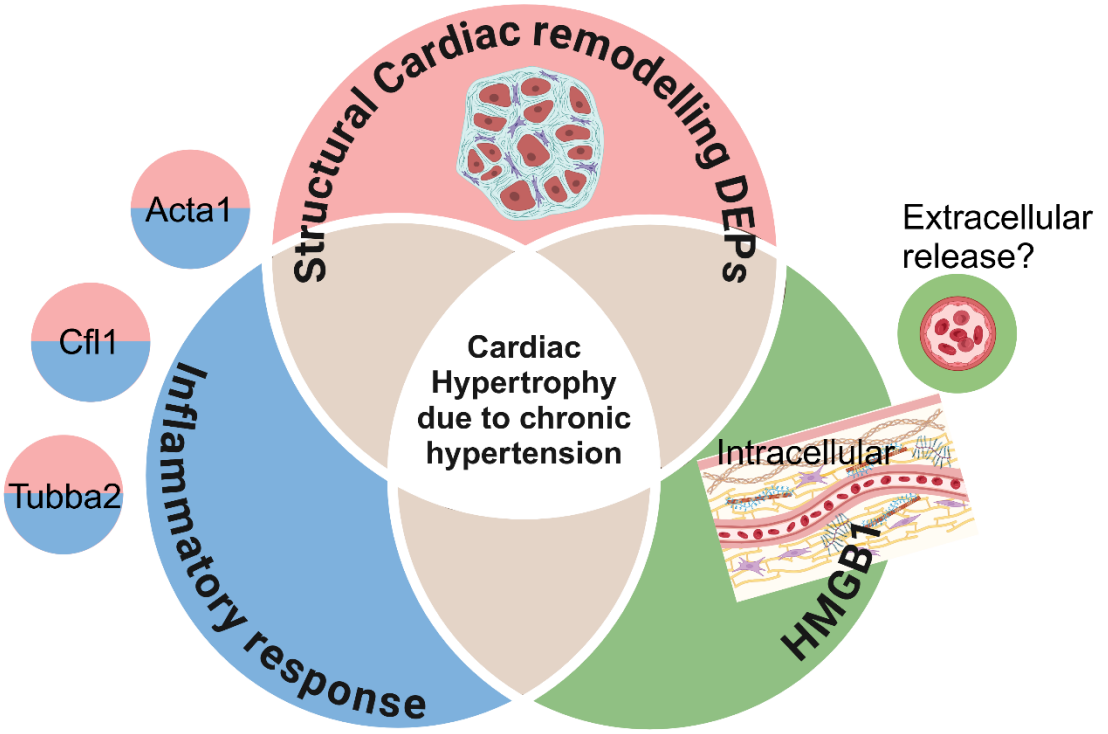

Figure 4.12: Summary of key findings based on LC-MS-based proteomics analysis of cardiac tissues.
Proteomic analyses have identified several hub proteins, including Acta1 (α-actin 1), Cfl1 (cofilin 1), and Tubb2a (β-tubulin 2a), besides cardiac remodelling as key mediators of inflammatory pathways that might influenced by HMGB1. These proteins contribute to cytoskeletal dynamics and cellular responses during inflammation, linking structural changes to signalling mechanisms within cardiac tissue. HMGB1's release as a damage-associated molecular pattern (DAMP) molecule during cardiac stress activates receptors such as TLRs and RAGE. This activation induces downstream signalling cascades, including those involving Acta1, Cfl1, and Tubb2a, which regulate cytoskeletal remodelling and cellular migration, critical for immune cell recruitment and ECM remodelling. For example: Acta1: Associated with cytoskeletal organisation, Acta1's modulation in the presence of HMGB1 suggests its role in contractile dysfunction and structural adaptations observed in remodelling. Cfl1: Cofilin 1 regulates actin filament turnover and plays a role in immune cell chemotaxis and fibroblast migration, processes driven by HMGB1-mediated inflammation. Tubb2a: This tubulin isoform is crucial for microtubule dynamics, which are affected during cellular stress and inflammation, further linking cytoskeletal changes to HMGB1's inflammatory effects. These findings could lead to future revelation of HMGB1's involvement in orchestrating cytoskeletal and inflammatory processes through proteins like Acta1, Cfl1, and Tubb2a, offering new insights into its role in cardiac remodelling. Targeting these downstream pathways may provide therapeutic opportunities to mitigate HMGB1-driven maladaptive remodelling.

4.4 Discussion

Blood pressure (BP) is a critical factor in understanding treatment strategies for heart failure (HF), but the molecular changes in BP related to inflammatory responses in cardiac remodelling, particularly in hypertensive pre-HF stages, remain unclear. This project represents the first unbiased, label-free proteomic characterisation of left ventricle tissue from non-genetically modified Ang II-induced chronic hypertension male SD rats.

While many findings in Chapter 3 align with the known pathophysiology of hypertension-induced hypertrophy, our proteomic analysis in Chapter 4 reveals potential new insights into the cellular processes involved in cardiac remodelling and inflammation. Though studying only left ventricle homogenate has its limitations, this exploratory study aims to generate hypotheses for further investigation.

The Ang II group exhibited notable concentric hypertrophy of cardiomyocytes, increased collagen deposition, and pronounced activation of pro-inflammatory HMGB1, compared to saline and control groups. To deepen our understanding of the pathophysiological changes in Ang II-induced chronic hypertension, differential protein expression and interactions were assessed using LC-MS-based proteomics. Despite capturing a limited portion of proteomic variability, our results reveal distinct proteomic signatures that highlight the structural remodelling of the heart. Notably, some differentially expressed proteins are linked to inflammation-mediated cytokine and chemokine pathways, offering valuable targets for future studies on the inflammatory mechanisms of cardiac remodelling, particularly fundamental microtubule biology within the heart.

Cardiomyocytes possess intricate cytoskeletal networks that play a pivotal role in their function. These networks are divided into two main components: the contractile sarcomere cytoskeleton, composed of actin-myosin filaments within myofibrils, and the non-sarcomere cytoskeleton, which includes β- and γ-actin,

microtubules, and intermediate filaments [308]. Microtubules, in particular, form a dynamic cross-linked scaffold that facilitates crucial cellular processes such as intracellular cargo transport, mechanical signal transmission, membrane shaping, and the organization of both myofibrils and organelles. Microtubules arise from the polymerisation of tubulin heterodimers, which consist of α- and β-tubulin subunits. These are integral components of the eukaryotic cytoskeleton and function synergistically with actin and intermediate filaments to maintain cellular integrity and function [309].

In the context of cardiac remodelling, microtubules undergo significant alterations, which can profoundly impact cardiomyocyte structure and function. The extent of these changes varies depending on the stage of pathological remodelling, influencing cardiac structure either as part of an adaptive response or a maladaptive mechanism. In the progression of HF, prolonged structural changes are maladaptive, impairing overall cardiac function. Alterations in the microtubule network—whether in terms of density, stability, or post-translational modifications are hallmark features of pathological cardiac remodelling. These changes can directly disrupt cardiomyocyte contractile function, contributing to the progression of various heart diseases [310]. The extensive interconnected transport network required to support cardiomyocytes' structure and function is illustrated in Figure 4.13. Sustained pressure overload increases MAP4 (Microtubule-Associated Protein 4, a key regulator of microtubule stability) levels and its dephosphorylation [311,312], leading to tighter microtubule binding, stabilization, and densification, which prolongs microtubule lifetime, facilitating detyrosination (the removal of a C-terminal tyrosine residue from α-tubulin, enhancing microtubule stability) and acetylation. Ultimately making microtubules more rigid and functional, affecting cell process and transport. Acta1 and Cfl1 identified in proteomic analysis are critical regulators of actin filament assembly and disassembly, influencing cardiac remodelling.

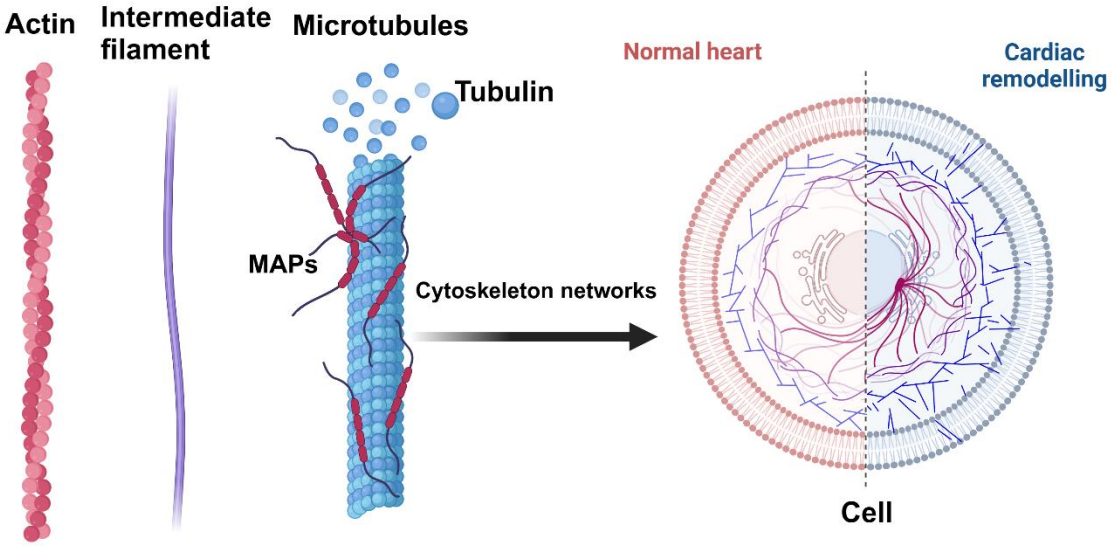

Figure 4.13: The Cytoskeleton Network and Its Components.
This figure illustrates the three main components of the cytoskeleton in mammalian cells: actin filaments, intermediate filaments, and microtubules. Actin filaments (left) are thin, flexible fibres composed of actin monomers, playing a crucial role in cell shape, motility, and intracellular transport. Intermediate filaments (centre) are more stable, rope-like structures that provide mechanical strength and structural support to the cell. Microtubules (right) are dynamic, hollow tubes made of tubulin subunits, essential for intracellular transport, mitotic spindle formation, and overall cell organization. Microtubules remain dynamic in normal heart, maintaining a balance between detyrosination and binding to microtubule-associated proteins (MAPs). However, in cardiac remodelling, microtubule network stabilisation and excessive detyrosination become prominent features. The rightmost diagram depicts the integration of these cytoskeletal components within a cell, forming an intricate network that supports cellular architecture and function. Image created with BioRender**.** Adapted from [310] .

In a normal heart, microtubules remain dynamic, maintaining a balance between detyrosination and binding to microtubule-associated proteins (MAPs), such as MAP4. However, in cardiac remodelling, microtubule network stabilization and excessive detyrosination become prominent features. At the microtubule level, mechanical stress induces hypo-phosphorylation of MAP4, promoting its accumulation on microtubules and leading to microtubule stabilization. As microtubules become more stable, they persist longer within the cell, accumulating post-translational modifications (PTMs) such as detyrosination and acetylation. These modifications further reinforce microtubule stability and enhance crosslinking between microtubules and the desmin intermediate filament network. This crosslinking occurs through structural proteins such as kinesin, plectin (actin filaments), and other MAPs.

4.4.1 Proteomic Insights into Early Cardiac Remodelling

4.4.1.1 Validating the Ang II-Induced Pre-Heart Failure Model in the Absence of Overt Dysfunction

The proteomic analysis conducted in this study, which included both significant and non-significant DEPs, provided further validation of the Ang II-induced model of cardiac remodelling in the absence of overt cardiac dysfunction. The identification of well-established cardiac biomarkers, including cardiac troponins (Tnni3 and Tnnt2), across all experimental groups, albeit without statistical significance (Table 4.4), suggests that while structural alterations occur, there is no evidence of substantial myocardial injury or contractile dysfunction. Cardiac troponins are integral components of the contractile apparatus in cardiac muscle [313], and their presence without significant alteration suggests that, despite structural remodelling, there is no substantial myocardial injury or compromise in contractile function. The study aimed to assess the prognostic value of high-sensitivity cardiac troponin T (hs-cTnT) levels in predicting HF and cardiovascular mortality among patients with stable coronary artery disease (CAD). A cohort of 3,679 patients with stable CAD was followed over a median period of 5.2 years. Baseline hs-cTnT concentrations were measured, and participants were categorized into four groups based on these levels: undetectable (<3 ng/L), low (3-8 ng/L), intermediate (9-14 ng/L), and high (≥15 ng/L) [314]. This aligns with the concept that while troponins are crucial markers of myocardial injury and dysfunction, their elevation is often associated with more advanced pathological changes leading to heart failure. The absence of significant changes in Tnni3 and Tnnt2 levels in my Ang II-induced chronic hypertension model suggests that, despite structural cardiac remodelling, there was no substantial myocardial injury or dysfunction indicative of heart failure. This finding is further supported by echocardiographic measurements, which confirmed the absence of significant cardiac dysfunction in the model.

Additionally, the significant downregulation of natriuretic peptide A (Nppa) in both Ang II vs. control and saline vs. control comparisons offers further insight. Nppa, encoding atrial natriuretic peptide (ANP), is typically upregulated in response to cardiac stress and hypertrophy, serving as a marker for cardiovascular dysfunction or injury [315]. A study investigated the role of Nppa in cardiac hypertrophy, fibrosis, and inflammation [316]. Nppa expression was found to be upregulated in response to hypertrophic stimuli, suggesting its involvement in the cardiac hypertrophic response. Additionally, Nppa exhibited antifibrotic properties by inhibiting collagen synthesis, thereby reducing myocardial fibrosis. Nppa demonstrated anti-inflammatory effects by suppressing pro-inflammatory cytokine production in disease progression. These findings highlight Nppa multifaceted protective role in cardiac remodelling. In this project, Nppa was found significantly downregulated in Ang II group aligning with its classification under the negative regulator of cell growth in GO analysis (see Table 4.8). Suggesting that Nppa downregulation may reflect an early adaptive response rather than a decompensatory shift toward heart failure and as a started protective mechanism, potentially contributing to progressive remodelling.

It is also important to acknowledge that surgical interventions themselves can introduce confounding molecular changes. Sham procedures and associated perioperative stress have been shown to alter systemic inflammatory responses and proteomic profiles independent of the primary intervention, which may partly explain the overlap observed between saline and Ang II groups in the PCA. For example, comparative proteomic analyses in brain injury models reported distinct protein expression changes in sham versus naïve animals [259] . Similarly, unbiased proteomic analysis in a neuropathic pain model demonstrated that even sham surgery alone can induce systemic inflammatory and proteomic alterations [260]. These findings highlight that sham procedures, while necessary for experimental controls, may not represent a completely “neutral” baseline and should be

considered when interpreting subtle molecular differences in high-throughput datasets such as proteomics.

4.4.2 Presence of HMGB1 in Proteomic Profiling: A Context-Dependent Regulator in Cardiac Remodelling

Shotgun proteomic analysis of LV tissue in Ang II-induced hypertension revealed HMGB1 presence in all groups with different expression (Table 4.5). Further pathway enrichment analysis using PANTHER revealed that HMGB1 was categorized under the p53 signalling pathway in all groups, though with different p-values (Section 4.3.6). While these values did not reach conventional significance thresholds, the trend suggests a potential involvement of HMGB1 in stress-related p53 mechanisms, which could be relevant to hypertensive cardiac remodelling. P53 serves as a key regulatory hub, coordinating cellular responses to various internal and external stress signals [317]. Chronic pressure overload significantly increases p53 expression in adipose tissue, accompanied by heightened adipose tissue inflammation [318]. Given that p53 is a regulator of hypertensive cardiac pathology through inflammatory response, further investigations using more stringent statistical analyses or targeted validation techniques could clarify HMGB1 functional significance in this context. Moreover, its expression level, localisation in nuclear vs. cytoplasmic, and functional state of PTM acetylated, oxidized, or secreted could differ between groups, influencing its role in either homeostasis or pathological remodelling. Determining whether HMGB1 is actively signalling in a DAMP capacity**.** This challenges the notion that HMGB1 presence alone is indicative of disease progression it necessitates further analysis of its modifications and cellular compartmentalisation.

Further investigations through STRING PPI analysis revealed that HMGB1 in Ang II group interacted with Histone H3.1 (H3c1), which was subsequently linked to Acta1, forming a significant protein network. The relevance of Histone interactions is it can modulate inflammation and chromatin remodelling, processes that are

crucial in hypertensive stress responses. Interestingly, the interaction between HMGB1 and histone H1, a linker histone involved in chromatin compaction and gene regulation, can exert a gene-specific repressive effect on immune-related functions. A study demonstrated that in severe systemic inflammation, the transcriptional silencing of TNFα occurs through the HMGB1-H1 interaction [319]. This process is associated with histone H3 lysine 9 (H3K9) methylation, a well-known epigenetic modification linked to transcriptional repression, and the recruitment of RelB, a noncanonical NF-κB subunit that acts as a transcriptional repressor in certain contexts, to the TNFα promoter, collectively leading to transcriptional repression. In alignment with these findings, the present study identification of interaction between HMGB1 and histone H3.1 in the Ang II group, suggesting a potential role of chromatin-associated HMGB1 in transcriptional regulation during Ang II-induced cardiac remodelling. Histone H3.1 is a variant of the core histone H3, primarily associated with the maintenance of chromatin integrity and epigenetic modifications influencing gene expression. The interaction between H3.1 and HMGB1 may reflect a similar mechanism to the HMGB1-H1 interaction, potentially contributing to inflammatory gene regulation in this disease model.

Additionally, the interaction between histone H3.1 and Acta1 (α-actin, skeletal muscle) in the same Ang II group further implicates cytoskeletal and nuclear dynamics in the remodelling process. Acta1 has been linked to inflammatory signalling pathways (Table 4.8), and its connection with H3.1 suggests a possible crosstalk between chromatin regulation and cytoskeletal reorganization. These interactions provide new insights into how chromatin modifications, cytoskeletal dynamics, and inflammatory pathways may converge in Ang II-induced hypertension, warranting further investigations into their functional consequences.

4.4.3 Distinct and Shared Proteomic Signatures of Cardiac Remodelling and Hypertrophy in Chronic Hypertension

Bioinformatics analysis revealed that there were biological themes unique to Ang II-infused rats when compared to control and saline rats. These caused more profound alterations comprising proteins involved in biological processes mostly including cardiac muscle contraction, cytoskeleton organisation, positive regulation of lamellipodium, regulation of the force of heart contraction, muscle organ development, negative regulation of cell growth and platelet aggregation. In addition, cellular localisation mostly includes the ruffle membrane, sarcolemma and cytoplasm. The molecular function analysis related to cardiac remodelling includes the macromolecular complex binding and structural constituent of the cytoskeleton (Figure 4.8 A, 4.9 A).

The DEPs alterations were also found to be related to the pathogenesis of cardiac remodelling and physiological process with 12 and 8 upregulated and 7 and 23 downregulated in left ventricles in Ang II vs Saline, Ang II vs Control respectively (see Section 4.3.4). These altered proteins were found to have interacted in PPI analysis with significant enriched pathways for Ang II groups related to the cardiac remodelling process and hypertrophy (Section 4.3.8, Figure 4.11). In addition, these proteins were classified under PANTHER pathways to narrow the enrichment terms in the Ang II group related to inflammatory response in cardiac remodelling. These includes cytoskeletal regulation by Rho GTPase, integrin signalling pathway, inflammation mediated by chemokine and cytokine signalling pathway (Section 4.3.9, Table 4.8).

A key observation in the results is that KEGG pathway analysis not only revealed pathways directly related to the Ang II hypertension model but also highlighted neurodegenerative diseases like Alzheimer's and Huntington's. This phenomenon occurs due to shared molecular mechanisms between diseases such as such as oxidative stress, inflammation and protein aggregation.

Hypertension has been linked to neurodegenerative diseases, as vascular dysfunction contributes to cognitive decline and neuroinflammation [320]. The presence of for example neurodegenerative disease pathways in your Ang II proteomic data suggests that hypertension may have broader systemic effects, potentially influencing pathways involved in neurodegeneration. This highlights the need for more refined statistical correction methods in pathway analysis to filter out results that may not be directly relevant to the experimental condition. Further targeted validation of key proteins would help determine their specific roles in cardiac related conditions. KEGG databases map proteins to broad biological functions based on known interactions, which sometimes results in the enrichment of disease pathways that are not directly relevant to the experimental condition but share common molecular players. Some DEPs were identified, while not specifically associated with hypertension or remodelling, were significantly overrepresented in the left ventricle. This suggests that their overexpression is not merely a result of redundancy but rather a necessary adaptation to meet the physiological demands.

A recent study examined left ventricle tissue from an essential hypertension model of spontaneous hypertensive rats compared to normotensive rats which revealed different GO functional and KEGG pathways results [299] . Results showed the most prominently enriched GO biological process for analysis showed xenobiotic catabolic process, molecular function for cholesterol binding and cellular component for mitochondrial function, and the most significantly enriched KEGG pathways were drug metabolism-cytochrome P450. This could be the result of genetic variation as a genetic model of spontaneous hypertensive rats was used and different from Ang II infusion model. Similarly, in the present project, a few DEPs located in mitochondria such as the upregulated, namely COX3, Hsp90aa1, and downregulated proteins were indicated to be related to metabolic pathways and diabetic cardiomyopathy.

4.4.2.1 Mitochondrial Dysfunction and Cardiac Remodelling

COX3 is a marker for mitochondrial injury [321] . Under cellular stress, it translocates to the cytosol, and during cell death, it is released extracellularly, where it may function as an immune mediator [322]. Circulating cytochrome was associated with MI progression and the apoptotic pathway and was investigated as a biomarker for reperfusion-associated apoptosis in patients with ST-segment elevation myocardial infarction [323]. Since Ang II-induced chronic hypertension occurred without overt cardiac dysfunction, it was considered a pre-heart failure (pre-HF) state. Despite this, evidence of cardiac remodelling was observed, including the upregulation of mitochondrial cytochrome c oxidase subunit 3 (COX3). Additionally, cytochrome c oxidase subunit 6A2 (COX6A2) was upregulated in the Ang II group (Figure 4.11), suggesting post-translational modifications of proteins involved in cardiac muscle contraction. This protein is also implicated in endothelial cell function and vascular tension regulation [324]. A study examined human myocardial cells with COX6A2 gene knockout which exhibited elevated oxidative stress levels, disrupted calcium transport activity, and reduced contractility [325]. The absence of this protein was associated with outcomes linked to heart failure (HF) or myocardial infarction (MI), highlighting its crucial role in maintaining muscle contraction and function. In the context of hypertension without cardiac dysfunction, as observed in the Ang II group, this protein appears to serve as an adaptive mechanism. In contrast, our study revealed cytochrome c oxidase subunit 6A2 (COX6A2, mitochondrial) was upregulated in the saline and control groups, likely due to physiological thermogenesis. The involvement of these protein subunits suggests a potential link to the effects of calorie restriction [326]. The findings from previous research observed diabetic cardiomyopathy in both groups as these protein subunits were possibly involved in different pathways. In addition, downregulated natriuretic peptides A showed in the saline and control group and profiled under the thermogenesis pathway which also possibly involved in this pathway. A subsequent *in vivo* study examined atrial natriuretic peptide (ANP) as a treatment that induces adipose tissue browning and

exerts thermogenic actions [327]. Another protein in the Ang II group found upregulated in the mitochondria is heat shock protein beta-6 (Hsp20/Hspb6) (Figure 4.11). This protein has a cardioprotective role against stress-induced damage [328] and is involved in cardiac structural process by regulating myocardial angiogenesis [329], as seen in the case of adaptive hypertension in the Ang II group.

4.4.2.2 Heat Shock Proteins and Fibrosis

Another heat shock protein has been implicated in the cardiac remodelling phase. Inhibition of extracellular Hsp90 alpha function significantly protected against BLM (bleomycin)-induced pulmonary fibrosis in mice by improving fibroblast overactivation and ECM production [330]. Overexpression and released Hsp90 participate in fibrosis and its extracellular release promotes fibroblast activation and migration. This protein was upregulated in the Ang II group (Figure 4.11) and was proposed to be involved in the positive regulation of lamellipodium assembly in GO classification (Table 4.6). This process increases the rate and extent of the lamellipodium formation, which is a thin sheetlike extension of the surface of a migrating cell [331] . Thus, it possibly enhances migrated cells that induce pro-inflammatory secretion that is involved in cardiac remodelling progression. Intercellular communication between these cell types, including cell-to-cell and cell-to-ECM interactions, is essential for maintaining proper cardiac function [332]. In addition to maintaining myocardial integrity and function, the intercellular communication networks between different cardiac cell populations are crucial for regulating cardiac repair following injury [333].

4.4.2.3 Cytoskeletal Remodelling and Tubulin Alterations

Another cardiac protein which may be involved in cell growth regulatory processes important for development and cellular differentiation is Csrp3. This protein has been previously examined in ventricle regeneration, as its expression increased in response to zebrafish heart injury [334]. Crp3 is part of the cysteine- and glycine-rich protein (CRP) family of muscle LIM protein-only proteins (MLP), which are involved in regulating smooth muscle cell (SMC) differentiation [335], migration, and

survival by facilitating the assembly of macromolecular signalosomes [336]. Macromolecular signalosomes are large, multi-protein complexes that enable and regulate cellular signalling pathways. LIM-only proteins primarily act as scaffolding molecules, facilitating the assembly of multi-protein complexes by binding to various signalling molecules and cytoskeletal components. This protein was upregulated in the Ang II group in the present project (Figure 4.11). Thus, it plays a role as a positive regulator in myocardium remodelling induced by hypertension. As it was involved in cardiac remodelling-related biological processes including cardiac muscle contraction, Regulation of the force of heart contraction and muscle organ development. However, prolonged cell stress and remodelling enhance proteins alterations and interactions as Csrp3 contributed to cardiac hypertrophy led to HF. This protein expression was increased in cardiac hypertrophic LV tissue with failing heart of mice [337].

The cell stress response is complex depending on disease progression, involves protein turnover either up or down-regulation, and changes in interactions, as well as molecule modifications and re-localisation. A study found that tubulin beta II colocalised with heart mitochondria in male Wistar rat ischemia/reperfusion model, and its displacement is damage time-dependent [338]. The microtubule tubulin beta 2A (Tubb2a) was downregulated (Figure 4.11) and localised in the cytoplasm which is involved in the structural constituent of the cytoskeleton in Ang II-infused rat LV tissue. This suggests that stress or disease progression affects protein function in its different expression and localisation. Another type of microtubule tubulin subunit found upregulated in the Ang II group was tubulin alpha-1A chain (Tuba1a) (Figure 4.11) involved in the molecular function structural constituent of the cytoskeleton in GO (Table 4.6). Alterations in the tubulin code at specific stages of pathological cardiac remodelling and its autoregulation during pathological progression in HF patients and murine [339]. Autoregulation is a process resulting from an internal adaptive mechanism that works to adjust the cardiac system's response to stimuli. Findings have revealed

a rapid and isoform-specific transcriptional induction and autoactivation of tubulin mRNA, combined with post-translational detyrosination, which promotes microtubule stabilisation and proliferation during the early phases of cardiac growth [339]. Microtubules are tube-like structures formed by the polymerisation of α- and β-tubulin dimers, essential for cell structure, intracellular transport, and division. They undergo dynamic growth and shrinkage, maintaining equilibrium between free and polymerized tubulin. In cardiomyocytes, microtubules regulate electrical activity, mitochondrial dynamics, protein degradation, and local translation, while also serving as load-bearing elements that affect cell mechanics and mechano-signalling [308]. Furthermore, in advanced heart failure, a shift towards autoinhibition was observed, resulting in decreased tubulin mRNA expression despite elevated tubulin protein levels. This study highlights the role of autoregulation in rewriting the tubulin code during cardiac remodelling. This explains tubulin isotypes opposite expression in the Ang II-induced cardiac remodelling group for adaptive mechanism, as two subunits were found one upregulated and the other downregulated.

A more targeted study compared patients of obstructive hypertrophic cardiomyopathy, sarcomere mutation-positive and sarcomere mutation-negative to examine tubulin's role in sarcomere-induced hypertrophy [340]. Hypertrophic cardiomyopathy (HCM) is characterised by diastolic dysfunction and asymmetrical LV hypertrophy which is a genetic hypertension whose causation differs from Ang II-induced hypertension. However, investigating the increased levels of specific proteins and their interactions specific to cardiac remodelling due to chronic hypertension could give insight into the close association of these proteins related to inflammation response. Another study examined myocardium from patients with dilated, ischaemic or advanced hypertrophic cardiomyopathy with preserved or reduced ejection fraction [341]. Super-resolution imaging has shown that failing cardiomyocytes are marked by a dense network of heavily detyrosinated microtubules, contributing to increased stiffness and impaired

contractility. Pharmacological suppression of detyrosinated microtubules reduces the viscoelasticity of failing myocytes, restoring 40–50% of lost contractile function. Similarly, reducing microtubule detyrosination through genetic approaches softens cardiomyocytes and improves contractile kinetics. These two proteomic assessments have defined the model of cytoskeletal remodelling in advanced HF in humans. As in the present project, Ang II-induced chronic hypertension without HF exhibits a similar starting point of cardiac remodelling protein alterations. A deeper understanding of cardiac remodelling mechanisms might help identify new targets for therapeutic intervention of both pre-HF and HF conditions.

4.4.2.4 Connection between Cardiac Muscle Contractility and Remodelling Markers

Another protein that is involved in cardiac remodelling is MYL4 (also known as ALC1 or MLC1) has traditionally been recognised as a myosin specific to the atria and the embryonic heart. It plays a crucial role in the contractile mechanisms of the sarcomere by enhancing cross-bridge kinetics and increasing calcium sensitivity, which leads to greater force production [342]. A study profiled genes related to cardiac contractile and contraction modulation in end-stage failing LV and found that MYL4 was downregulated [343]. Mutant variants in the MYL4 gene lead to progressive atrial cardiomyopathy in both humans and rats. Results establish MYL4 as a critical gene essential for maintaining atrial contractile function, as well as electrical and structural integrity [344]. Similarly in the present project, MYL4 was found downregulated in the Ang II group (Figure 4.11) and was involved in cardiac muscle contraction and regulation of the force of heart contraction (Table 4.7). Prolonged cardiac remodelling due to hypertension starts to affect cardiac function, as this protein is also involved in adrenergic signalling in the cardiomyocyte pathway. Furthermore, in mice with conditional knockout of guanylyl cyclase-A receptor in microcirculatory pericytes, the vasodilatory effects of ANP on precapillary arterioles and capillaries were eliminated and elevated

blood pressure [345]. As a negative regulation of cell growth, Natriuretic peptides A (Nppa) were found downregulated in the Ang II group (Figure 4.11) and involved in the cGMP-PKG signalling KEGG pathway (Table 4.7). Suggesting the role of ANP/Naap on microvascular tone is involved in the moderation of atrial blood pressure through cGMP signalling. In addition, this protein is a marker of HF case, however, here Ang II group exhibits cardiac remodelling without HF.

Four and a half LIM domains protein 1 (Fhl1), is involved in pathological cardiac hypertrophy. Fhl1 knock-out mice model of TAC exhibits a reduced reactivation of fetal gene markers, including atrial natriuretic factor and skeletal α-actin, indicating a diminished hypertrophic response [346]. This protein was found upregulated in Ang II group and involved in the biological process of negative regulation of cell growth and muscle organ development (Figure 4.11, Table 4.6). These studies provide insight into the physiological regulation of sarcomeres in response to hypertrophic stress. The sarcomere is long, cylindrical organelles that enable muscle contraction, and each is composed of overlapping thick and thin filaments made primarily of the proteins myosin and actin [347].

Protein kinase C and casein kinase substrate in neurons 2 protein (Pacsin2) found downregulated in Ang II group and was involved in cytoskeleton organisation and ruffle membrane (figure 4.11, Table 4.7). Pacsins represent a family of proteins crucial for regulating the cellular cytoskeleton, intracellular trafficking, and signalling pathways [348]. These proteins play significant roles in various physiological processes, including tissue repair across different organs, and their functional disruptions have been linked to multiple disease pathologies. Pacsin2 is expressed in both atrial and ventricular myocytes. In adult Pacsin2 knockout mice, numerous cardiac genes show downregulation within heart tissue; however, these knockout mice maintain normal cardiac morphology [349]. This suggests that Pacsin2 may be crucial in regulating the beating frequency of the heart by modulating atrial functions, where action potentials are initiated. In addition, proteins known to interact or function with Pacsin2 in cytoskeleton regulation is

actin and alpha tubulin, however, this protein showed no interaction in the present project as this model is an early stage of cardiac remodelling with no cardiac dysfunction.

4.4.2.5 Cytoskeleton Organisation Mechanotransduction and ECM-Integrin Signalling

A potent trigger of fibroblast activation and hypertrophic growth is mechanotransduction which is a molecular process converting a physical stimulus into a biological response [350]. Mechanotransduction and its downstream signalling pathways initially act as adaptive responses, serving as compensatory mechanisms to manage the early stages of load adaptation. However, with sustained or abnormal loading, these remodelling processes can transition to maladaptive responses, resulting in impaired physiological function and the progression of pathological cardiac hypertrophy and heart failure. Actin is a key cytoskeletal protein in eukaryotic cells, essential for various cellular processes, including mechano-resistance and the generation of contractile force [351]. In the present project, Actin alpha skeletal muscle (Acta1) was upregulated in the Ang II group (Figure 4.11). In end-stage failing hearts of mice models, striated actin was identified as actin alpha skeletal muscle, as observed in samples from the interventricular septum of patients with hypertrophic obstructive cardiomyopathy [352]. Similar observations in the human study of concentric LV hypertrophy due to hypertension, examined the distribution of actin alpha skeletal muscle with a high number of positively stained cardiomyocytes [353]. The actin dynamics key regulators are actin-binding protein cofilin and its upstream activator slingshot phosphatase (SSH1) [354]. SSH1 has been implicated in inflammatory signalling by regulating the NF-κB activity in endothelial cells by thrombin activation [355].

4.2.2.6 Actin Cytoskeleton Remodelling and the Role of Cofilin-1 and Integrin Signalling in Hypertensive Hearts

Cofilin-1 (Cfl1) also was upregulated in Ang II group (Figure 4.11) and involved in the positive regulator of lamellipodium assembly as well as cytoskeleton organisation in KEGG (Table 4.6) and further categorised in PANTHER under cytoskeletal regulation by Rho GTPase (Table 4.8). Cofilins belong to the actin depolymerising protein family [356]. Cfl1 is more efficient in actin depolymerization than Cfl2 [357], also mainly expressed in tissues with elevated actin turnover rates. A study found that a specific PTM of Cfl1 is a critical regulator of actin depolarisation [358]. Thus, these proteins have interacted with each other controlling the protein's key function in cardiac remodelling. This was confirmed in PPI analysis as shown interaction between Cfl1 and Acta1 and further with Hsp90aa1 and Flnc, and Flnc interacts with Itga7 all of which are involved in the structural remodelling theme. Integrin receptors interact directly or indirectly with various molecules, including actin cytoskeleton filaments. Upon activation, these interactions initiate multiple signalling cascades that regulate key cellular processes [359]. The ECM-integrin-cytoskeleton connection also plays a key role in mediating mechanotransduction signalling [360].

Integrins are heterodimeric cell receptors, consisting of α and β subunits, that function as cellular mechanosensory and mechanotransducers [361]. They provide a transmembrane linkage system, connecting extracellular matrix proteins to cortical actin within the cell. Itga7 was found upregulated in Ang II group (Figure 4.11 Ang II vs Saline) and involved in sarcolemma cellular localisation in KEGG and further categorised in PANTHER under integrin signalling pathway. Loss of integrin α7 causes a novel form of adult-onset cardiac dysfunction indicating its critical role for the in normal cardiac function [362]. Thus, integrin type is a modifier in cardiac hypertrophy as its upregulation in the present project of cardiac remodelling in Ang II group.

The hallmark of cardiac remodelling in the chronic hypertension model includes changes in cardiac structure along with function with disease progression and the activation of various signalling pathways due to protein alteration. Specifically, is because of myocardial interstitial and perivascular structural changes that involve excessive collagen deposition and are quantitatively characterised by an increase in the percentage of total myocardial tissue containing collagen fibres [363].

The subsequent tissue damage triggers an inflammatory response, activating local immune cells, primarily macrophages, and allowing various blood cells to infiltrate the injured sites. Both resident and invading immune cells release a wide range of biologically active soluble mediators, such as cytokines and chemokines, which in turn activate fibroblasts. These fibroblasts produce fibrillar collagen and other ECM components, further amplifying the production of proinflammatory cytokines, chemokines, and growth factors. This is the initiation of the fibrotic process which with prolonged activation leads to cardiac remodelling progression and ends with cardiovascular complications related to the inflammatory response. In reactive myocardial interstitial and perivascular fibrosis, diverse stimuli can induce fibrosis without cell death by activating various fibrotic signalling pathways in mesenchymal cells. This includes mechanical stress resulting from pressure overload in hypertensive heart disease. In the present project, the Ang II-induced chronic hypertension effect on the left ventricle results in up-down regulated proteins that are specifically related to structural cardiac remodelling as linked to GO functional and KEGG pathways analysis as well as in PANTHER analysis.

4.4.3 LV DEPs Interactions Related to Cardiac Remodelling that Link to Cardiac Inflammation

Cardiomyocytes undergo hypertrophy through increased protein synthesis and sarcomere reorganisation, leading to an overall increase in cardiac muscle mass [10]. The STRING database further classified protein interaction networks based on

biological processes to highlight their function which can be extrapolated by understanding the roles of their binding partners.

Proteomic analysis of Ang II groups showed key protein alterations characterised by the significant pathways related to cardiac remodelling. The hub proteins were Acta1, Flnc and Clf1 upregulated in Ang II vs saline (Figure 4.11), Hrg, Pzp, Apoa4, Fga and Cp downregulated and Csrp3 upregulated in Ang II vs control (Figure 4.11). Acta1 interacted with three upregulated proteins including Cfl1 which was involved in KEGG in the positive regulation of lamellipodium, cytoskeleton organisation and ruffle membrane, Flnc which is engaged in the sarcolemma and interacted with Csrp3. Further interactions were observed between Acta1 and H3c1, which is involved in neutrophil extracellular trap formation in KEGG, and Eno3, which both downregulated.

Interestingly, HMGB1 was found interacted with H3c1 which further linked to Acta1 (Figure 4.7) was discussed in section 4.4.2 above. Cardiac remodelling in response to Ang II-induced chronic hypertension involves structural, molecular, and inflammatory changes that contribute to disease progression. In this study, the detection of chromatin-associated HMGB1 suggests a potential role in transcriptional regulation, particularly through interactions with key nuclear proteins such as H3c1. This variant of the core histone H3, is essential for maintaining chromatin integrity and the interaction between HMGB1 and H3c1 in the Ang II model may parallel the previously reported HMGB1-H1 interaction, which is implicated in inflammatory gene regulation [319]. This suggests that HMGB1 may act as a chromatin modulator, influencing the transcriptional landscape of genes involved in inflammation and fibrosis during cardiac remodelling.

Additionally, H3c1 was found to interact with Acta1, a cytoskeletal protein associated with cardiomyocyte structure and contractility. This link further supports a nuclear-to-cytoskeletal interplay, potentially bridging inflammatory signalling with structural cardiac adaptation. Furthermore, Acta1 was found in

PANTHER category under cytoskeletal regulation by Rho GTPase with Cfl1 and Tubba2 and in inflammation mediated by chemokine and cytokine signalling pathways as well as in integrin signalling pathway with Itga7. In cell shape alteration, the cytoskeleton must undergo dynamic rearrangements, involving the disassembly and reassembly of filaments. This pathway is regulated by Rho GTPase. In general, Rho GTPase regulation and signalling involves many players including adhesion and cytokines that switch on signalling cascades that influence cell migration, endocytosis and contraction, which all regulate immune cell responses during CVD progression [364]. Cells receive extracellular stimuli through various mechanisms, including the binding of soluble molecules like growth factors, cytokines, and hormones to cell-surface receptors, adhesion interactions with the extracellular matrix, and direct cell-cell adhesions. These stimuli induce localised changes in the actin cytoskeleton, primarily mediated by Rho proteins [365]. Rho GTPases are signalling proteins essential for initiating various immune functions [366]. By interacting with a diverse set of effectors and kinases, they regulate cytoskeletal dynamics and the trafficking and proliferation of immune cells. Various isoforms of filament building blocks are produced, often specific to cell type, and combined with extensive post-translational modifications to create highly diverse actin, microtubule, or intermediate filaments [367]. This structural heterogeneity allows specific modification of cytoskeleton-mediated signalling to control cardiac remodelling, however, the inflammatory response involvement in this case still need further examination. The pro-inflammatory cytokines TNFα, IL1, and IL6 play critical roles in the pathogenesis of HF [368]. These inflammatory cytokines influence the phenotype and function of all myocardial cells by suppressing contractile function in cardiomyocytes, activating inflammatory responses in macrophages, inducing microvascular inflammation and dysfunction, and promoting a matrix degrading phenotype in fibroblasts.

Despite the underlying cause of heart failure, the induction of cytokines and chemokines contributes to myocardial dysfunction and progressive remodelling.

Inflammatory cytokines may promote apoptosis in cardiomyocytes [369]. In addition, pro-inflammatory cytokines can activate a matrix-degrading program, inducing matrix metalloproteinases that degrade the ECM, thereby eliminating essential matrix-driven signals necessary for cardiomyocyte homeostasis [370]. Finally, chronic activation of pro-inflammatory cytokines may initiate a fibrogenic program, inducing fibrogenic growth factors, expanding activated fibroblasts, and resulting in ECM protein deposition within the cardiac interstitium [371]. Moreover, evidence suggests that TLR4 plays a role in the progression of chronic HF [372]. TLR4 is expressed on the cell surface of cardiomyocytes [373]. Further studies are needed to examine this receptor molecules signalling activator such as HMGB1 which may contribute to cardiac remodelling and CVD progression, as well as the crosslink signalling.

Collectively, these findings suggest a complex interplay between HMGB1, histone modulation, and cytoskeletal regulation in Ang II-induced cardiac remodelling, emphasizing the need for targeted validation studies to confirm these mechanistic insights.

4.5 Chapter Conclusions

This study provides a comprehensive proteomic analysis of Ang II-induced chronic hypertension in the left ventricle, revealing key molecular pathways underpinning hypertensive cardiac remodelling. Bottom-up proteomics identified differentially expressed proteins linked to inflammation, extracellular matrix (ECM) reorganisation, and structural adaptation of the hypertensive heart. Network-based analyses highlighted hub proteins within cytoskeletal and ECM-related pathways, suggesting a convergence of mechanical stress and inflammatory signalling in maladaptive remodelling.

These findings deepen our understanding of the molecular landscape of hypertensive remodelling and offer a framework for future studies. Comparative proteomic analyses of other cardiac compartments, such as the right atrium or atrial–ventricular interface, may uncover region-specific mechanisms of disease.

Further validation of the key proteins identified through targeted functional assays, and *in vivo* models will be critical for confirming their roles in ECM remodelling and inflammatory regulation. Exploring their translational potential as biomarkers or therapeutic targets may provide new strategies for the management of hypertensive heart disease.

Overall, this study advances knowledge of proteomic alterations in hypertension-induced cardiac remodelling and lays the groundwork for mechanistic and therapeutic investigations in cardiovascular dysfunction.

Chapter 5:
General Discussion

5.1 Overview of key findings

Understanding the role of HMGB1, particularly the newly identified high molecular weight (HMW) form (HMW-HMGB1), cardiovascular dysfunction remains an important area of investigation. This study aimed to assess changes in HMGB1 expression and determine the presence of HMW-HMGB1 in an *in vivo* model of Ang II-induced chronic hypertension, while also exploring broader proteomic changes to identify potential biomarkers and therapeutic targets.

The study successfully established and validated a male rat model of Ang II-induced chronic hypertension (Chapter 3). Disease progression was confirmed by elevated blood pressure, increased heart weight/body weight ratio, and echocardiographic parameters consistent with hypertrophy [374] [242] . Interstitial and perivascular fibrosis were evident through Masson's trichrome staining, confirming pathological tissue remodelling [375] . Western blot analysis detected both HMGB1 and HMW-HMGB1, though expression differences across groups did not reach statistical significance. Notably, HMW-HMGB1 was present in saline and Ang II hearts but absent in naïve controls, suggesting that surgical stress may itself contribute to HMW-HMGB1 induction [161] . In contrast, immunofluorescence revealed significantly increased HMGB1 signal and altered nuclear-to-cytoplasmic distribution in Ang II tissue, highlighting its potential role in extracellular release [198] .

To investigate whether HMGB1 redistribution could reflect extracellular release, extracellular vesicles (EVs) were examined. While Ang II serum samples were limited by poor recovery, control EVs confirmed the feasibility of isolation and size characterisation by DLS. These findings complement the *in vivo* immunofluorescence data by supporting a model in which cytoplasmic HMGB1 may be secreted into extracellular vesicles. To strengthen this mechanistic link, MEG-01 cell experiments were performed, demonstrating HMGB1 release in EV cargo under basal conditions, with increased release following thrombin

stimulation [376]. This surrogate system provided additional support for non-classical HMGB1 secretion pathways that may be relevant to the Ang II model.

Finally, proteomic analysis of left ventricular tissue (Chapter 4) contextualised these findings, with principal component analysis (PCA) showing overlap between Ang II and saline groups but clear separation from naïve controls, indicating that surgical intervention may contribute to proteomic variation, but that Ang II drives a distinct hypertension-associated signature. proteomic profiling identified distinct molecular signatures associated with cytoskeletal remodelling (Acta1, Cfl1, Tubb2a), histone regulation (H3.1), and inflammatory pathways, some of which overlapped with HMGB1 biology. These findings suggest that HMGB1-linked cytoskeletal and inflammatory alterations may contribute to hypertensive cardiac remodelling and highlight candidate proteins for further validation.

In summary, this project established a robust Ang II rat model of chronic hypertension and demonstrated structural and molecular features of cardiac remodelling, including fibrosis and HMGB1 redistribution. Proteomics revealed distinct molecular signatures associated with cytoskeletal remodelling and inflammation, while PCA emphasised the need to interpret surgical confounders. Together with the EV/MEG-1 findings, these results highlight HMGB1 as a candidate mediator of inflammation-driven cardiac remodelling and suggest potential avenues for future validation as a biomarker or therapeutic target.

5.2 Ang II-induced chronic hypertension hypertrophy model in the absence of heart failure

Essentially the model in this study displayed structural hypertension-hypertrophy with pathologic cardiac hypertrophy involving cellular and molecular remodelling. We observed myocyte growth without significant proliferation, with alterations in cardiac remodelling with increased level of collagen disposition and fibrosis progression (Figure 3.6 and Figure 3.7). These cellular and molecular alterations within the myocyte are typically accompanied by changes in the ECM [377]. ECM

structural remodelling regulates the expression of fibrillar collagen synthesis and directs cell morphology, migration, differentiation, and mediates cell-cell interactions [378]. Hypertension promotes leukocyte infiltration into the heart, where interactions among macrophages, T cells, and monocytic fibroblast precursor cells modulate the imbalance between pro-inflammatory and anti-inflammatory factors [379] . The inflammatory microenvironment in the hypertensive heart promotes a positive feedback loop, enhancing leukocyte infiltration and monocyte differentiation, and driving myofibroblast formation. Elevated number of myofibroblasts, the primary contributors to ECM production, leads to collagen deposition forming fibrosis and drives cardiac remodelling [380,381]. In the present study, high level collagen disposition was exhibited in Ang II infused rats in both perivascular and interstitial areas (Figure 3.6). The progression of this cardiac remodelling leads to fibrosis by excessive deposition in the interstitial and perivascular regions, which represents a key pathological response to chronic inflammation [253].

Different forms of fibrosis, such as interstitial and perivascular, may evolve in distinct ways. Collagen volume fraction (CVF) is often considered a more accurate measure of myocardial interstitial fibrosis, as it accounts for total collagen volume rather than the percentage area of a single cross-section [255]. In this project, collagen area fraction was used as a fibrosis marker, which remains widely applied and informative but does not fully capture volume-based remodelling. Automated macro-based image analysis has been proposed as a more objective, reproducible, and cost-effective method for collagen quantification [382]. Such approaches could complement conventional analysis, particularly in regions with low collagen content where manual assessment may be less reliable.

Fibrosis progression also depends on cellular and molecular characteristics. Features such as immune cell infiltration, fibroblast activation, matricellular protein expression, and ECM cross-linking influence whether fibrosis is reversible. Increased inflammatory activity and interstitial cellularity have been associated

with recovery of myocardial function following revascularisation [383] [384], whereas hypocellular fibrotic lesions with high cross-linking are more likely irreversible [385]. Thus, the degree and type of fibrosis provide important mechanistic and prognostic information in hypertensive cardiac remodelling. These structural observations connect directly with inflammatory pathways. Fibroblasts express various pattern-recognition receptors (PRRs), including TLR4, and their activation can drive differentiation into collagen-producing myofibroblasts [386]. While inhibiting TLR4 has been proposed as a therapeutic approach, the diversity of its ligands means that selectively targeting stress-associated DAMPs such as HMGB1 may provide a more effective strategy. Persistent fibroblast activation leads to excessive ECM deposition and cross-linking, reinforcing pathological cardiac remodelling.

Ang II-treated models have demonstrated that tissue injury and inflammatory mediators further promote immune infiltration into damaged myocardium [387]. Locally generated Ang II exacerbates remodelling by sustaining a low-grade inflammatory state [388]. Importantly, TLR4 deficiency does not prevent hypertension in Ang II-infused mice but significantly reduces inflammation: IL-1β and IL-6 expression are attenuated, and Ang II-induced cardiomyocyte hypertrophy is abolished despite elevated blood pressure [247]. These findings suggest that TLR4 contributes to cardiac remodelling independently of blood pressure effects, with HMGB1 acting as a key upstream mediator. Together, these observations highlight the dual haemodynamic and inflammatory drivers of hypertension-induced cardiac pathology.

5.2.1 Is HMGB1 implicated in the Ang II-induced chronic hypertension hypertrophy model in the absence of heart failure

In the present study, high level of HMGB1 localisation and re-distribution of HMGB1 was observed in cardiac sections taken from Ang II-infused rat hearts (Figure 3.8). HMGB1 localisation was accompanied with the collagen disposition (Figure 3.11). Fibrosis progression involves a notable alteration in both the

quantity and distribution of interstitial and basement membrane collagens. This process is further characterised by modifications in vascularisation, immune cell infiltration, and is shaped by the specific underlying aetiologies and their progression [245]. HMGB1 as DAMPs molecule released under cellular stress or chronic tissue injury and induced inflammatory cells infiltration [389]. Further investigation of inflammatory cells infiltration beside HMGB1 could provide insight into immune cell-cell interaction in fibrosis area.

Interestingly in our investigations, changes in cardiac HMGB1 expression and localisation were most evident through indirect-immunofluorescence-based imaging experiments. The same changes were not significantly detected when the different compartments of the heart were dissected and processed for protein analysis via Western blotting (Figure 3.8). Instead, we noted the appearance of a higher molecular weight proteoform of HMGB1 (HMW-HMGB1) in Sal and Ang II cardiac samples, but not control samples, which raised the question of the role of surgery as a potential regulator HMGB1 expression, independent of disease.

5.2.2 Is increased HMW-HMGB1 expression linked to surgical stress during the mini-pump implantation in the experimental rodent model?

HMW-HMGB1 was detected in both saline (Sal) and Ang II groups but was absent in control groups (without surgical intervention), suggesting that surgery itself may be a sufficient trigger for increased HMW-HMGB1 expression. The role of surgery in HMGB1 regulation has been noted in previous studies [390,391], where post-operative increases in HMGB1 have been observed [392]. Evidence suggests that HMGB1 release is an early response to surgical trauma and may serve as a prognostic biomarker.

Surgical procedures are known to induce a systemic inflammatory response in patients [393], which may account for the observed increases in HMW-HMGB1 in both Sal and Ang II groups in the present study. The mini-pump model is a well-

established approach to disease induction in rodents [394], however the impact of surgery involved in this procedure upon HMGB1 levels has not been published before. This is the first study to observe changes to HMGB1 in control Sal and Ang II HMGB1 levels in the rodent minipump model.

Trauma and surgical stress can trigger immune cell activation, leading to the rapid release of DAMPs such as HMGB1 [390,395]. This is particularly relevant given that HMGB1 can act as both a passive by-product of cellular damage and an active pro-inflammatory mediator when secreted by immune cells. Interestingly in these cases, serum HMGB1 expression peaked within 1-3-days post-operation, whereas in our study HMW-HMGB1 expressed within Sal and Ang II cardiac tissue was stably observed after 28 days (Chapter 3). Given that our sham Sal and Ang II observed an increase in HMW-HMGB1, this could be an adaptive response to post-surgical wound healing, rather than an immediate pro-inflammatory-mediated event. A critical factor that has been proposed to influence the role of HMGB1 in inflammation vs wound healing is its post-translational modified (PTM) status [396]. The presence of DTT (dithiothreitol, 50mM) as a reducing agent in blotting experiments mean that the HMGB1 proteoforms observed already have had the disulfide bonds between cysteine residues reduced. It could be proposed that the HMW-HMGB1 is therefore not reliant on disulfide bonds, however non-reducing conditions would have to be carried out for comparison. This may also suggest that expression is not associated with a change in the redox state, but rather a direct increase in its synthesis, secretion, or release [397]. This could indicate a low-grade chronic inflammatory response sustained through surgery-induced tissue damage.

Much debate, unreliable reporting and significant retractions in the HMGB1 PTM field [398] has hampered progress in the HMGB1 field. Studies that have solely relied upon serum measurements are now subject to reappraisal (reviewed in [398]), with researchers now recommending the use of plasma or tissue-derived investigations for the evaluation of HMGB1 proteoforms in pathological

conditions. Our studies experienced challenges with the quality and reliability of HMGB1 detection in serum derived from our experimental rodent models. Whilst control serum could be optimised, we were unable to obtain quality reproducible data from Sal and Ang II serum samples isolated.

At present, due to the poor reliability and selectivity issues of detecting PTM HMGB1 proteoforms with current commercially available tools, we are unable to confirm the nature of the HMW-HMGB1 proteoform found in our experiments. We do not believe that the HMW-HMGB1 is a pathological feature of the Ang II model given the expression of this in the Sal samples. We propose that expression of HMW-HMGB1 in cardiac sections was an adaptive response to surgery following the implantation of the minipumps in Sal and Ang II rodent groups. This hypothesis is currently being followed up as a separate project that was beyond the scope of this thesis.

These findings potentially highlight the necessity of carefully considering surgical stress as a contributing factor in studies examining HMGB1 and its role in disease pathology, particularly in models reliant on invasive surgical procedures. Given the extent of retractions and expressions of concern within the HMGB1 field, caution should be taken when interpreting or attributing a role for changes in HMGB1 expression in pathological settings where animals were subjected to trauma such as surgery.

5.2.3 Altered HMGB1 localisation in Ang II but not Control or Sal groups – Experimental artifact or a pathological marker of the Ang II disease model?

In this present project, cardiac expression of HMGB1 was increased, with cardiomyocyte HMGB1 redistribution evident following Ang II induction. These events were not evident in any of the control cardiac tissue taken (Figure 3.9). Ang II is proposed to elevate protein levels of RAGE, TLR4, and the pro-inflammatory HMGB1, and even AT1R itself by activating NF-κB, thereby

establishing a positive feedback loop [399,400]. Considering the findings from this project, we suggest that extracellular HMGB1, as a downstream signal of AT1R stimulation in Ang II infused rats, is one of the major mediators of TLR4 activation. Studies have shown the critical roles of extracellular HMGB1 in many cardiac complications [401]. In the present study, it could be proposed that cardiac HMGB1 expression was increased (via RAGE-TLR4-dependent mechanisms) during the pathological process of pressure overload during Ang II-induced cardiac hypertrophy. Previous *in vitro* studies have proposed similar roles for HMGB1, with increased HMGB1 expression being involved in aggravated mechanical stress in cardiomyocytes [402]. Interestingly, *in vivo* studies using a transverse aortic constriction (TAC) model of cardiac hypertrophy and LV dysfunction have attributed this role to extracellular HMGB1 [403].

One of the major limitations of the HMGB1 field is the lack of transparency in the band size reporting. In most cases, protein bands are published cropped with no molecular weight marker or annotation of the band size to indicate the HMGB1 proteoform presented. Mechanical stretching of isolated cardiomyocyte cells from the Ang II-induced model would be a good experiment to conduct to compare HMGB1 changes with those published with using TAC model. This would strengthen existing data that suggests pathological changes in HMGB1 expression, with more transparent reporting to confirm the specific HMGB1 proteoform that changes.

5.2.4 Extracellular release of HMGB1via extracellular vesicles (EV) - A potential consequence of cardiac myocyte HMGB1 redistribution

Follow-up investigation into the potential consequence of HMGB1 re-distribution in cardiac sections was hampered by the inability to collect high quality blood-related products in the Sal/Ang II-treatment groups. One of the major HMGB1 secretory mechanisms that we sought to investigate was through extracellular vesicle (EV) release. The aim was to characterise the different types of EV

released by size, type and cargo to understand the potential mechanisms of HMGB1 expression changes observed at the end-point of the Ang II model. Extracellular HMGB1 is a delayed mediator of inflammation that is released late via non-classical secretion pathways [166]. In addition, other danger signals or pro-inflammatory stimuli could induce HMGB1 hyper acetylation and nuclear translocation. For example, a study reported LPS-induced HMGB1 cytoplasmic accumulation [404], however, extracellular HMGB1 was not examined. The secretion and release of HMGB1 are tightly regulated by various factors, including its post-translational modifications, such as acetylation, ADP-ribosylation, phosphorylation, and methylation, as well as the mechanisms of cell death of its extracellular release [198]. The regulatory mechanisms governing HMGB1 secretion and release are crucial areas of study.

In our study, in addition to evaluating the ability of cardiac myocytes to release HMGB1 EVs, we originally intended to determine if increased HMGB1 and its redistribution could be a consequence of enhanced circulatory HMGB levels and pathological paracrine uptake of HMGB1-enriched EVs [405]. The preference was to use serum rather than plasma, so that we could evaluate platelet-derived EVs [406]. Optimisation was complete where EVs sizes were examined from control rats' serum which are ranging from 10-1000 nm in diameter represents different types (Figure 3.12). EVs including exosomes, which are typically 50-150 nm in size and are released through the exocytosis of multivesicular bodies, and micro-vesicles (MVs), also known as microparticles or ectosomes, which are vesicles ranging from 0.1 to 1 μm in diameter and are shed from the plasma membrane [213]. EVs facilitate intercellular communication, frequently facilitating the transfer of biomolecular cargo between cells, including those of the heart [212]. During vascular endothelial cell injury, platelets release a large quantities of extracellular disulfide-HMGB1 which has cytokine like activity by inducing NETs formation, platelet aggregation and myocyte activation [192]. Haemolysis was a significant issue faced when isolating blood from Saline and Ang II-animal groups. Previous studies have

highlighted that rat erythrocytes are more sensitive to haemolysis when compared to other laboratory animal models or human blood [407,408].

Serum isolated from control rats, not subjected to surgical mini-pump implantation, was successfully achieved. The EV levels isolated from 1 control rat serum was sufficient to measure EV size via DLS but was insufficient to adequately process further as part of cargo characterisation. The animal numbers required to effectively conduct cargo characterisation would be >7-10 per animal group. When haemolysis was experienced with the Sal and Ang II animals, it was deemed unethical to sacrifice further control animals just for the purposes of characterisation in the absence of comparative analysis.

Our findings also raise the possibility that HMGB1 is released through non-classical secretion pathways, including extracellular vesicles. Although serum-based validation was limited, the *in vitro* MEG-01 model provided supportive evidence, as thrombin stimulation markedly increased HMGB1 release. This aligns with prior work showing that activated platelets and megakaryocytes can package HMGB1 into EV cargo, linking platelet activation to vascular inflammation [409]. Such vesicle-mediated secretion may represent a key mechanism coupling hypertension-induced cellular stress with fibrosis progression, bypassing classical secretion routes.

5.2.5 Translating HMGB1 EV release to a human megakaryocytic cell line that secretes platelet-like particles

In the absence of sufficient quality and quantity of rat serum, a qualitative characterisation of megakaryocyte-derived platelet-like particles was carried out to ascertain if EV's derived from PLPs isolated from MEG-01 cells contain HMGB1 cargo. As MEG-01 cells are easy to culture and spontaneously released platelet-like particles into the culture medium, we were able to mass produce cells to conduct basic EV characterisation experiments. MEG-01 displaying proplatelets then the release of PLP (Figure 3.14). This was comparable to previous published

literature of megakaryocytes and MEG-01 differentiation with different methods [410,411], with similar observations. DLS was used to differentiate the cell sizes (Figure 3.17). Three types of extracellular vesicles were found in this cell line and using flow cytometric analysis of EVs expression in MEG-01 could further used for markers identification [411]. These basic characterisation experiments will help to guide future work into *in vitro* investigation into HMGB1-EV release and its implications in a model that can be more ethically designed.

5.2.6 Implications of HMGB1 EV release to cardiovascular dysfunction

HMGB1 can be released through EVs cargo and influence other cells linking endothelial dysfunction to inflammatory response and cardiovascular diseases. Proteomic analysis of VSMCs exposed to EC-derived EVs revealed an upregulation of HMGB1 [412]. Pharmacological inhibition of HMGB1 as well as siRNA-mediated depletion of HMGB1 in VSMCs, significantly reduced EC EV-induced VCAM-1 expression and leukocyte adhesion, highlighting its inflammatory role in hypertension. Studies have demonstrated that HMGB1 is elevated in the cardiac tissue of HFpEF mice. Inhibition of HMGB1 decreases neutrophil infiltration, reduces NET formation, and improves diastolic function, highlighting its role in driving inflammation and cardiac dysfunction [413]. Platelets release a large amount of extracellular HMGB1 in injured vascular endothelial in the form of a disulfide-HMGB1, which has cytokine like activity by inducing NETs formation, platelet aggregation and myocyte activation [192]. Disulfide HMGB1 mediates cytokine secretion and cellular motility, mainly through TLR4 and induces different bone-marrow-derived macrophages phenotypes migration [414], which could advance upon the immune-coagulative nexus in CV dysfunction.

5.3 Did shotgun proteomic analysis of LV tissue offer any new insights into mechanisms of Ang II-induced Hypertension?

This study represents the first unbiased, label-free proteome changes in left ventricular tissue from non-genetically modified male Sprague-Dawley rats with Ang II-induced chronic hypertension compared to control (no surgery) and Saline control sham groups. Although the study focuses solely on left ventricular tissue homogenates, which poses certain limitations, it serves as an exploratory effort to generate testable hypotheses for further future investigation.

The Shotgun proteomic analysis further validated the characterization of the Ang II-induced chronic hypertension model as a pre-heart failure (pre-HF) condition, given the absence of significant cardiac dysfunction. By examining the DEPs, key cardiac function markers were identified, supporting this classification. Nppa, a well-established marker of progress pathological cardiac remodelling [315], was detected and significantly downregulated across two groups (Table 4.4), indicating early cardiac adaptation rather than overt failure. Nppb, another critical marker of heart failure [415], was not detected in the proteomic profile, reinforcing the notion that the model represents a pre-HF state rather than progressing to decompensated cardiac dysfunction. Additionally, cardiac troponins Tnni3 and Tnnt2 are essential for contractile function [313], were present in all groups but did not exhibit significant differential expression (Table 4.4), further supporting the absence of functional impairment. Furthermore, the connective tissue growth factor (Ctgf), also known as CCN2 is a pro-fibrotic factor acting downstream of growth factor TGFβ [416], which plays a key role in pathological extracellular matrix remodelling, was not detected, aligning with histological findings that fibrosis in the Ang II group was minor yet significant. Collectively, these proteomic findings provide molecular evidence that the Ang II-induced hypertensive model in this study represents an early-stage remodelling phase without substantial cardiac dysfunction, reinforcing its validity as a pre-HF model.

Interestingly, further proteomic analysis of LV tissue revealed HMGB1 presence in all groups even though was not significant, with pathway analysis linking it to p53 signalling (see Section 4.3.6). STRING PPI analysis identified condition-specific HMGB1 interactions, particularly with histones and actin-associated proteins, forming significant networks in hypertensive tissue. Histone H3.1 (H3c1) was found in KEGG involved neutrophil extracellular trap formation (Table 4.7), suggesting a role in inflammatory responses. Acta1, Cfl1, and Tubb2a were differentially expressed in cytoskeletal pathways, with Acta1 found in inflammation-mediated signalling and Acta1 and Cfl1 significantly enriched in cytoskeletal regulation via Rho GTPases (Table 4.8), highlighting potential links between hypertension induced cytoskeletal remodelling and inflammatory response.

Importantly, the interpretation of these proteomic findings must consider both biological and technical caveats. For example, our PCA analysis showed an overlap between saline and Ang II groups, which may reflect shared molecular effects of surgery and perioperative stress rather than treatment alone. Previous studies have demonstrated that sham surgery can itself drive systemic inflammatory and proteomic alterations independent of the primary insult [259,260]. This highlights the need for careful contextualisation of proteomic separation and reinforces that not all observed differences can be attributed solely to Ang II infusion.

In addition, while our study represents an important animal model dataset, translational value increases when considered alongside human cardiac proteomics. Large-scale proteomic profiling of human LV tissue, such as the human heart proteome atlas and cross-species comparative studies, has identified consistent alterations in cytoskeletal organisation, mitochondrial energy metabolism, and inflammatory signalling in dilated cardiomyopathy and heart failure patients [417,418]. Many of these processes overlap with the pathways highlighted in our dataset, particularly the enrichment of cytoskeletal regulators

(Acta1, Cfl1, Tubb2a) and HMGB1-associated inflammatory signatures. This overlap reinforces the biological plausibility of our findings, even though the model reflects a pre-HF hypertrophy stage rather than end-stage failure. Importantly, our observation that these proteins change early, before overt dysfunction, may indicate that cytoskeletal and HMGB1-related remodelling are early drivers of pathology rather than secondary consequences. This distinction has not been consistently captured in human studies, where tissue is typically obtained at advanced stages of disease. Therefore, our dataset provides new insights into the temporal sequence of these molecular events. However, caution is warranted, as our study reflects an early-stage, pre-HF hypertrophy model, whereas human studies often examine end-stage failing hearts. This distinction highlights the need for further data from both longitudinal animal studies and well-phenotyped human cohorts to confirm whether these molecular pathways are conserved across disease stages and to clarify their role in the transition from adaptive to maladaptive remodelling. While we cannot claim direct equivalence between rodent and human proteomes, the convergence of findings supports the translational relevance of Ang II-induced hypertension as a pre-HF model and highlights candidate pathways that may serve as biomarkers for early disease detection or targets for antifibrotic therapies.

Collectively, these findings suggest a complex interplay between HMGB1, histone modulation, and cytoskeletal regulation in Ang II-induced cardiac remodelling, and underscore the need for cautious, clinically oriented validation studies to confirm these mechanistic insights.

5.3.1. HMGB1-associated pathways feature in LV proteomics analysis

The observed presence of HMGB1 in the Ang II-treated group, despite being non-significant (Table 4.4), presents attracting implications for its role in cardiac remodelling. This is consistent with findings that Ang II can increase HMGB1 expression and release in cardiac tissues [307] and decreased nuclear HMGB1

expression has been observed in human failing hearts, which is linked to cardiomyocyte hypertrophy and fibrosis [222]. However, the potential role of extracellular HMGB1 in this context has yet to be examined.

This study provides novel insights into HMGB1-associated pathways in Ang II-induced cardiac remodelling, particularly in relation to fibrosis and cytoskeletal reorganisation. Using Masson's trichrome staining, we confirmed the presence of collagen deposition in the cardiac tissue of Ang II-treated rats, indicating enhanced ECM remodelling (see Section 3.3.2) align with HMGB1 present in both interstitial and perivascular fibrotic area (Figure 3.13). However, proteomic analysis revealed that HMGB1 was present in all groups with varying p-values (Table 4.5) and was found to be involved in the p53 signalling pathway, though without statistical significance in PANTHER analysis (Section 4.3.6). In a study, disrupting p53 activation showed that not only improves insulin resistance but also mitigates cardiac dysfunction caused by chronic pressure overload, suggesting a crucial role of adipose p53 in the heart-adipose axis in disease progression [318]. The study findings suggest that pressure overload-induced metabolic stress via p53 activation contributes to inflammation and systemic insulin resistance, which could parallel Ang II-induced cardiac remodelling through HMGB1-dependent mechanisms. The fact that HMGB1 was present in the p53 pathway even in control tissue suggests that it may be a constitutive component of baseline cellular regulation rather than solely an injury-induced signal. Additionally, the connection between p53, inflammation, and cardiac dysfunction highlights a potential interplay in myocardial adaptation to chronic hypertension as in our model of Ang II induced pre-HF case, where HMGB1 may serve as a key modulator of inflammatory signalling, cytoskeletal reorganization, and fibrosis. Given that p53 was observed in both hypertensive and control samples in my study, this suggests a possible homeostatic role in maintaining cardiac structure under normal conditions, but a pathological role in inflammatory-driven remodelling under Ang II stimulation. While the current data do not establish a definitive link, the potential

involvement of HMGB1 in p53-mediated pathways merits further exploration, particularly in the context of cytoskeletal dynamics and cellular stress responses in cardiac remodelling.

Further analysis using STRING Protein-Protein Interaction analysis revealed that in Ang II vs. Saline, HMGB1 interacted with H3c1, and H3c.1 was linked to Acta1, a cytoskeletal protein was involved in inflammatory and cytoskeleton pathways (Table 4.6). The significance of this interaction suggests that HMGB1 may influence chromatin remodelling via histone modifications, which in turn could regulate fibrosis-associated genes. This aligns with prior studies showing that HMGB1 modulates histone modifications to regulate inflammatory gene expression, including TNFα suppression through H1-mediated chromatin compaction [319]. The observed interaction between H3c1 and Acta1 in the Ang II group suggests a link between chromatin remodelling and cytoskeletal dynamics during structural cardiac remodelling. Histone H3.1 is a replication-dependent histone variant that plays a crucial role in chromatin structure and gene regulation[419]. While direct interactions between H3.1 and Acta1 have not been extensively documented, the potential crosstalk between chromatin regulation and cytoskeletal reorganisation warrants further investigation to elucidate their roles in Ang II-induced hypertension.

Interestingly, Acta1 and Cfl1 were significantly upregulated in the Cytoskeletal Regulation by Rho GTPase pathway (Table 4.8), suggesting a role in cytoskeletal remodelling in response to Ang II-induced stress. However, Acta1 was also identified in the Inflammation-Mediated by Chemokine and Cytokine Signalling Pathway but was not significant (Table 4.8), raising the possibility that Acta1 contributes to inflammatory processes but with a more indirect regulatory role.

Additionally, Histone H3.1 was downregulated and linked to Neutrophil Extracellular Trap (NET) formation in KEGG analysis, suggesting a potential role in inflammation resolution or immune regulation. Since NETs have been implicated in cardiovascular inflammation and fibrosis [420], further studies should

investigate whether HMGB1-histone interactions influence chromatin remodelling in fibroblast activation and NET formation in hypertensive hearts. As further HMGB1 was detected in the cargo of MEG-01 cells (Figure 3.20) and actively released upon thrombin stimulation (Figure 3.21). HMGB1 involvement in cardiac hypertrophy and remodelling induced by Ang II which might be influencing the disease progression in different pathway, or its activity could depend on other factors like post-translational modification. In our study, we detected HMW form of HMGB1 across all heart tissue samples of all groups using Western blot analysis (Figure 3.8). However, the differences in HMGB1 expression among these groups were not statistically significant, as reflected in the bar graph representations. This lack of significant variation suggests that while HMGB1 is present, its role in disease progression may not be solely dependent on its expression levels. In support of the potential regulatory roles of HMGB1 in cardiac remodelling, an *in vitro* study has indicated that Ang II induces HMGB1 release, contributing to inflammatory signalling in cardiac tissues. The inhibition of HMGB1 increased phosphorylation of extracellular signal-related kinase 1/2 and NF-κB, which was rescued by DDR inhibitor treatment [222]. This suggests that Ang II can promote the release of HMGB1 from cardiac myocytes, which activates inflammatory pathways such as NF-κB signalling.

Similarly, a study showed that blocking HMGB1 in an isoproterenol-induced hypertensive mouse model alleviated inflammation and reduced myocardial fibrosis [421]. However, when linking this to our proteomic findings, it is important to consider the complexity of HMGB1 role in cardiac hypertrophy and remodelling. In our study, the identified protein Acta1 that is involved in inflammatory pathways and potentially contribute to HMGB1 expression in the context of Ang II-induced remodelling. This suggests that the mechanism by which HMGB1 exacerbates inflammation and fibrosis might involve a broader network of proteins that are differentially expressed or post-translationally modified in response to Ang II.

Thus, a critical aspect to explore further would be whether the proteins identified in our study, particularly those involved in actin dynamics and cytoskeletal remodelling (Acta1 and Cfl1), interact with HMGB1 in the context of Ang II-induced cardiac remodelling, as their expression and activity may be influenced by HMGB1 or other inflammatory mediators. This could provide deeper insights into the proteomic landscape associated with HMGB1 and inflammation, ultimately offering a more comprehensive understanding of its role in cardiac hypertrophy and fibrosis.

In conclusion, although HMGB1 expression itself may not dramatically change in response to Ang II-induced cardiac remodelling, its activity might be modulated through post-translational modifications and compartmentalization. This warrants further investigation to better understand its potential contribution to the pathophysiology of hypertension and cardiac remodelling. Understanding these subtler regulatory mechanisms could help in identifying novel therapeutic targets for cardiovascular diseases associated with chronic inflammation.

5.3.2. Critical evaluation of existing LV proteomic analysis compared to Ang II-induced hypertension experiments

5.3.2.1 LV proteomic approaches reveal critical changes in cytoskeletal protein clusters

New proteomic analysis showed differentially expressed proteins involved in structural cardiac remodelling involving muscle contraction, positive regulation of the force of heart contraction. The molecular function analysis mostly revealed proteins that were structural constituent of the cytoskeleton and macromolecular complex binding. These DEPs alterations play a significant role in structural cardiac remodelling, as seen in the case of adaptive hypertension in the Ang II group.

One notable finding is the upregulation of skeletal muscle alpha-actin (Acta1) in the Ang II group in the top 5 significant listed DEPs (Table 4.1). This leads to the hypothesis that Acta1 upregulation in response to Ang II contributes to structural changes in the myocardium, potentially facilitating the adaptation mechanism to increased workload. This aligns with studies indicating that Acta1 expression is associated with cardiac hypertrophy and remodelling [422] and a human study of concentric left ventricular hypertrophy caused by hypertension, the distribution of alpha-skeletal muscle actin was examined, revealing a high number of cardiomyocytes with positive staining [353]. Furthermore, in our study the upregulated Acta1 was identified within the inflammation mediated by chemokine and cytokine signalling pathway in the Ang II group, as revealed by PANTHER classification (Table 4.8). The hypothesis here is that Acta1 not only contributes to structural remodelling but also plays a role in mediating inflammatory responses, potentially exacerbating the remodelling process. These findings align with Key regulators of actin dynamics, such as the actin-binding protein cofilin and its upstream activator, slingshot phosphatase (SSH1), were identified [354]. In addition, SSH1 has been implicated in inflammatory signalling by modulating NF-κB activity in endothelial cells following thrombin activation [355]. Notably, STRING analysis of protein-protein interactions revealed that Acta1 clusters with Cfl1 (Figure 4.11), indicating a potential functional association between these proteins. Given that Acta1 encodes α-actin, a fundamental component of the contractile apparatus in cardiomyocytes, its co-clustering with Cfl1 suggests a coordinated regulation of actin cytoskeletal dynamics. This implies that Acta1, alongside Cfl1, may play a crucial role not only in cytoskeletal remodelling but also in inflammation response pathway. Potentially impacting cellular mechanism, mechanical stress adaptation, and overall myocardial structural integrity in response to Ang II-induced hypertensive remodelling.

Another protein which is crucial for microtubule dynamics and affected during cellular stress is Tubb2a which was downregulated in Ang II infused LV tissue

(Table 4.7) and localised in the cytoplasm, where it plays a role in the structural constituent of the cytoskeleton as classified by GO. While a study demonstrated that tubulin beta II colocalises with cardiac mitochondria in the male Wistar rat ischemia/reperfusion model, with its displacement being time-dependent in relation to the extent of damage [338]. These findings suggest that stress or disease progression influences protein function through alterations in both expression levels and subcellular localisation. Employ immunofluorescence microscopy to visualise changes in cytoskeletal organization following gene manipulation in different time point. Thus, modulating the expression of Acta1, Cfl1, or Tubb2a is expected to result in observable changes in cytoskeletal architecture, supporting their roles in cardiac remodelling progression.

5.3.2.2 LV proteomic approaches reveal critical changes in mitochondrial proteins

A previous study examined LV tissue from an essential hypertension model of spontaneous hypertensive rats compared to normotensive rats which revealed different GO functional and KEGG pathways results [299]. The analysis revealed that the most prominently enriched GO terms for diseased group included the xenobiotic catabolic process in the biological process category, and components related to mitochondrial function in the cellular component category. These findings may reflect the influence of genetic variation, as the study utilized a genetic model of spontaneously hypertensive rats, which differs from the Ang II infusion model.

During cardiac hypertrophy and heart failure, Nppa is re-expressed in ventricular cardiomyocytes, serving as a highly conserved biomarker of heart disease progression [423,424]. As observed in our study, Nppa was significantly downregulated in Ang II (Table 4.4) which suggests the pre-HF condition. In this model, other proteins such as COX3, Hsp90aa1 located in mitochondria and were

upregulated (Table 4.6). In contrast, circulating cytochrome c has been reported as a potential biomarker for reperfusion-associated apoptosis in patients with ST-segment elevation myocardial infarction [323]. In addition, post-translational modifications of proteins involved in cardiac muscle contraction such as COX6A2 was upregulated in the Ang II group highlighting its crucial role in maintaining muscle contraction and function. In support of this results, human myocardial cells with COX6A2 gene knockout revealed increased oxidative stress, impaired calcium transport activity, and decreased contractility [325]. This was associated with outcomes linked progressive heart disease such as HF or MI. Collectively, in the context of pre-HF the condition of hypertension without cardiac dysfunction, as observed in our study in the Ang II group, this protein appears to serve as an adaptive mechanism.

5.3.3. Testable hypothesis – the role of Cofilin-associated protein networks as a potential new avenue for experimental follow-up

In this study, we focused exclusively on the left ventricle (LV) to generate testable hypotheses regarding the molecular mechanisms underlying Ang II-induced cardiac remodelling. The LV is the primary chamber responsible for systemic circulation and is particularly susceptible to pathological remodelling in response to chronic hypertension [28]. By conducting proteomic analysis on LV tissue, we aimed to identify differentially expressed proteins (DEPs) associated with cytoskeletal remodelling, inflammation, and fibrosis—key processes implicated in hypertensive cardiac adaptation. This approach allowed us to investigate protein networks potentially linked to structural and functional changes in the myocardium. Among the identified DEPs, cofilin-associated proteins emerged as a critical node in cytoskeletal dynamics, prompting further exploration of their role in myocardial remodelling. These findings provide a foundation for targeted experimental follow-ups to assess the contribution of cofilin-mediated signalling pathways in hypertensive heart disease.

Protein expression differences between the atria and the left ventricle reflect functional chamber specialization [425], highlighting the importance of assessing multiple cardiac regions for a comprehensive understanding of disease mechanisms. Our study focused exclusively on the left ventricle, given its central role in systemic circulation and its susceptibility to hypertensive remodelling. However, this approach may have overlooked key molecular adaptations occurring in the atria, which are known to play a crucial role in cardiac remodelling, fibrosis, and electrophysiological changes in response to hypertension. Investigating proteomic differences across different cardiac chambers could provide a more holistic view of how hypertensive stress influences the entire heart, potentially revealing novel biomarkers or therapeutic targets that are region-specific. Future studies incorporating both atrial and ventricular tissue could further clarify chamber-specific remodelling processes and their contributions to overall cardiac remodelling and dysfunction.

Proteomic analyses of the LV tissues have revealed significant alterations in proteins associated with actin dynamics and cytoskeletal regulation, notably the upregulation of Acta1 and Cfl1, alongside the downregulation of Tubb2a. These findings were verified through KEGG and Gene Ontology analyses, underscoring the pivotal role of these proteins in maintaining cytoskeletal integrity and function. The concurrent upregulation of Acta1 and Cfl1 suggests a coordinated response to modulate actin filament dynamics. Cfl1 activity is tightly regulated by phosphorylation, primarily mediated by LIM kinases, which, upon inhibition, lead to actin cytoskeleton disorganization and impaired cell motility [426]. The observed upregulation of Cfl1 may reflect a cellular adaptation to promote actin filament disassembly, facilitating cytoskeletal remodelling in response to specific stimuli. The interplay between Acta1 and Cfl1 is crucial, as cofilin-mediated actin depolymerization necessitates a balanced actin monomer pool, potentially sustained by Acta1 expression. Conversely, the significant downregulation of Tubb2a, a constituent of microtubules, points to a disruption in microtubule

dynamics. Microtubules, in conjunction with actin filaments, are essential for various cellular processes, including intracellular transport and maintenance of cell shape. The reduced expression of Tubb2a may lead to compromised microtubule stability, thereby influencing overall cytoskeletal architecture. Notably, Acta1 was identified within the inflammation mediated by chemokine and cytokine signalling pathways in PANTHER analysis (Table 4.8). This suggests a potential role for Acta1 in inflammatory responses, warranting further investigation with more stringent statistical approaches. Moreover, Acta1, Cfl1, and Tubb2a were significantly associated with the cytoskeletal regulation by Rho GTPase pathway. Rho GTPases are pivotal regulators of the cytoskeleton, orchestrating actin and microtubule dynamics to influence cell morphology and motility which consist with starting point of hypertrophy case.

The interaction between HMGB1, H3c1, and Acta1 suggests a potential link between chromatin remodelling, inflammatory signalling, and cytoskeletal adaptation in cardiac remodelling. HMGB1, a chromatin-associated protein, is known for its dual role in nuclear DNA organization and extracellular inflammatory signalling. Its association with H3c1, a histone H3 variant, indicates a possible involvement in transcriptional regulation during Ang II-induced cardiac remodelling. This interaction may contribute to the epigenetic control of genes related to inflammation and structural remodelling. Furthermore, the connection between H3c1 and Acta1, a cytoskeletal protein essential for cardiomyocyte contractility, highlights a nuclear-to-cytoskeletal signalling axis. This suggests that chromatin-associated HMGB1, through its interaction with H3c1, may influence Acta1 expression or organization, thereby linking inflammatory pathways to cytoskeletal remodelling. Such a mechanism could play a critical role in the structural adaptations seen in cardiac hypertrophy and fibrosis in pre-HF, reinforcing the need for further studies on nuclear-cytoskeletal crosstalk in cardiac disease.

The nuanced role of HMGB1 warrants additional investigation to elucidate its contribution to cardiac remodelling. These hypotheses provide a foundation for future studies aimed at understanding the molecular mechanisms underlying Ang II-induced cardiac remodelling. A key testable hypothesis for future work is to assess whether HMGB1 is released into circulation in this model. Since HMGB1 can act as a DAMP when secreted extracellularly, testing blood samples from this Ang II-induced hypertensive model could provide insight into whether HMGB1 is actively released into the serum. This would help confirm whether its presence in LV tissue reflects a localized intracellular role or if it contributes to systemic inflammatory signalling. Such findings could further elucidate HMGB1 involvement in cardiac remodelling and its potential as a biomarker for hypertension-induced cardiac changes.

The absence of a marked increase in HMGB1 expression levels in the current proteomic analysis of the LV tissue challenges the notion of its further contribution through extracellular release as HMW-HMGB1 was detected by western bot. This indicates the potential for other mechanisms at play in the Ang II-induced remodelling process. A reasonable hypothesis is that in the early stages of Ang II-induced cardiac remodelling, HMGB1 may undergo post-translational modifications or undergo cellular compartmentalisation shifts that modify its activity. Such modifications may include acetylation, methylation, or phosphorylation.

Further investigation into HMGB1 role in Ang II-induced cardiac remodelling can be supported through techniques such as targeted proteomics of quantitative interactomes such as in BioID proximity labelling, a technique used to identify proteins that are in close proximity to a protein of interest [427]. Which allows interactions in intact, living cells to be detected could identify specific post-translational modifications of HMGB1 in response to Ang II samples. Additionally, quantitative immunofluorescence analysis of nuclear versus cytoplasmic HMGB1 fractions would provide insight into the cellular compartmentalisation of HMGB1

during remodelling, as the translocation of HMGB1 from the nucleus to the cytoplasm is known to alter its activity and its interaction with inflammatory pathways. A study provides evidence for the nuclear-cytoplasmic translocation of HMGB1 during liver ischemia-reperfusion injury [428], emphasising the importance of HMGB1 subcellular localisation in the inflammatory response induced by injury or stress. Similar to our study hypertension can be classified as a stress condition, although different pathway would be tested to identify HMGB1 mechanism in this case of cardiac remodelling.

In summary, the proteomic alterations observed in Acta1, Cfl1, and Tubb2a highlight a coordinated modulation of the cytoskeleton, potentially mediated by Rho GTPase signalling pathways. The nuanced roles of these proteins in inflammation and p53-associated pathways, as suggested by pathway analyses, open avenues for future research to outline their precise functions and interactions. Understanding these dynamics could provide insights into the molecular mechanisms governing cytoskeletal regulation and its implications in cardiac remodelling progression.

5.4 Limitations of research Conclusion

While this study provides important insights into Ang II-induced chronic hypertension and its role in cardiac remodelling, several limitations must be acknowledged. One key limitation was the absence of blood sample analysis for differential expression of HMGB1, and other proteins identified in the LV proteomic profiling. Incorporating serum or plasma proteomic data would have allowed evaluation of whether proteins involved in cardiac remodelling are also released into the circulation, thereby strengthening the link between local cardiac changes and systemic inflammatory responses. In addition, although extracellular vesicles (EVs) were successfully isolated and characterised from control rat serum, low blood yield and poor protein recovery in Ang II-infused rats prevented full evaluation of EV cargo and HMGB1 release. This restricted the direct

integration of circulating extracellular HMGB1 findings with the *in vivo* cardiac localisation data.

Another limitation relates to the proteomics analyses. The number of biological replicates was modest (n = 3 per group), which limits statistical power and the generalisability of the findings. Moreover, although multiple pathway analysis tools were employed to improve robustness, statistical corrections such as false discovery rate (FDR) eliminated many of the observed pathways, likely reflecting the variability inherent in proteomic datasets. In response, uncorrected p-values were reported, an accepted approach in exploratory proteomics [429]. However, this inevitably increases the risk of false positives, and therefore the enriched pathways should be considered hypothesis-generating rather than conclusive. These limitations highlight the importance of further validation in larger experimental cohorts.

5.5 Future Work

Future work should build upon these findings with targeted functional validation and complementary approaches. Since HMGB1 was consistently identified as a key inflammatory mediator in tissue remodelling and was observed in proximity to collagen deposition and cytoskeletal regulators such as Acta1, Cfl1, and Tubb2a, its role in cytoskeletal reorganisation warrants deeper investigation. Experimental strategies such as microtubule stability assays and co-localisation studies could clarify the extent to which HMGB1 directly influences cytoskeletal dynamics in Ang II-induced cardiac remodelling. This direction is further supported by evidence that intracellular HMGB1 contributes to cardiac growth and remodelling [430], suggesting that detailed analysis of its nuclear, cytoplasmic, and extracellular distribution may uncover new mechanistic insights.

Parallel investigations should also expand the evaluation of fibrotic and inflammatory markers. Quantification of collagen I/III and α-SMA, together with

cytokines such as TNF-α, IL-6, IL-1β, TGF-β, MCP-1, and MMPs, would provide more definitive evidence of whether HMGB1-driven inflammation correlates with fibrotic progression. Incorporating Western blot, ELISA, and immunofluorescence approaches in combination would ensure robust validation across multiple platforms. Moreover, future studies could leverage circulating biomarkers such as serum carboxy-terminal pro-peptide of procollagen type I (PICP), which has been proposed as a marker of myocardial fibrosis [431]. Testing whether circulating HMGB1, alongside PICP, offers prognostic value in hypertensive patients would provide important translational relevance, allowing earlier detection of pre-HF fibrosis.

Finally, future proteomic work should involve larger sample sizes to improve statistical power and enable more stringent corrections without losing biological signal. The integration of multiple pathway tools such as KEGG, PANTHER, and GO remains important, but results must always be considered within the biological context and confirmed by orthogonal experimental methods. By combining these targeted validations with systemic biomarker analysis, future studies will be able to confirm the significance of HMGB1-associated pathways and establish their contribution to hypertensive cardiac remodelling.

Concluding Remarks

This research established a male rat model of Ang II-induced chronic hypertension, which exhibited cardiac remodelling without overt cardiac dysfunction, as confirmed by echocardiographic measurements. Fibrosis assessment through Masson's trichrome staining revealed minor but significant collagen deposition in the Ang II group, indicating early structural remodelling. HMGB1 expression and its high-molecular-weight (HMW) isoform were analysed in cardiac tissues, but their differences were not statistically significant across different heart regions, as seen in Western blot analysis. However, immunofluorescence analysis demonstrated a significant increase in HMGB1

localization, which was further validated using intensity mapping techniques, suggesting a role in localized tissue responses rather than global expression changes.

Given the challenges in isolating whole blood from Ang II rats, the human megakaryoblastic leukemia cell line (MEG-01) was utilized as an alternative model to investigate extracellular vesicle (EV) expression of HMGB1. Dynamic Light Scattering (DLS) analysis of control rat serum and MEG-01-derived EVs confirmed that exosomes from both sources fell within the same size range. MEG-01 cells were used as a model for platelet-like particles, where stimulation confirmed the release of HMGB1 within the cargo.

To gain deeper insights into the molecular mechanisms underlying hypertensive cardiac remodelling, we performed LC-MS-based proteomic analysis of left ventricular tissues. Differentially expressed proteins (DEPs) were identified and analysed using KEGG and GO pathway enrichment, PANTHER classification, and STRING-based protein-protein interaction (PPI) networks. A targeted search in the raw proteomic data confirmed the presence of HMGB1 across all experimental groups, albeit with varying statistical significance. Key findings from this study indicate that Acta1, Cfln1, Tubb2a, Itga7, and HMGB1 are likely involved in the remodelling process of hypertensive cardiac tissue and may contribute to the transition toward heart failure. These findings provide novel insights into the proteomic landscape of hypertensive remodelling in this stage and highlight potential molecular targets for future investigations into early-stage heart failure mechanisms.

References

1. Mensah GA, Fuster V, Murray CJL, et al. Global Burden of Cardiovascular Diseases and Risks, 1990-2022. *J Am Coll Cardiol*. 2023;82(25). doi:10.1016/j.jacc.2023.11.007

2. Zhou B, Perel P, Mensah GA, Ezzati M. Global epidemiology, health burden and effective interventions for elevated blood pressure and hypertension. *Nat Rev Cardiol*. 2021;18(11):785-802. doi:10.1038/s41569-021-00559-8

3. Litviňuková M, Talavera-López C, Maatz H, et al. Cells of the adult human heart. *Nature*. 2020;588(7838):466-472. doi:10.1038/s41586-020-2797-4

4. Morano I. The Contractile Machines of the Heart. In: Rickert-Sperling S, Kelly RG, Haas N, eds. *Congenital Heart Diseases: The Broken Heart: Clinical Features, Human Genetics and Molecular Pathways*. Springer International Publishing; 2024:417-433. doi:10.1007/978-3-031-44087-8_21

5. van Eif VWW, Devalla HD, Boink GJJ, Christoffels VM. Transcriptional regulation of the cardiac conduction system. *Nat Rev Cardiol*. 2018;15(10):617-630. doi:10.1038/s41569-018-0031-y

6. Ng SY, Wong CK, Tsang SY. Differential gene expressions in atrial and ventricular myocytes: insights into the road of applying embryonic stem cell-derived cardiomyocytes for future therapies. *Am J Physiol-Cell Physiol*. 2010;299(6):C1234-C1249. doi:10.1152/ajpcell.00402.2009

7. Sweeney HL, Hammers DW. Muscle Contraction. *Cold Spring Harb Perspect Biol*. 2018;10(2):a023200. doi:10.1101/cshperspect.a023200

8. Ehler E. Cardiac cytoarchitecture — why the “hardware” is important for heart function! *Biochim Biophys Acta*. 2016;1863(7Part B):1857-1863. doi:10.1016/j.bbamcr.2015.11.006

9. Metzger JM, Westfall MV. Covalent and Noncovalent Modification of Thin Filament Action. *Circ Res*. 2004;94(2):146-158. doi:10.1161/01.RES.0000110083.17024.60

10. Nakamura M, Sadoshima J. Mechanisms of physiological and pathological cardiac hypertrophy. *Nat Rev Cardiol*. 2018;15(7):387-407. doi:10.1038/s41569-018-0007-y

11. Fedele L, Brand T. The Intrinsic Cardiac Nervous System and Its Role in Cardiac Pacemaking and Conduction. *J Cardiovasc Dev Dis*. 2020;7(4):54. doi:10.3390/jcdd7040054

12. Pinto AR, Ilinykh A, Ivey MJ, et al. Revisiting Cardiac Cellular Composition. *Circ Res*. 2016;118(3):400-409. doi:10.1161/CIRCRESAHA.115.307778

13. Gimbrone MA, García-Cardeña G. Vascular endothelium, hemodynamics, and the pathobiology of atherosclerosis. *Cardiovasc Pathol Off J Soc Cardiovasc Pathol*. 2013;22(1):9-15. doi:10.1016/j.carpath.2012.06.006

14. Mitchell JA, Ali F, Bailey L, Moreno L, Harrington LS. Role of nitric oxide and prostacyclin as vasoactive hormones released by the endothelium. *Exp Physiol*. 2008;93(1):141-147. doi:10.1113/expphysiol.2007.038588

15. Topper JN, Jr MAG. Blood flow and vascular gene expression: fluid shear stress as a modulator of endothelial phenotype. Accessed September 10, 2024. https://www.cell.com/molecular-medicine/abstract/S1357-4310(98)01372-0

16. Korenaga R, Ando J, Kosaki K, Isshiki M, Takada Y, Kamiya A. Negative transcriptional regulation of the VCAM-1 gene by fluid shear stress in murine endothelial cells. *Am J Physiol-Cell Physiol*. 1997;273(5):C1506-C1515. doi:10.1152/ajpcell.1997.273.5.C1506

17. Alexander Y, Osto E, Schmidt-Trucksäss A, et al. Endothelial function in cardiovascular medicine: a consensus paper of the European Society of Cardiology Working Groups on Atherosclerosis and Vascular Biology, Aorta and Peripheral Vascular Diseases, Coronary Pathophysiology and Microcirculation, and Thrombosis. *Cardiovasc Res*. 2020;117(1):29-42. doi:10.1093/cvr/cvaa085

18. Janaszak-Jasiecka A, Płoska A, Wierońska JM, Dobrucki LW, Kalinowski L. Endothelial dysfunction due to eNOS uncoupling: molecular mechanisms as potential therapeutic targets. *Cell Mol Biol Lett*. 2023;28(1):21. doi:10.1186/s11658-023-00423-2

19. Sun HJ, Wu ZY, Nie XW, Bian JS. Role of Endothelial Dysfunction in Cardiovascular Diseases: The Link Between Inflammation and Hydrogen Sulfide. *Front Pharmacol*. 2020;10. doi:10.3389/fphar.2019.01568

20. Kario K, Okura A, Hoshide S, Mogi M. The WHO Global report 2023 on hypertension warning the emerging hypertension burden in globe and its treatment strategy. *Hypertens Res*. 2024;47(5):1099-1102. doi:10.1038/s41440-024-01622-w

21. Zhou B, Carrillo-Larco RM, Danaei G, et al. Worldwide trends in hypertension prevalence and progress in treatment and control from 1990 to 2019: a pooled analysis of 1201 population-representative studies with 104 million participants. *The Lancet*. 2021;398(10304):957-980. doi:10.1016/S0140-6736(21)01330-1

22. Choudhry NK, Kronish IM, Vongpatanasin W, et al. Medication Adherence and Blood Pressure Control: A Scientific Statement From the American Heart Association. *Hypertension*. 2022;79(1):e1-e14. doi:10.1161/HYP.0000000000000203

23. Redon J, Carmena R. Present and future of drug therapy in hypertension: an overview. *Blood Press*. 2024;33(1):2320401. doi:10.1080/08037051.2024.2320401

24. Freeman Mason W., Halvorsen Yuan-Di, Marshall William, et al. Phase 2 Trial of Baxdrostat for Treatment-Resistant Hypertension. *N Engl J Med*. 2023;388(5):395-405. doi:10.1056/NEJMoa2213169

25. Murray EC, Nosalski R, MacRitchie N, et al. Therapeutic targeting of inflammation in hypertension: from novel mechanisms to translational perspective. *Cardiovasc Res*. 2021;117(13):2589-2609. doi:10.1093/cvr/cvab330

26. Varagic J, Ahmad S, Nagata S, Ferrario CM. ACE2: Angiotensin II/Angiotensin-(1–7) Balance in Cardiac and Renal Injury. *Curr Hypertens Rep*. 2014;16(3):420. doi:10.1007/s11906-014-0420-5

27. Xiao L, Harrison DG. Inflammation in Hypertension. *Can J Cardiol*. 2020;36(5):635-647. doi:10.1016/j.cjca.2020.01.013

28. Cuspidi C, Sala C, Negri F, Mancia G, Morganti A. Prevalence of left-ventricular hypertrophy in hypertension: an updated review of echocardiographic studies. *J Hum Hypertens*. 2012;26(6):343-349. doi:10.1038/jhh.2011.104

29. Turakhia MP, Schiller NB, Whooley MA. Prognostic Significance of Increased Left Ventricular Mass Index to Mortality and Sudden Death in Patients With Stable Coronary Heart Disease (from the Heart and Soul Study). *Am J Cardiol*. 2008;102(9):1131-1135. doi:10.1016/j.amjcard.2008.06.036

30. Ha ET, Cohen M, Peterson SJ, Aronow WS. Eccentric hypertrophy predicts adverse events in patients undergoing percutaneous coronary intervention for acute coronary syndrome. *Arch Med Sci Atheroscler Dis*. 2021;6:e21-e27. doi:10.5114/amsad.2021.105175

31. Bots ML, Nikitin Y, Salonen JT, et al. Left ventricular hypertrophy and risk of fatal and non-fatal stroke. EUROSTROKE: a collaborative study among research centres in Europe. *J Epidemiol Community Health*. 2002;56(suppl 1):i8-i13. doi:10.1136/jech.56.suppl_1.i8

32. Cambronero F, Marín F, Roldán V, Hernández-Romero D, Valdés M, Lip GYH. Biomarkers of pathophysiology in hypertrophic cardiomyopathy: implications for clinical management and prognosis. *Eur Heart J*. 2009;30(2):139-151. doi:10.1093/eurheartj/ehn538

33. Saheera S, Krishnamurthy P. Cardiovascular Changes Associated with Hypertensive Heart Disease and Aging. *Cell Transplant*. 2020;29:0963689720920830. doi:10.1177/0963689720920830

34. Azevedo PS, Polegato BF, Minicucci MF, Paiva SAR, Zornoff LAM. Cardiac Remodeling: Concepts, Clinical Impact, Pathophysiological Mechanisms and Pharmacologic Treatment. *Arq Bras Cardiol*. 2016;106(1):62-69. doi:10.5935/abc.20160005

35. Pitoulis FG, Terracciano CM. Frontiers | Heart Plasticity in Response to Pressure- and Volume-Overload: A Review of Findings in Compensated and Decompensated Phenotypes. doi:10.3389/fphys.2020.00092

36. Concentric vs. eccentric remodelling in heart failure with reduced ejection fraction: clinical characteristics, pathophysiology and response to treatment - Nauta - 2020 - European Journal of Heart Failure - Wiley Online Library. Accessed September 6, 2024. https://onlinelibrary.wiley.com/doi/full/10.1002/ejhf.1632?msockid=32cf26d0eb416cfd0ce83572eacd6dc9

37. Frangogiannis NG. Cardiac fibrosis. *Cardiovasc Res*. 2021;117(6):1450. doi:10.1093/cvr/cvaa324

38. López B, Ravassa S, Moreno MU, et al. Diffuse myocardial fibrosis: mechanisms, diagnosis and therapeutic approaches. *Nat Rev Cardiol*. 2021;18(7):479-498. doi:10.1038/s41569-020-00504-1

39. González A, Schelbert EB, Díez J, Butler J. Myocardial Interstitial Fibrosis in Heart Failure: Biological and Translational Perspectives. *J Am Coll Cardiol*. 2018;71(15):1696-1706. doi:10.1016/j.jacc.2018.02.021

40. Díez J, de Boer RA. Management of cardiac fibrosis is the largest unmet medical need in heart failure. *Cardiovasc Res*. 2022;118(2):e20-e22. doi:10.1093/cvr/cvab228

41. Lindsay MM, Maxwell P, Dunn FG. Timp-1. *Hypertension*. 2002;40(2):136-141. doi:10.1161/01.HYP.0000024573.17293.23

42. Agrinier N, Thilly N, Boivin JM, Dousset B, Alla F, Zannad F. Prognostic value of serum PIIINP, MMP1 and TIMP1 levels in hypertensive patients: a community-based prospective cohort study. *Fundam Clin Pharmacol*. 2013;27(5):572-580. doi:10.1111/j.1472-8206.2012.01053.x

43. Spinale FG, Villarreal F. Targeting Matrix Metalloproteinases in Heart Disease: Lessons from Endogenous Inhibitors. *Biochem Pharmacol*. 2014;90(1):7-15. doi:10.1016/j.bcp.2014.04.011

44. Goh VJ, Le TT, Bryant J, et al. Novel Index of Maladaptive Myocardial Remodeling in Hypertension. *Circ Cardiovasc Imaging*. 2017;10(9):e006840. doi:10.1161/CIRCIMAGING.117.006840

45. Tan J, Hua Q, Xing X, Wen J, Liu R, Yang Z. Impact of the Metalloproteinase-9/Tissue Inhibitor of Metalloproteinase-1 System on Large Arterial Stiffness in Patients with Essential Hypertension. *Hypertens Res*. 2007;30(10):959-963. doi:10.1291/hypres.30.959

46. Travers JG, Kamal FA, Robbins J, Yutzey KE, Blaxall BC. Cardiac Fibrosis. *Circ Res*. 2016;118(6):1021-1040. doi:10.1161/CIRCRESAHA.115.306565

47. Mayorca-Guiliani AE, Leeming DJ, Henriksen K, et al. ECM formation and degradation during fibrosis, repair, and regeneration. *Npj Metab Health Dis*. 2025;3(1):25. doi:10.1038/s44324-025-00063-4

48. Hinderer S, Schenke-Layland K. Cardiac fibrosis – A short review of causes and therapeutic strategies. *Adv Drug Deliv Rev*. 2019;146:77-82. doi:10.1016/j.addr.2019.05.011

49. Chute M, Aujla P, Jana S, Kassiri Z. The Non-Fibrillar Side of Fibrosis: Contribution of the Basement Membrane, Proteoglycans, and Glycoproteins to Myocardial Fibrosis. *J Cardiovasc Dev Dis*. 2019;6(4):35. doi:10.3390/jcdd6040035

50. de Jong S, van Veen TAB, de Bakker JMT, Vos MA, van Rijen HVM. Biomarkers of Myocardial Fibrosis. *J Cardiovasc Pharmacol*. 2011;57(5):522. doi:10.1097/FJC.0b013e31821823d9

51. Yokota T, McCourt J, Ma F, et al. Type V collagen in scar tissue regulates the size of scar after heart injury. *Cell*. 2020;182(3):545-562.e23. doi:10.1016/j.cell.2020.06.030

52. Weber KT. Cardiac interstitium in health and disease: The fibrillar collagen network. *J Am Coll Cardiol*. 1989;13(7):1637-1652. doi:10.1016/0735-1097(89)90360-4

53. Bashey RI, Martinez-Hernandez A, Jimenez SA. Isolation, characterization, and localization of cardiac collagen type VI. Associations with other extracellular matrix components. *Circ Res*. 1992;70(5):1006-1017. doi:10.1161/01.RES.70.5.1006

54. Fan D, Creemers EE, Kassiri Z. Matrix as an Interstitial Transport System. *Circ Res*. 2014;114(5):889-902. doi:10.1161/CIRCRESAHA.114.302335

55. Bonnans C, Chou J, Werb Z. Remodelling the extracellular matrix in development and disease. *Nat Rev Mol Cell Biol*. 2014;15(12):786-801. doi:10.1038/nrm3904

56. Pozzi A, Yurchenco PD, Iozzo RV. The nature and biology of basement membranes. *Matrix Biol J Int Soc Matrix Biol*. 2017;57-58:1-11. doi:10.1016/j.matbio.2016.12.009

57. Valiente-Alandi I, Schafer AE, Blaxall BC. Extracellular matrix-mediated cellular communication in the heart. *J Mol Cell Cardiol*. 2016;91:228-237. doi:10.1016/j.yjmcc.2016.01.011

58. Chang CW, Dalgliesh AJ, López JE, Griffiths LG. “Cardiac extracellular matrix proteomics: challenges, techniques, and clinical implications.” *Proteomics Clin Appl*. 2016;10(1):39-50. doi:10.1002/prca.201500030

59. Walker CA, Spinale FG. The structure and function of the cardiac myocyte: A review of fundamental concepts. Accessed August 25, 2024. https://www.jtcvs.org/article/S0022-5223(99)70233-3/fulltext#

60. Structural and functional characterisation of cardiac fibroblasts | Cardiovascular Research | Oxford Academic. Accessed August 25, 2024. https://academic.oup.com/cardiovascres/article/65/1/40/310243?login=false

61. Jabłońska-Trypuć A, Matejczyk M, Rosochacki S. Matrix metalloproteinases (MMPs), the main extracellular matrix (ECM) enzymes in collagen degradation, as a target for anticancer drugs. *J Enzyme Inhib Med Chem*. 2016;31(sup1):177-183. doi:10.3109/14756366.2016.1161620

62. Chen K, Xu M, Lu F, He Y. Development of Matrix Metalloproteinases-Mediated Extracellular Matrix Remodeling in Regenerative Medicine: A Mini Review. *Tissue Eng Regen Med*. 2023;20(5):661-670. doi:10.1007/s13770-023-00536-x

63. Bloksgaard M, Lindsey M, Martinez-Lemus LA. Extracellular matrix in cardiovascular pathophysiology. *Am J Physiol - Heart Circ Physiol*. 2018;315(6):H1687-H1690. doi:10.1152/ajpheart.00631.2018

64. Lerman LO, Kurtz TW, Touyz RM, et al. Animal Models of Hypertension: A Scientific Statement From the American Heart Association. *Hypertension*. 2019;73(6):e87-e120. doi:10.1161/HYP.0000000000000090

65. Riehle C, Bauersachs J. Small animal models of heart failure. *Cardiovasc Res*. 2019;115(13):1838-1849. doi:10.1093/cvr/cvz161

66. Szpirer C. Rat Models of Human Diseases and Related Phenotypes: A Novel Inventory of Causative Genes. *Mamm Genome*. 2022;33(1):88-90. doi:10.1007/s00335-021-09876-2

67. Lin HY, Lee YT, Chan YW, Tse G. Animal models for the study of primary and secondary hypertension in humans. *Biomed Rep*. 2016;5(6):653-659. doi:10.3892/br.2016.784

68. Gómez GI, Velarde V. Boldine Improves Kidney Damage in the Goldblatt 2K1C Model Avoiding the Increase in TGF-β. *Int J Mol Sci*. 2018;19(7):1864. doi:10.3390/ijms19071864

69. Leite R, Salgado MC. Increased vascular formation of angiotensin II in one-kidney, one clip hypertension. *Hypertension*. 1992;19(6_pt_1):575-581. doi:10.1161/01.HYP.19.6.575

70. Fan ML, Tong HQ, Sun T, et al. Animal model of coronary microembolization under transthoracic echocardiographic guidance in rats. *Biochem Biophys Res Commun*. 2021;568:174-179. doi:10.1016/j.bbrc.2021.05.045

71. Vanegas V, Ferrebuz A, Quiroz Y, Rodríguez-Iturbe B. Hypertension in Page (cellophane-wrapped) kidney is due to interstitial nephritis. *Kidney Int*. 2005;68(3):1161-1170. doi:10.1111/j.1523-1755.2005.00508.x

72. Pechanova O, Vrankova S, Cebova M. Chronic L-Name-Treatment Produces Hypertension by Different Mechanisms in Peripheral Tissues and Brain: Role of Central eNOS. *Pathophysiology*. 2020;27(1):46-54. doi:10.3390/pathophysiology27010007

73. Rodriguez-Iturbe B. Environmental stress and hypertension: the disregarded role of HSP70. *J Hum Hypertens*. 2024;38(6):538-541. doi:10.1038/s41371-024-00917-2

74. Rassler B, Hawlitschek C, Brendel J, Zimmer HG. How Do Young and Old Spontaneously Hypertensive Rats Respond to Antihypertensive Therapy? Comparative Studies on the Effects of Combined Captopril and Nifedipine Treatment. *Biomedicines*. 2022;10(12):3059. doi:10.3390/biomedicines10123059

75. Liang M, Lee NH, Wang H, et al. Molecular networks in Dahl salt-sensitive hypertension based on transcriptome analysis of a panel of consomic rats. *Physiol Genomics*. 2008;34(1):54-64. doi:10.1152/physiolgenomics.00031.2008

76. Jaimes EA, Zhou MS, Pearse DD, Puzis L, Raij L. Upregulation of cortical COX-2 in salt-sensitive hypertension: role of angiotensin II and reactive oxygen species. *Am J Physiol-Ren Physiol*. 2008;294(2):F385-F392. doi:10.1152/ajprenal.00302.2007

77. Graham D, McBride MW, Brain NJR, Dominiczak AF. Congenic/Consomic Models of Hypertension. Accessed September 9, 2024. https://link.springer.com/protocol/10.1385/1-59259-850-1:003

78. Ames MK, Atkins CE, Pitt B. The renin-angiotensin-aldosterone system and its suppression. *J Vet Intern Med*. 2019;33(2):363-382. doi:10.1111/jvim.15454

79. Zhou C, Huang J, Chen J, et al. CYP2J2-Derived EETs Attenuated Angiotensin II-Induced Adventitial Remodeling via Reduced Inflammatory Response. *Cell Physiol Biochem*. 2016;39(2):721-739. doi:10.1159/000445663

80. Forrester SJ, Booz GW, Sigmund CD, et al. Angiotensin II Signal Transduction: An Update on Mechanisms of Physiology and Pathophysiology. *Physiol Rev*. 2018;98(3):1627-1738. doi:10.1152/physrev.00038.2017

81. Mehta PK, Griendling KK. Angiotensin II cell signaling: physiological and pathological effects in the cardiovascular system. *Am J Physiol-Cell Physiol*. 2007;292(1):C82-C97. doi:10.1152/ajpcell.00287.2006

82. Kumar U, Garimella PS, Wettersten N. Cardiorenal syndrome-Pathophysiology. *Cardiol Clin*. 2019;37(3):251-265. doi:10.1016/j.ccl.2019.04.001

83. Advani A, Kelly DJ, Cox AJ, et al. The (Pro)Renin Receptor. *Hypertension*. 2009;54(2):261-269. doi:10.1161/HYPERTENSIONAHA.109.128645

84. Santos RAS, Sampaio WO, Alzamora AC, et al. The ACE2/Angiotensin-(1–7)/MAS Axis of the Renin-Angiotensin System: Focus on Angiotensin-(1–7). *Physiol Rev*. 2018;98(1):505-553. doi:10.1152/physrev.00023.2016

85. Lo J, Patel VB, Wang Z, et al. Angiotensin-converting enzyme 2 antagonizes angiotensin II-induced pressor response and NADPH oxidase activation in Wistar–Kyoto rats and spontaneously hypertensive rats. *Exp Physiol*. 2013;98(1):109-122. doi:10.1113/expphysiol.2012.067165

86. Liu Z, Huang XR, Chen HY, Fung E, Liu J, Lan HY. Deletion of Angiotensin-Converting Enzyme-2 Promotes Hypertensive Nephropathy by Targeting Smad7 for Ubiquitin Degradation. *Hypertension*. 2017;70(4):822-830. doi:10.1161/HYPERTENSIONAHA.117.09600

87. Lautner RQ, Villela DC, Fraga-Silva RA, et al. Discovery and Characterization of Alamandine. *Circ Res*. 2013;112(8):1104-1111. doi:10.1161/CIRCRESAHA.113.301077

88. Jesus ICG de, Scalzo S, Alves F, et al. Alamandine acts via MrgD to induce AMPK/NO activation against ANG II hypertrophy in cardiomyocytes. *Am J Physiol-Cell Physiol*. 2018;314(6):C702-C711. doi:10.1152/ajpcell.00153.2017

89. Paz Ocaranza M, Riquelme JA, García L, et al. Counter-regulatory renin–angiotensin system in cardiovascular disease. *Nat Rev Cardiol*. 2020;17(2):116-129. doi:10.1038/s41569-019-0244-8

90. Oliveira V, Kwitek AE, Sigmund CD, Morselli LL, Grobe JL. Recent Advances in Hypertension. *Hypertension*. 2021;77(4):1061-1068. doi:10.1161/HYPERTENSIONAHA.120.14513

91. Wu CH, Mohammadmoradi S, Chen JZ, Sawada H, Daugherty A, Lu HS. Renin-Angiotensin System and Cardiovascular Functions. *Arterioscler Thromb Vasc Biol*. 2018;38(7):e108-e116. doi:10.1161/ATVBAHA.118.311282

92. Santos RAS, Oudit GY, Verano-Braga T, Canta G, Steckelings UM, Bader M. The renin-angiotensin system: going beyond the classical paradigms. *Am J Physiol - Heart Circ Physiol*. 2019;316(5):H958-H970. doi:10.1152/ajpheart.00723.2018

93. Sparks MA, Crowley SD, Gurley SB, Mirotsou M, Coffman TM. Classical Renin-Angiotensin System in Kidney Physiology. *Compr Physiol*. 2014;4(3):1201-1228. doi:10.1002/cphy.c130040

94. Karnik SS, Unal H, Kemp JR, et al. International Union of Basic and Clinical Pharmacology. XCIX. Angiotensin Receptors: Interpreters of Pathophysiological Angiotensinergic Stimuli. Ohlstein EH, ed. *Pharmacol Rev*. 2015;67(4):754-819. doi:10.1124/pr.114.010454

95. Guo DF, Sun YL, Hamet P, Inagami T. The angiotensin II type 1 receptor and receptor-associated proteins. *Cell Res*. 2001;11(3):165-180. doi:10.1038/sj.cr.7290083

96. AbdAlla S, Lother H, Abdel-tawab AM, Quitterer U. The Angiotensin II AT2 Receptor Is an AT1Receptor Antagonist *. *J Biol Chem*. 2001;276(43):39721-39726. doi:10.1074/jbc.M105253200

97. Miura S ichiro, Zhang J, Boros J, Karnik SS. TM2-TM7 Interaction in Coupling Movement of Transmembrane Helices to Activation of the Angiotensin II Type-1 Receptor *. *J Biol Chem*. 2003;278(6):3720-3725. doi:10.1074/jbc.M211338200

98. Patel S, Hussain T. Dimerization of AT2 and Mas Receptors in Control of Blood Pressure. *Curr Hypertens Rep*. 2018;20(5):41. doi:10.1007/s11906-018-0845-3

99. Fatima N, Patel SN, Hussain T. Angiotensin II Type 2 Receptor. *Hypertens Dallas Tex 1979*. 2021;77(6):1845-1856. doi:10.1161/HYPERTENSIONAHA.120.11941

100. Vargas Vargas RA, Varela Millán JM, Fajardo Bonilla E. Renin–angiotensin system: Basic and clinical aspects—A general perspective. *Endocrinol Diabetes Nutr*. 2022;69(1):52-62. doi:10.1016/j.endien.2022.01.005

101. Abdel Ghafar MT. An overview of the classical and tissue-derived renin-angiotensin-aldosterone system and its genetic polymorphisms in essential hypertension. *Steroids*. 2020;163:108701. doi:10.1016/j.steroids.2020.108701

102. Tsilosani A, Gao C, Zhang W. Aldosterone-Regulated Sodium Transport and Blood Pressure. *Front Physiol*. 2022;13:770375. doi:10.3389/fphys.2022.770375

103. Mentz RJ, Bakris GL, Waeber B, et al. The past, present and future of renin–angiotensin aldosterone system inhibition. *Int J Cardiol*. 2013;167(5):1677-1687. doi:10.1016/j.ijcard.2012.10.007

104. 2020 International Society of Hypertension Global Hypertension Practice Guidelines | Hypertension. Accessed July 29, 2024.

https://www.ahajournals.org/doi/full/10.1161/HYPERTENSIONAHA.120.15026

105. Thomopoulos C, Bazoukis G, Tsioufis C, Mancia G. Beta-blockers in hypertension: overview and meta-analysis of randomized outcome trials. *J Hypertens*. 2020;38(9):1669. doi:10.1097/HJH.0000000000002523

106. Basile J. The Role of Existing and Newer Calcium Channel Blockers in the Treatment of Hypertension. *J Clin Hypertens*. 2007;6(11):621-629. doi:10.1111/j.1524-6175.2004.03683.x

107. Lee EM. Calcium channel blockers for hypertension: old, but still useful. *Cardiovasc Prev Pharmacother*. 2023;5(4):113-125. doi:10.36011/cpp.2023.5.e16

108. López B, Querejeta R, González A, Sánchez E, Larman M, Díez J. Effects of loop diuretics on myocardial fibrosis and collagen type I turnover in chronic heart failure. *JACC*. 2004;43(11):2028-2035. doi:10.1016/j.jacc.2003.12.052

109. Jorde UP, Ennezat PV, Lisker J, et al. Maximally Recommended Doses of Angiotensin-Converting Enzyme (ACE) Inhibitors Do Not Completely Prevent ACE-Mediated Formation of Angiotensin II in Chronic Heart Failure. *Circulation*. 2000;101(8):844-846. doi:10.1161/01.CIR.101.8.844

110. Bomback AS, Toto R. Dual Blockade of the Renin–Angiotensin–Aldosterone System: Beyond the ACE Inhibitor and Angiotensin-II Receptor Blocker Combination. *Am J Hypertens*. 2009;22(10):1032-1040. doi:10.1038/ajh.2009.138

111. Ghatage T, Goyal SG, Dhar A, Bhat A. Novel therapeutics for the treatment of hypertension and its associated complications: peptide- and nonpeptide-based strategies. *Hypertens Res*. 2021;44(7):740-755. doi:10.1038/s41440-021-00643-z

112. Ridker PM, Everett BM, Thuren T, et al. Antiinflammatory Therapy with Canakinumab for Atherosclerotic Disease. *N Engl J Med*. 2017;377(12):1119-1131. doi:10.1056/NEJMoa1707914

113. Thupakula S, Nimmala SSR, Ravula H, Chekuri S, Padiya R. Emerging biomarkers for the detection of cardiovascular diseases. *Egypt Heart J*. 2022;74:77. doi:10.1186/s43044-022-00317-2

114. Counseller Q, Aboelkassem Y. Recent technologies in cardiac imaging. *Front Med Technol*. 2023;4:984492. doi:10.3389/fmedt.2022.984492

115. Hoffman KA, Reynolds C, Bottazzi ME, Hotez P, Jones K. Improved Biomarker and Imaging Analysis for Characterizing Progressive Cardiac Fibrosis in a Mouse Model of Chronic Chagasic Cardiomyopathy. *J Am Heart Assoc*. 2019;8(22):e013365. doi:10.1161/JAHA.119.013365

116. Blake GJ, Ridker PM. Novel Clinical Markers of Vascular Wall Inflammation. *Circ Res*. 2001;89(9):763-771. doi:10.1161/hh2101.099270

117. Held C, White HD, Stewart RAH, et al. Inflammatory Biomarkers Interleukin-6 and C-Reactive Protein and Outcomes in Stable Coronary Heart Disease: Experiences From the STABILITY (Stabilization of Atherosclerotic Plaque by Initiation of Darapladib Therapy) Trial. *J Am Heart Assoc*. 2017;6(10):e005077. doi:10.1161/JAHA.116.005077

118. Sun M, Chen M, Dawood F, et al. Tumor Necrosis Factor-α Mediates Cardiac Remodeling and Ventricular Dysfunction After Pressure Overload State. *Circulation*. 2007;115(11):1398-1407. doi:10.1161/CIRCULATIONAHA.106.643585

119. Padmanabhan S, Caulfield M, Dominiczak AF. Genetic and Molecular Aspects of Hypertension. *Circ Res*. 2015;116(6):937-959. doi:10.1161/CIRCRESAHA.116.303647

120. Drummond GR, Vinh A, Guzik TJ, Sobey CG. Immune mechanisms of hypertension. *Nat Rev Immunol*. 2019;19(8):517-532. doi:10.1038/s41577-019-0160-5

121. Epelman S, Liu PP, Mann DL. Role of innate and adaptive immune mechanisms in cardiac injury and repair. *Nat Rev Immunol*. 2015;15(2):117-129. doi:10.1038/nri3800

122. Prabhu SD, Frangogiannis NG. The Biological Basis for Cardiac Repair After Myocardial Infarction. *Circ Res*. 2016;119(1):91-112. doi:10.1161/CIRCRESAHA.116.303577

123. Mann DL. Innate Immunity and the Failing Heart. *Circ Res*. 2015;116(7):1254-1268. doi:10.1161/CIRCRESAHA.116.302317

124. Buscher K, Marcovecchio P, Hedrick CC, Ley K. Patrolling Mechanics of Non-Classical Monocytes in Vascular Inflammation. *Front Cardiovasc Med*. 2017;4:80. doi:10.3389/fcvm.2017.00080

125. Latet SC, Hoymans VY, Van Herck PL, Vrints CJ. The cellular immune system in the post-myocardial infarction repair process. *Int J Cardiol*. 2015;179:240-247. doi:10.1016/j.ijcard.2014.11.006

126. Rurik JG, Aghajanian H, Epstein JA. Immune Cells and Immunotherapy for Cardiac Injury and Repair. *Circ Res*. 2021;128(11):1766-1779. doi:10.1161/CIRCRESAHA.121.318005

127. Li D, Wu M. Pattern recognition receptors in health and diseases. *Signal Transduct Target Ther*. 2021;6(1):1-24. doi:10.1038/s41392-021-00687-0

128. Chen GY, Nuñez G. Sterile inflammation: sensing and reacting to damage. *Nat Rev Immunol*. 2010;10(12):826-837. doi:10.1038/nri2873

129. Gong T, Liu L, Jiang W, Zhou R. DAMP-sensing receptors in sterile inflammation and inflammatory diseases. *Nat Rev Immunol*. 2020;20(2):95-112. doi:10.1038/s41577-019-0215-7

130. Lu F, Lan Z, Xin Z, et al. Emerging insights into molecular mechanisms underlying pyroptosis and functions of inflammasomes in diseases. *J Cell Physiol*. 2020;235(4):3207-3221. doi:10.1002/jcp.29268

131. van Hensbergen VP, Hu X. Chapter 21 - Pattern recognition receptors and the innate immune network. In: Tang YW, Hindiyeh MY, Liu D, Sails A, Spearman P, Zhang JR, eds. *Molecular Medical Microbiology (Third Edition)*. Academic Press; 2024:407-441. doi:10.1016/B978-0-12-818619-0.00131-3

132. Vidya MK, Kumar VG, Sejian V, Bagath M, Krishnan G, Bhatta R. Toll-like receptors: Significance, ligands, signaling pathways, and functions in mammals. *Int Rev Immunol*. 2018;37(1):20-36. doi:10.1080/08830185.2017.1380200

133. Kawai T, Akira S. Toll-like Receptors and Their Crosstalk with Other Innate Receptors in Infection and Immunity. *Immunity*. 2011;34(5):637-650. doi:10.1016/j.immuni.2011.05.006

134. McCarthy CG, Goulopoulou S, Wenceslau CF, Spitler K, Matsumoto T, Webb RC. Toll-like receptors and damage-associated molecular patterns: novel links between inflammation and hypertension. *Am J Physiol-Heart Circ Physiol*. 2014;306(2):H184-H196. doi:10.1152/ajpheart.00328.2013

135. El-Zayat SR, Sibaii H, Mannaa FA. Toll-like receptors activation, signaling, and targeting: an overview. *Bull Natl Res Cent*. 2019;43(1):187. doi:10.1186/s42269-019-0227-2

136. Kawai T, Akira S. The role of pattern-recognition receptors in innate immunity: update on Toll-like receptors. *Nat Immunol*. 2010;11(5):373-384. doi:10.1038/ni.1863

137. Vaure C, Liu Y. A Comparative Review of Toll-Like Receptor 4 Expression and Functionality in Different Animal Species. *Front Immunol*. 2014;5. doi:10.3389/fimmu.2014.00316

138. Toll-Like Receptor 4 Upregulation by Angiotensin II Contributes to Hypertension and Vascular Dysfunction through Reactive Oxygen Species Production | PLOS ONE. Accessed September 16, 2024. https://journals.plos.org/plosone/article?id=10.1371/journal.pone.0104020

139. Kagan JC, Su T, Horng T, Chow A, Akira S, Medzhitov R. TRAM couples endocytosis of Toll-like receptor 4 to the induction of interferon-β. *Nat Immunol*. 2008;9(4):361-368. doi:10.1038/ni1569

140. Yamamoto M, Sato S, Hemmi H, et al. Essential role for TIRAP in activation of the signalling cascade shared by TLR2 and TLR4. *Nature*. 2002;420(6913):324-329. doi:10.1038/nature01182

141. Suzuki N, Suzuki S, Duncan GS, et al. Severe impairment of interleukin-1 and Toll-like receptor signalling in mice lacking IRAK-4. *Nature*. 2002;416(6882):750-754. doi:10.1038/nature736

142. Fisch D, Zhang T, Sun H, et al. Molecular definition of the endogenous Toll-like receptor signalling pathways. *Nature*. 2024;631(8021):635-644. doi:10.1038/s41586-024-07614-7

143. Vollmer S, Strickson S, Zhang T, et al. The mechanism of activation of IRAK1 and IRAK4 by interleukin-1 and Toll-like receptor agonists. *Biochem J*. 2017;474(12):2027-2038. doi:10.1042/BCJ20170097

144. Lin SC, Lo YC, Wu H. Helical assembly in the MyD88:IRAK4:IRAK2 complex in TLR/IL-1R signaling. *Nature*. 2010;465(7300):885-890. doi:10.1038/nature09121

145. Israël A. The IKK Complex, a Central Regulator of NF-κB Activation. *Cold Spring Harb Perspect Biol*. 2010;2(3):a000158. doi:10.1101/cshperspect.a000158

146. Pereira M, Durso DF, Bryant CE, et al. The IRAK4 scaffold integrates TLR4-driven TRIF and MYD88 signaling pathways. *Cell Rep*. 2022;40(7). doi:10.1016/j.celrep.2022.111225

147. Morrison DK. MAP Kinase Pathways. Published online November 1, 2012. doi:10.1101/cshperspect.a011254

148. Nunes KP, de Oliveira AA, Mowry FE, Biancardi VC. Targeting toll-like receptor 4 signalling pathways: can therapeutics pay the toll for

hypertension? *Br J Pharmacol*. 2019;176(12):1864-1879. doi:10.1111/bph.14438

149. Yamamoto M, Sato S, Hemmi H, et al. Role of Adaptor TRIF in the MyD88-Independent Toll-Like Receptor Signaling Pathway. *Science*. 2003;301(5633):640-643. doi:10.1126/science.1087262

150. Ullah MO, Sweet MJ, Mansell A, Kellie S, Kobe B. TRIF-dependent TLR signaling, its functions in host defense and inflammation, and its potential as a therapeutic target. *J Leukoc Biol*. 2016;100(1):27-45. doi:10.1189/jlb.2RI1115-531R

151. Phosphorylation of innate immune adaptor proteins MAVS, STING, and TRIF induces IRF3 activation | Science. Accessed September 19, 2024. https://www.science.org/doi/10.1126/science.aaa2630?url_ver=Z39.88-2003&rfr_id=ori:rid:crossref.org&rfr_dat=cr_pub%20%200pubmed

152. Sato S, Sugiyama M, Yamamoto M, et al. Toll/IL-1 Receptor Domain-Containing Adaptor Inducing IFN-β (TRIF) Associates with TNF Receptor-Associated Factor 6 and TANK-Binding Kinase 1, and Activates Two Distinct Transcription Factors, NF-κB and IFN-Regulatory Factor-3, in the Toll-Like Receptor Signaling 1. *J Immunol*. 2003;171(8):4304-4310. doi:10.4049/jimmunol.171.8.4304

153. Evavold CL, Ruan J, Tan Y, Xia S, Wu H, Kagan JC. The pore forming protein gasdermin D regulates interleukin-1 secretion from living macrophages. *Immunity*. 2018;48(1):35-44.e6. doi:10.1016/j.immuni.2017.11.013

154. McKee CM, Coll RC. NLRP3 inflammasome priming: A riddle wrapped in a mystery inside an enigma. *J Leukoc Biol*. 2020;108(3):937-952. doi:10.1002/JLB.3MR0720-513R

155. Wang L, Hauenstein AV. The NLRP3 inflammasome: Mechanism of action, role in disease and therapies. *Mol Aspects Med*. 2020;76:100889. doi:10.1016/j.mam.2020.100889

156. Franchi L, Eigenbrod T, Núñez G. TNF-α Mediate Sensitization to ATP and Silica via the NLRP3 Inflammasome in the Absence of Microbial Stimulation. *J Immunol Baltim Md 1950*. 2009;183(2):792-796. doi:10.4049/jimmunol.0900173

157. Bauerfeld CP, Rastogi R, Pirockinaite G, et al. TLR4-mediated AKT Activation is MyD88/TRIF-dependent and Critical for Induction of OxPhos and Mitochondrial Transcription Factor A in Murine Macrophages. *J*

Immunol Baltim Md 1950. 2012;188(6):2847-2857. doi:10.4049/jimmunol.1102157

158. Deng M, Tang Y, Li W, et al. The Endotoxin Delivery Protein HMGB1 Mediates Caspase-11-Dependent Lethality in Sepsis. *Immunity*. 2018;49(4):740-753.e7. doi:10.1016/j.immuni.2018.08.016

159. Wahid A, Chen W, Wang X, Tang X. High-mobility group box 1 serves as an inflammation driver of cardiovascular disease. *Biomed Pharmacother*. 2021;139:111555. doi:10.1016/j.biopha.2021.111555

160. Goodwin GH, Sanders C, Johns EW. A New Group of Chromatin-Associated Proteins with a High Content of Acidic and Basic Amino Acids. *Eur J Biochem*. 1973;38(1):14-19. doi:https://doi.org/10.1111/j.1432-1033.1973.tb03026.x

161. Kang R, Chen R, Zhang Q, et al. HMGB1 in health and disease. *Mol Aspects Med*. 2014;40:1-116. doi:10.1016/j.mam.2014.05.001

162. Štros M. HMGB proteins: Interactions with DNA and chromatin. *Biochim Biophys Acta BBA - Gene Regul Mech*. 2010;1799(1):101-113. doi:10.1016/j.bbagrm.2009.09.008

163. The structure of a chromosomal high mobility group protein–DNA complex reveals sequence-neutral mechanisms important for non-sequence-specific DNA recognition. *EMBO J*. 1999;18(23):6610-6618. doi:10.1093/emboj/18.23.6610

164. Mallik R, Kundu A, Chaudhuri S. High mobility group proteins: the multifaceted regulators of chromatin dynamics. *The Nucleus*. 2018;61(3):213-226. doi:10.1007/s13237-018-0257-4

165. Hock R, Furusawa T, Ueda T, Bustin M. HMG chromosomal proteins in development and disease. *Trends Cell Biol*. 2007;17(2):72-79. doi:10.1016/j.tcb.2006.12.001

166. Gardella S, Andrei C, Ferrera D, et al. The nuclear protein HMGB1 is secreted by monocytes via a non-classical, vesicle-mediated secretory pathway. *EMBO Rep*. 2002;3(10):995-1001. doi:10.1093/embo-reports/kvf198

167. Peng HH, Liu YJ, Ojcius DM, et al. Mineral particles stimulate innate immunity through neutrophil extracellular traps containing HMGB1. *Sci Rep*. 2017;7(1):16628. doi:10.1038/s41598-017-16778-4

168. Wu CX, Sun H, Liu Q, Guo H, Gong JP. LPS Induces HMGB1 Relocation and Release by Activating the NF-κB-CBP Signal Transduction Pathway in the Murine Macrophage-Like Cell Line RAW264.7. *J Surg Res*. 2012;175(1):88-100. doi:10.1016/j.jss.2011.02.026

169. Xu B, Lang L min, Lian S, et al. Neuroinflammation induced by secretion of acetylated HMGB1 from activated microglia in hippocampi of mice following chronic cold exposure. *Brain Res*. 2020;1726:146495. doi:10.1016/j.brainres.2019.146495

170. Vogel S, Bodenstein R, Chen Q, et al. Platelet-derived HMGB1 is a critical mediator of thrombosis. *J Clin Invest*. 2015;125(12):4638-4654. doi:10.1172/JCI81660

171. Pawlinski R. Platelet HMGB1: the venous clot coordinator. *Blood*. 2016;128(20):2376-2378. doi:10.1182/blood-2016-09-738740

172. Dyer MR, Chen Q, Haldeman S, et al. Deep vein thrombosis in mice is regulated by platelet HMGB1 through release of neutrophil-extracellular traps and DNA. *Sci Rep*. 2018;8:2068. doi:10.1038/s41598-018-20479-x

173. Mullins GE, Sunden-Cullberg J, Johansson AS, et al. Activation of Human Umbilical Vein Endothelial Cells Leads to Relocation and Release of High-Mobility Group Box Chromosomal Protein 1. *Scand J Immunol*. 2004;60(6):566-573. doi:10.1111/j.0300-9475.2004.01518.x

174. Kang L, Guo N, Liu X, et al. High mobility group box-1 protects against Aflatoxin G1-induced pulmonary epithelial cell damage in the lung inflammatory environment. *Toxicol Lett*. 2020;331:92-101. doi:10.1016/j.toxlet.2020.05.013

175. Chi JH, Seo GS, Cheon JH, Lee SH. Isoliquiritigenin inhibits TNF-α-induced release of high-mobility group box 1 through activation of HDAC in human intestinal epithelial HT-29 cells. *Eur J Pharmacol*. 2017;796:101-109. doi:10.1016/j.ejphar.2016.12.026

176. Alsousi AA, Igwe OJ. Redox-active trace metal-induced release of high mobility group box 1(HMGB1) and inflammatory cytokines in fibroblast-like synovial cells is Toll-like receptor 4 (TLR4) dependent. *Biochim Biophys Acta BBA - Mol Basis Dis*. 2018;1864(11):3847-3858. doi:10.1016/j.bbadis.2018.08.029

177. An K, Rong H, Ni H, et al. Spinal PKC activation — Induced neuronal HMGB1 translocation contributes to hyperalgesia in a bone cancer pain model in rats. *Exp Neurol*. 2018;303:80-94. doi:10.1016/j.expneurol.2018.02.003

178. Li W, Deng M, Loughran PA, et al. LPS Induces Active HMGB1 Release From Hepatocytes Into Exosomes Through the Coordinated Activities of TLR4 and Caspase-11/GSDMD Signaling. *Front Immunol*. 2020;0. doi:10.3389/fimmu.2020.00229

179. Tao A, Song J, Lan T, et al. Cardiomyocyte–fibroblast interaction contributes to diabetic cardiomyopathy in mice: Role of HMGB1/TLR4/IL-33 axis. *Biochim Biophys Acta BBA - Mol Basis Dis*. 2015;1852(10, Part A):2075-2085. doi:10.1016/j.bbadis.2015.07.015

180. Yang H, Antoine DJ, Andersson U, Tracey KJ. The many faces of HMGB1: molecular structure-functional activity in inflammation, apoptosis, and chemotaxis. *J Leukoc Biol*. 2013;93(6):865-873. doi:10.1189/jlb.1212662

181. Blair RH, Horn AE, Pazhani Y, Grado L, Goodrich JA, Kugel JF. The HMGB1 C-Terminal Tail Regulates DNA Bending. *J Mol Biol*. 2016;428(20):4060-4072. doi:10.1016/j.jmb.2016.08.018

182. Postnikov YV, Bustin M. Functional Interplay Between Histone H1 and HMG Proteins in Chromatin. *Biochim Biophys Acta*. 2016;1859(3):462-467. doi:10.1016/j.bbagrm.2015.10.006

183. Watson M, Stott K, Fischl H, Cato L, Thomas JO. Characterization of the interaction between HMGB1 and H3—a possible means of positioning HMGB1 in chromatin. *Nucleic Acids Res*. 2014;42(2):848-859. doi:10.1093/nar/gkt950

184. Jung Y, Lippard SJ. Nature of Full-Length HMGB1 Binding to Cisplatin-Modified DNA. *Biochemistry*. 2003;42(9):2664-2671. doi:10.1021/bi026972w

185. Lee SA, Kwak MS, Kim S, Shin JS. The Role of High Mobility Group Box 1 in Innate Immunity. *Yonsei Med J*. 2014;55(5):1165-1176. doi:10.3349/ymj.2014.55.5.1165

186. Bonaldi T, Talamo F, Scaffidi P, et al. Monocytic cells hyperacetylate chromatin protein HMGB1 to redirect it towards secretion. *EMBO J*. 2003;22(20):5551-5560. doi:10.1093/emboj/cdg516

187. Huttunen HJ, Fages C, Kuja-Panula J, Ridley AJ, Rauvala H. Receptor for Advanced Glycation End Products-binding COOH-terminal Motif of Amphoterin Inhibits Invasive Migration and Metastasis. *Cancer Res*. 2002;62(16):4805-4811. Accessed February 26, 2021. https://cancerres.aacrjournals.org/content/62/16/4805

188. Li J, Kokkola R, Tabibzadeh S, et al. Structural Basis for the Proinflammatory Cytokine Activity of High Mobility Group Box 1. *Mol Med*. 2003;9(1-2):37-45. Accessed February 23, 2021. https://www.ncbi.nlm.nih.gov/pmc/articles/PMC1430376/

189. Ito Takashi, Kawahara Ko-ichi, Okamoto Kohji, et al. Proteolytic Cleavage of High Mobility Group Box 1 Protein by Thrombin-Thrombomodulin Complexes. *Arterioscler Thromb Vasc Biol*. 2008;28(10):1825-1830. doi:10.1161/ATVBAHA.107.150631

190. Yang H, Ochani M, Li J, et al. Reversing established sepsis with antagonists of endogenous high-mobility group box 1. *Proc Natl Acad Sci U S A*. 2004;101(1):296-301. doi:10.1073/pnas.2434651100

191. Rowell JP, Simpson KL, Stott K, Watson M, Thomas JO. HMGB1-Facilitated p53 DNA Binding Occurs via HMG-Box/p53 Transactivation Domain Interaction, Regulated by the Acidic Tail. *Structure*. 2012;20(12):2014-2024. doi:10.1016/j.str.2012.09.004

192. Stark K, Philippi V, Stockhausen S, et al. Disulfide HMGB1 derived from platelets coordinates venous thrombosis in mice. *Blood*. 2016;128(20):2435-2449. doi:10.1182/blood-2016-04-710632

193. Sekiguchi F, Kawabata A. Role of HMGB1 in Chemotherapy-Induced Peripheral Neuropathy. *Int J Mol Sci*. 2021;22(1):367. doi:10.3390/ijms22010367

194. Lotze MT, Tracey KJ. High-mobility group box 1 protein (HMGB1): nuclear weapon in the immune arsenal. *Nat Rev Immunol*. 2005;5(4):331-342. doi:10.1038/nri1594

195. Walko TD, Di Caro V, Piganelli J, Billiar TR, Clark RS, Aneja RK. Poly(ADP-Ribose) Polymerase 1–Sirtuin 1 Functional Interplay Regulates LPS-Mediated High Mobility Group Box 1 Secretion. *Mol Med*. 2015;20(1):612-624. doi:10.2119/molmed.2014.00156

196. Scaffidi P, Misteli T, Bianchi ME. Release of chromatin protein HMGB1 by necrotic cells triggers inflammation. *Nature*. 2002;418(6894):191-195. doi:10.1038/nature00858

197. Kim J, Gee HY, Lee MG. Unconventional protein secretion – new insights into the pathogenesis and therapeutic targets of human diseases. *J Cell Sci*. 2018;131(12). doi:10.1242/jcs.213686

198. Chen R, Kang R, Tang D. The mechanism of HMGB1 secretion and release. *Exp Mol Med*. 2022;54(2):91-102. doi:10.1038/s12276-022-00736-w

199. Schaefer L. Complexity of Danger: The Diverse Nature of Damage-associated Molecular Patterns. *J Biol Chem*. 2014;289(51):35237-35245. doi:10.1074/jbc.R114.619304

200. Park JS, Gamboni-Robertson F, He Q, et al. High mobility group box 1 protein interacts with multiple Toll-like receptors. *Am J Physiol-Cell Physiol*. 2006;290(3):C917-C924. doi:10.1152/ajpcell.00401.2005

201. Park JS, Svetkauskaite D, He Q, et al. Involvement of Toll-like Receptors 2 and 4 in Cellular Activation by High Mobility Group Box 1 Protein *. *J Biol Chem*. 2004;279(9):7370-7377. doi:10.1074/jbc.M306793200

202. Yang H, Wang H, Andersson U. Targeting Inflammation Driven by HMGB1. *Front Immunol*. 2020;11. doi:10.3389/fimmu.2020.00484

203. Kierdorf K, Fritz G. RAGE regulation and signaling in inflammation and beyond. *J Leukoc Biol*. 2013;94(1):55-68. doi:https://doi.org/10.1189/jlb.1012519

204. Cheng C, Tsuneyama K, Kominami R, et al. Expression profiling of endogenous secretory receptor for advanced glycation end products in human organs. *Mod Pathol*. 2005;18(10):1385-1396. doi:10.1038/modpathol.3800450

205. Fuentes E, Rojas A, Palomo I. Role of multiligand/RAGE axis in platelet activation. *Thromb Res*. 2014;133(3):308-314. doi:10.1016/j.thromres.2013.11.007

206. Tanji N, Markowitz GS, Fu C, et al. Expression of Advanced Glycation End Products and Their Cellular Receptor RAGE in Diabetic Nephropathy and Nondiabetic Renal Disease. *J Am Soc Nephrol*. 2000;11(9):1656-1666. doi:10.1681/ASN.V1191656

207. Zhao CB, Bao JM, Lu YJ, et al. Co-expression of RAGE and HMGB1 is associated with cancer progression and poor patient outcome of prostate cancer. *Am J Cancer Res*. 2014;4(4):369-377. Accessed March 1, 2021. https://www.ncbi.nlm.nih.gov/pmc/articles/PMC4106654/

208. Kong Y, Wang F, Wang J, et al. Pathological Mechanisms Linking Diabetes Mellitus and Alzheimer's Disease: the Receptor for Advanced Glycation End Products (RAGE). *Front Aging Neurosci*. 2020;0. doi:10.3389/fnagi.2020.00217

209. Cai Z, Liu N, Wang C, et al. Role of RAGE in Alzheimer's Disease. *Cell Mol Neurobiol*. 2016;36(4):483-495. doi:10.1007/s10571-015-0233-3

210. Egaña-Gorroño L, López-Díez R, Yepuri G, et al. Receptor for Advanced Glycation End Products (RAGE) and Mechanisms and Therapeutic Opportunities in Diabetes and Cardiovascular Disease: Insights From Human Subjects and Animal Models. *Front Cardiovasc Med*. 2020;0. doi:10.3389/fcvm.2020.00037

211. Hally K, Fauteux-Daniel S, Hamzeh-Cognasse H, Larsen P, Cognasse F. Revisiting Platelets and Toll-Like Receptors (TLRs): At the Interface of Vascular Immunity and Thrombosis. *Int J Mol Sci*. 2020;21(17):6150. doi:10.3390/ijms21176150

212. Wagner KT, Radisic M. A New Role for Extracellular Vesicles in Cardiac Tissue Engineering and Regenerative Medicine. *Adv NanoBiomed Res*. 2021;1(11):2100047. doi:10.1002/anbr.202100047

213. Szatanek R, Baj-Krzyworzeka M, Zimoch J, Lekka M, Siedlar M, Baran J. The Methods of Choice for Extracellular Vesicles (EVs) Characterization. *Int J Mol Sci*. 2017;18(6):1153. doi:10.3390/ijms18061153

214. Doyle LM, Wang MZ. Overview of Extracellular Vesicles, Their Origin, Composition, Purpose, and Methods for Exosome Isolation and Analysis. *Cells*. 2019;8(7):727. doi:10.3390/cells8070727

215. Kenneweg F, Bang C, Xiao K, et al. Long Noncoding RNA-Enriched Vesicles Secreted by Hypoxic Cardiomyocytes Drive Cardiac Fibrosis. *Mol Ther - Nucleic Acids*. 2019;18:363-374. doi:10.1016/j.omtn.2019.09.003

216. Yang Y, Li Y, Chen X, Cheng X, Liao Y, Yu X. Exosomal transfer of miR-30a between cardiomyocytes regulates autophagy after hypoxia. *J Mol Med*. 2016;94(6):711-724. doi:10.1007/s00109-016-1387-2

217. Gorgulho CM, Romagnoli GG, Bharthi R, Lotze MT. Johnny on the Spot-Chronic Inflammation Is Driven by HMGB1. *Front Immunol*. 2019;10. doi:10.3389/fimmu.2019.01561

218. Alfaddagh A, Martin SS, Leucker TM, et al. Inflammation and cardiovascular disease: From mechanisms to therapeutics. *Am J Prev Cardiol*. 2020;4:100130. doi:10.1016/j.ajpc.2020.100130

219. Foglio E, Pellegrini L, Russo MA, Limana F. HMGB1-Mediated Activation of the Inflammatory-Reparative Response Following Myocardial Infarction. *Cells*. 2022;11(2):216. doi:10.3390/cells11020216

220. Funayama A, Shishido T, Netsu S, et al. Cardiac nuclear high mobility group box 1 prevents the development of cardiac hypertrophy and heart failure. *Cardiovasc Res*. 2013;99(4):657-664. doi:10.1093/cvr/cvt128

221. Hwang JS, Choi HS, Ham SA, et al. Deacetylation-mediated interaction of SIRT1-HMGB1 improves survival in a mouse model of endotoxemia. *Sci Rep*. 2015;5(1):15971. doi:10.1038/srep15971

222. Takahashi T, Shishido T, Kinoshita D, et al. Cardiac Nuclear High-Mobility Group Box 1 Ameliorates Pathological Cardiac Hypertrophy by Inhibiting DNA Damage Response. *JACC Basic Transl Sci*. 2019;4(2):234-247. doi:10.1016/j.jacbts.2018.11.011

223. Kwak MS, Kim HS, Lee B, Kim YH, Son M, Shin JS. Immunological Significance of HMGB1 Post-Translational Modification and Redox Biology. *Front Immunol*. 2020;11. Accessed February 22, 2023. https://www.frontiersin.org/articles/10.3389/fimmu.2020.01189

224. Martin TP, Robinson E, Harvey AP, et al. Surgical optimization and characterization of a minimally invasive aortic banding procedure to induce cardiac hypertrophy in mice. *Exp Physiol*. 2012;97(7):822-832. doi:10.1113/expphysiol.2012.065573

225. Ribeiro S, Pereira ARS, Pinto AT, et al. Echocardiographic Assessment of Cardiac Anatomy and Function in Adult Rats. *JoVE J Vis Exp*. 2019;(154):e60404. doi:10.3791/60404

226. Yu G, Wang LG, Han Y, He QY. clusterProfiler: an R Package for Comparing Biological Themes Among Gene Clusters. *OMICS J Integr Biol*. 2012;16(5):284-287. doi:10.1089/omi.2011.0118

227. Protocol Update for large-scale genome and gene function analysis with the PANTHER classification system (v.14.0) | Nature Protocols. Accessed October 6, 2024. https://www.nature.com/articles/s41596-019-0128-8

228. van der Velden J, Asselbergs FW, Bakkers J, et al. Animal models and animal-free innovations for cardiovascular research: current status and routes to be explored. Consensus document of the ESC Working Group on Myocardial Function and the ESC Working Group on Cellular Biology of the Heart. *Cardiovasc Res*. 2022;118(15):3016-3051. doi:10.1093/cvr/cvab370

229. Zeiss CJ, Johnson LK. Bridging the Gap between Reproducibility and Translation: Data Resources and Approaches. *ILAR J*. 2017;58(1):1-3. doi:10.1093/ilar/ilx017

230. Reichlin TS, Vogt L, Würbel H. The Researchers' View of Scientific Rigor—Survey on the Conduct and Reporting of In Vivo Research. *PLOS ONE*. 2016;11(12):e0165999. doi:10.1371/journal.pone.0165999

231. Sjoberg EA. Logical fallacies in animal model research. *Behav Brain Funct*. 2017;13(1):3. doi:10.1186/s12993-017-0121-8

232. Animals in Science Regulation Unit. GOV.UK. June 14, 2017. Accessed September 20, 2024. https://www.gov.uk/government/collections/animals-in-science-regulation-unit

233. Naderi SH, Bestwick JP, Wald DS. Adherence to Drugs That Prevent Cardiovascular Disease: Meta-analysis on 376,162 Patients. *Am J Med*. 2012;125(9):882-887.e1. doi:10.1016/j.amjmed.2011.12.013

234. Brown IAM, Diederich L, Good ME, et al. Vascular Smooth Muscle Remodeling in Conductive and Resistance Arteries in Hypertension: VSMC in hypertension. *Arterioscler Thromb Vasc Biol*. 2018;38(9):1969-1985. doi:10.1161/ATVBAHA.118.311229

235. McMaster WG, Kirabo A, Madhur MS, Harrison DG. Inflammation, Immunity, and Hypertensive End-Organ Damage. *Circ Res*. 2015;116(6):1022-1033. doi:10.1161/CIRCRESAHA.116.303697

236. Zhu YC, Zhu YZ, Lu N, Wang MJ, Wang YX, Yao T. Role of angiotensin AT1 and AT2 receptors in cardiac hypertrophy and cardiac remodelling. *Clin Exp Pharmacol Physiol*. 2003;30(12):911-918. doi:10.1111/j.1440-1681.2003.03942.x

237. O'Rourke SA, Dunne A, Monaghan MG. Frontiers | The Role of Macrophages in the Infarcted Myocardium: Orchestrators of ECM Remodeling. doi:10.3389/fcvm.2019.00101

238. Boytard L, Hadi T, Silvestro M, et al. Lung-derived HMGB1 is detrimental for vascular remodeling of metabolically imbalanced arterial macrophages. *Nat Commun*. 2020;11(1):4311. doi:10.1038/s41467-020-18088-2

239. Jama HA, Muralitharan RR, Xu C, et al. Rodent models of hypertension. *Br J Pharmacol*. 2022;179(5):918-937. doi:10.1111/bph.15650

240. Edgley A, Kett M, Anderson W. 'Slow Pressor' Hypertension From Low-Dose Chronic Angiotensin II Infusion. *Clin Exp Pharmacol Physiol*. 2001;28(12):1035-1039. doi:10.1046/j.1440-1681.2001.03590.x

241. Kawada N, Imai E, Karber A, Welch WJ, Wilcox CS. A Mouse Model of Angiotensin II Slow Pressor Response: Role of Oxidative Stress. *J Am*

Soc Nephrol. 2002;13(12):2860. doi:10.1097/01.ASN.0000035087.11758.ED

242. Guzik TJ, Nosalski R, Maffia P, Drummond GR. Immune and inflammatory mechanisms in hypertension. *Nat Rev Cardiol*. Published online January 3, 2024:1-21. doi:10.1038/s41569-023-00964-1

243. Schmieder RE. End Organ Damage In Hypertension. *Dtsch Ärztebl Int*. 2010;107(49):866-873. doi:10.3238/arztebl.2010.0866

244. Jellis C, Martin J, Narula J, Marwick TH. Assessment of Nonischemic Myocardial Fibrosis. *J Am Coll Cardiol*. 2010;56(2):89-97. doi:10.1016/j.jacc.2010.02.047

245. Karsdal MA, Nielsen SH, Leeming DJ, et al. The good and the bad collagens of fibrosis – Their role in signaling and organ function. *Adv Drug Deliv Rev*. 2017;121:43-56. doi:10.1016/j.addr.2017.07.014

246. Patel SR, Hartwig JH, Italiano JE. The biogenesis of platelets from megakaryocyte proplatelets. *J Clin Invest*. 2005;115(12):3348-3354. doi:10.1172/JCI26891

247. Singh MV, Cicha MZ, Nunez S, Meyerholz DK, Chapleau MW, Abboud FM. Angiotensin II-induced hypertension and cardiac hypertrophy are differentially mediated by TLR3- and TLR4-dependent pathways. *Am J Physiol - Heart Circ Physiol*. 2019;316(5):H1027-H1038. doi:10.1152/ajpheart.00697.2018

248. Lundin M, Heiberg E, Nordlund D, et al. Prognostic utility and characterization of left ventricular hypertrophy using global thickness. *Sci Rep*. 2023;13(1):22806. doi:10.1038/s41598-023-48173-7

249. Fliegner D, Schubert C, Penkalla A, et al. Female sex and estrogen receptor-β attenuate cardiac remodeling and apoptosis in pressure overload. *Am J Physiol-Regul Integr Comp Physiol*. 2010;298(6):R1597-R1606. doi:10.1152/ajpregu.00825.2009

250. Kararigas G, Fliegner D, Forler S, et al. Comparative Proteomic Analysis Reveals Sex and Estrogen Receptor β Effects in the Pressure Overloaded Heart. *J Proteome Res*. 2014;13(12):5829-5836. doi:10.1021/pr500749j

251. Skavdahl M, Steenbergen C, Clark J, et al. Estrogen receptor-β mediates male-female differences in the development of pressure overload hypertrophy. *Am J Physiol-Heart Circ Physiol*. 2005;288(2):H469-H476. doi:10.1152/ajpheart.00723.2004

252. Montalvo C, Villar AV, Merino D, et al. Androgens Contribute to Sex Differences in Myocardial Remodeling under Pressure Overload by a Mechanism Involving TGF-β. *PLoS ONE*. 2012;7(4):e35635. doi:10.1371/journal.pone.0035635

253. Antar SA, Ashour NA, Marawan ME, Al-Karmalawy AA. Fibrosis: Types, Effects, Markers, Mechanisms for Disease Progression, and Its Relation with Oxidative Stress, Immunity, and Inflammation. *Int J Mol Sci*. 2023;24(4):4004. doi:10.3390/ijms24044004

254. Nagao K, Inada T, Tamura A, et al. Circulating markers of collagen types I, III, and IV in patients with dilated cardiomyopathy: relationships with myocardial collagen expression. *ESC Heart Fail*. 2018;5(6):1044-1051. doi:10.1002/ehf2.12360

255. Dai Z, Aoki T, Fukumoto Y, Shimokawa H. Coronary perivascular fibrosis is associated with impairment of coronary blood flow in patients with non-ischemic heart failure. *J Cardiol*. 2012;60(5):416-421. doi:10.1016/j.jjcc.2012.06.009

256. Khalil H, Kanisicak O, Vagnozzi RJ, et al. Cell-specific ablation of Hsp47 defines the collagen-producing cells in the injured heart. *JCI Insight*. 4(15):e128722. doi:10.1172/jci.insight.128722

257. Su Z, Yin J, Wang T, et al. Up-regulated HMGB1 in EAM directly led to collagen deposition by a PKCβ/Erk1/2-dependent pathway: cardiac fibroblast/myofibroblast might be another source of HMGB1. *J Cell Mol Med*. 2014;18(9):1740-1751. doi:10.1111/jcmm.12324

258. Zile MR, DeSantis SM, Baicu CF, et al. Plasma Biomarkers That Reflect Determinants of Matrix Composition Identify the Presence of Left Ventricular Hypertrophy and Diastolic Heart Failure. *Circ Heart Fail*. 2011;4(3):246-256. doi:10.1161/CIRCHEARTFAILURE.110.958199

259. Candamo-Lourido M, Dopico-López A, López-Arias E, et al. Comparative Brain Proteomic Analysis between Sham and Cerebral Ischemia Experimental Groups. *Int J Mol Sci*. 2024;25(14):7538. doi:10.3390/ijms25147538

260. Zhou WBS, Shi XQ, Liu Y, Tran SD, Beaudry F, Zhang J. Unbiased proteomic analysis detects painful systemic inflammatory profile in the serum of nerve-injured mice. *PAIN*. 2023;164(2):e77. doi:10.1097/j.pain.0000000000002695

261. Wang W ke, Wang B, Lu Q hua, et al. Inhibition of high-mobility group box 1 improves myocardial fibrosis and dysfunction in diabetic

cardiomyopathy. *Int J Cardiol*. 2014;172(1):202-212. doi:10.1016/j.ijcard.2014.01.011

262. Sadamura-Takenaka Y, Ito T, Noma S, et al. HMGB1 Promotes the Development of Pulmonary Arterial Hypertension in Rats. *PLOS ONE*. 2014;9(7):e102482. doi:10.1371/journal.pone.0102482

263. Jiang M, Wu W, Xia Y, Wang X, Liang J. Platelet-derived extracellular vesicles promote endothelial dysfunction in sepsis by enhancing neutrophil extracellular traps. *BMC Immunol*. 2023;24(1):22. doi:10.1186/s12865-023-00560-5

264. Dai X, Shen L. Advances and Trends in Omics Technology Development. *Front Med*. 2022;9:911861. doi:10.3389/fmed.2022.911861

265. Karczewski KJ, Snyder MP. Integrative omics for health and disease. *Nat Rev Genet*. 2018;19(5):299-310. doi:10.1038/nrg.2018.4

266. Thomas R, Pontius JU, Borst LB, Breen M. Development of a Genome-Wide Oligonucleotide Microarray Platform for Detection of DNA Copy Number Aberrations in Feline Cancers. *Vet Sci*. 2020;7(3):88. doi:10.3390/vetsci7030088

267. Neagu AN, Jayathirtha M, Baxter E, Donnelly M, Petre BA, Darie CC. Applications of Tandem Mass Spectrometry (MS/MS) in Protein Analysis for Biomedical Research. *Molecules*. 2022;27(8):2411. doi:10.3390/molecules27082411

268. Pitt JJ. Principles and Applications of Liquid Chromatography-Mass Spectrometry in Clinical Biochemistry. *Clin Biochem Rev*. 2009;30(1):19-34. Accessed July 4, 2024. https://www.ncbi.nlm.nih.gov/pmc/articles/PMC2643089/

269. Gas Chromatography and Mass Spectrometry: The Technique | SpringerLink. Accessed July 25, 2024. https://link.springer.com/chapter/10.1007/978-3-031-30288-6_1

270. Hu Y, Cheng K, He L, et al. NMR-Based Methods for Protein Analysis. *Anal Chem*. 2021;93(4):1866-1879. doi:10.1021/acs.analchem.0c03830

271. May C, Brosseron F, Chartowski P, Meyer HE, Marcus K. Differential Proteome Analysis Using 2D-DIGE. In: Marcus K, ed. *Quantitative Methods in Proteomics*. Humana Press; 2012:75-82. doi:10.1007/978-1-61779-885-6_6

272. Marouga R, David S, Hawkins E. The development of the DIGE system: 2D fluorescence difference gel analysis technology. *Anal Bioanal Chem*. 2005;382(3):669-678. doi:10.1007/s00216-005-3126-3

273. Haag AM. Mass Analyzers and Mass Spectrometers. In: Mirzaei H, Carrasco M, eds. *Modern Proteomics – Sample Preparation, Analysis and Practical Applications*. Springer International Publishing; 2016:157-169. doi:10.1007/978-3-319-41448-5_7

274. Tian X, Permentier HP, Bischoff R. Chemical isotope labeling for quantitative proteomics. *Mass Spectrom Rev*. 2023;42(2):546-576. doi:10.1002/mas.21709

275. An Overview of Label-Free Quantitation Methods in Proteomics by Mass Spectrometry | SpringerLink. Accessed July 25, 2024. https://link.springer.com/protocol/10.1007/978-1-60761-444-9_18

276. Al-Amrani S, Al-Jabri Z, Al-Zaabi A, Alshekaili J, Al-Khabori M. Proteomics: Concepts and applications in human medicine. *World J Biol Chem*. 2021;12(5):57-69. doi:10.4331/wjbc.v12.i5.57

277. Bludau I, Aebersold R. Proteomic and interactomic insights into the molecular basis of cell functional diversity. *Nat Rev Mol Cell Biol*. 2020;21(6):327-340. doi:10.1038/s41580-020-0231-2

278. Holman JD, Dasari S, Tabb DL. Informatics of Protein and Posttranslational Modification Detection via Shotgun Proteomics. *Methods Mol Biol Clifton NJ*. 2013;1002:167-179. doi:10.1007/978-1-62703-360-2_14

279. Cox J, Mann M. Quantitative, High-Resolution Proteomics for Data-Driven Systems Biology. Published online July 7, 2011. doi:10.1146/annurev-biochem-061308-093216

280. Aslam B, Basit M, Nisar MA, Khurshid M, Rasool MH. Proteomics: Technologies and Their Applications. *J Chromatogr Sci*. 2017;55(2):182-196. doi:10.1093/chromsci/bmw167

281. Adua E. Decoding the mechanism of hypertension through multiomics profiling. *J Hum Hypertens*. 2023;37(4):253-264. doi:10.1038/s41371-022-00769-8

282. Cupp-Sutton KA, Wu S. High-throughput quantitative top-down proteomics. *Mol Omics*. 2020;16(2):91-99. doi:10.1039/c9mo00154a

283. Chen B, Brown KA, Lin Z, Ge Y. Top-Down Proteomics: Ready for Prime Time? *Anal Chem*. 2018;90(1):110-127. doi:10.1021/acs.analchem.7b04747

284. Bateman NW, Goulding SP, Shulman NJ, et al. Maximizing Peptide Identification Events in Proteomic Workflows Using Data-Dependent Acquisition (DDA). *Mol Cell Proteomics MCP*. 2014;13(1):329-338. doi:10.1074/mcp.M112.026500

285. Zhang Y, Fonslow BR, Shan B, Baek MC, Yates JRI. Protein Analysis by Shotgun/Bottom-up Proteomics. *Chem Rev*. 2013;113(4):2343-2394. doi:10.1021/cr3003533

286. Orsburn BC. Proteome Discoverer—A Community Enhanced Data Processing Suite for Protein Informatics. *Proteomes*. 2021;9(1):15. doi:10.3390/proteomes9010015

287. Lakoski SG, Cushman M, Siscovick DS, et al. The relationship between inflammation, obesity and risk for hypertension in the Multi-Ethnic Study of Atherosclerosis (MESA). *J Hum Hypertens*. 2011;25(2):73-79. doi:10.1038/jhh.2010.91

288. Schirone L, Forte M, Palmerio S, et al. A Review of the Molecular Mechanisms Underlying the Development and Progression of Cardiac Remodeling. *Oxid Med Cell Longev*. 2017;2017:3920195. doi:10.1155/2017/3920195

289. Jin X, Xia L, Wang LS, et al. Differential protein expression in hypertrophic heart with and without hypertension in spontaneously hypertensive rats. *PROTEOMICS*. 2006;6(6):1948-1956. doi:10.1002/pmic.200500337

290. Lam L, Tsoutsman T, Arthur J, Semsarian C. Differential protein expression profiling of myocardial tissue in a mouse model of hypertrophic cardiomyopathy. *J Mol Cell Cardiol*. 2010;48(5):1014-1022. doi:10.1016/j.yjmcc.2009.08.015

291. Al Ashmar S, Anlar GG, Krzyslak H, et al. Proteomic Analysis of Prehypertensive and Hypertensive Patients: Exploring the Role of the Actin Cytoskeleton. *Int J Mol Sci*. 2024;25(9):4896. doi:10.3390/ijms25094896

292. Kanehisa M, Goto S, Sato Y, Furumichi M, Tanabe M. KEGG for integration and interpretation of large-scale molecular data sets. *Nucleic Acids Res*. 2012;40(D1):D109-D114. doi:10.1093/nar/gkr988

293. Croft D, O'Kelly G, Wu G, et al. Reactome: a database of reactions, pathways and biological processes. *Nucleic Acids Res*. 2011;39(suppl_1):D691-D697. doi:10.1093/nar/gkq1018

294. Interpreting omics data with pathway enrichment analysis - ScienceDirect. Accessed October 3, 2024. https://www.sciencedirect.com/science/article/pii/S0168952523000185

295. On the influence of several factors on pathway enrichment analysis | Briefings in Bioinformatics | Oxford Academic. Accessed October 3, 2024. https://academic.oup.com/bib/article/23/3/bbac143/6572658

296. Salomonis N, Hanspers K, Zambon AC, et al. GenMAPP 2: new features and resources for pathway analysis. *BMC Bioinformatics*. 2007;8(1):217. doi:10.1186/1471-2105-8-217

297. Mi H, Guo N, Kejariwal A, Thomas PD. PANTHER version 6: protein sequence and function evolution data with expanded representation of biological pathways. *Nucleic Acids Res*. 2007;35(suppl_1):D247-D252. doi:10.1093/nar/gkl869

298. Franceschini A, Szklarczyk D, Frankild S, et al. STRING v9.1: protein-protein interaction networks, with increased coverage and integration. *Nucleic Acids Res*. 2013;41(Database issue):D808-D815. doi:10.1093/nar/gks1094

299. Wang T, Cai X, Li J, Xie L. Proteomics analysis in myocardium of spontaneously hypertensive rats. *Sci Rep*. 2023;13(1):276. doi:10.1038/s41598-023-27590-8

300. Wojtkiewicz M, Berg Luecke L, Castro C, Burkovetskaya M, Mesidor R, Gundry RL. Bottom-up proteomic analysis of human adult cardiac tissue and isolated cardiomyocytes. *J Mol Cell Cardiol*. 2022;162:20-31. doi:10.1016/j.yjmcc.2021.08.008

301. Turkieh A, Fertin M, Bouvet M, et al. Expression and Implication of Clusterin in Left Ventricular Remodeling After Myocardial Infarction. *Circ Heart Fail*. 2018;11(6):e004838. doi:10.1161/CIRCHEARTFAILURE.117.004838

302. Willforss J, Chawade A, Levander F. NormalyzerDE: Online Tool for Improved Normalization of Omics Expression Data and High-Sensitivity Differential Expression Analysis. *J Proteome Res*. 2019;18(2):732-740. doi:10.1021/acs.jproteome.8b00523

303. Wang S, Li W, Hu L, Cheng J, Yang H, Liu Y. NAguideR: performing and prioritizing missing value imputations for consistent bottom-up proteomic analyses. *Nucleic Acids Res*. 2020;48(14):e83. doi:10.1093/nar/gkaa498

304. Hayakawa K, Sakakibara S, Sokabe M, Tatsumi H. Single-molecule imaging and kinetic analysis of cooperative cofilin–actin filament interactions. *Proc Natl Acad Sci U S A*. 2014;111(27):9810-9815. doi:10.1073/pnas.1321451111

305. McGrath J, Tung CY, Liao X, et al. Actin at stereocilia tips is regulated by mechanotransduction and ADF/cofilin. *Curr Biol CB*. 2021;31(6):1141. doi:10.1016/j.cub.2020.12.006

306. Thirone ACP, Speight P, Zulys M, et al. Hyperosmotic stress induces Rho/Rho kinase/LIM kinase-mediated cofilin phosphorylation in tubular cells: key role in the osmotically triggered F-actin response. *Am J Physiol Cell Physiol*. 2009;296(3):C463-C475. doi:10.1152/ajpcell.00467.2008

307. Zhang L, Zhang B, Yu Y, et al. Angiotensin II Increases HMGB1 Expression in the Myocardium Through AT1 and AT2 Receptors When Under Pressure Overload. *Int Heart J*. 2021;62(1):162-170. doi:10.1536/ihj.20-384

308. Caporizzo MA, Chen CY, Prosser BL. Cardiac microtubules in health and heart disease. *Exp Biol Med*. 2019;244(15):1255. doi:10.1177/1535370219868960

309. Grimes KM, Prasad V, McNamara JW. Supporting the heart: Functions of the cardiomyocyte's non-sarcomeric cytoskeleton. *J Mol Cell Cardiol*. 2019;131:187-196. doi:10.1016/j.yjmcc.2019.04.002

310. Caporizzo MA, Prosser BL. The microtubule cytoskeleton in cardiac mechanics and heart failure. *Nat Rev Cardiol*. 2022;19(6):364-378. doi:10.1038/s41569-022-00692-y

311. Li L, Zhang Q, Zhang X, et al. Microtubule associated protein 4 phosphorylation leads to pathological cardiac remodeling in mice. *EBioMedicine*. 2018;37:221-235. doi:10.1016/j.ebiom.2018.10.017

312. Chinnakkannu P, Samanna V, Cheng G, et al. Site-specific Microtubule-associated Protein 4 Dephosphorylation Causes Microtubule Network Densification in Pressure Overload Cardiac Hypertrophy. *J Biol Chem*. 2010;285(28):21837-21848. doi:10.1074/jbc.M110.120709

313. Hausner EA. Cardiac Muscle and the Troponins. In: Jagadeesh G, Balakumar P, Maung-U K, eds. *Pathophysiology and Pharmacotherapy of*

Cardiovascular Disease. Springer International Publishing; 2015:179-192. doi:10.1007/978-3-319-15961-4_10

314. Zhang C, Liu R, Yuan J, et al. Significance and Determinants of Cardiac Troponin I in Patients With Obstructive Hypertrophic Cardiomyopathy. *Am J Cardiol*. 2015;116(11):1744-1751. doi:10.1016/j.amjcard.2015.09.006

315. Giovou AE, Gladka MM, Christoffels VM. The Impact of Natriuretic Peptides on Heart Development, Homeostasis, and Disease. *Cells*. 2024;13(11):931. doi:10.3390/cells13110931

316. Wang D, Oparil S, Feng JA, et al. Effects of Pressure Overload on Extracellular Matrix Expression in the Heart of the Atrial Natriuretic Peptide–Null Mouse. *Hypertension*. 2003;42(1):88-95. doi:10.1161/01.HYP.0000074905.22908.A6

317. Liu Y, Tavana O, Gu W. p53 modifications: exquisite decorations of the powerful guardian. *J Mol Cell Biol*. 2019;11(7):564-577. doi:10.1093/jmcb/mjz060

318. Shimizu I, Yoshida Y, Katsuno T, et al. p53-Induced Adipose Tissue Inflammation Is Critically Involved in the Development of Insulin Resistance in Heart Failure. *Cell Metab*. 2012;15(1):51-64. doi:10.1016/j.cmet.2011.12.006

319. Gazzar ME, Yoza BK, Chen X, Garcia BA, Young NL, McCall CE. Chromatin-Specific Remodeling by HMGB1 and Linker Histone H1 Silences Proinflammatory Genes during Endotoxin Tolerance. *Mol Cell Biol*. 2009;29(7):1959-1971. doi:10.1128/MCB.01862-08

320. Iadecola C, Gottesman RF. Neurovascular and Cognitive Dysfunction in Hypertension. *Circ Res*. 2019;124(7):1025-1044. doi:10.1161/CIRCRESAHA.118.313260

321. Radhakrishnan J, Wang S, Ayoub IM, Kolarova JD, Levine RF, Gazmuri RJ. Circulating levels of Cytochrome c after Resuscitation from Cardiac Arrest: A Marker of Mitochondrial Injury and Predictor of Survival. *Am J Physiol Heart Circ Physiol*. 2007;292(2):H767-H775. doi:10.1152/ajpheart.00468.2006

322. Zhou Z, Arroum T, Luo X, et al. Diverse functions of cytochrome c in cell death and disease. *Cell Death Differ*. 2024;31(4):387-404. doi:10.1038/s41418-024-01284-8

323. Liu ZB, Fu XH, Wei G, Gao JL. Cytochrome c release in acute myocardial infarction predicts poor prognosis and myocardial reperfusion on contrast-

enhanced magnetic resonance imaging. *Coron Artery Dis*. 2014;25(1):66. doi:10.1097/MCA.0000000000000040

324. Anto Michel N, Ljubojevic-Holzer S, Bugger H, Zirlik A. Cellular Heterogeneity of the Heart. *Front Cardiovasc Med*. 2022;9:868466. doi:10.3389/fcvm.2022.868466

325. Jiang M, Song Y, Chen X, et al. COX6A2 deficiency leads to cardiac remodeling in human pluripotent stem cell-derived cardiomyocytes. *Stem Cell Res Ther*. 2023;14(1):357. doi:10.1186/s13287-023-03596-x

326. Kim SE, Mori R, Komatsu T, et al. Upregulation of cytochrome c oxidase subunit 6b1 (Cox6b1) and formation of mitochondrial supercomplexes: implication of Cox6b1 in the effect of calorie restriction. *AGE*. 2015;37(3):45. doi:10.1007/s11357-015-9787-8

327. Kimura H, Nagoshi T, Oi Y, et al. Treatment with atrial natriuretic peptide induces adipose tissue browning and exerts thermogenic actions in vivo. *Sci Rep*. 2021;11(1):17466. doi:10.1038/s41598-021-96970-9

328. Fan GC, Ren X, Qian J, et al. Novel Cardioprotective Role of a Small Heat-Shock Protein, Hsp20, Against Ischemia/Reperfusion Injury. *Circulation*. 2005;111(14):1792-1799. doi:10.1161/01.CIR.0000160851.41872.C6

329. Zhang X, Wang X, Zhu H, et al. Hsp20 Functions as a Novel Cardiokine in Promoting Angiogenesis via Activation of VEGFR2. *PLoS ONE*. 2012;7(3):e32765. doi:10.1371/journal.pone.0032765

330. Dong H, Luo L, Zou M, et al. Blockade of extracellular heat shock protein 90α by 1G6-D7 attenuates pulmonary fibrosis through inhibiting ERK signaling. *Am J Physiol-Lung Cell Mol Physiol*. 2017;313(6):L1006-L1015. doi:10.1152/ajplung.00489.2016

331. Forces generated by lamellipodial actin filament elongation regulate the WAVE complex during cell migration | Nature Cell Biology. Accessed February 6, 2025. https://www.nature.com/articles/s41556-021-00786-8

332. Howard CM, Baudino TA. Dynamic cell–cell and cell–ECM interactions in the heart. *J Mol Cell Cardiol*. 2014;70:19-26. doi:10.1016/j.yjmcc.2013.10.006

333. Martins-Marques T. Connecting different heart diseases through intercellular communication. *Biol Open*. 2021;10(9):bio058777. doi:10.1242/bio.058777

334. Liang S, Zhou Y, Chang Y, et al. A novel gene-trap line reveals the dynamic patterns and essential roles of cysteine and glycine-rich protein 3 in zebrafish heart development and regeneration. *Cell Mol Life Sci*. 2024;81(1):1-14. doi:10.1007/s00018-024-05189-0

335. Chang DF, Belaguli NS, Iyer D, et al. Cysteine-Rich LIM-Only Proteins CRP1 and CRP2 Are Potent Smooth Muscle Differentiation Cofactors. *Dev Cell*. 2003;4(1):107-118. doi:10.1016/S1534-5807(02)00396-9

336. Chen CH, Ho YC, Ho HH, et al. Cysteine-rich protein 2 alters p130Cas localization and inhibits vascular smooth muscle cell migration. *Cardiovasc Res*. 2013;100(3):461-471. doi:10.1093/cvr/cvt207

337. Kang JO, Ha TW, Jung HU, Lim JE, Oh B. A cardiac-null mutation of Prdm16 causes hypotension in mice with cardiac hypertrophy via increased nitric oxide synthase 1. *PLoS ONE*. 2022;17(7):e0267938. doi:10.1371/journal.pone.0267938

338. Bagur R, Tanguy S, Foriel S, et al. The impact of cardiac ischemia/reperfusion on the mitochondria–cytoskeleton interactions. *Biochim Biophys Acta BBA - Mol Basis Dis*. 2016;1862(6):1159-1171. doi:10.1016/j.bbadis.2016.03.009

339. Phyo SA, Uchida K, Chen CY, et al. Transcriptional, Post-Transcriptional, and Post-Translational Mechanisms Rewrite the Tubulin Code During Cardiac Hypertrophy and Failure. *Front Cell Dev Biol*. 2022;10:837486. doi:10.3389/fcell.2022.837486

340. Schuldt M, Pei J, Harakalova M, et al. Proteomic and Functional Studies Reveal Detyrosinated Tubulin as Treatment Target in Sarcomere Mutation-Induced Hypertrophic Cardiomyopathy. *Circ Heart Fail*. 2021;14(1):e007022. doi:10.1161/CIRCHEARTFAILURE.120.007022

341. Chen CY, Caporizzo MA, Bedi K, et al. Suppression of detyrosinated microtubules improves cardiomyocyte function in human heart failure. *Nat Med*. 2018;24(8):1225-1233. doi:10.1038/s41591-018-0046-2

342. Wang TY, Lee D, Fox-Talbot K, Arking DE, Chakravarti A, Halushka MK. Cardiomyocytes have mosaic patterns of protein expression. *Cardiovasc Pathol Off J Soc Cardiovasc Pathol*. 2018;34:50-57. doi:10.1016/j.carpath.2018.03.002

343. Gao Z, Xu H, DiSilvestre D, et al. Transcriptomic profiling of the canine tachycardia-induced heart failure model: global comparison to human and murine heart failure. *J Mol Cell Cardiol*. 2006;40(1):76-86. doi:10.1016/j.yjmcc.2005.08.002

344. Peng W, Li M, Li H, et al. Dysfunction of Myosin Light-Chain 4 (MYL4) Leads to Heritable Atrial Cardiomyopathy With Electrical, Contractile, and Structural Components: Evidence From Genetically-Engineered Rats. *J Am Heart Assoc*. 6(11):e007030. doi:10.1161/JAHA.117.007030

345. Špiranec Spes K, Chen W, Krebes L, et al. Heart-Microcirculation Connection. *Hypertension*. 2020;76(5):1637-1648. doi:10.1161/HYPERTENSIONAHA.120.15772

346. An FHL1-containing complex within the cardiomyocyte sarcomere mediates hypertrophic biomechanical stress responses in mice - PMC. Accessed October 22, 2024. https://pmc.ncbi.nlm.nih.gov/articles/PMC2575833/

347. Sliding Filament Theory, Sarcomere, Muscle Contraction, Myosin | Learn Science at Scitable. Accessed October 28, 2024. https://www.nature.com/scitable/topicpage/the-sliding-filament-theory-of-muscle-contraction-14567666/

348. Dumont V, Lehtonen S. PACSIN proteins in vivo: Roles in development and physiology. *Acta Physiol Oxf Engl*. 2022;234(3):e13783. doi:10.1111/apha.13783

349. Semmler J, Kormann J, Srinivasan SP, et al. Pacsin 2 is required for the maintenance of a normal cardiac function in the developing mouse heart. *Pharmacol Res*. 2018;128:200-210. doi:10.1016/j.phrs.2017.10.004

350. Fibroblast and myofibroblast activation in normal tissue repair and fibrosis | Nature Reviews Molecular Cell Biology. Accessed June 25, 2024. https://www.nature.com/articles/s41580-024-00716-0

351. Pathak S, Kale A, Kumar CMS, Sheikh M. Role of Cytoskeletal Protein, Actin in Various Diseases. In: Egbuna C, Hassan S, eds. *Dietary Phytochemicals: A Source of Novel Bioactive Compounds for the Treatment of Obesity, Cancer and Diabetes*. Springer International Publishing; 2021:95-124. doi:10.1007/978-3-030-72999-8_6

352. Copeland O, Nowak KJ, Laing NG, et al. Investigation of changes in skeletal muscle α-actin expression in normal and pathological human and mouse hearts. *J Muscle Res Cell Motil*. 2010;31(3):207-214. doi:10.1007/s10974-010-9224-7

353. Suurmeijer AJ, Clément S, Francesconi A, et al. α-Actin isoform distribution in normal and failing human heart: a morphological, morphometric, and biochemical study. *J Pathol*. 2003;199(3):387-397. doi:10.1002/path.1311

354. Huang TY, DerMardirossian C, Bokoch GM. Cofilin phosphatases and regulation of actin dynamics. *Curr Opin Cell Biol*. 2006;18(1):26-31. doi:10.1016/j.ceb.2005.11.005

355. Leonard A, Marando C, Rahman A, Fazal F. Thrombin selectively engages LIM kinase 1 and slingshot-1L phosphatase to regulate NF-κB activation and endothelial cell inflammation. *Am J Physiol-Lung Cell Mol Physiol*. 2013;305(9):L651-L664. doi:10.1152/ajplung.00071.2013

356. Maciver SK, Hussey PJ. The ADF/cofilin family: actin-remodeling proteins. *Genome Biol*. 2002;3(5):reviews3007.1. doi:10.1186/gb-2002-3-5-reviews3007

357. Vartiainen MK, Mustonen T, Mattila PK, et al. The Three Mouse Actin-depolymerizing Factor/Cofilins Evolved to Fulfill Cell-Type–specific Requirements for Actin Dynamics. *Mol Biol Cell*. 2002;13(1):183-194. doi:10.1091/mbc.01-07-0331

358. N-terminal α-amino SUMOylation of cofilin-1 is critical for its regulation of actin depolymerization | Nature Communications. Accessed October 14, 2024. https://www.nature.com/articles/s41467-023-41520-2

359. Askari JA, Buckley PA, Mould AP, Humphries MJ. Linking integrin conformation to function. *J Cell Sci*. 2009;122(2):165-170. doi:10.1242/jcs.018556

360. Jansen KA, Atherton P, Ballestrem C. Mechanotransduction at the cell-matrix interface. *Semin Cell Dev Biol*. 2017;71:75-83. doi:10.1016/j.semcdb.2017.07.027

361. Barczyk M, Carracedo S, Gullberg D. Integrins. *Cell Tissue Res*. 2009;339(1):269. doi:10.1007/s00441-009-0834-6

362. Bugiardini E, Nunes AM, Oliveira-Santos A, et al. Integrin α7 Mutations Are Associated With Adult-Onset Cardiac Dysfunction in Humans and Mice. *J Am Heart Assoc*. 2022;11(23):e026494. doi:10.1161/JAHA.122.026494

363. Díez J, González A, Kovacic JC. Myocardial Interstitial Fibrosis in Nonischemic Heart Disease, Part 3/4: JACC Focus Seminar. *J Am Coll Cardiol*. 2020;75(17):2204-2218. doi:10.1016/j.jacc.2020.03.019

364. Mosaddeghzadeh N, Ahmadian MR. The RHO Family GTPases: Mechanisms of Regulation and Signaling. *Cells*. 2021;10(7):1831. doi:10.3390/cells10071831

365. Rho GTPases and their role in organizing the actin cytoskeleton | Journal of Cell Science | The Company of Biologists. Accessed October 26, 2024. https://journals.biologists.com/jcs/article/124/5/679/32109/Rho-GTPases-and-their-role-in-organizing-the-actin

366. RHO GTPases: from new partners to complex immune syndromes | Nature Reviews Immunology. Accessed October 28, 2024. https://www.nature.com/articles/s41577-021-00500-7

367. Moujaber O, Stochaj U. The Cytoskeleton as Regulator of Cell Signaling Pathways. *Trends Biochem Sci*. 2020;45(2):96-107. doi:10.1016/j.tibs.2019.11.003

368. Dick SA, Epelman S. Chronic Heart Failure and Inflammation. *Circ Res*. 2016;119(1):159-176. doi:10.1161/CIRCRESAHA.116.308030

369. Kubota T, McTiernan CF, Frye CS, et al. Dilated Cardiomyopathy in Transgenic Mice With Cardiac-Specific Overexpression of Tumor Necrosis Factor-α. *Circ Res*. 1997;81(4):627-635. doi:10.1161/01.RES.81.4.627

370. Siwik DA, Chang DLF, Colucci WS. Interleukin-1β and Tumor Necrosis Factor-α Decrease Collagen Synthesis and Increase Matrix Metalloproteinase Activity in Cardiac Fibroblasts In Vitro. *Circ Res*. 2000;86(12):1259-1265. doi:10.1161/01.RES.86.12.1259

371. Frangogiannis NG. The extracellular matrix in ischemic and non-ischemic heart failure. *Circ Res*. 2019;125(1):117-146. doi:10.1161/CIRCRESAHA.119.311148

372. Liu L, Wang Y, Cao ZY, et al. Up-regulated TLR4 in cardiomyocytes exacerbates heart failure after long-term myocardial infarction. *J Cell Mol Med*. 2015;19(12):2728. doi:10.1111/jcmm.12659

373. Frantz S, Kobzik L, Kim YD, et al. Toll4 (TLR4) expression in cardiac myocytes in normal and failing myocardium. *J Clin Invest*. 1999;104(3):271-280. doi:10.1172/JCI6709

374. Gunadi JW, Tarawan VM, Setiawan I, Lesmana R, Wahyudianingsih R, Supratman U. Cardiac hypertrophy is stimulated by altered training intensity and correlates with autophagy modulation in male Wistar rats. *BMC Sports Sci Med Rehabil*. 2019;11(1):9. doi:10.1186/s13102-019-0121-0

375. Díez J, González A, Kovacic JC. Myocardial Interstitial Fibrosis in Nonischemic Heart Disease: JACC Focus Seminar: Part 3 of 4. *J Am Coll Cardiol*. 2020;75(17):2204-2218. doi:10.1016/j.jacc.2020.03.019

376. Willis WL, Wang L, Wada TT, et al. The proinflammatory protein HMGB1 is a substrate of transglutaminase-2 and forms high-molecular weight complexes with autoantigens. *J Biol Chem*. 2018;293(22):8394-8409. doi:10.1074/jbc.RA117.001078

377. Kehat I, Molkentin JD. Molecular pathways underlying cardiac remodeling during pathophysiologic stimulation. *Circulation*. 2010;122(25):10.1161/CIRCULATIONAHA.110.942268. doi:10.1161/CIRCULATIONAHA.110.942268

378. Hu M, Ling Z, Ren X. Extracellular matrix dynamics: tracking in biological systems and their implications. *J Biol Eng*. 2022;16(1):13. doi:10.1186/s13036-022-00292-x

379. Nguyen BA, Alexander MR, Harrison DG. Immune mechanisms in the pathophysiology of hypertension. *Nat Rev Nephrol*. 2024;20(8):530-540. doi:10.1038/s41581-024-00838-w

380. Liu M, López de Juan Abad B, Cheng K. Cardiac fibrosis: Myofibroblast-mediated pathological regulation and drug delivery strategies. *Adv Drug Deliv Rev*. 2021;173:504-519. doi:10.1016/j.addr.2021.03.021

381. Umbarkar P, Ejantkar S, Tousif S, Lal H. Mechanisms of Fibroblast Activation and Myocardial Fibrosis: Lessons Learned from FB-Specific Conditional Mouse Models. *Cells*. 2021;10(9):2412. doi:10.3390/cells10092412

382. Kammerer J, Cirnu A, Williams T, et al. Macro-based collagen quantification and segmentation in picrosirius red-stained heart sections using light microscopy. *Biol Methods Protoc*. 2024;9(1):bpae027. doi:10.1093/biomethods/bpae027

383. Frangogiannis NG, Shimoni S, Chang S, et al. Active interstitial remodeling: an important process in the hibernating human myocardium. *J Am Coll Cardiol*. 2002;39(9):1468-1474. doi:10.1016/S0735-1097(02)01792-8

384. Frangogiannis NG, Shimoni S, Chang SM, et al. Evidence for an Active Inflammatory Process in the Hibernating Human Myocardium. *Am J Pathol*. 2002;160(4):1425-1433. doi:10.1016/S0002-9440(10)62568-0

385. Frangogiannis NG. Can Myocardial Fibrosis Be Reversed?∗. *J Am Coll Cardiol*. 2019;73(18):2283-2285. doi:10.1016/j.jacc.2018.10.094

386. Bhattacharyya S, Kelley K, Melichian DS, et al. Toll-Like Receptor 4 Signaling Augments Transforming Growth Factor-β Responses. *Am J Pathol*. 2013;182(1):192-205. doi:10.1016/j.ajpath.2012.09.007

387. Cambier L, Giani JF, Liu W, et al. Angiotensin II–Induced End-Organ Damage in Mice Is Attenuated by Human Exosomes and by an Exosomal Y RNA Fragment. *Hypertension*. 2018;72(2):370-380. doi:10.1161/HYPERTENSIONAHA.118.11239

388. Xu J, Carretero OA, Liao TD, et al. Local angiotensin II aggravates cardiac remodeling in hypertension. *Am J Physiol - Heart Circ Physiol*. 2010;299(5):H1328-H1338. doi:10.1152/ajpheart.00538.2010

389. Schiraldi M, Raucci A, Muñoz LM, et al. HMGB1 promotes recruitment of inflammatory cells to damaged tissues by forming a complex with CXCL12 and signaling via CXCR4. *J Exp Med*. 2012;209(3):551-563. doi:10.1084/jem.20111739

390. Manganelli V, Signore M, Pacini I, et al. Increased HMGB1 expression and release by mononuclear cells following surgical/anesthesia trauma. *Crit Care*. 2010;14(6):R197. doi:10.1186/cc9316

391. Zhang Z, Wu Y, Zhao Y, Xiao X, Liu J, Zhou X. Dynamic changes in HMGB1 levels correlate with inflammatory responses during cardiopulmonary bypass. *Exp Ther Med*. 2013;5(5):1523-1527. doi:10.3892/etm.2013.1026

392. Kim N, Lee S, Lee JR, Kwak YL, Jun JH, Shim JK. Prognostic role of serum high mobility group box 1 concentration in cardiac surgery. *Sci Rep*. 2020;10(1):6293. doi:10.1038/s41598-020-63051-2

393. Smajic J, Tupkovic LR, Husic S, Avdagic SS, Hodzic S, Imamovic S. Systemic Inflammatory Response Syndrome in Surgical Patients. *Med Arch*. 2018;72(2):116-119. doi:10.5455/medarh.2018.72.116-119

394. Kuroki MT, Fink GD, Osborn JW. Comparison of arterial pressure and plasma ANG II responses to three methods of subcutaneous ANG II administration. *Am J Physiol - Heart Circ Physiol*. 2014;307(5):H670-H679. doi:10.1152/ajpheart.00922.2013

395. Dąbrowska AM, Słotwiński R. The immune response to surgery and infection. *Cent-Eur J Immunol*. 2014;39(4):532-537. doi:10.5114/ceji.2014.47741

396. Ranzato E, Martinotti S, Pedrazzi M, Patrone M. High Mobility Group Box Protein-1 in Wound Repair. *Cells*. 2012;1(4):699-710. doi:10.3390/cells1040699

397. Yang H, Lundbäck P, Ottosson L, et al. Redox modifications of cysteine residues regulate the cytokine activity of HMGB1. *Mol Med*. 2021;27(1):58. doi:10.1186/s10020-021-00307-1

398. Pirnie R, P Gillespie K, Mesaros C, Blair IA. Reappraisal of Oxidized HMGB1 As a Mediator and Biomarker. *Future Sci OA*. 2022;8(10):FSO828. doi:10.2144/fsoa-2022-0052

399. Jeong J, Lee J, Lim J, et al. Soluble RAGE attenuates AngII-induced endothelial hyperpermeability by disrupting HMGB1-mediated crosstalk between AT1R and RAGE. *Exp Mol Med*. 2019;51(9):1-15. doi:10.1038/s12276-019-0312-5

400. Feng Q, Liu D, Lu Y, Liu Z. The Interplay of Renin-Angiotensin System and Toll-Like Receptor 4 in the Inflammation of Diabetic Nephropathy. *J Immunol Res*. 2020;2020(1):6193407. doi:10.1155/2020/6193407

401. Andrassy M, Volz HC, Igwe JC, et al. High-Mobility Group Box-1 in Ischemia-Reperfusion Injury of the Heart. *Circulation*. 2008;117(25):3216-3226. doi:10.1161/CIRCULATIONAHA.108.769331

402. Zhang L, Yang X, Jiang G, et al. HMGB1 enhances mechanical stress-induced cardiomyocyte hypertrophy in vitro via the RAGE/ERK1/2 signaling pathway. *Int J Mol Med*. 2019;44(3):885-892. doi:10.3892/ijmm.2019.4276

403. Zhang L, Liu M, Jiang H, et al. Extracellular high-mobility group box 1 mediates pressure overload-induced cardiac hypertrophy and heart failure. *J Cell Mol Med*. 2016;20(3):459-470. doi:10.1111/jcmm.12743

404. Lu B, Antoine DJ, Kwan K, et al. JAK/STAT1 signaling promotes HMGB1 hyperacetylation and nuclear translocation. *Proc Natl Acad Sci U S A*. 2014;111(8):3068-3073. doi:10.1073/pnas.1316925111

405. Rizzuto AS, Faggiano A, Macchi C, Carugo S, Perrino C, Ruscica M. Extracellular vesicles in cardiomyopathies: A narrative review. *Heliyon*. 2024;10(1):e23765. doi:10.1016/j.heliyon.2023.e23765

406. Zhang X, Takeuchi T, Takeda A, Mochizuki H, Nagai Y. Comparison of serum and plasma as a source of blood extracellular vesicles: Increased levels of platelet-derived particles in serum extracellular vesicle fractions

alter content profiles from plasma extracellular vesicle fractions. *PLoS ONE*. 2022;17(6):e0270634. doi:10.1371/journal.pone.0270634

407. Chin BH, Tyler TR, Kozbelt SJ. The Interfering Effects of Hemolyzed Blood on Rat Serum Chemistry. *Toxicol Pathol*. 1979;7(1):19-22. doi:10.1177/019262337900700104

408. da SilveiraCavalcante L, Acker JP, Holovati JL. Differences in Rat and Human Erythrocytes Following Blood Component Manufacturing: The Effect of Additive Solutions. *Transfus Med Hemotherapy*. 2015;42(3):150-157. doi:10.1159/000371474

409. Ebeyer-Masotta M, Eichhorn T, Weiss R, Lauková L, Weber V. Activated Platelets and Platelet-Derived Extracellular Vesicles Mediate COVID-19-Associated Immunothrombosis. *Front Cell Dev Biol*. 2022;10:914891. doi:10.3389/fcell.2022.914891

410. Machlus KR, Italiano JE Jr. The incredible journey: From megakaryocyte development to platelet formation. *J Cell Biol*. 2013;201(6):785-796. doi:10.1083/jcb.201304054

411. Takeuchi K, Satoh M, Kuno H, Yoshida T, Kondo H, Takeuchi M. Platelet-like particle formation in the human megakaryoblastic leukaemia cell lines, MEG-01 and MEG-01s. *Br J Haematol*. 1998;100(2):436-444. doi:https://doi.org/10.1046/j.1365-2141.1998.00576.x

412. Zhang Q, Chen Y, Wang Q, et al. HMGB1-induced activation of ER stress contributes to pulmonary artery hypertension in vitro and in vivo. *Respir Res*. 2023;24(1):149. doi:10.1186/s12931-023-02454-x

413. Zhang X, Wang T, Chen Z, et al. HMGB1-Promoted Neutrophil Extracellular Traps Contribute to Cardiac Diastolic Dysfunction in Mice. *J Am Heart Assoc*. 2022;11(4):e023800. doi:10.1161/JAHA.121.023800

414. Salo H, Qu H, Mitsiou D, et al. Disulfide and Fully Reduced HMGB1 Induce Different Macrophage Polarization and Migration Patterns. *Biomolecules*. 2021;11(6):800. doi:10.3390/biom11060800

415. van VDJ, Linssen GCM, Jaarsma T, et al. B-Type Natriuretic Peptide and Prognosis in Heart Failure Patients With Preserved and Reduced Ejection Fraction. *JACC*. 2013;61(14):1498-1506. doi:10.1016/j.jacc.2012.12.044

416. Lipson KE, Wong C, Teng Y, Spong S. CTGF is a central mediator of tissue remodeling and fibrosis and its inhibition can reverse the process of fibrosis. *Fibrogenesis Tissue Repair*. 2012;5(Suppl 1):S24. doi:10.1186/1755-1536-5-S1-S24

417. Linscheid N, Santos A, Poulsen PC, et al. Quantitative proteome comparison of human hearts with those of model organisms. *PLOS Biol*. 2021;19(4):e3001144. doi:10.1371/journal.pbio.3001144

418. Doll S, Dreßen M, Geyer PE, et al. Region and cell-type resolved quantitative proteomic map of the human heart. *Nat Commun*. 2017;8(1):1469. doi:10.1038/s41467-017-01747-2

419. Scott WA, Campos EI. Interactions With Histone H3 & Tools to Study Them. *Front Cell Dev Biol*. 2020;8. doi:10.3389/fcell.2020.00701

420. Hofbauer TM, Mangold A, Scherz T, et al. Neutrophil extracellular traps and fibrocytes in ST-segment elevation myocardial infarction. *Basic Res Cardiol*. 2019;114(5):33. doi:10.1007/s00395-019-0740-3

421. Wu RN, Yu TY, Zhou JC, et al. Targeting HMGB1 ameliorates cardiac fibrosis through restoring TLR2-mediated autophagy suppression in myocardial fibroblasts. *Int J Cardiol*. 2018;267:156-162. doi:10.1016/j.ijcard.2018.04.103

422. Lim DS, Roberts R, Marian AJ. Expression profiling of cardiac genes in human hypertrophic cardiomyopathy: insight into the pathogenesis of phenotypes. *J Am Coll Cardiol*. 2001;38(4):1175-1180. doi:10.1016/S0735-1097(01)01509-1

423. Horsthuis T, Houweling AC, Habets PEMH, et al. Distinct Regulation of Developmental and Heart Disease–Induced Atrial Natriuretic Factor Expression by Two Separate Distal Sequences. *Circ Res*. 2008;102(7):849-859. doi:10.1161/CIRCRESAHA.107.170571

424. Man JCK, van Duijvenboden K, Krijger PHL, et al. Genetic Dissection of a Super Enhancer Controlling the Nppa-Nppb Cluster in the Heart. *Circ Res*. 2021;128(1):115-129. doi:10.1161/CIRCRESAHA.120.317045

425. Linscheid N, Poulsen PC, Pedersen ID, et al. Quantitative Proteomics of Human Heart Samples Collected *In Vivo* Reveal the Remodeled Protein Landscape of Dilated Left Atrium Without Atrial Fibrillation. *Mol Cell Proteomics*. 2020;19(7):1132-1144. doi:10.1074/mcp.RA119.001878

426. Prudent R, Demoncheaux N, Diemer H, et al. A quantitative proteomic analysis of cofilin phosphorylation in myeloid cells and its modulation using the LIM kinase inhibitor Pyr1. *PLoS ONE*. 2018;13(12):e0208979. doi:10.1371/journal.pone.0208979

427. Varnaitė R, MacNeill SA. Meet the neighbors: Mapping local protein interactomes by proximity-dependent labeling with BioID. *Proteomics*. 2016;16(19):2503-2518. doi:10.1002/pmic.201600123

428. Zhao G, Fu C, Wang L, et al. Down-regulation of nuclear HMGB1 reduces ischemia-induced HMGB1 translocation and release and protects against liver ischemia-reperfusion injury. *Sci Rep*. 2017;7(1):46272. doi:10.1038/srep46272

429. Karp PD, Midford PE, Caspi R, Khodursky A. Pathway size matters: the influence of pathway granularity on over-representation (enrichment analysis) statistics. *BMC Genomics*. 2021;22(1):191. doi:10.1186/s12864-021-07502-8

430. Yu P, Liu M, Zhang B, et al. Cardiomyocyte-restricted high-mobility group box 1 (HMGB1) deletion leads to small heart and glycolipid metabolic disorder through GR/PGC-1α signalling. *Cell Death Discov*. 2020;6(1):1-11. doi:10.1038/s41420-020-00340-9

431. Querejeta R, López B, González A, et al. Increased Collagen Type I Synthesis in Patients With Heart Failure of Hypertensive Origin. *Circulation*. 2004;110(10):1263-1268. doi:10.1161/01.CIR.0000140973.60992.9A